

MECHANISMS OF DRUG-INDUCED LIVER INJURY:
THE ROLE OF HEPATIC TRANSPORT PROTEINS

Kyunghee Yang

A dissertation submitted to the faculty of the University of North Carolina at Chapel Hill
in partial fulfillment of the requirements for the degree of Doctor of Philosophy
in the Eshelman School of Pharmacy

Chapel Hill
2014

Approved by:

Kim L.R. Brouwer

Paul B. Watkins

Dhiren Thakker

Harvey J. Clewell III

Brett A. Howell

©2014
Kyunghee Yang
ALL RIGHTS RESERVED

ABSTRACT

Kyunghee Yang: Mechanisms of Drug-Induced Liver Injury: The Role of Hepatic Transport Proteins
(Under the direction of Kim L.R. Brouwer)

The objectives of this research were to investigate mechanisms of drug-induced liver injury (DILI) that involve drug-bile acid (BA) interactions at hepatic transporters, and develop a novel strategy to reliably predict human DILI. Troglitazone (TGZ), an antidiabetic withdrawn from the market due to severe DILI, was employed as a model hepatotoxic drug. Pharmacokinetic modeling of taurocholic acid (TCA, a model BA) disposition data from human and rat sandwich-cultured hepatocytes (SCH) revealed that species differences exist in TCA hepatocellular efflux pathways; in human SCH, TCA biliary excretion predominated, whereas biliary and basolateral excretion contributed equally to TCA efflux in rat SCH. This finding explains, in part, why rats are less susceptible to DILI compared to humans after administration of drugs that inhibit BA biliary excretion. The present study also revealed for the first time that TGZ sulfate (TS), a major TGZ metabolite, inhibits BA basolateral efflux in addition to biliary excretion. These findings support the hypothesis that TS is an important mediator of altered hepatic BA disposition; increased hepatic TS exposure due to impaired canalicular transport function might predispose a subset of patients to hepatotoxicity. A novel in vitro model system, rat SCH lacking selected canalicular transporters [breast cancer resistance protein (Bcrp) and multidrug resistance-associated protein 2 (Mrp2)] was established to test this hypothesis; biliary excretion of hepatically-generated TS was not significantly altered, suggesting that alternate transporters can excrete TS into bile, and loss of Bcrp and/or Mrp2 function would not necessarily be risk factors for increased hepatocellular TS accumulation in rats. To translate experimental data to in vivo humans, a mechanistic model that incorporated TGZ/TS disposition, BA physiology/pathophysiology, hepatocyte life cycle, and liver injury

biomarkers was developed; intracellular BA concentrations and toxicity measured in SCH were used to link BA homeostasis and hepatotoxicity. This mechanistic model adequately predicted the incidence, delayed presentation, and species differences in TGZ hepatotoxicity. This dissertation research revealed a number of important and novel findings that improve our understanding about mechanisms underlying BA-mediated DILI, and establish a framework to integrate biological information and experimental data to evaluate DILI mechanisms and predict hepatotoxic potential of chemical entities.

ACKNOWLEDGEMENTS

First of all, I want to thank Dr. Kim Brouwer for her constant support, guidance, and encouragement, and for having been there as a great mentor at every stage of my growth over the last four years. I also want to thank all the members of my dissertation committee who have been influential on my scientific and personal development: Dr. Watkins for serving as my chair and all of the guidance, advice, and opportunities he has provided during my dissertation research and also for future career; Dr. Thakker for insights on drug metabolism and transport, and exciting scientific discussions; Dr. Howell for all of the modeling advice and expertise which have enabled me to carry out the mechanistic modeling project; Dr. Clewell for all of the helpful comments and insights on pharmacokinetic modeling; Dr. Paine for serving as my early committee and continuing support.

This dissertation would not have been possible without the help of so many people in so many ways. I would like to thank the past and present Brouwer lab members, for intellectual interactions as well as being such great lab mates: Grace Yan, Tracy Marion, LaToya Griffin, Wei Yue, Brian Ferslew, Kevin Watt, Jason Slizgi, and Cen Guo. And my special thanks to Nathan Pfeifer, Kathleen Köck and Rhiannon Hardwick for all the times we shared working in the lab day and night, and all the adventures we took outside the lab. All of our undergraduate work-study students who have helped with many experiments and keeping lab space clean and neat, notably: Kevin Harris, Pearl Nguyen, Matthew Sanchez, and Kevin Le. PK/PD and T32 postdoctoral fellows for their insights and helpful suggestions on modeling projects and manuscript preparation: Dora Dumitrescu, Christina Mayer, Mario Sampson, Curtis Johnston, Danny Gonzalez, and Eleftheria Tsakalozou. Arlo Brown and Kathy Maboll who have helped me with important processes and document in the program step by step. I could not have made it without fellow graduate

students of my year, Nicole Zane, Akinyemi Oni-Orisan, and Dan Crona, who were there with me enduring together the coursework and the qualifying exam, and celebrating survival. I also want to thank a number of ESOP members who have helped me throughout the graduate school years: Christina Won, Julie Lauffenburger, Melea Ward, Scott Brantley, Brandon Gufford, Garrett Ainslie, and Kristina Wolf. I cannot thank the DILIsim team and the folks at the Hamner Institutes enough for their support and all the times we spent together; Jeffrey Woodhead, Scott Siler, Yuching Yang, Lisl Shoda, Patti Steele, and Geoffrey Bock. There are so many people who had brought expertise from various fields and help strengthen my research: Alexander Sedykh, Alexander Tropsha, Bob St. Claire, Cassandra Hubert, and Paul Stewart. I also thank my previous advisors and mentors, Myung Gull Lee and Hyunyoung Jeong, who led me to the exciting world of science and have been watching my development ever since.

I also need to thank many people whom I met in this home far away from my home in South Korea. Without their personal and emotional support, I could not made it through. “Baity Hill sisters” who had been with me during good times and bad times since I arrived in Chapel Hill: Jane Lim, Gina Song, Sujeong Kim, and Younjee Chung. All the members of Nehemiah at Duraleigh Presbyterian Church and my group members at Bible Study Fellowship for their support and prayer. Denise Dietrich, for our fellowship and the wonderful times we spent together every Monday night. My friends from Chicago who cares and supports me: Kwi Hye Koh, Su-Young Choi, Yeonjoo Lee, and Hyunjoo Lee. I also want to thank my old friends for being there whenever I need encouragement: Sora Park who has known me since I was a little child, and Seojin Huh with whom I spent my exciting years in the Pharmacy School. Finally, and most importantly, my family: my cheering sisters Kyungjin and Kyungjee, who can always make me laugh even during the hard times. I also would like to thank my parents-in-law, Youngki Yang and Sungsook Lee, for their continuing prayer and loving support for me. Mom and Dad, thanks for everything you have done for me – for your nurturing love, support for my dreams, and countless things I cannot even list all. This work is for my beloved husband, Sihyung Yang; I could not have made this journey without your faithful love and support, and look forward to a lifelong journey with you. Lastly, I would like to thank my greatest mentor, friend, and savior: God. I know that you have been with

me and guiding me during all the paths of my life. I will never forget what a great fortune I have had in being here, and that it comes with a responsibility. I am thankful for your presence and for all the things you allowed and did not allow in my life, and hope I am doing the work you have planned me to do for your good purpose.

TABLE OF CONTENTS

LIST OF TABLES	ix
LIST OF FIGURES	x
CHAPTER 1. Introduction.....	1
CHAPTER 2. Analysis of Hepatic Transport Proteins	53
CHAPTER 3. Species Differences in Hepatobiliary Disposition of Taurocholic acid in Human and Rat Sandwich-Cultured Hepatocytes; Implications for Drug-Induced Liver Injury	98
CHAPTER 4. An Experimental Approach to Evaluate the Impact of Impaired Transport Function on Hepatobiliary Drug Disposition using Mrp2-deficient TR ⁻ Rat Sandwich-Cultured Hepatocytes in Combination with Bcrp Knockdown.....	124
CHAPTER 5. Hepatocellular Exposure of Generated Metabolites, Troglitazone Sulfate and Glucuronide, is Determined by the Interplay between Formation and Excretion in Rat Sandwich-Cultured Hepatocytes Lacking Selected Canalicular Transporters	153
CHAPTER 6. Quantitative Relationship between Intracellular Lithocholic Acid, Chenodeoxycholic Acid and Toxicity in Sandwich-Cultured Hepatocytes; Incorporation into a Mechanistic Model of Drug-Induced Liver Injury	179
CHAPTER 7. Mechanistic Modeling of Drug-Induced Liver Injury Predicts Delayed Presentation and Species Differences in Bile Acid -Mediated Troglitazone Hepatotoxicity	211
CHAPTER 8. Summary and Future Directions	261
APPENDIX.....	287

LIST OF TABLES

Table 1.1. Physicochemical and pharmacokinetic properties of drugs with different mechanisms of cholestasis.	25
Table 1.2. Relationship between mechanism of cholestasis (impaired formation of bile and obstruction of bile flow) and the extent of metabolism and excretion, BDDCS, and BSEP inhibition for 77 cholestatic compounds.....	31
Table 1.3. Computational models of small molecule interactions with bile acid transporters.	32
Table 1.4. Computational models of PXR and FXR activation.	33
Table 2.1. Human hepatic influx transporter proteins.	74
Table 2.2. Human hepatic efflux transporter proteins.	76
Table 2.3. Summary of advantages and disadvantages of in vitro models used to study hepatobiliary drug transport.	78
Table 2.4. Summary of advantages and disadvantages of in vivo models used to study hepatobiliary drug transport.	81
Table 2.5. Preferred approaches to answer specific questions regarding hepatobiliary drug transport.	82
Table 3.1. Summary of parameter estimates based on the model scheme depicted in Figure 3.2 describing taurocholic acid (TCA) disposition in human and rat sandwich-cultured hepatocytes (SCH) without (Control) or with 10 μ M Troglitazone (+TGZ) pre-incubation.....	113
Table 4.1. Total Accumulation and BEI (mean \pm SEM) of probe substrates at MOI=5 vs. non infected control.	141
Table 6.1. Parameter values describing the relationship between hepatocellular lithocholic acid (LCA) and chenodeoxycholic acid (CDCA) concentrations, and intracellular ATP.	196
Table 7.1. Summary of troglitazone-mediated hepatotoxicity in human SimPops and clinical trials.	224
Table 7.2. List of parameters varied in the human and rat SimPops and results of multiple regression analysis in human SimPops administered 600 mg/day troglitazone (TGZ) for 6 months.	225

LIST OF FIGURES

Figure 1.1. Localization of bile acid transporters in human hepatocytes (A) and enterocytes (B).	34
Figure 1.2. Mechanisms of altered bile acid transport by cholestatic drugs.	35
Figure 2.1. In vivo architecture of polarized hepatocytes with distinct apical and basolateral domains facing respectively the bile canaliculus and bloodstream.	83
Figure 2.2. In vitro models and the related methods to study hepatobiliary drug transport.	84
Figure 3.1. Schemes depicting the uptake and efflux protocol.	114
Figure 3.2. Model schemes depicting the disposition of taurocholic acid (TCA) in sandwich-cultured hepatocytes (SCH) studies based on the experimental design depicted in Figure 3.1.	115
Figure 3.3. Taurocholic acid (TCA) mass versus time data in rat and human sandwich-cultured hepatocytes (SCH) in the absence (Control) or presence of 10 μ M troglitazone (TGZ) pre-incubation.	116
Figure 3.4. Inhibition of multidrug resistance-associated protein 4 (MRP4)-mediated transport of [3 H]dehydroepiandrosterone sulfate (DHEAS) by troglitazone sulfate (TS) in membrane vesicles from MRP4-overexpressing and control human embryonic kidney cells.	117
Figure 3.5. Impact of impaired function of canalicular and/or basolateral efflux transporters on hepatic TCA exposure.	118
Figure 3.6. Net effects of inhibition of uptake and efflux transporters on hepatic TCA exposure.	119
Figure 4.1. Efficient knockdown of Bcrp in WT and TR ⁻ rat SCH.	142
Figure 4.2. Effects of Bcrp knockdown on mean relative levels of Oatp1a1, Ntcp, Bsep, P gp, Mrp4, and Mrp2 proteins in WT and TR ⁻ rat SCH infected with Ad siNT Ad siBcrp.	143
Figure 4.3. Effects of non-targeted and targeted adenoviral infection in WT and TR ⁻ SCH at increasing MOI.	144
Figure 5.1. Proposed mechanism of troglitazone (TGZ)-mediated hepatotoxicity.	167
Figure 5.2. Intracellular accumulation of troglitazone (TGZ) and generated metabolites [TGZ sulfate (TS) and TGZ glucuronide (TG)] in WT and TR ⁻ rat SCH in the absence or presence of Bcrp Knockdown.	168
Figure 5.3. Accumulation of troglitazone (TGZ) and generated metabolites [TGZ sulfate (TS) and TGZ glucuronide (TG)] in the medium of WT and TR ⁻ rat SCH in the absence or presence of Bcrp Knockdown.	169
Figure 5.4. Recovery of troglitazone (TGZ) and generated metabolites [TGZ sulfate (TS), TGZ glucuronide (TG), and TGZ quinone (TQ)] in WT and TR ⁻ rat SCH in the absence or presence of Bcrp Knockdown.	170
Figure 5.5. Bsep-mediated transport of taurocholate (TC) and troglitazone sulfate (TS) in membrane vesicles.	171
Figure 5.6. Hepatobiliary disposition of troglitazone (TGZ) and generated metabolites [TGZ sulfate (TS) and TGZ glucuronide (TG)] in WT and TR ⁻ rat SCH in the absence or presence of GF120918.	172

Figure 5.7. Metabolism of troglitazone (TGZ) in S9 fraction prepared from liver tissues of WT and TR ⁻ rats.....	173
Figure 6.1. Schematic overview of the bile acid (BA) transport inhibition model in DILI _{sym} [®]	197
Figure 6.2. Toxicity and bile acid (BA) accumulation in lithocholic acid (LCA)-treated rat, human, mouse, and dog sandwich-cultured hepatocytes (SCH).....	198
Figure 6.3. Toxicity and bile acid (BA) accumulation in chenodeoxycholic acid (CDCA)-treated rat and human sandwich-cultured hepatocytes (SCH).	199
Figure 6.4. Relationship between intracellular lithocholic acid (LCA) and chenodeoxycholic acid (CDCA) concentrations and ATP.....	200
Figure 7.1. Schematic overview of the bile acid transport inhibition module in DILI _{sym}	227
Figure 7.2. Predicted and observed plasma concentration of troglitazone (TGZ) and TGZ sulfate (TS) in humans and rats.....	228
Figure 7.3. Simulated DILI responses in human and rat populations (SimPops) at specified troglitazone (TGZ) dose levels.	229
Figure 7.4. Simulated serum ALT and viable liver mass in susceptible individuals.	231
Figure 7.5. Sensitivity analysis of transporter inhibition constants.	232

CHAPTER 1. Introduction

An Updated Review on Drug-Induced Cholestasis: Mechanisms and Investigation of Physicochemical Properties and Pharmacokinetic Parameters¹

INTRODUCTION

The liver is the major organ responsible for the metabolism and excretion of endogenous and exogenous compounds, including drugs. The liver is predisposed to drug toxicity because of its anatomical location and the expression of uptake transporters that facilitate accumulation of drugs in hepatocytes. Drug-induced liver injury (DILI) is the most common cause of acute liver failure (1), and is one of the primary reasons for the failure of pharmaceutical agents during drug development.

Unfortunately, current *in vitro* screening approaches or *in vivo* preclinical studies do not adequately predict the likelihood of DILI. Even Phase III clinical trials that involve a few thousand patients often fail to detect DILI. In some cases, instances of severe liver injury and death only were observed after drug approval and administration to tens or hundreds of thousands of patients. These unexpected findings led to blackbox warnings, or in severe cases, withdrawal of the drug from the market. Recent examples include troglitazone and bromfenac (withdrawn), and bosentan and diclofenac (blackbox warnings).

DILI is classified into hepatocellular, mixed, or cholestatic injury based on the major underlying mechanism (2). Among 784 DILI cases reviewed by the Swedish adverse drug reactions advisory committee between 1970 and 2004, almost one-half of the cases had either cholestatic or mixed cholestatic hepatic toxicity (3). Acute cholestatic injury comprised approximately 16% of all hepatic

¹This chapter has been published in *Journal of Pharmaceutical Sciences*, and is presented in the style of that Journal: *J Pharm Sci* 2013 Sep;102(9):3037-57.

adverse drug reactions in a Danish study of 1100 DILI cases from 1978 to 1987 (4). In the United States, drugs were responsible for approximately 20% of cases of jaundice in the elderly population (5). However, reported reactions are thought to be only a small fraction of all the instances of drug-related cholestasis in the community because drug-induced cholestasis can present with asymptomatic disease where the only clinical manifestation is an elevation in liver enzymes, which often is not detected or reported. Therefore, the actual number of cases and medical costs associated with drug-induced cholestasis could exceed what has either been reported or estimated. In the present paper, the clinical presentation and mechanisms of bile-acid mediated drug-induced cholestasis are reviewed. In addition, we investigated whether the physicochemical properties or pharmacokinetic parameters of selected drugs, or the ability of these compounds to inhibit BSEP, influenced the type of cholestatic liver injury (impaired bile formation vs. obstruction of bile flow). Furthermore, existing *in silico* models developed to predict drug effects on bile acid transporters and nuclear receptors that are involved in bile acid homeostasis are reviewed.

CLINICAL FEATURES OF DRUG-INDUCED CHOLESTASIS

Diagnosis

Biochemical tests (liver function tests) typically are used to define drug-induced cholestasis. The Council of International Organizations of Medical Sciences (CIOMS) defines cholestatic injury as an elevation of serum alkaline phosphatase (AP) to greater than 2x the upper limit of normal (ULN) combined with a major elevation of γ -glutamyl transpeptidase (GGT) in the presence of a normal alanine transaminase (ALT) value. Alternatively, cholestasis is thought to be present when there is an increase in both ALT and AP, but with an ALT/AP ratio of < 2 . In severe cases of cholestasis, an increase in serum conjugated bilirubin also is observed. Mixed hepatocellular/cholestatic injury is defined as an ALT/AP ratio of 2 – 5, whereas hepatocellular injury is defined as $ALT > 2x ULN$ or $ALT/AP \geq 5$ (6). An accurate diagnosis of DILI also requires careful causality assessment, interpretation of clinical features and

laboratory tests including liver biopsy findings, if available, and the exclusion of other potential causes for liver injury.

Clinical Presentation

Drug-induced cholestasis may present as an acute illness that promptly diminishes after withdrawal of the offending drug. Drug-induced cholestasis may present with or without jaundice, and symptoms may occur weeks or months after the start of treatment. Nonspecific symptoms such as nausea, malaise, anorexia, and fatigue may be elicited due to parenchymal liver injury. For some drugs (e.g., amoxicillin-clavulanate, erythromycin), abdominal pain or discomfort has been reported (7). Chronic drug-induced cholestasis can result in the development of xanthomas, pruritus, and melanoderma. Symptoms often resolve following withdrawal of the offending drug, but in some cases, if there is significant loss of the interlobular bile ducts, chronic liver disease may develop and even progress to liver failure (8). Rarely, drugs can induce cholelithiasis (gall stones) or mimic large duct sclerosing cholangitis, resulting in extrahepatic obstruction (9). Drug-induced cholestasis can be classified into the following categories:

Acute Drug-Induced Cholestasis without Hepatitis (Bland Cholestasis): This is a rare type of drug-induced cholestasis that typically is produced by estrogens or anabolic steroids, and manifests histologically as pure canalicular cholestasis. Bland cholestasis causes abnormal biliary secretions without hepatocellular damage.

Acute Drug-Induced Cholestasis with Hepatitis (Cholestatic Hepatitis): This type of drug-induced cholestasis is associated with concomitant hepatic parenchymal damage. Cholestatic hepatitis is characterized by portal inflammation and varying degrees of hepatocyte injury and necrosis.

Acute Drug-Induced Cholestasis with Bile Duct Injury: This type of drug-induced cholestasis involves bile duct injury (ductular, cholangiolar, or cholangiolytic) but minimal parenchymal liver cell injury.

Chronic Drug-Induced Cholangiopathies: These drug-induced cholestatic disorders vary from mild, nonspecific bile duct injury (mild elevation in AP or GGT) to vanishing bile duct syndrome (VBDS), sclerosing cholangitis, and cholelithiasis (10).

PHYSIOLOGY OF BILE ACID HOMEOSTASIS

Cholestasis may occur if there is impaired formation of bile or if there is a physical obstruction to the flow of bile after it has been secreted from hepatocytes. To understand the pathogenesis of cholestasis, it is important to understand the physiological principles involved in bile flow.

Synthesis and Conjugation

Primary bile acids are synthesized from cholesterol in hepatocytes. Approximately 16 enzymes are involved in this process; the rate limiting step is 7 α -hydroxylation by Cytochrome P450 7A1 (CYP7A1) (11, 12). Chenodeoxycholic acid (CDCA) and cholic acid (CA) are the most common primary bile acids in humans while rodents have high levels of muricholic acid (MCA) and hyocholic acid (HCA). Secondary bile acids are formed by gut bacteria-mediated dehydroxylation of primary bile acids. The most common secondary bile acids include lithocholic acid (LCA) and deoxycholic acid (DCA), which are formed by 7-dehydroxylation of CDCA and CA, respectively. Bile acids are conjugated extensively with glycine or taurine in the liver, and more than 98% of bile acids excreted from the liver are amidated. Bile acids also may undergo sulfation or glucuronidation. Conjugated bile acids are more water soluble and therefore, are excreted more readily into feces and urine. Bile acid synthesis has been comprehensively reviewed elsewhere (11, 13).

Hepatobiliary Transport

Bile acids undergo vectorial transport from sinusoidal blood across the basolateral membranes into hepatocytes, and across the canalicular membranes into bile. Bile acids are taken up from the sinusoidal blood into hepatocytes by the uptake transport proteins sodium taurocholate cotransporting polypeptide (NTCP) and organic anion transporting polypeptides (OATPs) (Figure 1A). NTCP is responsible for sodium-dependent bile acid uptake, while sodium-independent transport is mediated by

OATPs. The efficiency of hepatic uptake varies depending on the bile acid structure: trihydroxy > dihydroxy bile acids, and conjugated > unconjugated bile acids (14). Individual bile acids may use different uptake transporters. The uptake of conjugated bile acids such as taurocholic acid (TCA) is mediated predominantly (>75%) by sodium-dependent NTCP. In contrast, sodium-dependent uptake accounts for less than half of the uptake of unconjugated bile acids (15-18). Within hepatocytes, bile acids are translocated by diffusion or undergo carrier-mediated transport after binding to cytosolic proteins such as glutathione S-transferases, liver fatty acid binding protein (L-FABP), and dehydrogenases (19). Vesicular transport of bile acids has been suggested, but confocal microscopy studies of fluorescent bile acid analogs in hepatocyte couplets showed no intracellular vesicular structure containing bile acids (20). However, characteristics and intracellular disposition of fluorescent bile acid analogs may differ between individual bile acids, and the significance of vesicular transport of bile acids in hepatocytes remains to be investigated. At the canalicular membrane, bile acids are excreted into bile predominantly via the bile salt export pump (BSEP) in an ATP-dependent manner (Figure 1A). Multidrug resistance-associated protein (MRP) 2, which is the main driving force for bile salt-independent bile flow through canalicular excretion of reduced glutathione, also transports glucuronide and sulfate conjugates of bile acids (21). The osmotic forces that are generated by bile acid secretion, coupled with the coordinated contraction of the actin filaments that surround the canaliculus, generate the pressure necessary to force bile to flow down the bile duct. The biliary tract itself is composed of a network of small to large ducts that are lined by cholangiocytes (bile duct epithelial cells). Cholangiocytes also express ion and organic anion transporters on the apical [i.e. apical sodium-dependent bile salt transporter (ASBT), OATP1A2] and basolateral [i.e. organic solute transporter (OST) α/β , MRP3] membranes that modify the composition of bile before it passes into the larger bile ducts (21-23). In humans, bile acids enter the gallbladder where they are stored and expelled into the duodenum in response to hormonal signals such as cholecystokinin. In addition to canalicular excretion, hepatocytes also are capable of effluxing bile acids across the basolateral membrane into sinusoidal blood via MRP3, MRP4, and a recently identified heteromeric organic solute transporter, OST α -OST β (Figure 1A). Human MRP3 and rat Mrp3 transported glycocholic acid (GCA) and

tauro lithocholate 3-sulfate (TLC-S), whereas TCA was transported to a significant degree only by rat Mrp3 (24). Unconjugated (CA, DCA) and conjugated bile acids [TCA, GCA, taurochenodeoxycholic acid (TCDCa), glycochenodeoxycholic acid (GCDCa)] were transported by MRP4 in the presence of glutathione with higher affinity than MRP3 (25), suggesting that MRP4 may play an important role in basolateral efflux of bile acids in humans. OST α -OST β transports glycine and taurine conjugated bile acid species by facilitated diffusion; OST α -OST β mediates cellular efflux or uptake depending on the electrochemical gradient (26, 27). The contribution of basolateral efflux to overall hepatic bile acid excretion is small under normal conditions, but expression of these transporters is up-regulated under cholestatic conditions as an important part of adaptive response to serve as a compensatory route of bile acid excretion (28-32). Assem et al. reported that Mrp4 and sulfotransferase (Sult) 2a1 are both upregulated during cholestasis suggesting that increased sulfation and hepatic basolateral efflux of sulfated bile acids leads to increased renal excretion as a compensatory excretion route (33). In healthy humans, the proportion of sulfated bile acids in the serum is less than 2% of bile acids, and the amount of total bile acids excreted in urine is minimal, whereas in patients with hepatobiliary/cholestatic disease, urinary excretion of bile acids increased more than 100-fold, with 25 – 80% of urinary bile acids excreted in the sulfated form (34). These studies demonstrate that sulfation and glucuronidation of bile acids are important detoxification pathways; conjugation increases the hydrophilicity of bile acids and, in most cases, decreases the toxicity and facilitates the urinary excretion of bile acids.

Intestinal Transport

Bile acids undergo efficient enterohepatic recirculation. The bile acid pool size is only about 2 – 3 g in humans, but 12 – 18 g of bile acids are secreted into bile per day because the pool recycles several times after each meal (35). Just a small fraction of the bile acid pool is lost in the feces (0.2 – 0.6 g/day), and about 0.3 g/day of bile acids are synthesized in hepatocytes to replace the portion that is excreted (35). In the intestinal lumen, taurine- or glycine-conjugated bile acids are de-conjugated by gut bacteria. Bile acids are reabsorbed by ASBT in the terminal ileum (Figure 1B) or by passive diffusion (36). From the enterocyte, bile acids enter the mesenteric blood via basolateral transport proteins such as MRP3 and

OST α -OST β (Figure 1B) (16, 23, 37-41), and return to the liver in portal blood followed by efficient uptake by hepatocyte transporters, as described above. It has been reported that MRP4 is expressed in the basolateral membrane of Caco-2 cells (42), but its expression and contribution to basolateral transport of bile acids in enterocytes remain to be investigated. Sulfate-conjugates of bile acids are not deconjugated readily and only a limited amount of sulfated bile acids are re-absorbed (34). Bile acids that are not absorbed from the colon are eliminated in the feces; fecal elimination is balanced by biosynthesis from cholesterol in the liver.

Bile Acid Toxicity

Bile acids are required for the digestion and absorption of fats and fat-soluble vitamins and they facilitate the excretion of bile pigments, cholesterol, and other medium-sized molecules by micellar solubilization. Bile acids induce biliary lipid secretion and solubilize cholesterol in bile, thereby promoting cholesterol elimination. Bile acids are potent activators of nuclear receptors such as farnesoid-X receptor (FXR) and pregnane X receptor (PXR), and they play an important role in the regulation of lipid homeostasis (43, 44).

However, bile acids can be cytotoxic when present in abnormally high concentrations in hepatocytes. Therefore, defects in bile acid excretion may lead to cholestasis. Defects in hepatocytes (especially at the canalicular membrane), altered fluidity of bile, impaired contraction of the actin filaments in the pericanalicular region, and changes in bile duct patency can reduce bile flow. Importantly, drugs also can affect bile flow at one or more of these steps, which will be discussed in more detail in the following sections. Bile acid toxicity is thought to be highly correlated with hydrophobicity; more hydrophobic bile acids are more cytotoxic. The rank order of bile acid cytotoxicity, from greatest to least is: LCA > CDCA, DCA > CA > ursodeoxycholic acid (UDCA) (45). Under normal conditions, it is likely that the unbound concentration of bile acids in the cytosol of hepatocytes is low because bile acids are highly bound to cytosolic proteins. However, if hepatic concentrations exceed the binding capacity of the cytosolic proteins, unbound bile acid concentrations would be expected to increase markedly. Accumulation of bile acids in hepatocytes leads to mitochondrial damage and ultimately to apoptosis or

necrosis (46, 47). LCA has been shown to induce biliary tract injury; oral administration of LCA to mice resulted in cholangitis (48).

MECHANISMS OF DRUG-INDUCED CHOLESTASIS

Cholestatic drugs may disrupt bile acid homeostasis by direct inhibition of bile acid transport (Figure 2A), or by indirect processes, which may include regulation of transporter localization (Figure 2B) or expression (Figure 2C). In the following section, the physiological mechanisms of drug-induced cholestasis that are associated with altered bile acid homeostasis are reviewed.

Role of hepatic transport proteins in drug-induced cholestasis

Hepatic biliary and basolateral transport proteins regulate the physiologic/pathophysiologic effects of endogenous compounds such as bile acids as well as exogenous compounds. Increasing evidence supports the hypothesis that drug-mediated functional disturbances in hepatic bile acid transporters can lead to intracellular accumulation of potentially harmful bile acids and subsequent development of cholestatic hepatocyte damage. In an effort to avoid drug-induced cholestasis, an *in vitro* test for BSEP inhibition during drug development may prove beneficial to screen for hepatotoxic compounds. However, bile acid-drug interactions are more complicated. The intracellular accumulation of bile acids is dependent upon both uptake and efflux (basolateral and canalicular) processes. Furthermore, the sensitivity of each transport protein to administered drugs may differ. Thus, to predict the hepatic exposure to bile acids, inhibitory effects of drugs on each transport protein, as well as drug concentrations at the site of interaction should be considered when translating *in vitro* data to *in vivo*. For the inhibition of uptake transporters, systemic concentrations of drugs are important, whereas intracellular drug concentrations are important when considering the inhibitory effects of drugs on bile acid efflux. However, measurement of intracellular hepatocyte drug concentrations is challenging, and these data typically are not available, particularly in humans. Additionally, most major human bile acids are >80% bound to plasma proteins (49), so it is likely that bile acids are highly bound to cytosolic proteins in

hepatocytes; total as well as unbound intracellular bile acid concentrations may be important in predicting drug-bile acid interactions.

Several transport proteins have been identified as potential loci for drug-induced cholestasis. These include the basolateral uptake transporters (NTCP and OATPs), canalicular efflux transporters (BSEP, MRP2, and MDR3), and basolateral efflux transporters (MRP3 and MRP4). The potential role(s) of each of these transport proteins in drug-induced cholestasis will be discussed in detail in the following paragraphs.

Hepatic Canalicular Efflux Transport Proteins. The rate-limiting step in bile formation is transport of biliary constituents across the canalicular membrane. This process is mediated predominantly by **BSEP**, a hepatic transport protein that is a member of the ATP-binding cassette (ABC) gene superfamily. Impaired BSEP function due to defects in gene coding or gene regulation can lead to inherited and acquired cholestatic disorders such as progressive familial intra-hepatic cholestasis type 2 (PFIC2), benign recurrent intrahepatic cholestasis type 2 (BRIC2), and intrahepatic cholestasis of pregnancy (50-52). Many drugs that cause either cholestatic or mixed hepatocellular/cholestatic liver injury (e.g., troglitazone, bosentan, cyclosporine, rifampin, sulindac, and glibenclamide) inhibit BSEP/Bsep-mediated biliary excretion of bile acids, potentially leading to increased hepatic exposure to cytotoxic bile acids (53-58). Two recent studies that systematically compared the potency of BSEP inhibition between cholestatic and non-cholestatic drugs revealed that drugs that caused cholestatic/mixed DILI in humans exhibited a markedly higher incidence and potency of BSEP inhibition compared to drugs that were non-cholestatic or caused hepatocellular liver damage (59, 60). In these studies, the inhibitory effects of test compounds on TCA uptake into inside-out membrane vesicles prepared from insect cells over-expressing BSEP/Bsep were investigated, and BSEP inhibition was demonstrated to be one of the risk factors for drug-induced cholestasis. These studies also showed a close correlation between inhibition potency for human BSEP- and rat Bsep-mediated TCA transport (59, 60). In most of the BSEP inhibition studies, including the above studies, TCA was used as a model bile acid. However, Kis et al. showed that troglitazone and glibenclamide inhibited the BSEP/Bsep-mediated transport of different bile

acids (TCA, GCA, TCDCA, and GCDCA) with similar potencies (IC_{50}), whereas cyclosporine A exhibited a 10-fold more potent inhibition of GCA and TCDCA transport compared to TCA and GCDCA (57). Thus, extrapolation of the results of transport inhibition from one bile acid to another may not be accurate. Also, one should note that membrane vesicles do not express metabolizing enzymes, thus inhibitory effects of metabolites cannot be detected unless the metabolite(s) are tested directly.

Whereas most of the BSEP inhibitors directly *cis*-inhibit BSEP, estradiol 17 β -glucuronide and progesterone metabolites indirectly *trans*-inhibit Bsep after secretion into the bile canaliculus by **Mrp2** (61). Bosentan stimulated Mrp2-dependent bilirubin excretion and bile salt-independent bile flow, while phospholipid and cholesterol secretion were markedly inhibited and uncoupled from bile salt secretion (62). Inhibition of biliary lipid secretion was not observed in Mrp2-deficient TR⁻ rats, which suggested that translocation of organic anions across the canalicular membrane is a prerequisite for the occurrence of the uncoupling effect (62).

MDR3, an ATP-dependent phospholipid flippase, translocates phosphatidylcholine from the inner to the outer leaflet of the canalicular membrane (63). Subsequently, canalicular phospholipids are solubilized by canalicular bile salts to form mixed micelles, thereby protecting cholangiocytes from the detergent properties of bile salts. Mutations in MDR3 result in impaired biliary excretion of phosphatidylcholine and cause PFIC3, a severe pediatric liver disease that usually requires liver transplantation (64). Yoshikado et al. noted that two patients with itraconazole-induced cholestatic liver injury exhibited markedly high serum itraconazole concentrations (65). In itraconazole-treated rats, biliary phospholipids, rather than bile acids, were markedly decreased compared to control rats (65). Itraconazole decreased MDR3-mediated efflux of phosphatidylcholine in MDR3-overexpressing cells, but did not alter BSEP-mediated TCA transport (65). These results suggest that inhibition of MDR3-mediated biliary phospholipid secretion can be a risk factor for drug-induced cholestasis even if bile acid excretion is not altered. *In vitro*, MDR3 transported verapamil and cyclosporine, which could potentially lead to competitive inhibition of phospholipid flippase activity and cholestatic injury (66).

Hepatic Basolateral Efflux Transport Proteins. As described above, BSEP inhibition is a risk factor for drug-induced cholestasis. However, not all drugs that inhibit BSEP cause cholestasis. This suggests that screening for BSEP inhibition alone cannot accurately predict the hepatotoxic potential of drugs. This might be due to compensatory mechanisms of bile acid transport. The basolateral efflux transporters, **MRP3** and **MRP4**, play a minor role in bile acid efflux under normal conditions, but they are up-regulated under cholestatic conditions to compensate for impaired biliary excretion (67-72). Compensatory basolateral efflux prevents hepatic bile acid accumulation and enables subsequent renal elimination of bile acids. Thus, impaired function of MRP3 and MRP4 by drugs, or genetic polymorphisms resulting in reduced-function variants may result in accumulation of toxic bile acids in hepatocytes. Troglitazone sulfate (TS), a major metabolite of troglitazone and a potent BSEP inhibitor, also inhibits MRP4-mediated dehydroepiandrosterone (DHEAS) transport; potent inhibition of both canalicular and basolateral efflux of bile acids by TS may predispose hepatocytes to toxicity (73). Our group has investigated the inhibitory effects of 88 compounds on MRP3 and MRP4, and reported that MRP4 inhibition was associated with an increased risk of cholestatic potential for drugs that are not BSEP inhibitors (74, 75). These results suggest that MRP4 inhibition also may represent a risk factor for the development of cholestatic DILI in humans.

Hepatic Uptake Transport Proteins. Basolateral uptake transporters are important in controlling hepatic and systemic exposure to drugs and toxins. The hepatic accumulation of bile acids is regulated by both uptake and efflux (basolateral and canalicular) processes, thus inhibition of hepatic bile acid uptake may exert protective effects by preventing the hepatic accumulation of bile acids. Bosentan, a potent inhibitor of human BSEP and rat Bsep, caused hepatic injury in humans, but bosentan-treated rats did not develop hepatotoxicity (54). Species difference in bosentan-induced hepatotoxicity might be explained by differential inhibition of human NTCP and rat Ntcp. Bosentan was a more potent inhibitor of sodium-dependent TCA uptake in rat ($IC_{50} = 5.4 \mu M$) than human ($IC_{50} = 30 \mu M$) suspended hepatocytes, resulting in less hepatocyte accumulation of TCA in rats after administration of bosentan (76). Drugs also may exert differential inhibitory effects on individual bile acids. Marion et al. reported that troglitazone

differentially affected the uptake and accumulation of CDCA species (CDCA and metabolites) compared with TCA in rat SCH, causing an intracellular increase in CDCA species but not TCA (18). Troglitazone inhibited both uptake and biliary excretion of TCA in rat and human hepatocytes, leading to unchanged or even decreased intracellular accumulation (18, 77-79). Hepatic accumulation of CDCA species was not altered after incubation with 10 μ M troglitazone, but was significantly increased with 100 μ M troglitazone suggesting that biliary excretion of CDCA species was inhibited to a greater extent than uptake processes by higher concentrations of troglitazone. CDCA is more abundant in humans, and is known to be more cytotoxic compared to TCA (80, 81). These results suggest that one should consider species differences as well as differential inhibitory effects of drugs on individual bile acids when predicting hepatotoxicity in humans.

Role of intestinal transport proteins in drug-induced cholestasis

Bile acid concentrations in enterocytes are important in the bile acid regulatory loop. Once activated by bile acids, intestinal FXR induces an intestinal hormone, fibroblast growth factor 19 (FGF19; or Fgf15 in mice), which migrates to the liver and activates hepatic FGF receptor 4 (FGFR4) signaling to inhibit hepatic bile acid synthesis (13). Activation of hepatic FXR also down-regulates bile acid synthesis by activation of small heterodimer partner (SHP) (13). In ASBT null mice, which were unable to absorb bile acids in the ileum, intestinal and hepatic FXR activity was impaired resulting in decreased Fgf15 and Shp in the ileum and liver, respectively (82). Because Fgf15 and Shp play important roles in the regulatory feedback loop of bile acid synthesis, mRNA levels of Cyp7a1 and bile acid synthesis were increased in ASBT null mice compared to wild-type mice (82). Similarly, inhibition of bile acid absorption in the intestine by ASBT inhibitors or bile acid sequestrants interrupted the normal feedback inhibition of bile acid synthesis, leading to increased hepatic Cyp7a1 expression and bile acid synthesis (82). On the other hand, inhibition of basolateral bile acid transport in enterocytes of OST α null mice increased intestinal Fgf15 expression and decreased bile acid synthesis in hepatocytes (40). Interruption of bile acid absorption by surgical procedures (i.e. partial external biliary diversion, partial ileal bypass) or bile acid sequestrants (i.e. cholestyramine, cholestipol) have been used to treat cholestasis and/or

pruritus (83-85). Bile acid sequestrants are non-digestible resins that bind to intestinal bile acids and form an insoluble complex, reducing absorption of bile acids. They are used to treat primary hypercholesterolemia, and also as a second-line treatment for pruritus in patients with incomplete biliary obstruction. ASBT inhibitors have been investigated to treat hypercholesterolaemia, but the effects on cholestatic liver disease have not been evaluated fully. Reduced absorption of bile acids through the enterohepatic circulation may have therapeutic effects in certain types of cholestatic liver disease, but effects on the feedback loop of bile acid synthesis also must be considered.

Indirect Interactions: Effects on Expression/Activity/Localization of Transport Proteins and Enzymes Involved in Bile Acid Homeostasis

Due to the critical physiological and pathophysiological role of bile acids, homeostasis is tightly regulated through multiple nuclear receptors including FXR, the retinoid-X receptor (RXR), the liver receptor homologue-1 (LRH-1), the constitutive androstane receptor (CAR) and the liver-X-receptor (LXR), as well as the cell surface bile acid receptors including the G-protein coupled receptor TGR5. In addition, bile acid transporters undergo post-transcriptional regulation including insertion/retrieval of transporters into/from the plasma membrane. These mechanisms allow fine tuning of bile acid synthesis and transport and, under normal physiological conditions, maintain enterohepatic circulation and regulate intracellular concentrations of bile acids through repression of bile acid synthesis, induction of bile acid metabolism (e.g. induction of phase I and II hydroxylation, sulfation and conjugation) as well as inhibition of hepatic bile acid uptake, and stimulation of bile acid efflux. The importance of nuclear receptors in the adaptive response to bile acids has been demonstrated in numerous knockout rodent models. For example, PXR or CAR knockout mice are more susceptible to cholestatic liver injury than wild-type mice (31, 86, 87). Nuclear receptor-mediated adaptive changes are likely caused by compounds normally excreted into bile (e.g. bile acids, hormones, drugs, or bilirubin) that are retained during cholestasis and act as nuclear receptor ligands (88, 89).

Drugs that act as nuclear receptor activators (e.g. rifampicin, dexamethasone) can increase the clearance of other drugs or induce the formation of reactive metabolites that can cause hepatotoxicity. For

example, acetaminophen liver toxicity was exacerbated by increased phase I-mediated oxidation to the reactive metabolite N-acetyl-p-benzoquinone-imine by CYP inducers (90, 91).

Several anticholestatic compounds such as UDCA, phenobarbital, and rifampicin are nuclear receptor agonists, which could explain their anticholestatic properties. In recent years, FXR agonists have been proposed as a treatment for cholestatic liver disease because they repress bile acid uptake and synthesis, and promote bile acid excretion by activation of canalicular bile acid transporters. However, the utility of FXR agonists in the treatment of cholestasis might depend on the type of cholestasis, and changes in the expression of transport proteins that are induced. For conditions that are characterized by bile duct destruction such as primary biliary cirrhosis (PBC) or primary sclerosing cholangitis (PSC), stimulation of canalicular bile acid excretion may worsen liver injury. Interestingly, FXR knockout mice but not wild-type mice adapted to bile duct obstruction by increasing expression of Mrp4 mRNA and were protected from liver injury after ligation of the common bile duct (92). It was suggested that FXR acts as a negative regulator of the basolateral bile acid transport protein MRP4, whose increased expression normally protects the liver from accumulation of potentially toxic bile acids through basolateral efflux and subsequent renal elimination. FXR competes with CAR for binding at the MRP4 promoter and represses MRP4 induction by CAR activation; activation of FXR could impair the MRP4-mediated basolateral efflux of bile acids (93). Because of this, FXR antagonists might be beneficial in certain types of cholestasis (e.g. total biliary obstruction) where increased renal bile acid excretion is desired. For more detail about FXR and PXR and their role as potential targets for cholestasis, see the review of Jonker et al (43).

Estrogen-induced cholestasis. While decreased expression or impaired function of transport proteins can contribute to or cause cholestasis, most changes in transport protein expression observed in cholestatic patients or animal models represent compensatory mechanisms providing alternate routes of excretion in response to the retention of bile acids. There are only a few examples where changes in transport protein expression or localization (as opposed to inhibition) due to drug treatment or other cholestatic agents, such as hormones and proinflammatory cytokines, are the **primary** cause of

cholestasis. The most prominent example of this type of cholestasis is estrogen- and C17-alkylated steroid-induced cholestasis, which causes a clinical picture that is similar to intrahepatic cholestasis of pregnancy in susceptible women who use oral contraceptives or postmenopausal estrogen replacement therapy. Estrogen-induced cholestasis can be induced experimentally in rodents with estradiol-17 β -D-glucuronide (E₂17G) or the synthetic estrogen ethinylestradiol (94, 95). Although trans-inhibition of BSEP-mediated bile acid transport by E₂17G has been demonstrated (61), the internalization of Bsep and Mrp2, which impairs the excretory function within minutes by reducing the amount of protein in the canalicular membrane, appears to be a key mechanism of cholestasis (96-98). E₂17G activates classical, Ca²⁺-dependent protein kinase C and phosphoinositol 3-kinase signaling pathways, which are cooperatively involved in internalization and intracellular retention of Bsep/Mrp2 (99, 100). Furthermore, E₂17G activates the estrogen receptor α (ER α) in isolated perfused rat liver (101). This might explain why chemical inhibition or knock-down of ER α partially prevented decreased Bsep/Mrp2 activity and reduced transporter internalization (101). This finding is substantiated further by the observation that ER α (-/-) mice are resistant to ethinylestradiol-induced hepatotoxicity (102). At the moment, it is not quite clear how the activation of the ER α leads to internalization of transporter proteins. Recent data suggest that phosphoinositol 3-kinase is not directly involved in this process, and it was shown that activation of protein kinase C actually precedes activation of ER α , suggesting that other yet unknown mediators are involved (101). Interestingly, the upregulation of Mrp3 expression and activity in rat liver after administration of ethinylestradiol was independent of cholestasis and required the estrogen receptor (103).

Inflammation-induced cholestasis. Inflammation often contributes to liver injury during cholestasis. However, cholestasis also can be induced by inflammation itself. This phenomenon is common in patients with extrahepatic infections or inflammatory processes in which inflammatory cytokines or bacterial endotoxins lead to profound reductions in bile flow (104, 105). The prototypical example of inflammation-induced cholestasis is sepsis-associated cholestasis. Lipopolysaccharide (LPS), an endotoxin from the cell wall of gram-negative bacteria, is a potent causal agent in inflammation. LPS often is released at extrahepatic sites and cleared from the systemic circulation by Kupffer cells in the

liver, which respond by producing proinflammatory cytokines and/or nitric oxide (NO). These cytokines and NO activate membrane receptors and after intracellular signal transduction, they alter hepatic and renal transport protein expression and function.

Most of our knowledge about inflammation-induced changes in hepatic transport proteins is based on animal models; reduced expression of the bile acid uptake proteins Ntcp and Oatp, decreased expression of the canalicular bile acid efflux pumps Bsep and Mrp2, and downregulation of phase I and II metabolizing enzymes have been described. There is also some regulation through internalization of Bsep and/or Mrp2 from the canalicular membrane to intracellular vesicles (106, 107). However, the key factor appears to be translational regulation resulting in reduced mRNA transcription and hence protein synthesis. Interestingly, signal transduction of inflammatory cytokines targets regulatory transcription factors (e.g. through phosphorylation or decreased binding of nuclear transcription factors) resulting in reduced nuclear quantities and function of these nuclear receptors. This has, for example, been demonstrated for RXR α , an important heterodimerization partner for numerous nuclear receptors such as FXR, RAR, PXR and CAR, in response to LPS or IL-1 β treatment (108-110).

So far, only a few studies have investigated the effects of inflammation-induced cholestasis in human disease. In PBC and PSC, cholestasis develops with a substantial inflammatory component; decreased expression of NTCP, OATP1B1, MRP2, and BSEP have been reported, whereas MRP3, MRP4, and OST α/β expression were increased (30, 32, 111). Furthermore, in patients with advanced stage PBC, the canalicular localization of MRP2 was disrupted and the expression of the uptake transporters, OATP1B1, OATP1B3, and NTCP was decreased (112). In another study, an increase in the severity of inflammation and the fibrosis score in patients with viral hepatitis was associated with decreased hepatic MRP2, MDR1, and OATP1B1, but not MRP3, mRNA expression (113).

ASSESSMENT OF PHYSICOCHEMICAL PROPERTIES AND PHARMACOKINETIC PARAMETERS OF DRUGS WITH DIFFERENT MECHANISMS OF CHOLESTASIS

In previous sections, direct and indirect mechanisms of drug-induced cholestasis mediated by interruption of bile acid homeostasis were reviewed. Since multiple processes are involved in bile acid homeostasis, an accurate prediction of the cholestatic potential of drugs mediated by these pathways is not straightforward. Several studies have investigated risk factors for the development of drug-induced cholestasis based on the drugs' inhibitory effects on BSEP and physicochemical properties and pharmacokinetic parameters (59, 60). In this type of analysis, it is critical to establish well-defined phenotypes (i.e. cholestasis). In general, there are two major mechanisms of drug-induced cholestasis: (1) impaired formation of bile due to drugs that interact with bile acid formation and/or hepatic bile acid transport (hepatic cholestasis), and (2) physical obstruction of bile flow after bile has been secreted from hepatocytes, which might be caused by drugs that damage the bile duct itself (ductular/ductal cholestasis). If cholestatic drugs with different mechanisms of cholestasis are all considered as one group, it may confound the study results and lead to inaccurate predictions of cholestatic potential. In the present investigation, we compared the physicochemical properties and pharmacokinetic parameters of 77 cholestatic drugs. The compounds selected for investigation included 50 drugs reported to cause cholestasis due to impaired bile acid formation (bland cholestasis or cholestatic hepatitis; classified into Group 1) and 27 drugs reported to cause cholestasis by obstruction of bile flow (classified into Group 2) (Table 1.1) (6, 114-117). Eleven drugs, including glyburide and carbamazepine, were reported to cause both impaired bile formation and obstruction of bile flow; these drugs were classified into Group 3 ("Mixed Cholestasis"; Table 1.1), and were not included in the statistical analysis (6, 114-117).

Relationship between Mechanism of Cholestasis and Physicochemical Properties of Drugs

To explore the relationship between the mechanism of cholestasis and physicochemical properties, we compared the molecular weight, lipophilicity, and solubility of the Group 1 and Group 2 cholestatic drugs. The physicochemical properties of the investigated compounds are summarized in Table 1.1; if experimentally determined logP and logS values were not available, then they were obtained

from Dragon Ver.5.5 (Talete SRL, Milano, Italy). The molecular weight distribution of these compounds ranged from 114.2 to 1202.8 g/mol. The median (range) molecular weights for Group 1 and Group 2 cholestatic drugs were 346.9 (114.2 – 1202.8) and 295.8 (136.1 – 814.1) g/mol, respectively. The log P value, which is an indicator of lipophilicity, varied from -1.8 to 8.6, with median (range) values of 2.6 (-1.4 – 8.6) and 2.3 (-1.8 – 5.1) for Group 1 and Group 2, respectively. The solubility, indicated by logS, ranged from -10.2 to 0.4, with median (range) values of -3.5 (-10.2 – 0.4) and -2.8 (-5.7 – -0.1) for Group 1 and Group 2, respectively. There were no statistically significant differences between drugs from these two different cholestatic groups with regard to any of the physicochemical properties discussed above.

Relationship between Mechanism of Cholestasis and Plasma Concentrations of Drugs

To explore the relationship between the mechanism of cholestasis and systemic exposure, we investigated the maximum plasma concentrations (C_{max}), maximum unbound plasma concentrations ($C_{max,u}$), and standard and maximum daily doses of the cholestatic drugs in humans. Information about C_{max} , standard and maximum daily doses were retrieved from Thompson's Micromedex DRUGDEX index, Lexicomp database, and PubMed. The $C_{max,u}$ was calculated for each drug using the C_{max} and experimentally determined plasma protein binding values available from published sources. If protein binding data were not available, estimated values were used (118); estimated and experimentally determined protein binding values were comparable for the drugs with available protein binding data. The C_{max} distribution ranged from 0.00004 to 492 $\mu\text{g/ml}$ (Table 1.1). The median (range) C_{max} values for Group 1 and Group 2 cholestatic drugs were 1.1 (0.00028 – 492) and 2.0 (0.004 – 150) $\mu\text{g/ml}$, respectively. $C_{max,u}$ values ranged from 0.00001 to 231.6 μM (Table 1.1), with median (range) values of 0.4 (0.00003 – 80.6) and 2.2 (0.0005 – 231.6) μM for Group 1 and Group 2, respectively. Plasma protein binding ranged from 0 to 99.8 %; median (range) values were 88 (0 – 99.8) and 90 (0.5 – 99) for Group 1 and Group 2, respectively. The median standard daily doses were 300 (4 – 6750) and 440 (1.3 – 6500) mg/day, whereas the maximum daily doses were 450 (8 – 12000) and 600 (15 – 12000) mg/day for Group 1 and Group 2, respectively. There were no significant differences in C_{max} , $C_{max,u}$, plasma protein binding,

standard daily doses or maximum daily doses between the two groups of cholestatic drugs, indicating that these values, by themselves, were not predictive of the mechanism of cholestasis.

Relationship between Mechanism of Cholestasis and the Metabolism and Excretion of Drugs

To explore the relationship between the mechanism of cholestasis and drug disposition, we investigated the extent of metabolism, renal excretion and biliary excretion of cholestatic drugs. Drugs were categorized as high, intermediate or low, if the extent of metabolism/excretion was $\geq 70\%$, between 30% and 70%, and $< 30\%$, respectively. The relationship between the mechanism of cholestasis and the biopharmaceutics drug disposition classification system (BDDCS) class also was investigated. The BDDCS categorizes drugs into four classes; class 1 represents drugs with high solubility and extensive metabolism, whereas class 2 drugs have low solubility and extensive metabolism. Drugs with high solubility and poor metabolism are categorized into class 3, and class 4 is composed of drugs with low solubility and poor metabolism (119). Information on metabolism, the routes of excretion, BDDCS class, and clinical parameters were retrieved from Thompson's Micromedex DRUGDEX index, Lexicomp database, PubMed, and WOMBAT-PK 2007 (120), and are presented in Table 1.1. Among the 50 cholestatic drugs categorized in Group 1, 26 (52%) drugs were classified as low with respect to the extent of metabolism. Among 27 cholestatic drugs categorized in Group 2, information about metabolism was available for 25 drugs; 60% (15 out of 25) of these were metabolized to a minimal extent. Drugs with low renal excretion accounted for 44% (22 out of 50) of Group 1 cholestatic drugs and 48% (13 out of 27) of Group 2 cholestatic drugs. Importantly, 64% (32 out of 50) of Group 1 and 78% (21 out of 27) of Group 2 cholestatic drugs were excreted extensively into bile ($\geq 70\%$). However, the classification of cholestatic drugs (Group 1 vs. 2) was not associated with the extent of metabolism or the extent of renal or biliary excretion when examined using the chi-square test (Table 1.2). Cholestatic drugs were categorized evenly as BDDCS class 1 – 3, with fewer drugs in BDDCS class 4. This is consistent with the previous report that only a small number of the approved drugs are categorized as BDDCS class 4 (119). There was no significant association between BDDCS class and the type of cholestasis when examined using the chi-square test (Table 1.2).

Relationship between Mechanism of Cholestasis and Inhibition of Bile Acid Transport Proteins by Drugs

Inhibition of bile acid transport is one important mechanism of drug-induced cholestasis. Thus, the relationship between the mechanism of cholestasis and the ability of drugs to inhibit bile acid transport was investigated. BSEP is a major transport protein responsible for the biliary excretion of bile acids. Inhibition data for BSEP is relatively abundant compared to inhibition of other bile acid transport proteins based on recent publications describing high-throughput screening approaches to analyze for BSEP inhibition (59, 60, 121). Information about BSEP inhibition was available for 41 cholestatic drugs (Table 1.1). Drugs with IC_{50} values less than 133 μ M were defined as BSEP inhibitors as reported previously (59). Chi-square analysis revealed that BSEP inhibitors are more abundant in Group 1 compared to Group 2 cholestatic drugs (61% vs 20%, $p=0.023$; Table 1.2); among the 31 Group 1 cholestatic drugs, 19 drugs (61%) were BSEP inhibitors. On the other hand, only 2 out of 10 Group 2 cholestatic drugs were BSEP inhibitors. Although this analysis was performed with only a limited number of drugs, the data suggest that BSEP inhibition might not play a major role in cholestasis that is caused by bile duct obstruction. Inhibition data for other bile acid transporters such as ASBT, NTCP, OATP and MRP4, as well as substrate information on major drug transporters such as OATP, MRP2, BCRP, and P-gp, might be necessary to understand the complex interplay of bile acid homeostasis, the pharmacokinetic behavior of drugs, and direct and indirect regulation of the pathogenesis of different types of cholestasis.

***IN SILICO* MODELING TO PREDICT DIRECT AND INDIRECT EFFECTS OF DRUGS ON BILE ACID HOMEOSTASIS**

Interruption of bile acid homeostasis plays a key role in the development of cholestasis. Therefore, in order to improve the prediction of cholestatic potential, it is important to understand how drugs affect bile acid disposition. However, for a large number of drugs, experimental data documenting an interaction with bile acid transporters are not available; high-throughput screening methods to test the inhibition potential of drugs have not been available until recently (59, 60, 122). Data regarding drug

effects on nuclear receptors involved in bile acid homeostasis are even more scarce because the role of nuclear receptors in bile acid homeostasis has been revealed only recently (123, 124). *In silico* modeling can be used to fill this data gap; existing datasets can be used to build *in silico* models based on the structural properties of drugs, and these models can be used to predict drug effects on bile acid homeostasis. When large datasets are available and resulting *in silico* models are well-validated, they can help reduce the financial burden in early drug discovery and development by limiting the need for extensive laboratory experiments. In the following section, *in silico* models to predict drug effects on bile acid transporters and nuclear receptors such as PXR and FXR are reviewed.

***In Silico* Modeling to Predict Drug Interactions with Bile Acid Transport Proteins**

The 3D structures of membrane transport proteins remain scarce. Thus, current computational transporter studies rely on a series of experimentally measured interactions of small molecules with membrane transporters and employ statistical learning approaches, such as quantitative structure-activity relationship (QSAR) and ligand-based pharmacophore construction. Available computational models of bile acid transporters (i.e., MRP2, MRP3, MRP4, BSEP, NTCP, ASBT, OATPs) are summarized in Table 1.3. Due to the great heterogeneity of experimental reports (e.g., from diverse assay types, test concentrations and experimental conditions), most of the computational studies present classification models (e.g., inhibitors vs. non-inhibitors). The few available quantitative models (such as for binding affinity or inhibition) usually are limited to small sets of compounds with the measurements from the same source.

For the canalicular efflux transporters BSEP and MRP2 (Table 1.3), Warner et al. reported classification of BSEP inhibitors (defined by an IC_{50} threshold of $300\mu\text{M}$) by a recursive partitioning QSAR for over 600 chemicals using molecular descriptors as covariates (121). An earlier study by Saito et al. reported a multiple linear regression model of BSEP inhibition (measured in % of taurocholate transport at $100\mu\text{M}$ test concentration) for 37 diverse drug-like compounds using chemical fragment descriptors, but this model has not been validated further (125). Several groups reported QSAR models

for MRP2 inhibition at various potency thresholds (Table 1.3) using linear (e.g., PLS – partial least squares regression and discriminant analysis) and non-linear modeling methods (SVM – Support Vector Machine, kNN – k Nearest Neighbors, RF – Random Forest) (126-128). The accuracy of these models on external data (judged by test sets) ranged from 70 to 90%. In addition, Ng et al. developed a QSAR model of binding affinity to rat Mrp2 for 25 methotrexate analogues as well as a pharmacophore for their binding model (129). Zhang et al. have constructed a pharmacophore for MRP2 inhibitors, which performed slightly worse than their SVM QSAR model (127).

Due to lack of experimental measurements, very few computational studies exist for the basolateral bile acid efflux transporters MRP3 and MRP4 (Table 1.3). Sedykh et al. reported classification models of MRP4 inhibitors at a 10 μ M threshold with external accuracy of 70%, however, the modeling was based on a rather small set of 64 molecules (128). In a recent study, Akanuma et al. attempted structural analysis of MRP4 transport for several groups of β -lactam antibiotics (130).

For the bile acid uptake transporters, there were appreciably more studies on ASBT and OATPs than on NTCP (Table 1.3), which reflects the importance of the former to the absorption, distribution, metabolism, excretion and toxicity of pharmaceuticals because they also are expressed in gut and kidney (131). Karlgren et al. reported classification models of OATP1B1, OATP1B3, and OATP2B1 inhibitors at a 20 μ M potency threshold, with expected accuracy of 75-93% (132). Several QSAR models of ASBT binding affinity as well as pharmacophores were developed by Zheng et al., Rais et al., and Gonzalez et al. with squared correlation coefficient (R^2) values of 0.68-0.89, albeit all were trained on small congeneric series of conjugated bile acid derivatives (133-137). Sedykh et al. and Zheng et al. reported classification QSARs of ASBT inhibitors based on 10 μ M and 100 μ M potency thresholds respectively (128, 133). In a recent study, Greupink et al. developed a 3D-pharmacophore model based on five NTCP substrates, which were then applied to screen large chemical libraries. Several NTCP inhibitors were identified among the top selected hits (138).

Based on the data presented in Table 1.3, the small size of the modeling data sets is the major limitation to accurate *in silico* prediction of drug interactions with bile acid transporters. Conformational flexibility of membrane transporters, their broad substrate specificity, as well as noisiness and limitations of experimental assays all require large and diverse sets of chemical structures for proper statistical learning. Large and diverse modeling sets also are necessary for the broad applicability of the resulting models, so that more structural classes of chemicals can be covered and reliably predicted. Presently, there are too few compounds with experimental data available for MRP3, MRP4 and NTCP transporters. Even though OST α/β is essential for bile acid transport, adequate data for *in silico* modeling is not yet available (27).

***In Silico* Models of Drug Interactions with the Nuclear Receptors, FXR and PXR**

A number of the resolved 3D protein structures of FXR and PXR are publicly available (e.g., 1OSH, 1OSV for FXR, 3R8D, 2QNV for PXR at www.pdb.org), which allows for application of modeling techniques such as docking and structure-based pharmacophore construction. However, accurate characterization of a drug-protein interaction by structure-based methods can be difficult, which is the case for PXR with its large and flexible pocket leading to promiscuous binding and poor docking results (139, 140). Therefore, statistical knowledge-inference methods, such as QSAR, are still applied widely. Currently available computational models of FXR and PXR are reviewed in Table 1.4. Although stand-alone docking yielded modest results (~60% accuracy), as demonstrated by Khandelwal et al., Kortagere et al., and Ekins et al., docking was used routinely to impute bound conformations of chemicals for the subsequent 3D-QSAR modeling studies (139, 141-144). Most of the classification models of PXR agonists have external accuracy in the 70-85% range (Table 1.4). A few quantitative models for the potency of PXR activation (measured as EC₅₀) also have been reported (139, 145), although it is important to note that these do not take into account the extent of activation (i.e., efficacy), which can vary substantially among the agonists.

Relatively few *in silico* studies are available for FXR activation, likely due to the limited availability of experimental data. Several quantitative models of FXR activation (Table 1.4) achieve

correlations in the 0.76-0.93 range (square of Pearson's correlation coefficient), albeit on rather small data sets. Recent studies by Shuster and Grinke employed a set of pharmacophores for classification of FXR agonists with accuracy of ~70% (146, 147). While diverse models for PXR activation currently are available (e.g., see the recent review by Kortagere et al.(140)) and further improvements are likely to be incremental, in the case of FXR, new models based on larger data samples definitely are needed for reliable use in drug design and risk assessment.

CONCLUSIONS AND FUTURE DIRECTIONS

Disruption of bile acid homeostasis is an important mechanism of drug-induced cholestasis. In order to accurately predict the cholestatic potential of drugs, an understanding of the molecule's effects on the many processes involved in bile acid homeostasis appears to be necessary. *In silico* modeling, which will diminish the time and resources required for laboratory experiments, is a promising approach to obtain this mechanistic information. Drugs may inhibit bile acid transporters directly, or alter the expression, function and/or localization of transporters by indirect interactions mediated by nuclear receptors and intracellular signaling pathways. In addition, patient-specific factors including genetic polymorphisms, underlying disease, and pregnancy may alter the function of bile acid transporters and predispose individuals to cholestasis. These data can be integrated and incorporated into mechanistic, mathematical models to improve predictions. Multi-scale modeling approaches incorporating both drug disposition and physiological processes (i.e. systems biology) is an exciting, emerging area. Recent efforts using mechanistic, mathematical modeling approaches have successfully predicted the hepatotoxicity induced by drugs such as acetaminophen and methapyrilene (148, 149). The same approach can be taken to predict drug-induced cholestatic injury, thereby allowing more accurate predictions during the early stages of drug development.

Table 1.1. Physicochemical and pharmacokinetic properties of drugs with different mechanisms of cholestasis.

Drug	MW	logP ^a	logS ^a	PPB ^a (%)	C _{max} ^b (µg/ml)	C _{max,u} ^c (uM)	Std Daily Dose ^{d,e} (mg /day)	Max Daily Dose ^d (mg/ day)	Meta- bolism ^f	Renal Excre- tion ^f	Fecal/ biliary Excre- tion ^f	BDD -CS ^g	BSEP Inhibi- tion ^h	IC ₅₀ for BSEP Inhibition (µM)
Group 1: Impaired Formation of Bile (n=50)														
6-Mercapto- purine	152.2	-0.4	-1.3	19.0	0.073	0.39	225	350	H	I	L	2	-	-
Acitretin	326.5	6.4	-6.7	99.0	0.42	0.013	37.5	75	I	I	I	2	Y	18(60)
Atorvastatin	540.7	5.7	-7.4	98.5	0.019	0.0005 ₃	45	80	H	L	H	2	-	-
Azithromycin	749.1	4.0	-1.3	28.5	0.40	0.38	875	1500	I	L	H	3	N	>1000 (121)
Bupropion	239.8	3.6	-2.9	84.0	0.14	0.093	300	450	H	H	L	1	N	>1000 (121)
Captopril	217.3	0.3	-0.1	27.5	0.93	3.1	234	450	I	H	L	3	-	-
Celecoxib	381.4	3.9	-4.9	97.0	1.2	0.091	400	600	H	I	I	2	-	-
Cephalexin	347.4	-0.7	-1.5	12.5	32	81	2500	4000	L	H	L	3	-	-
Cetirizine	388.9	1.7	-3.6	93.0	0.31	0.056	7.5	10	L	H	L	3	-	-
Chlorambucil	304.2	3.3	-1.4	99.0	492	16	15.0	28	H	I	L	1	-	-
Clarithro- mycin	748.1	3.2	-2.6	50.5	3.7	2.4	1000	1500	H	I	L	3	Y	<13(121)
Cyclosporine	1203	3.0	-5.2	93.7	0.93	0.049	525	1260	H	L	H	2	Y	0.3-10 (59, 60, 121, 150- 152)
Danazol	337.5	0.5	-5.6	96.2*	0.025	0.0028	450	800	H	L	I	2	Y	<10 (121)
Dapsone	248.3	1.0	-3.1	75.3	0.93	0.93	175	300	H	H	L	2	N	>1000 (60, 121)
Dextro- methorphan	271.4	3.6	-1.3	74.8*	0.0077	0.0071	120	180	H	H	L	1	-	-
Dicloxacillin	470.4	2.9	-5.1	96.9	91	6.0	1750	2000	L	I	I	3	Y	<10(121), 70(60)

Fenofibrate	360.9	5.3	-5.7	99.0	4.4	0.12	100	160	I	I	L	2	Y	15(59)
Fosinopril	563.7	6.3	-4.4	94.4	0.37	0.037	22.5	40	I	I	I	2	Y	<13(121)
Gabapentin	171.3	-1.1	-1.2	1.5	2.5	14	2700	3600	L	H	L	3	N	>1000 (121)
Gemcitabine	263.2	-1.4	-1.2	6.4	7.0	25	1912.5	2125	H	H	L	1	-	-
Glimepiride	490.7	3.5	-5.6	99.5	0.55	0.0056	4.5	8	I	I	I	2	Y	<10(121), 16(59)
Griseofulvin	352.8	2.2	-4.6	83.8*	1.6	0.73	540	750	H	I	I	2	-	-
Hydrochloro- thiazides	297.8	-0.1	-2.7	67.9	0.49	0.53	56.25	100	L	H	L	3	-	-
Isoniazid	137.2	-0.8	0.0	5.0	11	73	300	300	H	H	L	1	N	>1000 (60, 121)
Itraconazole	705.7	5.7	-8.9	99.0	2.0	0.028	450	800	H	I	L	2	Y	18(59) 2.9-65 (59, 60, 121, 153)
Ketoconazole	531.5	4.4	-4.9	99.0	3.5	0.066	700	1200	I	L	I	2	Y	
Loracarbef	349.8	0.5	-0.9	25.0	13	27	500	800	L	H	L	3	-	-
Mesalamine	153.2	1.2	-2.2	43.0	5.0	19	3600	4800	H	L	H	2	N	381(121)
Metformin	129.2	-0.5	0.0	2.5	1.0	7.5	1250	2550	L	H	L	3	N	>1000 (121)
Methimazole	114.2	-0.3	0.4	0.0	0.21	1.9	37.5	60	H	H	L	1	N	>1000 (60, 121)
Methyldopa	211.2	0.4	-1.3	20.0	3.1	12	1750	3000	I	H	L	3	N	>1000 (60)
Metolazone	365.9	2.5	-3.8	95.0	22	3.1	10.25	20	L	H	L	4	-	-
Nevirapine	266.3	1.8	-3.4	60.0	2.3	3.4	300	400	H	H	L	2	N	295(121)
Nifedipine	346.4	2.2	-4.8	96.0	0.094	0.011	45	180	H	H	L	2	Y	19-40 (60, 121, 154)
Nitro- furantoin	238.2	-0.1	-3.1	60.0	0.50	0.84	300	400	I	I	L	4	N	>1000 (60, 121)
Norfloxacin	319.4	-1.0	-2.6	12.5	2.4	6.6	800	800	L	I	L	4	-	-
Ofloxacin	361.4	-0.4	-2.0	22.5	2.8	5.9	700	800	L	H	L	3	N	>1000 (121)

Orlistat	495.8	8.6	-10.2*	99.0	0.10	0.0020	270	360	L	L	H	4	-	-
Oxacillin	401.5	2.4	-4.5	92.0	43	8.6	6750	12000	I	H	L	3	-	-
Propafenone	341.5	3.2	-3.6	96.0	0.00028	0.000032	675	900	H	I	I	2	Y	54(121)
Propyl-thiouracil	170.3	0.4	-2.2	80.0	6.5	7.6	500	900	H	I	L	1	-	-
Repaglinide	452.7	5.9	-5.9*	98.0	0.051	0.0023	8.5	16	H	L	H	2	-	-
Risperidone	410.5	3.0	-3.2	89.0	0.033	0.0088	8.5	16	H	H	L	1	Y	<10(121)
Rofecoxib	314.4	3.2	-3.5	87.0	0.32	0.13	31.25	50	H	H	L	2	Y	95(121)
Rosiglitazone	357.5	2.4	-4.0	99.8	0.37	0.0021	4	8	I	I	L	1	Y	4.4-6.4 (56, 57, 118)
Roxithromycin	837.2	2.8	-3.9	86.0	12	2.0	387.5	600	I	L	I	4	-	-
Tamoxifen	371.6	7.1	-6.3	99.0	0.060	0.0016	30	40	H	L	I	1	Y	10-23 (121, 150, 153)
Ticlopidine	263.8	2.9	0.0	98.0	2.1	0.16	500	500	I	I	L	1	Y	27-74 (60, 121)
Troglitazone	441.6	3.6	-5.9*	99.0	2.8	0.064	400	600	H	L	H	4	Y	4-66 (121, 153, 154)
Warfarin	308.4	2.6	-4.2	99.5	1.5	0.026	6	10	H	H	L	2	Y	115(121)
Group 2: Obstruction of Bile Flow (n=27)														
Ajmaline	326.5	1.8	-2.8	46.0	1.5	2.4	42.5	50	H	L	H	1.5	-	-
Allopurinol	136.1	-0.6	-2.4	0.5	1.9	14	450	800	H	H	L	2	-	-
Amineptine	337.5	5.1*	-4.7*	95.3*	0.77	0.11	150	200	-	H	L	-	-	-
Amitriptyline	277.4	4.9	-4.5	94.8	0.029	0.0054	187.5	300	H	I	L	1	-	-
Ampicillin	349.5	1.4	-1.7	24.0	107	232	6500	12000	L	H	L	3	-	-
Carmustine	214.1	1.5	-1.8	80.0	1.7	1.6	297.5	340	I	I	L	1	N.D.	97(121), >1000 (60)

Chloro-thiazide	295.8	-0.2	-2.8	50.0	0.50	0.85	750	1000	L	H	L	4	-	-
Cimetidine	252.4	0.4	-1.6	17.5	1.1	3.7	800	1600	I	I	L	3	N	>1000 (121, 153)
Ciprofloxacin	331.4	0.3	-3.3	30.0	3.8	8.0	1000	1500	I	H	L	4	N	>1000 (121)
Clindamycin	425.1	2.2	-1.1	93.0	4.5	0.73	1600	2600	H	L	H	1	-	-
Cromolyn	468.4	1.9	-0.4	69.5	0.0092	0.0060	440	800	L	L	H	3	N	>1000 (57, 118)
Cypro-heptadine	287.4	4.7	-1.9	90.1*	30	10	12	20	H	I	I	1	-	-
Diazepam	284.8	2.8	-3.7	96.8	0.17	0.019	22	40	H	H	L	1	-	-
D-penicillamine	149.2	-1.8	-0.1	80.6	5.6	7.3	187.5	4000	L	H	L	3	N	>1000 (60)
Floxuridine	246.2	-1.4	-1.3	7.7*	3.3	12	24.5	42	H	L	L	-	-	-
Haloperidol	375.9	4.3	-4.0	92.0	0.020	0.0043	1.25	15	H	H	L	2	Y	23(121) >790 (121, 154), 599(60)
Ibuprofen	206.3	4.0	-3.7	99.0	57	2.8	1000	3200	H	H	L	2	N	
Imipramine	280.5	4.8	-4.2	92.0	0.025	0.0070	162.5	300	H	H	L	1	-	-
Methyl-testosterone	302.5	3.5*	-4.8*	98.0	0.032	0.0021	30	50	H	H	L	2	-	-
Phenyl-butazone	308.4	3.2	-2.6	98.5	150	7.3	450	600	I	I	L	1	-	-
Phenytoin	252.3	2.5	-4.1	90.0*	5.5	2.2	450	600	H	L	H	2	-	-
Prochlor-perazine	374.0	4.9	-3.6	95.2*	0.0040	0.0005 1	27.5	40	H	L	H	1	Y	<10(121)
Tenoxicam	337.4	1.9	-2.6	98.5	2.0	0.089	30	40	I	I	L	1	-	-
Tetracycline	444.5	-1.3	-2.4	65.0	9.3	7.3	1125	2000	L	I	L	3	N	>1000 (121)
Thiaben-dazole	201.3	2.5	-3.6	74.6*	5.0	6.3	3000	3000	H	H	L	2	N	560(121)
Tolbutamide	270.4	2.3	-3.4	96.0	100	14.8	1125	3000	H	H	L	2	N	>1000 (57, 118)

Troleandomycin	814.1	4.2*	-5.7*	61.6*	2.0	0.94	1500	2000	-	I	L	-	-	-
Group 3: Mixed Cholestasis (n=11)														
Azathioprine	277.3	0.1	-1.4	30.0	1.0	2.5	192.5	350	H	H	L	1	N	>1000 (57, 118)
Carbamazepine	236.3	2.5	-3.0	74.0	12	13	1000	1600	H	H	L	2	N	>1000 (121) 31-91
Chlorpromazine	318.9	5.4	-5.0	97.5	0.30	0.024	400	2000	H	I	L	1	N.D.	(121, 153), 148(60)
Chlorpropamide	276.8	1.9	-2.1	92.0	150	43	300	750	L	H	L	0	N	>1000 (57, 118) >983
Erythromycin	734.1	3.1	-2.5	60.0	1.3	0.72	1000	1000	L	L	H	3	N.D.	(121), 4.1- 13 (59, 60)
Estradiol	272.4	4.0	-3.5	93.5*	0.0000 43	0.0000 1	15.5	30	H	H	L	1	-	-
Flucloxacillin	453.9	2.6	-5.8*	94.0	8.0	1.1	3500	6000	L	H	L	4	N.D.	<10(121), 209(60) 5.3-60
Glyburide	494.1	4.7	-5.1	99.0	0.22	0.0045	10.6	20	H	I	I	2	Y	(57, 118, 152-154)
Pioglitazone	356.5	2.3	-4.6*	99.0	1.1	0.029	22.5	45	H	L	H	2	Y	0.3 (56, 57, 118)
Propoxyphene	339.5	4.2	-4.3	78.0	0.085	0.055	325	390	H	L	H	2	-	-
Terbinafine	291.5	6.0	-6.4*	99.0	1.0	0.034	625	1000	H	H	L	2	-	-

MW, molecular weight; PPB, plasma protein binding; BDDCS, biopharmaceutics drug disposition classification system;

^aObtained from Dragon Ver.5.5, measured data if not stated otherwise (*calculated).

^bRetrieved from Thompson's Micromedex DRUGDEX index and Lexicomp database if not stated otherwise.

^cCalculated using C_{max} , MW, and PPB.

^dRetrieved from Thompson's Micromedex DRUGDEX index and Lexicomp database. Administered orally if not stated otherwise.

^eIf a dose range was recommended (e.g. for different indications), the average of minimum and maximum recommended daily dose was calculated.

If dosing was given as mg/kg or mg/m², the maximum and average doses were calculated based on a 70 kg adult with a body surface area of 1.7.

^rThe extent of metabolism, renal excretion, and fecal/biliary excretion. H, High ($\geq 70\%$); I, Intermediate ($\geq 30\%$ and $< 70\%$); L, Low ($< 30\%$). Retrieved from Thompson's Micromedex DRUGDEX index and Lexicomp database if not stated otherwise.

^sClass 1, high solubility/extensive metabolism; class 2, low solubility/extensive metabolism; class 3, high solubility/poor metabolism; class 4, low solubility/poor metabolism.

^hDrugs with $IC_{50} < 133 \mu M$ are defined as BSEP inhibitors.(59)

ⁱN.D: Inhibitory effects of chlorpromazine, erythromycin, flucloxacillin, and carmustin were not determined because reported IC_{50} values of these drugs spanned the cutoff value of $133 \mu M$.

Table 1.2. Relationship between mechanism of cholestasis (impaired formation of bile and obstruction of bile flow) and the extent of metabolism and excretion, BDDCS, and BSEP inhibition for 77 cholestatic compounds.

Drugs with no information were excluded from the analysis. P-values from chi-square tests are presented.

Metabolism (n=75)^a			
	Group 1 (Impaired formation of bile)	Group 2 (Obstruction of bile flow)	P-value
High	11	5	0.7881
Intermediate	13	5	
Low	26	15	
Renal Excretion (n=77)^a			
	Group 1 (Impaired formation of bile)	Group 2 (Obstruction of bile flow)	P-value
High	11	6	0.9186
Intermediate	17	8	
Low	22	13	
Biliary Excretion (n=77)^a			
	Group 1 (Impaired formation of bile)	Group 2 (Obstruction of bile flow)	P-value
High	32	21	0.1065
Intermediate	11	1	
Low	7	5	
BDDCS (n=73)^b			
	Group 1 (Impaired formation of bile)	Group 2 (Obstruction of bile flow)	P-value
Class I	20	7	0.503
Class II	13	5	
Class III	11	9	
Class IV	6	2	
BSEP Inhibition (n=41)^c			
	Group 1 (Impaired formation of bile)	Group 2 (Obstruction of bile flow)	P-value
Yes	19	2	0.023
No	12	8	

^aHigh ($\geq 70\%$); Intermediate ($\geq 30\%$ and $< 70\%$); Low ($< 30\%$)

^bClass 1, high solubility/extensive metabolism; class 2, low solubility/extensive metabolism; class 3, high solubility/poor metabolism; class 4, low solubility/poor metabolism.

^cDrugs with $IC_{50} < 133 \mu M$ are defined as BSEP inhibitors.

Table 1.3. Computational models of small molecule interactions with bile acid transporters.

Transporter	Model description	External Accuracy ^a	Data size ^b (train/test)	Reference
BSEP	%inhibition at 100 μ M	R ² =0.95	37/0	Saito et al 2009(125)
BSEP	Classification of inhibitors at 300 μ M	87%	437/187	Warner et al 2012(121)
MRP2	Binding affinity, K _i	R ² =0.82	20/5	Ng et al 2005(129)
MRP2	Classification of inhibitors at 80 μ M	72%	79/39	Pedersen et al 2008(126, 127)
MRP2	Classification of inhibitors	74-77%	257/61	Zhang et al 2009(127)
MRP2	Classification of substrates	87%	150/38	Sedykh et al 2013(128)
MRP2	Classification of inhibitors at 10 μ M	89%	77/19	Sedykh et al 2013(128)
MRP3	Classification of substrates	98%	50/12	Sedykh et al 2013(128)
MRP4	Classification of substrates	92%	74/18	Sedykh et al 2013(128)
MRP4	Classification of inhibitors at 10 μ M	70%	51/13	Sedykh et al 2013(128)
ASBT	Binding affinity, K _i	R ² =0.73	29/1	Gonzalez et al 2009(137)
ASBT	Classification of inhibitors at 100 μ M	54-88%	38/19-30	Zheng et al 2009(133)
ASBT	Binding affinity, K _i	R ² =0.68	23/4	Zheng et al 2010(134)
ASBT	Binding affinity, K _i Transport constraints, K _m /V _{max}	R ² =0.89 R ² =0.68	32/1	Rais et al 2010(135, 136)
ASBT	Classification of substrates	93%	80/20	Sedykh et al 2013(128)
ASBT	Classification of inhibitors at 10 μ M	92%	120/30	Sedykh et al 2013(128)
NTCP	Ligand-based 3D pharmacophore	60%	5/10	Greupink et al 2012(138)
OATP1B1		81-93%	98/48	Karlgren et al 2012(132, 155)
OATP1B1	Classification of inhibitors at 20 μ M	79%	134/67	Karlgren et al 2012(132)
OATP1B3		92%	125/62	Karlgren et al 2012(132)
OATP2B1		75%	118/60	Karlgren et al 2012(132)
OATP2B1	Classification of inhibitors at 100 μ M	80%	109/27	Sedykh et al 2013(128)
OATP2B1	Classification of substrates	75%	42/11	Sedykh et al 2013(128)

^aAccuracy of the model when evaluated on external data (i.e., data not known to the model)

^bNumber of data points (i.e., distinct molecules) available for modeling

Table 1.4. Computational models of PXR and FXR activation.

Model description	External Accuracy ^a	Data size ^b (train/test)	Reference
<i>Pregnane X Receptor (PXR)</i>			
Classification of agonists at 100μM	73-87%	175/15	Ung et al 2007(156)
Classification of agonists at 100μM	63-67%	177/145	Khandelwal et al 2008(141)
Classification of agonists at 100μM	72-81%	168/130	Kortagere et al 2009(142)
Classification of agonists at 10μM Activation, EC ₅₀	77% R ² =0.45	95/20	Ekins et al 2009(139)
Classification of agonists (0.5nM – 38.3μM)	82-85%	316/315	Dybdahl et al 2012(157)
Classification of agonists at 100μM Activation, EC ₅₀	85% 78% R ² =0.45	405/29 586/50 273/33	Matter et al 2012(145)
<i>Farnesoid X Receptor (FXR)</i>			
Activation by non-steroidal agonists, EC ₅₀	R ² =0.76	82/20	Honorio et al 2005(143, 158)
Activation by non-steroidal agonists, EC ₅₀	R ² =0.77	77/20	Honorio et al 2007(143)
Activation by non-steroidal agonists, EC ₅₀	R ² =0.93	58/10	Zhang et al 2007(144)
Structure-Activity relationship analysis	-	50/0	Genet et al 2010(159)
Classification of agonists at 100μM by structure-based pharmacophores	73%	-/221	Shuster et al 2011(146) Grienke et al 2011(147)

^aAccuracy of the model when evaluated on external data (i.e., data not known to the model)

^bNumber of data points (i.e., distinct molecules) available for modeling

Figure 1.1. Localization of bile acid transporters in human hepatocytes (A) and enterocytes (B).

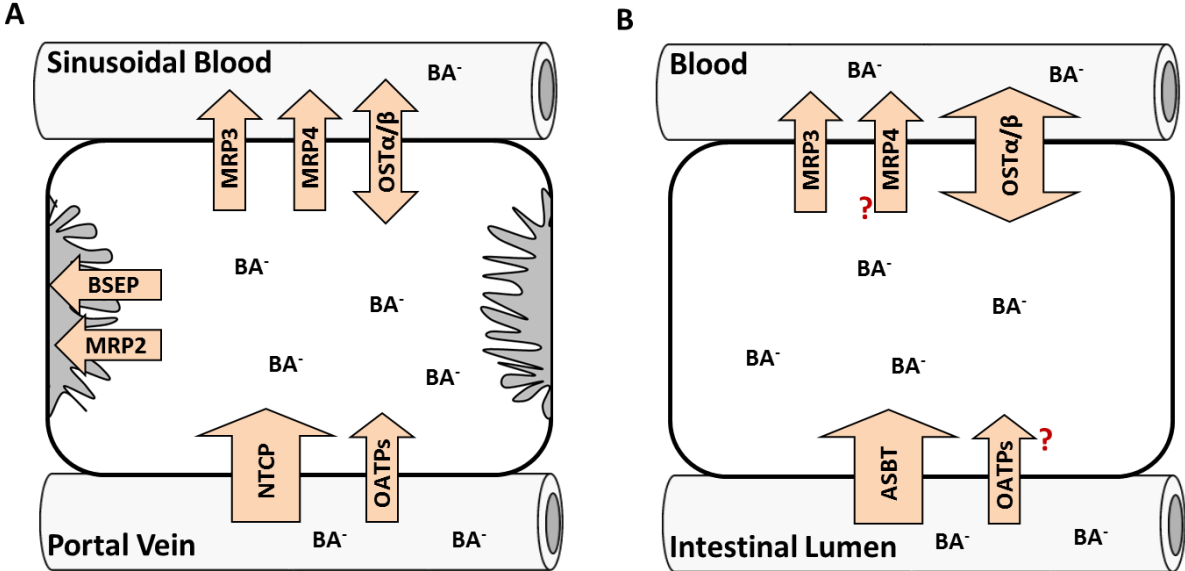
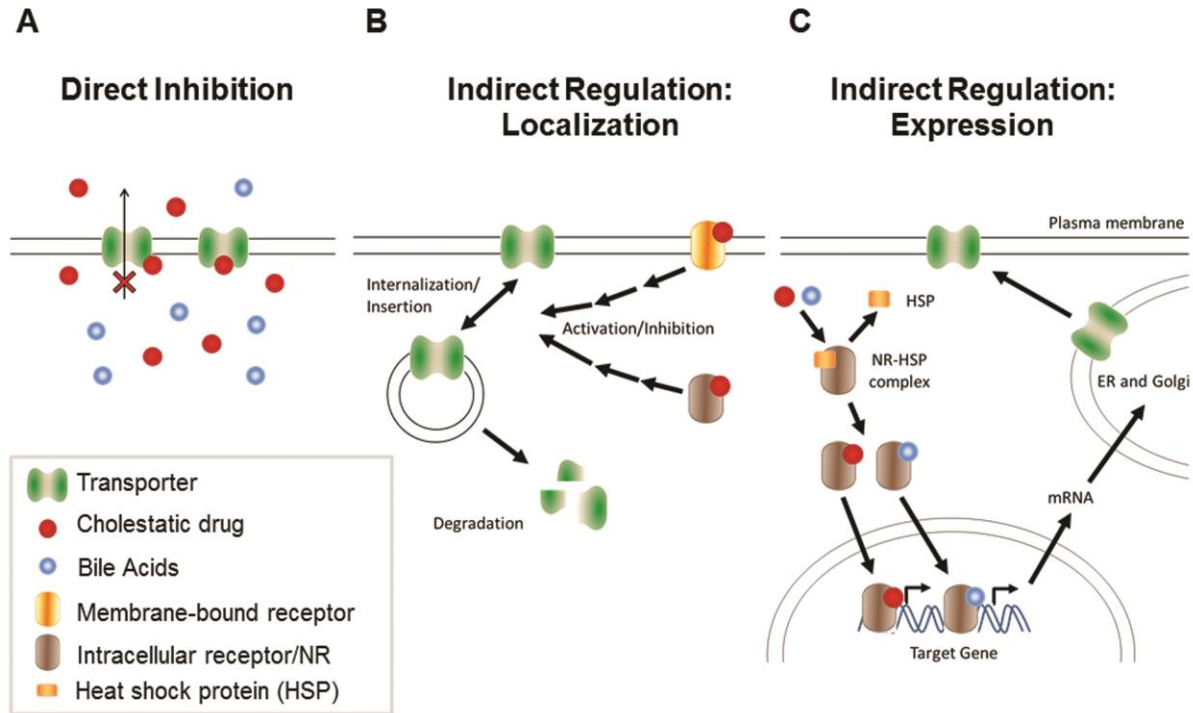


Figure 1.2. Mechanisms of altered bile acid transport by cholestatic drugs.

(A) Direct inhibition of transport proteins. Cholestatic drugs might directly interfere with bile acid transport through inhibition of transporter function. **(B) Altered localization of transport proteins.** Certain cholestatic drugs can activate membrane-bound and intracellular receptors resulting in activation or inhibition of intracellular signal transduction and increased insertion into or internalization from the plasma membrane. Internalized proteins can be degraded or undergo recycling to the plasma membrane. **(C) Altered transport protein expression.** Bile acids and certain cholestatic drugs are activators of nuclear receptors (NR). Binding of ligands results in dissociation of heat-shock proteins from the NR, homo-dimerization and subsequent translocation to the nucleus where they bind to response elements of target genes and activate gene transcription.



Project Rationale and Specific Aims

The objectives of this research project were to investigate the mechanisms of drug-induced liver injury (DILI) that involves transporter-mediated drug-bile acid interactions, and develop a novel strategy to reliably predict DILI liability of drugs in humans. This includes improving our understanding of species differences in bile acid disposition, specifically differential effects of transporter inhibitors on hepatic bile acid exposure in humans and rats, and impact of altered transport function on hepatic disposition of drugs. A mechanistic model that incorporates bile acid physiology and drug disposition was developed to translate data from in vitro systems to in vivo, and from preclinical species to humans, for the reliable prediction of human DILI. Troglitazone, an anti-diabetic drug withdrawn from worldwide markets due to severe DILI, was used as a model hepatotoxic drug. TGZ and its major metabolite, TGZ sulfate (TS) are potent inhibitors of multiple bile acid transporters. The experimental and analytical methods to study hepatic transporters are discussed in the next chapter (**Chapter 2**).

The first aim (**Aim #1**) of this dissertation research was to characterize the species differences in hepatobiliary disposition of taurocholic acid (TCA, a prototypical model bile acid) and its interaction with TGZ and TS using experimental data obtained in human and rat sandwich-cultured hepatocytes (SCH) combined with pharmacokinetic modeling and simulation (**Chapter 3**). The second objective (**Aim #2**) was to evaluate the impact of loss-of-function of canalicular transporters, which is a potential risk factor for DILI, on disposition of TS that is predominantly eliminated into bile. To this end, a novel in vitro model system, rat SCH lacking breast cancer resistance protein (Bcrp) and multidrug resistance-associated protein 2 (Mrp2), was established (**Chapter 4**), and altered disposition of TGZ and derived metabolites was evaluated (**Chapter 5**). Finally, a mechanistic, mathematical model was developed to improve our predictability of DILI caused by altered hepatobiliary disposition of bile acids (**Aim #3**). The quantitative relationship between the intracellular concentrations of bile acids and toxicity, which was critical for the model development, was determined in human and rat SCH, and incorporated into the mechanistic model (**Chapter 6**). This mechanistic model was used to assess the contribution of bile acid

transport inhibition associated with TGZ hepatotoxicity in humans and to investigate the mechanism(s) for differential hepatotoxicity of TGZ in humans and rats (**Chapter 7**).

Aim #1. Characterize the species differences in hepatobiliary disposition of taurocholic acid (TCA) and the influence of hepatic transport protein modulation by troglitazone (TGZ) and TGZ sulfate (TS) on TCA disposition.

Hypothesis: Species differences in hepatic disposition of bile acids may be responsible for poor predictability of human DILI using preclinical animals. Bile acid disposition data from human and rat SCH combined with pharmacokinetic (PK) modeling/simulations will provide insights regarding species differences in transporter-mediated drug-bile acid interactions.

- 1.a. Characterize the hepatobiliary disposition (basolateral uptake and efflux, canalicular efflux) of TCA and predict altered TCA disposition by functional modulation of transporters in human and rat SCH using PK modeling and simulation.
- 1.b. Determine the impact of TGZ and TS on the hepatobiliary disposition of TCA using human and rat SCH and isolated membrane vesicles.

Aim #2. Elucidate the mechanisms responsible for increased cellular accumulation of TS, which is a potential risk factor of TGZ-induced hepatotoxicity.

Hypothesis: TS, a potent bile acid transport inhibitor, is mainly excreted into bile via breast cancer resistance protein (Bcrp) and multidrug resistance-associated protein 2 (Mrp2). Impaired biliary transport (due to genetic polymorphisms, drug-drug interactions, and underlying disease) will increase hepatocellular exposure to TS and further inhibit bile acid transport, leading to hepatotoxicity in susceptible patients.

- 2.a. Establish an in vitro model system to evaluate the impact of loss-of-function of Bcrp and/or Mrp2 using SCH from WT and Mrp2-deficient (TR⁻) rats and RNA interference (RNAi).

- 2.b. Quantify the consequences of impaired function of Bcrp and/or Mrp2 on hepatocellular accumulation of TS using SCH from WT and TR⁻ rats, in the absence and presence of Bcrp knockdown.

Aim #3. Develop a mechanistic, mathematical model to predict DILI caused by altered hepatobiliary disposition of bile acids.

Hypothesis: A mechanistic, mathematical model incorporating dynamic interactions between drug(s) and the biological system will improve the understanding and the prediction of bile acid-mediated hepatotoxicity in humans.

- 3.a. Determine the quantitative relationship between the intracellular concentrations of bile acids [lithocholic acid (LCA) and chenodeoxycholic acid (CDCA)] and toxicity in human and rat SCH.
- 3.b. Develop a mechanistic, mathematical model to predict altered hepatic disposition of bile acids and subsequent hepatotoxicity using TGZ as a model hepatotoxic drug.

REFERENCES

- (1) Lee, W.M. Drug-induced hepatotoxicity. *N Engl J Med* **349**, 474-85 (2003).
- (2) Benichou, C. Criteria of drug-induced liver disorders. Report of an international consensus meeting. *J Hepatol* **11**, 272-6 (1990).
- (3) Bjornsson, E. & Olsson, R. Outcome and prognostic markers in severe drug-induced liver disease. *Hepatology* **42**, 481-9 (2005).
- (4) Friis, H. & Andreasen, P.B. Drug-induced hepatic injury: an analysis of 1100 cases reported to the Danish Committee on Adverse Drug Reactions between 1978 and 1987. *J Intern Med* **232**, 133-8 (1992).
- (5) Lewis, J.H. Drug-induced liver disease. *Med Clin North Am* **84**, 1275-311, x (2000).
- (6) Padda, M.S., Sanchez, M., Akhtar, A.J. & Boyer, J.L. Drug-induced cholestasis. *Hepatology* **53**, 1377-87 (2011).
- (7) Viteri, A.L., Greene, J.F., Jr. & Dyck, W.P. Erythromycin ethylsuccinate-induced cholestasis. *Gastroenterology* **76**, 1007-8 (1979).
- (8) Moradpour, D. *et al.* Chlorpromazine-induced vanishing bile duct syndrome leading to biliary cirrhosis. *Hepatology* **20**, 1437-41 (1994).
- (9) Erlinger, S. Drug-induced cholestasis. *J Hepatol* **26 Suppl 1**, 1-4 (1997).
- (10) Geubel, A.P., Sempoux, C. & Rahier, J. Bile duct disorders. *Clin Liver Dis* **7**, 295-309 (2003).
- (11) Russell, D.W. The enzymes, regulation, and genetics of bile acid synthesis. *Annu Rev Biochem* **72**, 137-74 (2003).
- (12) Norlin, M. & Wikvall, K. Enzymes in the conversion of cholesterol into bile acids. *Curr Mol Med* **7**, 199-218 (2007).
- (13) Chiang, J.Y. Bile acids: regulation of synthesis. *J Lipid Res* **50**, 1955-66 (2009).
- (14) Hofmann, A.F. *Bile Acids. In The Liver: Biology and pathobiology.* (Raven Press Limited.: New York, 1994).

- (15) Reichen, J. & Paumgartner, G. Uptake of bile acids by perfused rat liver. *Am J Physiol* **231**, 734-42 (1976).
- (16) Van Dyke, R.W., Stephens, J.E. & Scharschmidt, B.F. Bile acid transport in cultured rat hepatocytes. *Am J Physiol* **243**, G484-92 (1982).
- (17) Kouzuki, H., Suzuki, H., Ito, K., Ohashi, R. & Sugiyama, Y. Contribution of sodium taurocholate co-transporting polypeptide to the uptake of its possible substrates into rat hepatocytes. *J Pharmacol Exp Ther* **286**, 1043-50 (1998).
- (18) Marion, T.L., Perry, C.H., St Claire, R.L., 3rd, Yue, W. & Brouwer, K.L. Differential disposition of chenodeoxycholic acid versus taurocholic acid in response to acute troglitazone exposure in rat hepatocytes. *Toxicol Sci* **120**, 371-80 (2011).
- (19) Agellon, L.B. & Torchia, E.C. Intracellular transport of bile acids. *Biochim Biophys Acta* **1486**, 198-209 (2000).
- (20) El-Seaidy, A.Z., Mills, C.O., Elias, E. & Crawford, J.M. Lack of evidence for vesicle trafficking of fluorescent bile salts in rat hepatocyte couplets. *Am J Physiol* **272**, G298-309 (1997).
- (21) Pauli-Magnus, C. & Meier, P.J. Hepatobiliary transporters and drug-induced cholestasis. *Hepatology* **44**, 778-87 (2006).
- (22) Rost, D., Konig, J., Weiss, G., Klar, E., Stremmel, W. & Keppler, D. Expression and localization of the multidrug resistance proteins MRP2 and MRP3 in human gallbladder epithelia. *Gastroenterology* **121**, 1203-8 (2001).
- (23) Ballatori, N. *et al.* OSTalpha-OSTbeta: a major basolateral bile acid and steroid transporter in human intestinal, renal, and biliary epithelia. *Hepatology* **42**, 1270-9 (2005).
- (24) Akita, H., Suzuki, H., Hirohashi, T., Takikawa, H. & Sugiyama, Y. Transport activity of human MRP3 expressed in Sf9 cells: comparative studies with rat MRP3. *Pharm Res* **19**, 34-41 (2002).
- (25) Rius, M., Hummel-Eisenbeiss, J., Hofmann, A.F. & Keppler, D. Substrate specificity of human ABCC4 (MRP4)-mediated cotransport of bile acids and reduced glutathione. *Am J Physiol Gastrointest Liver Physiol* **290**, G640-9 (2006).
- (26) Ballatori, N. Biology of a novel organic solute and steroid transporter, OSTalpha-OSTbeta. *Exp Biol Med (Maywood)* **230**, 689-98 (2005).

- (27) Ballatori, N., Li, N., Fang, F., Boyer, J.L., Christian, W.V. & Hammond, C.L. OST alpha-OST beta: a key membrane transporter of bile acids and conjugated steroids. *Front Biosci* **14**, 2829-44 (2009).
- (28) Akita, H., Suzuki, H. & Sugiyama, Y. Sinusoidal efflux of taurocholate is enhanced in Mrp2-deficient rat liver. *Pharm Res* **18**, 1119-25 (2001).
- (29) Trauner, M., Wagner, M., Fickert, P. & Zollner, G. Molecular regulation of hepatobiliary transport systems: clinical implications for understanding and treating cholestasis. *J Clin Gastroenterol* **39**, S111-24 (2005).
- (30) Zollner, G. *et al.* Expression of bile acid synthesis and detoxification enzymes and the alternative bile acid efflux pump MRP4 in patients with primary biliary cirrhosis. *Liver Int* **27**, 920-9 (2007).
- (31) Teng, S. & Piquette-Miller, M. Hepatoprotective role of PXR activation and MRP3 in cholic acid-induced cholestasis. *Br J Pharmacol* **151**, 367-76 (2007).
- (32) Boyer, J.L. *et al.* Upregulation of a basolateral FXR-dependent bile acid efflux transporter OSTalpha-OSTbeta in cholestasis in humans and rodents. *Am J Physiol Gastrointest Liver Physiol* **290**, G1124-30 (2006).
- (33) Assem, M. *et al.* Interactions between hepatic Mrp4 and Sult2a as revealed by the constitutive androstane receptor and Mrp4 knockout mice. *J Biol Chem* **279**, 22250-7 (2004).
- (34) Alnouti, Y. Bile Acid sulfation: a pathway of bile acid elimination and detoxification. *Toxicol Sci* **108**, 225-46 (2009).
- (35) Hofmann, A.F. The continuing importance of bile acids in liver and intestinal disease. *Arch Intern Med* **159**, 2647-58 (1999).
- (36) Dietschy, J.M. Mechanisms for the intestinal absorption of bile acids. *J Lipid Res* **9**, 297-309 (1968).
- (37) Shneider, B.L. Intestinal bile acid transport: biology, physiology, and pathophysiology. *J Pediatr Gastroenterol Nutr* **32**, 407-17 (2001).
- (38) Hagenbuch, B. & Dawson, P. The sodium bile salt cotransport family SLC10. *Pflugers Arch* **447**, 566-70 (2004).

- (39) Dawson, P.A. *et al.* The heteromeric organic solute transporter alpha-beta, Ostalpha-Ostbeta, is an ileal basolateral bile acid transporter. *J Biol Chem* **280**, 6960-8 (2005).
- (40) Rao, A., Haywood, J., Craddock, A.L., Belinsky, M.G., Kruh, G.D. & Dawson, P.A. The organic solute transporter alpha-beta, Ostalpha-Ostbeta, is essential for intestinal bile acid transport and homeostasis. *Proc Natl Acad Sci U S A* **105**, 3891-6 (2008).
- (41) Trauner, M. & Boyer, J.L. Bile salt transporters: molecular characterization, function, and regulation. *Physiol Rev* **83**, 633-71 (2003).
- (42) Ming, X. & Thakker, D.R. Role of basolateral efflux transporter MRP4 in the intestinal absorption of the antiviral drug adefovir dipivoxil. *Biochem Pharmacol* **79**, 455-62 (2010).
- (43) Jonker, J.W., Liddle, C. & Downes, M. FXR and PXR: potential therapeutic targets in cholestasis. *J Steroid Biochem Mol Biol* **130**, 147-58 (2012).
- (44) Claudel, T., Staels, B. & Kuipers, F. The Farnesoid X receptor: a molecular link between bile acid and lipid and glucose metabolism. *Arterioscler Thromb Vasc Biol* **25**, 2020-30 (2005).
- (45) Perez, M.J. & Briz, O. Bile-acid-induced cell injury and protection. *World J Gastroenterol* **15**, 1677-89 (2009).
- (46) Rodrigues, C.M., Fan, G., Ma, X., Kren, B.T. & Steer, C.J. A novel role for ursodeoxycholic acid in inhibiting apoptosis by modulating mitochondrial membrane perturbation. *J Clin Invest* **101**, 2790-9 (1998).
- (47) Roberts, L.R. *et al.* Cathepsin B contributes to bile salt-induced apoptosis of rat hepatocytes. *Gastroenterology* **113**, 1714-26 (1997).
- (48) Fickert, P. *et al.* Lithocholic acid feeding induces segmental bile duct obstruction and destructive cholangitis in mice. *Am J Pathol* **168**, 410-22 (2006).
- (49) Salvioli, G., Lugli, R., Pradelli, J.M. & Gigliotti, G. Bile acid binding in plasma: the importance of lipoproteins. *FEBS Lett* **187**, 272-6 (1985).
- (50) Davit-Spraul, A., Gonzales, E., Baussan, C. & Jacquemin, E. Progressive familial intrahepatic cholestasis. *Orphanet J Rare Dis* **4**, 1 (2009).
- (51) Dixon, P.H. *et al.* Contribution of variant alleles of ABCB11 to susceptibility to intrahepatic cholestasis of pregnancy. *Gut* **58**, 537-44 (2009).

- (52) Kagawa, T. *et al.* Phenotypic differences in PFIC2 and BRIC2 correlate with protein stability of mutant Bsep and impaired taurocholate secretion in MDCK II cells. *Am J Physiol Gastrointest Liver Physiol* **294**, G58-67 (2008).
- (53) Lee, J.K., Paine, M.F. & Brouwer, K.L. Sulindac and its metabolites inhibit multiple transport proteins in rat and human hepatocytes. *J Pharmacol Exp Ther* **334**, 410-8 (2010).
- (54) Fattinger, K. *et al.* The endothelin antagonist bosentan inhibits the canalicular bile salt export pump: a potential mechanism for hepatic adverse reactions. *Clin Pharmacol Ther* **69**, 223-31 (2001).
- (55) Bohme, M., Muller, M., Leier, I., Jedlitschky, G. & Keppler, D. Cholestasis caused by inhibition of the adenosine triphosphate-dependent bile salt transport in rat liver. *Gastroenterology* **107**, 255-65 (1994).
- (56) Funk, C. *et al.* Troglitazone-induced intrahepatic cholestasis by an interference with the hepatobiliary export of bile acids in male and female rats. Correlation with the gender difference in troglitazone sulfate formation and the inhibition of the canalicular bile salt export pump (Bsep) by troglitazone and troglitazone sulfate. *Toxicology* **167**, 83-98 (2001).
- (57) Kis, E., Ioja, E., Nagy, T., Szente, L., Heredi-Szabo, K. & Krajcsi, P. Effect of membrane cholesterol on BSEP/Bsep activity: species specificity studies for substrates and inhibitors. *Drug Metab Dispos* **37**, 1878-86 (2009).
- (58) Mano, Y., Usui, T. & Kamimura, H. Effects of bosentan, an endothelin receptor antagonist, on bile salt export pump and multidrug resistance-associated protein 2. *Biopharm Drug Dispos* **28**, 13-8 (2007).
- (59) Morgan, R.E. *et al.* Interference with bile salt export pump function is a susceptibility factor for human liver injury in drug development. *Toxicol Sci* **118**, 485-500 (2010).
- (60) Dawson, S., Stahl, S., Paul, N., Barber, J. & Kenna, J.G. In vitro inhibition of the bile salt export pump correlates with risk of cholestatic drug-induced liver injury in humans. *Drug Metab Dispos* **40**, 130-8 (2012).
- (61) Stieger, B., Fattinger, K., Madon, J., Kullak-Ublick, G.A. & Meier, P.J. Drug- and estrogen-induced cholestasis through inhibition of the hepatocellular bile salt export pump (Bsep) of rat liver. *Gastroenterology* **118**, 422-30 (2000).
- (62) Fouassier, L. *et al.* Contribution of mrp2 in alterations of canalicular bile formation by the endothelin antagonist bosentan. *J Hepatol* **37**, 184-91 (2002).

- (63) van Erpecum, K.J. Biliary lipids, water and cholesterol gallstones. *Biol Cell* **97**, 815-22 (2005).
- (64) Gonzales, E., Davit-Spraul, A., Baussan, C., Buffet, C., Maurice, M. & Jacquemin, E. Liver diseases related to MDR3 (ABCB4) gene deficiency. *Front Biosci* **14**, 4242-56 (2009).
- (65) Yoshikado, T. *et al.* Itraconazole-induced cholestasis: involvement of the inhibition of bile canalicular phospholipid translocator MDR3/ABCB4. *Mol Pharmacol* **79**, 241-50 (2011).
- (66) Smith, A.J. *et al.* MDR3 P-glycoprotein, a phosphatidylcholine translocase, transports several cytotoxic drugs and directly interacts with drugs as judged by interference with nucleotide trapping. *J Biol Chem* **275**, 23530-9 (2000).
- (67) Denk, G.U., Soroka, C.J., Takeyama, Y., Chen, W.S., Schuetz, J.D. & Boyer, J.L. Multidrug resistance-associated protein 4 is up-regulated in liver but down-regulated in kidney in obstructive cholestasis in the rat. *J Hepatol* **40**, 585-91 (2004).
- (68) Wang, R., Sheps, J.A. & Ling, V. ABC transporters, bile acids, and inflammatory stress in liver cancer. *Curr Pharm Biotechnol* **12**, 636-46 (2011).
- (69) Keitel, V. *et al.* Expression and localization of hepatobiliary transport proteins in progressive familial intrahepatic cholestasis. *Hepatology* **41**, 1160-72 (2005).
- (70) Chai, J. *et al.* Changes of organic anion transporter MRP4 and related nuclear receptors in human obstructive cholestasis. *J Gastrointest Surg* **15**, 996-1004 (2011).
- (71) Soroka, C.J., Lee, J.M., Azzaroli, F. & Boyer, J.L. Cellular localization and up-regulation of multidrug resistance-associated protein 3 in hepatocytes and cholangiocytes during obstructive cholestasis in rat liver. *Hepatology* **33**, 783-91 (2001).
- (72) Donner, M.G. & Keppler, D. Up-regulation of basolateral multidrug resistance protein 3 (Mrp3) in cholestatic rat liver. *Hepatology* **34**, 351-9 (2001).
- (73) Yang, K., Yue, W., Koeck, K., Pfeifer, N.D. & Brouwer, K.L.R. Interaction of Troglitazone Sulfate with Hepatic Basolateral and Canalicular Transport Proteins. In 2011 AAPS Annual Meeting and Exposition M1301.
- (74) Köck, K. *et al.* Inhibition of the hepatic basolateral bile acid transporter MRP4 predicts cholestatic drug-induced liver injury (DILI). In AASLD Liver meeting.

- (75) Köck, K., Ferslew, B.C., Yang, K. & Brouwer, K.L.R. Inhibition of hepatic bile acid transporter MRP4: a potential risk factor for drug-induced liver injury (DILI). In SOT Annual Meeting and ToxExpo 495.
- (76) Leslie, E.M., Watkins, P.B., Kim, R.B. & Brouwer, K.L. Differential inhibition of rat and human Na⁺-dependent taurocholate cotransporting polypeptide (NTCP/SLC10A1) by bosentan: a mechanism for species differences in hepatotoxicity. *J Pharmacol Exp Ther* **321**, 1170-8 (2007).
- (77) Marion, T.L., Leslie, E.M. & Brouwer, K.L. Use of sandwich-cultured hepatocytes to evaluate impaired bile acid transport as a mechanism of drug-induced hepatotoxicity. *Mol Pharm* **4**, 911-8 (2007).
- (78) Ansele, J.H., Smith, W.R., Perry, C.H., St Claire, R.L., 3rd & Brouwer, K.R. An in vitro assay to assess transporter-based cholestatic hepatotoxicity using sandwich-cultured rat hepatocytes. *Drug Metab Dispos* **38**, 276-80 (2010).
- (79) Kemp, D.C., Zamek-Gliszczynski, M.J. & Brouwer, K.L. Xenobiotics inhibit hepatic uptake and biliary excretion of taurocholate in rat hepatocytes. *Toxicol Sci* **83**, 207-14 (2005).
- (80) Trottier, J., Caron, P., Straka, R.J. & Barbier, O. Profile of serum bile acids in noncholestatic volunteers: gender-related differences in response to fenofibrate. *Clin Pharmacol Ther* **90**, 279-86 (2011).
- (81) Miyazaki, K., Nakayama, F. & Koga, A. Effect of chenodeoxycholic and ursodeoxycholic acids on isolated adult human hepatocytes. *Dig Dis Sci* **29**, 1123-30 (1984).
- (82) Jung, D. *et al.* FXR agonists and FGF15 reduce fecal bile acid excretion in a mouse model of bile acid malabsorption. *J Lipid Res* **48**, 2693-700 (2007).
- (83) Hollands, C.M., Rivera-Pedrogo, F.J., Gonzalez-Vallina, R., Loret-de-Mola, O., Nahmad, M. & Burnweit, C.A. Ileal exclusion for Byler's disease: an alternative surgical approach with promising early results for pruritus. *J Pediatr Surg* **33**, 220-4 (1998).
- (84) Emond, J.C. & Whittington, P.F. Selective surgical management of progressive familial intrahepatic cholestasis (Byler's disease). *J Pediatr Surg* **30**, 1635-41 (1995).
- (85) Whittington, P.F. & Whittington, G.L. Partial external diversion of bile for the treatment of intractable pruritus associated with intrahepatic cholestasis. *Gastroenterology* **95**, 130-6 (1988).
- (86) Stedman, C.A. *et al.* Nuclear receptors constitutive androstane receptor and pregnane X receptor ameliorate cholestatic liver injury. *Proc Natl Acad Sci U S A* **102**, 2063-8 (2005).

- (87) Beilke, L.D. *et al.* Constitutive androstane receptor-mediated changes in bile acid composition contributes to hepatoprotection from lithocholic acid-induced liver injury in mice. *Drug Metab Dispos* **37**, 1035-45 (2009).
- (88) Zollner, G., Marschall, H.U., Wagner, M. & Trauner, M. Role of nuclear receptors in the adaptive response to bile acids and cholestasis: pathogenetic and therapeutic considerations. *Mol Pharm* **3**, 231-51 (2006).
- (89) Geier, A., Wagner, M., Dietrich, C.G. & Trauner, M. Principles of hepatic organic anion transporter regulation during cholestasis, inflammation and liver regeneration. *Biochim Biophys Acta* **1773**, 283-308 (2007).
- (90) Madhu, C., Maziasz, T. & Klaassen, C.D. Effect of pregnenolone-16 alpha-carbonitrile and dexamethasone on acetaminophen-induced hepatotoxicity in mice. *Toxicol Appl Pharmacol* **115**, 191-8 (1992).
- (91) Seo, K.W., Park, M., Kim, J.G., Kim, T.W. & Kim, H.J. Effects of benzothiazole on the xenobiotic metabolizing enzymes and metabolism of acetaminophen. *J Appl Toxicol* **20**, 427-30 (2000).
- (92) Stedman, C. *et al.* Benefit of farnesoid X receptor inhibition in obstructive cholestasis. *Proc Natl Acad Sci U S A* **103**, 11323-8 (2006).
- (93) Renga, B. *et al.* Farnesoid X receptor suppresses constitutive androstane receptor activity at the multidrug resistance protein-4 promoter. *Biochim Biophys Acta* **1809**, 157-65 (2011).
- (94) Vore, M., Liu, Y. & Huang, L. Cholestatic properties and hepatic transport of steroid glucuronides. *Drug Metab Rev* **29**, 183-203 (1997).
- (95) Eurenus, K., Dalton, T.V., Lokey, H.J. & McIntyre, O.R. The mechanism of glucocorticoid action on the phytohemagglutinin-stimulated lymphocyte. I. In vitro binding of corticosteroids to lymphoid tissue. *Biochim Biophys Acta* **177**, 572-8 (1969).
- (96) Crocenzi, F.A. *et al.* Estradiol-17beta-D-glucuronide induces endocytic internalization of Bsep in rats. *Am J Physiol Gastrointest Liver Physiol* **285**, G449-59 (2003).
- (97) Mottino, A.D., Crocenzi, F.A., Pozzi, E.J., Veggi, L.M., Roma, M.G. & Vore, M. Role of microtubules in estradiol-17beta-D-glucuronide-induced alteration of canalicular Mrp2 localization and activity. *Am J Physiol Gastrointest Liver Physiol* **288**, G327-36 (2005).

- (98) Mottino, A.D., Cao, J., Veggi, L.M., Crocenzi, F., Roma, M.G. & Vore, M. Altered localization and activity of canalicular Mrp2 in estradiol-17beta-D-glucuronide-induced cholestasis. *Hepatology* **35**, 1409-19 (2002).
- (99) Dawson, E.R. & Platt, B.S. The Phosphate Ion and Hydrolysis by Pancreatic Lipase. *J Gen Physiol* **11**, 357-60 (1928).
- (100) Boaglio, A.C. *et al.* Phosphoinositide 3-kinase/protein kinase B signaling pathway is involved in estradiol 17beta-D-glucuronide-induced cholestasis: complementarity with classical protein kinase C. *Hepatology* **52**, 1465-76 (2010).
- (101) Barosso, I.R. *et al.* Sequential Activation of Classic PKC and Estrogen Receptor alpha Is Involved in Estradiol 17ss-D-Glucuronide-Induced Cholestasis. *PLoS One* **7**, e50711 (2012).
- (102) Yamamoto, Y. *et al.* Estrogen receptor alpha mediates 17alpha-ethynylestradiol causing hepatotoxicity. *J Biol Chem* **281**, 16625-31 (2006).
- (103) Ruiz, M.L. *et al.* Induction of Hepatic Multidrug Resistance Associated Protein 3 by Ethynylestradiol is Independent of Cholestasis and Mediated by Estrogen Receptor. *Drug Metab Dispos*, (2012).
- (104) Trauner, M., Fickert, P. & Stauber, R.E. Inflammation-induced cholestasis. *J Gastroenterol Hepatol* **14**, 946-59 (1999).
- (105) Moseley, R.H. Sepsis-associated cholestasis. *Gastroenterology* **112**, 302-6 (1997).
- (106) Zinchuk, V., Zinchuk, O. & Okada, T. Experimental LPS-induced cholestasis alters subcellular distribution and affects colocalization of Mrp2 and Bsep proteins: a quantitative colocalization study. *Microsc Res Tech* **67**, 65-70 (2005).
- (107) Kubitz, R., Wettstein, M., Warskulat, U. & Haussinger, D. Regulation of the multidrug resistance protein 2 in the rat liver by lipopolysaccharide and dexamethasone. *Gastroenterology* **116**, 401-10 (1999).
- (108) Denson, L.A., Auld, K.L., Schiek, D.S., McClure, M.H., Mangelsdorf, D.J. & Karpen, S.J. Interleukin-1beta suppresses retinoid transactivation of two hepatic transporter genes involved in bile formation. *J Biol Chem* **275**, 8835-43 (2000).
- (109) Ghose, R., Zimmerman, T.L., Thevananther, S. & Karpen, S.J. Endotoxin leads to rapid subcellular re-localization of hepatic RXRalpha: A novel mechanism for reduced hepatic gene expression in inflammation. *Nucl Recept* **2**, 4 (2004).

- (110) Trauner, M., Arrese, M., Lee, H., Boyer, J.L. & Karpen, S.J. Endotoxin downregulates rat hepatic ntcp gene expression via decreased activity of critical transcription factors. *J Clin Invest* **101**, 2092-100 (1998).
- (111) Zollner, G. *et al.* Adaptive changes in hepatobiliary transporter expression in primary biliary cirrhosis. *J Hepatol* **38**, 717-27 (2003).
- (112) Kojima, H. *et al.* Changes in the expression and localization of hepatocellular transporters and radixin in primary biliary cirrhosis. *J Hepatol* **39**, 693-702 (2003).
- (113) Congiu, M., Mashford, M.L., Slavin, J.L. & Desmond, P.V. Coordinate regulation of metabolic enzymes and transporters by nuclear transcription factors in human liver disease. *J Gastroenterol Hepatol* **24**, 1038-44 (2009).
- (114) Levy, C. & Lindor, K.D. Drug-induced cholestasis. *Clin Liver Dis* **7**, 311-30 (2003).
- (115) Mohi-ud-din, R. & Lewis, J.H. Drug- and chemical-induced cholestasis. *Clin Liver Dis* **8**, 95-132, vii (2004).
- (116) Chitturi, S. & Farrell, G.C. Drug-induced cholestasis. *Semin Gastrointest Dis* **12**, 113-24 (2001).
- (117) Hamilton, J.P. & Laurin, J.M. *Drug-induced cholestasis* (Humana Press Inc.: Totowa, NJ, 2008).
- (118) Zhu, X., Sedykh, A., Zhu, H., Liu, S. & Tropsha, S. The Use of Pseudo-equilibrium Constant Affords Improved QSAR Models of Human Plasma Protein Binding (Accepted). *Pharm Res*, (2012).
- (119) Benet, L.Z., Broccatelli, F. & Oprea, T.I. BDDCS applied to over 900 drugs. *AAPS J* **13**, 519-47 (2011).
- (120) Olah, M. *et al.* WOMBAT and WOMBAT-PK: Bioactivity Databases for Lead and Drug Discovery. In: *Chemical Biology: From Small Molecules to Systems Biology and Drug Design* (eds. Schreiber, S.L., Kapoor, T.M. and Wess, G.) 760-86 (Wiley-VCH, New York, 2007).
- (121) Warner, D.J. *et al.* Mitigating the inhibition of human bile salt export pump by drugs: opportunities provided by physicochemical property modulation, in silico modeling, and structural modification. *Drug Metab Dispos* **40**, 2332-41 (2012).

- (122) van Staden, C.J., Morgan, R.E., Ramachandran, B., Chen, Y., Lee, P.H. & Hamadeh, H.K. Membrane vesicle ABC transporter assays for drug safety assessment. *Curr Protoc Toxicol* **Chapter 23**, Unit 23 5 (2012).
- (123) Modica, S., Gadaleta, R.M. & Moschetta, A. Deciphering the nuclear bile acid receptor FXR paradigm. *Nucl Recept Signal* **8**, e005 (2010).
- (124) Goodwin, B. & Kliewer, S.A. Nuclear receptors. I. Nuclear receptors and bile acid homeostasis. *Am J Physiol Gastrointest Liver Physiol* **282**, G926-31 (2002).
- (125) Saito, H., Osumi, M., Hirano, H., Shin, W., Nakamura, R. & Ishikawa, T. Technical pitfalls and improvements for high-speed screening and QSAR analysis to predict inhibitors of the human bile salt export pump (ABCB11/BSEP). *AAPS J* **11**, 581-9 (2009).
- (126) Pedersen, J.M., Matsson, P., Bergstrom, C.A., Norinder, U., Hoogstraate, J. & Artursson, P. Prediction and identification of drug interactions with the human ATP-binding cassette transporter multidrug-resistance associated protein 2 (MRP2; ABCC2). *J Med Chem* **51**, 3275-87 (2008).
- (127) Zhang, H., Xiang, M.L., Zhao, Y.L., Wei, Y.Q. & Yang, S.Y. Support vector machine and pharmacophore-based prediction models of multidrug-resistance protein 2 (MRP2) inhibitors. *Eur J Pharm Sci* **36**, 451-7 (2009).
- (128) Sedykh, A. *et al.* Human Intestinal Transporter Database: QSAR Modeling and Virtual Profiling of Drug Uptake, Efflux and Interactions. *Pharm Res*, (2012).
- (129) Ng, C., Xiao, Y.D., Lum, B.L. & Han, Y.H. Quantitative structure-activity relationships of methotrexate and methotrexate analogues transported by the rat multispecific resistance-associated protein 2 (rMrp2). *Eur J Pharm Sci* **26**, 405-13 (2005).
- (130) Akanuma, S. *et al.* Molecular-weight-dependent, anionic-substrate-preferential transport of beta-lactam antibiotics via multidrug resistance-associated protein 4. *Drug Metab Pharmacokinet* **26**, 602-11 (2011).
- (131) Giacomini, K.M. *et al.* Membrane transporters in drug development. *Nat Rev Drug Discov* **9**, 215-36 (2010).
- (132) Karlgren, M. *et al.* Classification of inhibitors of hepatic organic anion transporting polypeptides (OATPs): influence of protein expression on drug-drug interactions. *J Med Chem* **55**, 4740-63 (2012).

- (133) Zheng, X., Ekins, S., Raufman, J.P. & Polli, J.E. Computational models for drug inhibition of the human apical sodium-dependent bile acid transporter. *Mol Pharm* **6**, 1591-603 (2009).
- (134) Zheng, X., Pan, Y., Acharya, C., Swaan, P.W. & Polli, J.E. Structural requirements of the ASBT by 3D-QSAR analysis using aminopyridine conjugates of chenodeoxycholic acid. *Bioconjug Chem* **21**, 2038-48 (2010).
- (135) Rais, R., Acharya, C., Mackerell, A.D. & Polli, J.E. Structural determinants for transport across the intestinal bile acid transporter using C-24 bile acid conjugates. *Mol Pharm* **7**, 2240-54 (2010).
- (136) Rais, R., Acharya, C., Tririya, G., Mackerell, A.D. & Polli, J.E. Molecular switch controlling the binding of anionic bile acid conjugates to human apical sodium-dependent bile acid transporter. *J Med Chem* **53**, 4749-60 (2010).
- (137) Gonzalez, P.M., Acharya, C., Mackerell, A.D., Jr. & Polli, J.E. Inhibition requirements of the human apical sodium-dependent bile acid transporter (hASBT) using aminopiperidine conjugates of glutamyl-bile acids. *Pharm Res* **26**, 1665-78 (2009).
- (138) Greupink, R. *et al.* In silico identification of potential cholestasis-inducing agents via modeling of Na(+)-dependent taurocholate cotransporting polypeptide substrate specificity. *Toxicol Sci* **129**, 35-48 (2012).
- (139) Ekins, S. *et al.* Challenges predicting ligand-receptor interactions of promiscuous proteins: the nuclear receptor PXR. *PLoS Comput Biol* **5**, e1000594 (2009).
- (140) Kortagere, S., Krasowski, M.D. & Ekins, S. Ligand- and structure-based pregnane X receptor models. *Methods Mol Biol* **929**, 359-75 (2012).
- (141) Khandelwal, A., Krasowski, M.D., Reschly, E.J., Sinz, M.W., Swaan, P.W. & Ekins, S. Machine learning methods and docking for predicting human pregnane X receptor activation. *Chem Res Toxicol* **21**, 1457-67 (2008).
- (142) Kortagere, S., Chekmarev, D., Welsh, W.J. & Ekins, S. Hybrid scoring and classification approaches to predict human pregnane X receptor activators. *Pharm Res* **26**, 1001-11 (2009).
- (143) Honorio, K.M., Garratt, R.C., Polikarpov, I. & Andricopulo, A.D. 3D QSAR comparative molecular field analysis on nonsteroidal farnesoid X receptor activators. *J Mol Graph Model* **25**, 921-7 (2007).

- (144) Zhang, T., Zhou, J.H., Shi, L.W., Zhu, R.X. & Chen, M.B. 3D-QSAR studies with the aid of molecular docking for a series of non-steroidal FXR agonists. *Bioorg Med Chem Lett* **17**, 2156-60 (2007).
- (145) Matter, H., Anger, L.T., Giegerich, C., Gussregen, S., Hessler, G. & Baringhaus, K.H. Development of in silico filters to predict activation of the pregnane X receptor (PXR) by structurally diverse drug-like molecules. *Bioorg Med Chem* **20**, 5352-65 (2012).
- (146) Schuster, D. *et al.* Pharmacophore-based discovery of FXR agonists. Part I: Model development and experimental validation. *Bioorg Med Chem* **19**, 7168-80 (2011).
- (147) Grienke, U. *et al.* Pharmacophore-based discovery of FXR-agonists. Part II: identification of bioactive triterpenes from *Ganoderma lucidum*. *Bioorg Med Chem* **19**, 6779-91 (2011).
- (148) Diaz Ochoa, J.G., Bucher, J., Pery, A.R., Zaldivar Comenges, J.M., Niklas, J. & Mauch, K. A multi-scale modeling framework for individualized, spatiotemporal prediction of drug effects and toxicological risk. *Front Pharmacol* **3**, 204 (2012).
- (149) Howell, B.A. *et al.* In vitro to in vivo extrapolation and species response comparisons for drug-induced liver injury (DILI) using DILIsym: a mechanistic, mathematical model of DILI. *J Pharmacokinet Pharmacodyn* **39**, 527-41 (2012).
- (150) Lecureur, V. *et al.* Cloning and expression of murine sister of P-glycoprotein reveals a more discriminating transporter than MDR1/P-glycoprotein. *Mol Pharmacol* **57**, 24-35 (2000).
- (151) Noe, J., Hagenbuch, B., Meier, P.J. & St-Pierre, M.V. Characterization of the mouse bile salt export pump overexpressed in the baculovirus system. *Hepatology* **33**, 1223-31 (2001).
- (152) Byrne, J.A., Strautnieks, S.S., Mieli-Vergani, G., Higgins, C.F., Linton, K.J. & Thompson, R.J. The human bile salt export pump: characterization of substrate specificity and identification of inhibitors. *Gastroenterology* **123**, 1649-58 (2002).
- (153) Wang, E.J., Casciano, C.N., Clement, R.P. & Johnson, W.W. Fluorescent substrates of sister-P-glycoprotein (BSEP) evaluated as markers of active transport and inhibition: evidence for contingent unequal binding sites. *Pharm Res* **20**, 537-44 (2003).
- (154) Hirano, H. *et al.* High-speed screening and QSAR analysis of human ATP-binding cassette transporter ABCB11 (bile salt export pump) to predict drug-induced intrahepatic cholestasis. *Mol Pharm* **3**, 252-65 (2006).

- (155) Karlgren, M., Ahlin, G., Bergstrom, C.A., Svensson, R., Palm, J. & Artursson, P. In vitro and in silico strategies to identify OATP1B1 inhibitors and predict clinical drug-drug interactions. *Pharm Res* **29**, 411-26 (2012).
- (156) Ung, C.Y., Li, H., Yap, C.W. & Chen, Y.Z. In silico prediction of pregnane X receptor activators by machine learning approaches. *Mol Pharmacol* **71**, 158-68 (2007).
- (157) Dybdahl, M., Nikolov, N.G., Wedebye, E.B., Jonsdottir, S.O. & Niemela, J.R. QSAR model for human pregnane X receptor (PXR) binding: screening of environmental chemicals and correlations with genotoxicity, endocrine disruption and teratogenicity. *Toxicol Appl Pharmacol* **262**, 301-9 (2012).
- (158) Honorio, K.M., Garratt, R.C. & Andricopulo, A.D. Hologram quantitative structure-activity relationships for a series of farnesoid X receptor activators. *Bioorg Med Chem Lett* **15**, 3119-25 (2005).
- (159) Genet, C. *et al.* Structure-activity relationship study of betulinic acid, a novel and selective TGR5 agonist, and its synthetic derivatives: potential impact in diabetes. *J Med Chem* **53**, 178-90 (2010).

CHAPTER 2. Analysis of Hepatic Transport Proteins¹

INTRODUCTION

The liver is one of the major organs responsible for the metabolism and excretion of endogenous and exogenous compounds. Hepatocytes contain transport proteins that facilitate the influx of many compounds from sinusoidal blood. Once inside the hepatocyte, compounds may be biotransformed by metabolizing enzymes and/or excreted. Hepatocytes are polarized cells with distinct apical and basolateral domains (Figure 2.1); transport proteins on the apical membrane are responsible for excretion of compounds into the bile canaliculus, whereas basolateral transport proteins mediate influx into hepatocytes and efflux back to sinusoidal blood. Biliary excretion of drugs and metabolites is an active process that requires energy, usually in the form of adenosine triphosphate (ATP); the multidrug and toxin extrusion (MATE) transporter is one exception that does not require ATP for drug transport into the bile canaliculus. ATP-dependent transport proteins also are located on the basolateral membrane, and are able to efflux drugs and metabolites from hepatocytes into sinusoidal blood.

In this chapter, the hepatic transport proteins important for drug disposition in humans are introduced based on their localization and function. The nomenclature and substrate specificity of hepatic transport proteins are summarized in Tables 2.1 and 2.2. *In vitro* and *in vivo* model systems and tools used to answer questions related to hepatic transport proteins are discussed, and more sophisticated approaches under development are introduced as future directions.

¹This chapter has been published in *Transporters in Drug Development*, and is presented in the style of that book: Chapter 9: Analysis of hepatic transport proteins. Sugiyama Y and Steffansen B (eds.), in: *Transporters in Drug Development*, Springer, pp201-233 (2013).

HEPATIC TRANSPORT PROTEINS

Hepatic Influx Transport Proteins

The solute carrier (*SLC*) and solute carrier organic anion (*SLCO*) gene families are two representative families of transport proteins that mediate the hepatic influx of xenobiotics across the basolateral hepatocyte membrane (Figure 2.1). The list of hepatic influx transporters and example substrates are included in Table 2.1.

NTCP (*SLC10A1*) The sodium-taurocholate cotransporting polypeptide (NTCP) is expressed exclusively in hepatocytes and plays a major role in the Na⁺-dependent hepatic influx of conjugated bile acids such as glycocholate and taurocholate (1). NTCP also is capable of transporting bromosulfophthalein (BSP), estrone 3-sulfate (E1S), and drugs such as pitavastatin and rosuvastatin, although the contribution of NTCP to the uptake of drug substrates into hepatocytes *in vivo* remains to be determined (Table 2.1). In rats, Ntcp also may be capable of transporting the thyroid hormones, and the mushroom toxin α -amanitin (2).

OATPs (*SLCO*, previously *SLC21A*) The family of organic anion transporting polypeptides (OATPs) plays an essential role in sodium-independent influx of endogenous and exogenous compounds into hepatocytes, and may be the rate-limiting step in the hepatobiliary clearance of some drugs, such as statins. OATPs exhibit broad and overlapping substrate specificity; the spectrum of OATP substrates includes organic anions, bulky organic cations (previously referred to as type II cations), and neutral steroids. Some OATP isoforms have been hypothesized to function as glutathione or bicarbonate antiporters (3-5), employing the high intracellular glutathione or bicarbonate concentrations as a driving force for hepatic influx of substrates with high efficiency.

Eleven human OATP isoforms have been identified so far; OATP1B1, OATP1B3, and OATP2B1 are the major human OATPs that play an important role in the hepatic influx of drugs across the basolateral membrane domain. OATP1B1 and 1B3 are liver-specific, whereas OATP2B1 is widely expressed (e.g. in intestine, brain, and kidney). OATP1B1 exhibits the largest diversity of substrates including bilirubin, BSP, bile salts, many antibiotics, angiotensin receptor antagonists, 3-hydroxy-3-

methyl-glutaryl Coenzyme A (HMG-CoA) reductase inhibitors (statins), and anticancer drugs (Table 2.1). OATP1B1 is the major human liver transport protein that is involved in sodium-independent bile salt and bilirubin influx. Inhibition of OATP1B1-mediated influx by drugs has been correlated with the incidence of hyperbilirubinemia (6). OATP1B1 is important in the hepatic influx of statins; genetic polymorphisms in *SLCO1B1* have been shown to be associated with increased systemic exposure of statins and increased risk of statin-induced myopathy (7). While OATP1B3 has overlapping substrate specificity with OATP1B1, distinct substrate specificity has been reported; repaglinide and troglitazone sulfate are more selective substrates for OATP1B1, while digoxin, cholecystokinin-8, and paclitaxel show selectivity for OATP1B3 (Table 2.1). Bile acids are known to be transported by OATP1A2, OATP1B1, and OATP1B3, but OATP2B1-mediated bile acid transport has not been investigated.

OATs (*SLC22A*) Organic anion transporters (OATs) mediate transport of small anionic compounds in exchange for dicarboxylate ions. Among six human OATs that have been functionally characterized, OAT2 (*SLC22A7*) is expressed in the basolateral membrane of hepatocytes and renal proximal tubule cells, while OAT7 (*SLC22A9*) is expressed exclusively in the liver (8). The known substrates for human OAT2 include prostaglandins, dehydroepiandrosterone sulfate (DHEAS), E1S, and anticancer drugs such as 5-fluorouracil and methotrexate (Table 2.1). OAT7, a recently characterized OAT, has been shown to transport sulfated hormones such as E1S and DHEAS when expressed in *X. Laevis* oocytes (9). Interestingly, typical OAT substrates such as para-aminohippurate, α -ketoglutarate, prostaglandins, cyclic nucleotides, and salicylic acid were not transported by OAT7, while OAT7 could transport the short-chain fatty acid butyrate (9).

OCTs (*SLC22A*) Organic cation transporters (OCTs) are electrogenic uniporters that primarily mediate the transport of small cations (previously referred to as type I cations) in a sodium-independent fashion. Human OCT1 (*SLC22A1*) is expressed exclusively at the basolateral membrane of the hepatocytes (10). OCT1 is known to transport antiviral drugs such as acyclovir and ganciclovir, as well as the H₂-receptor antagonists famotidine and ranitidine (Table 2.1). OCT3 (*SLC22A3*) and OCTN2

(*SLC22A5*) also are expressed in the liver, but expression levels are relatively low compared to OCT1 and the functional role of these proteins in hepatic drug transport remains to be elucidated (8).

OST α/β (*SLC51A/51B*) Organic solute transporter (OST) α/β is a heteromeric transporter that is expressed widely in the liver, small intestine, kidney, testis, and adrenal gland. In hepatocytes, OST α/β is expressed in the basolateral membrane, and is able to transport bile acids, E1S, and DHEAS. Since OST α/β mediates substrate transport by facilitated diffusion, OST α/β -mediated transport is bidirectional depending on the substrate's electrochemical gradient (10). Gene expression levels of *SLC51A* and *SLC51B* are positively regulated by bile acids through farnesoid X receptor (FXR), and it has been shown that hepatic OST α/β is up-regulated in patients with chronic cholestatic disease such as primary biliary cirrhosis (PBC) (11).

Hepatic Canalicular Efflux Transport Proteins

Biliary excretion is an important elimination pathway for many endogenous and exogenous substances. Canalicular transport proteins responsible for biliary excretion of substances primarily belong to the ATP-binding cassette (ABC) family of proteins that mediate ATP-dependent transport of solutes.

P-glycoprotein (MDR1, *ABCB1*) P-glycoprotein (P-gp) was first identified in multidrug-resistant (MDR) tumor cells (12), and is the most well characterized ABC transport protein. P-gp is widely distributed in liver, intestine, kidney, and brain. In hepatocytes, P-gp is expressed in the canalicular membrane and is responsible for biliary excretion of bulky hydrophobic and cationic substrates including many chemotherapeutic agents (e.g., daunorubicin, doxorubicin, etoposide, paclitaxel, vinblastine, vincristine), cardiac glycosides (e.g., digoxin), rhodamine 123, cyclosporine A, and protease inhibitors (e.g., amprenavir, indinavir, nelfinavir, ritonavir, saquinavir). Substrate specificity of P-gp largely overlaps with that of CYP3A4, resulting in synergistic defense mechanisms against xenobiotics. The *ABCB1* gene is highly polymorphic, and hepatic expression levels of P-gp are highly variable between different individuals.

MDR3 (*ABCB4*) MDR3, a phospholipid flippase, is involved in the biliary secretion of phospholipids and cholephilic compounds that form micelles with bile acids. Biliary excretion of

phospholipids protects the lumen of the bile canaliculus by solubilizing toxic bile acids (13). A deficiency in the *ABCB4* gene leads to progressive familial intrahepatic cholestasis type 3 (PFIC3), a disease that is characterized by increased γ -glutamyltranspeptidase levels, ductular proliferation, and inflammatory infiltrate that can progress to biliary cirrhosis. Individuals with decreased MDR3 activity are susceptible to cholesterol gallstone formation, which is known as low-phospholipid associated cholelithiasis (14). Inhibition of MDR3-mediated biliary phospholipids excretion is one proposed mechanism of hepatotoxicity induced by drugs such as itraconazole.

BSEP (*ABCB11*) The bile salt export pump (BSEP) is the major transport protein that mediates the biliary excretion of conjugated and unconjugated bile acids. Some drugs such as pravastatin may be substrates for BSEP based on membrane vesicle studies (15); however, the relative role of BSEP versus other canalicular transport proteins in the biliary excretion of pravastatin in hepatocytes or the intact liver remains to be determined (16). PFIC2 patients do not express BSEP protein due to a genetic polymorphism in the *ABCB11* gene; this leads to hepatocellular injury and necrosis caused by increased intracellular concentrations of detergent-like bile acids (17). Inhibition of BSEP-mediated bile acid transport is purported to be one mechanism of drug-induced liver injury associated with hepatotoxic drugs such as troglitazone, bosentan, and cyclosporine.

MRP2 (*ABCC2*) Multidrug resistance-associated protein (MRP) 2 plays an important role in the biliary excretion of organic anions, including bilirubin-diglucuronide, glutathione conjugates, sulfated bile acids, and divalent bile acid conjugates, as well as numerous drugs such as sulfapyrazone, indomethacin, penicillin, vinblastine, methotrexate, and telmisartan (Table 2.2). The absence of functional MRP2 due to genetic mutations in *ABCC2* results in Dubin-Johnson syndrome (DJS), which is characterized by decreased biliary excretion of bilirubin conjugates and hyperbilirubinemia (18).

BCRP (*ABCG2*) Breast cancer resistance protein (BCRP) is highly expressed in the canalicular membrane of hepatocytes as well as in the intestine, breast, and placenta. BCRP is a half-transport protein that forms a functional homodimer, and is responsible for transport of glucuronide and sulfate conjugates (e.g., E1S, estradiol-17 β -D-glucuronide (E₂17G), SN38-glucuronide), anticancer drugs (e.g., irinotecan,

SN-38, methotrexate, daunorubicin, doxorubicin), and some statins (e.g., pitavastatin, rosuvastatin) (Table 2.2).

MATE1 (SLC47A1) Human MATE1 is expressed predominantly in the canalicular membrane of hepatocytes and the luminal membrane of renal tubular cells. MATE1 has been shown to transport organic cations across the membrane in a bidirectional manner dependent on the proton gradient. Substrate specificity of MATE1 primarily overlaps with the OCTs; MATE1 substrates include acyclovir, N-methylpyridinium, and tetraethylammonium (Table 2.2).

Hepatic Basolateral Efflux Transport Proteins

Xenobiotics in the liver also may be excreted across the basolateral membrane into sinusoidal blood. MRP1, 3, 4, 5, and 6 are involved in cellular transport of both hydrophobic uncharged molecules and hydrophilic anionic compounds. OATPs also may function as basolateral efflux transport proteins under certain conditions, although the *in vivo* role of OATPs in basolateral efflux remains to be elucidated (4).

MRP3 (ABCC3) MRP3 was first localized in human and rat hepatocytes, and is also expressed widely in kidney, pancreas, enterocytes, cholangiocytes, and the gallbladder (19). The expression level of MRP3 in hepatocytes is low in normal liver, but markedly increased in patients with DJS who lack functional MRP2, and in patients with cholestatic liver disease, consistent with the important compensatory role of MRP3 when the function of biliary transport proteins is impaired (20-22). MRP3 is responsible for the basolateral efflux of glutathione and glucuronide conjugates (e.g., acetaminophen glucuronide), methotrexate, and E₂17G.

MRP4 (ABCC4) MRP4 is localized in many different tissues including liver, kidney, brain, and prostate (19). The expression level of MRP4 in normal hepatocytes is low, but is markedly induced under cholestatic conditions. MRP4 is responsible for the basolateral efflux of bile acids when the normal vectorial transport of bile acids from the hepatocyte into bile is compromised (23). MRP4-mediated bile acid transport requires glutathione, because bile acids and glutathione are co-transported by MRP4 (24). MRP4 also transports cyclic nucleotides (e.g., cAMP and cGMP), nucleoside analogs (e.g., zidovudine,

lamivudine, and stavudine), purine analogs (e.g., 6-mercaptopurine and 6-thioguanine), and non-nucleotide substrates such as methotrexate (25).

Other MRPs MRP1 (*ABCC1*) is expressed in several tissues including liver, lung, testis, kidney, skeletal and cardiac muscle, placenta, and macrophages (19). MRP1 is responsible for the efflux of various organic anions, such as glucuronide, glutathione, and sulfate conjugates of drugs. MRP5 (*ABCC5*) transports cyclic nucleotides (e.g., cAMP and cGMP) and purine analogs (e.g., 6-mercaptopurine and 6-thioguanine). The expression levels of MRP1 and MRP5 in healthy liver are relatively low, but protein levels of hepatic MRP1 and MRP5 were significantly increased in patients with PBC (26). Protein expression of hepatic MRP5 also was increased in acetaminophen-induced liver failure, suggesting a protective role for this protein in hepatic injury (26). MRP6 (*ABCC6*) is localized in the basolateral membrane of hepatocytes and transports glutathione conjugates and the endothelin receptor antagonist BQ-123 (Table 2.2). Expression of MRP6 was not altered in patients with PBC or acetaminophen-induced liver failure, and the functional roles of MRP6 remain to be explored (26).

***IN VITRO* MODELS AND METHODS TO STUDY HEPATOBILIARY DRUG TRANSPORT**

Membrane Vesicle System

With the development of membrane vesicle assays, it became possible to perform functional studies to identify and characterize distinct efflux transport systems. Historically, vesicle transport assays were performed using membranes isolated from hepatic tissue from the relevant species. Functional studies of hepatic efflux transporters in either canalicular liver plasma membrane (cLPM) or basolateral liver plasma membrane (bLPM) vesicles were enabled by the development of a method to separate these two membrane leaflets in the early 1980s (27, 28). This assay system was used to identify and characterize bile acid and bilirubin glucuronide transport across the canalicular membrane, and led to the discovery of BSEP and MRP2 (29, 30). The isolation of high-purity apical and basolateral membranes from tissue is labor intensive and technically challenging. Since inside-out and right-side-out vesicles coexist, ATP-dependent basolateral efflux data generated with bLPMs may be confounded by influx

transporters. Naturally, these membranes contain multiple transport proteins; therefore, it is impossible to identify specific substrates for ABC efflux proteins.

Due to evolving molecular biology techniques and identification of individual transport proteins, this tissue-based assay system has been replaced by vector-transfected and virus-infected cell lines expressing a single ABC-transporter. In the early 1990s, baculovirus-infected insect cells (*Spodoptera frugiperda*, Sf9) were used widely to generate membrane vesicles containing the transport protein of interest because this system allowed high expression of transport proteins (31). Disadvantages of these membrane vesicles are the different glycosylation pattern and a lower cholesterol content in Sf9 cells compared to mammalian cell lines (32), which may affect the localization and function of transporters. For example, MRP2-mediated transport and ATPase activity were altered by membrane cholesterol content (32). Therefore, either transiently or stably transfected mammalian cell lines from human embryonic kidney (HEK) 293, Madin-Darby canine kidney (MDCK) II, or porcine kidney epithelial (LLC-PK1) cells are now used more frequently for preparation of membrane vesicles for transporter studies. These systems are suitable for high-throughput screening of substrates and inhibitors for a single transport protein.

The most commonly used membrane system for efflux transporters is the vesicular transport system that detects direct translocation of substrates into inside-out vesicles (Figure 2.2). Substrates taken up into inside-out vesicles are separated from the incubation solution using rapid filtration and quantified by high performance liquid chromatography (HPLC), liquid chromatography mass spectrometry (LC/MS), scintillation counting, or fluorescence detection. ATP-dependent transport is calculated by subtracting the transport of substrate in the presence of AMP from that in the presence of ATP; endogenous transporter-mediated transport is excluded by subtracting ATP-dependent transport of substrate in control vesicles from that in transporter-expressing vesicles. This method detects direct transport of substrate, and kinetic parameters such as the Michaelis-Menten constant (K_m) and the maximal transport velocity (V_{max}) can be calculated. This method is ideal for the detection of drug-drug interactions (DDIs) or drug-endogenous compound interactions using a probe substrate. However, it is

difficult to detect the transport of highly permeable compounds due to passive diffusion out of the membrane vesicles.

The ATPase method, which detects the hydrolysis of ATP in the presence of an interacting compound, is more suitable for determining the transport of highly permeable compounds. The ATPase method is based on the principle that ABC transporters utilize the chemical energy of ATP cleavage to mediate the transport of substrates across membranes. The inorganic phosphate produced during this process is directly proportional to the activity of the transporter and can, for example, be monitored by colorimetric detection. This method is most commonly used for high-throughput screening for P-gp and BCRP, although it also is available commercially for other ABC efflux transporters. However, ATPase systems are indirect measures of transport, and are not always suitable for distinguishing between potential substrates, inhibitors or modulators. Major applications of the membrane vesicle systems as well as their advantages and disadvantages when used to study hepatobiliary drug transport are summarized in Table 2.3.

Transfected Cells

Bacterial, insect as well as mammalian cells have been transfected with vector constructs allowing overexpression of transport proteins for identification of transport processes. The transfected cell model is illustrated in Figure 2.2. Non-polarized cells such as Sf9 and HEK293 cells have been used for overexpression of a single transport protein, while polarized cells have been employed for the overexpression of one or more basolateral proteins in concert with apical protein(s). Transfected cell models can be used for high-throughput screening of substrates and inhibitors of a specific over-expressed transport protein. The major limitation of this model is that generally it is not suitable for the study of efflux transporters. Hypothetically, in transfected cells expressing a single efflux protein, transported substrates should demonstrate lower cellular accumulation, and inhibitors should increase drug accumulation compared to the parental cell line. However, substrates of drug efflux transporters are usually organic anions that do not easily penetrate into the cell in the absence of influx transport proteins. To overcome this limitation, polarized mammalian cells (e.g., MDCKII, LLC-PK1) have been used for

transfection of one or more influx and/or efflux transport proteins. Depending on the transporter, the protein will be routed to the apical or basolateral membrane in polarized cells; expression of influx transporters allows import of the substrates transported by the ABC efflux transporters. Furthermore, the combined expression of influx and efflux proteins enabled the analysis of vectorial transport, which is a key step in hepatobiliary elimination (33, 34). These double-transfected polarized cell lines were first developed by Cui et al. in the early 2000s (34) and are now valuable tools to study transcellular transport. Using MDCKII cells expressing both Oatp1b2 and Mrp2, Sasaki et al. demonstrated a good correlation between the clearance values obtained from *in vitro* transcellular transport and *in vivo* biliary clearance (35). Triple and quadruple transfected cell lines OATP1B1/MRP2/MRP3 or MRP4, as well as OATP1B1/OATP1B3/OATP2B1/MRP2 have been developed to better predict hepatobiliary processes (36, 37). Recently, a triple-transfected cell line expressing influx and efflux transporters as well as the drug-metabolizing enzyme uridine diphosphate glucuronosyl transferase (UGT) 1A1 has been described to study transporter-metabolism interplay (38). As our understanding of the role of influx and efflux transporters in facilitating the vectorial transport of xenobiotics across the hepatocyte has evolved, the use of polarized mammalian cells has become more popular to identify substrates and inhibitors of hepatic transport proteins. However, protein trafficking or localization in transfected cells may differ from human hepatocytes, depending on the species or type of transfected cells. Also, it is difficult to standardize the relative expression levels of transporters, and the relative contribution of a particular transport protein to overall transport of the substrate cannot be determined. The major applications of transfected cells together with their advantages and disadvantages when used to study hepatobiliary drug transport are summarized in Table 2.3.

Hepatocytes

Freshly isolated hepatocytes are the most comprehensive cell-based model to study hepatic drug transport and remain the gold standard. However, the scarcity of fresh, healthy human liver tissue suitable for hepatocyte isolation is a significant limitation, and isolation of human hepatocytes is technically challenging. Recent advances in technology have made good-quality cryopreserved human hepatocytes

commercially available at the user's convenience. Cryopreserved human hepatocytes have been used widely to study drug metabolism (39) and substrate influx in suspension (40-42); cryopreserved hepatocytes cultured in a sandwich configuration repolarize and form bile canalicular networks (43). Both the suspended and sandwich-cultured hepatocyte models are illustrated in Figure 2.2. However, not all batches of cryopreserved hepatocytes are qualified for sandwich-culture due to limitations in cell attachment and the loss of expression, localization, and/or function of transport proteins and metabolizing enzymes. Thus, further research is needed to improve the cryopreservation process.

Suspended Hepatocytes Fresh or cryopreserved suspended hepatocytes are a useful tool to characterize hepatic influx and metabolism processes, and inhibition studies can be performed with this system. However, suspended hepatocytes cannot be used for induction studies because the viability of hepatocytes in suspension cannot be maintained longer than several hours. Additionally, hepatocytes lose their cellular polarity during isolation and internalization of canalicular transport proteins has been demonstrated, which precludes the use of suspended hepatocytes to predict biliary clearance (44).

Sandwich-Cultured Hepatocytes In contrast to conventionally plated hepatocytes, hepatocytes cultured between two layers of gelled collagen ("sandwich-configuration") develop functional canalicular domains with proper localization of transport proteins and metabolic enzyme expression. (45) Liu et al. demonstrated that rat sandwich-cultured hepatocytes (SCH) could be used to investigate the hepatobiliary disposition of substrates using Ca^{2+} depletion methods (46, 47). This method involves pre-incubation of SCH with Hanks' balanced salt solution (HBSS) containing Ca^{2+} (standard HBSS) or Ca^{2+} -free HBSS for 10 minutes. Ca^{2+} -free HBSS disrupts tight junctions and opens the bile canalicular networks, while incubation with standard HBSS maintains tight junction integrity. Subsequently, cells are rinsed and incubated with substrate in standard HBSS for a predetermined period of time. Accumulation of substrate in cells+bile vs. cells can be determined in standard and Ca^{2+} -free HBSS buffers, respectively. The amount of substrate excreted into the bile canaliculi can be estimated as the difference in accumulation in standard and Ca^{2+} -free HBSS buffers, and *in vitro* biliary clearance may be obtained by dividing the amount of drug in the bile compartment by the area under the concentration-time curve (AUC) in the

dosing medium. This system has been applied to hepatocytes from many species, and has been used extensively to assess biliary clearance as a measure to improve hepatic clearance predictions (45). Biliary clearance values scaled from *in vitro* intrinsic biliary clearance measurements obtained in SCH have been shown to correlate well with *in vivo* biliary clearance data in rats (48-51) and humans (52, 53).

To determine the contribution of a specific transport protein to the disposition of a substrate, a transporter-specific reference compound can be employed in hepatocytes as well as transport protein overexpressing cells (54). Basically, this method compares the ratio of influx clearances of the test and the reference compound in both systems. However, the results are based on the assumption that the reference compound is specific for the respective transport protein, which – due to the overlapping substrate spectrum of transport proteins – is hardly ever the case.

SCH from naturally occurring, genetically deficient rodents lacking a specific transport protein, such as the Mrp2-deficient Wistar (TR⁻) and Eisai-hyperbilirubinemic Sprague-Dawley (SD) rats (EHBR), and the Mdr1a-deficient CF-1 mice, have been useful tools to evaluate the role of a transporter in the disposition of substrates (48). Also, genetically modified animals that lack specific transporter(s) can be used to assess the potential involvement of specific transport protein(s) in drug-drug interactions or polymorphisms that impair the function of drug transport proteins. However, care must be taken in interpreting the results of these studies because compensatory changes in drug metabolizing enzymes and/or other transport proteins may exist. Also, species difference in the expression, localization, and function of transport proteins between humans and genetically modified animals may limit clinical applicability of the data.

RNA interference (RNAi) of single or multiple transport proteins is a powerful tool to explore the consequences of loss of transport protein function. Synthetic small interfering RNA (siRNA) was transfected into rat SCH to specifically knock down Mrp2 and Mrp3 (55). Infection of rat SCH with adenoviral vectors expressing short hairpin RNA (shRNA) targeting Bcrp showed a significant decrease in protein expression and activity of this canalicular transport protein (56). Recently, Liao et al. successfully knocked down OATP1B1, 1B3, and 2B1 in sandwich-cultured human hepatocytes using

special delivery media containing siRNA (57). These studies have demonstrated the utility of knock down of specific transport proteins in SCH. However, careful optimization is required because knock down of one transport protein may alter the expression/function of metabolic enzymes and other transport proteins.

Other Hepatocyte Models Limited exposure of liver tissue to collagenase results in **hepatocyte couplets** preserving closed canalicular vacuoles and hepatocyte polarity (58). Hepatocyte couplets have been used to study hepatobiliary transport mechanisms underlying bile secretion (59, 60). **HepaRG** cells, a human hepatoma cell line, maintain specific liver functions such as drug metabolizing enzymes and transport proteins. In HepaRG cells, mRNA expression levels and functional activity of basolateral and canalicular transport proteins were comparable to those of human hepatocytes (61). Also, expression levels of transport proteins were up-regulated by known inducers, indicating that HepaRG cells maintain transactivation pathways that regulate expression of transport proteins (61). Since HepaRG cells are readily available compared to human hepatocytes, they may be a useful system to study hepatobiliary transport of compounds. However, HepaRG cells differentiate into biliary epithelial cells as well as hepatocytes, and the fraction of cells that differentiate into hepatocytes varies among different cultures and plates. In addition, more characterization is warranted including cell polarity and polarized expression of relevant transport proteins. Human **inducible pluripotent stem (iPS) cells** have been successfully differentiated into hepatocyte-like cells that exhibit human hepatocyte function such as inducible CYP450 activity (62). Although the expression and function of transport proteins still needs to be characterized, hepatocytes derived from individual-specific iPS cells may serve as a novel tool to study hepatobiliary transport of compounds in specific individuals. Newer three-dimensional microfluidic models (e.g. liverchip, H_µrel) that more closely resemble *in vivo* liver physiology are currently under development. Further investigations are needed to explore the utility of these more complex models. The major applications of hepatocytes as well as their advantages and disadvantages when used to study hepatobiliary drug transport are summarized in Table 2.3.

Isolated Perfused Liver Models

For decades, *in situ* or isolated perfused liver (IPL) studies have been used to investigate the physiology and pathophysiology of the liver. The model is illustrated in Figure 2.2. Publications regarding the use of IPLs date back to the 1950s, when the metabolism of drugs and endogenous compounds was first studied using this approach. In contrast to *in vitro* models such as isolated hepatocytes and liver slices, the IPL preserves hepatic architecture, cell polarity and bile flow. Furthermore, this model enables simultaneous sampling of bile as well as inflow and outflow perfusate; liver tissue may be obtained at the end of the study. Thus, the IPL provides a rich dataset amenable to pharmacokinetic modeling, and makes this system useful for mechanistic studies of hepatobiliary transport.

In IPL studies, the liver may be perfused in a single-pass or recirculating mode. A single-pass perfusion system is used to determine directly the steady-state hepatic extraction ratio of a compound. In the single-pass system, outflow perfusate from the liver does not re-enter the system, and the perfusion medium is pumped into the liver at a constant rate. Thus, steady-state conditions can be achieved readily, and drug and metabolite disposition can be examined at different dose levels in a single preparation. Also, experiments can be designed so that each liver serves as its own control. Hemoglobin-free oxygenated perfusate often is used in the single-pass perfusion system because a large volume of perfusate is required. Furthermore, flow rates that are 2 - 3 times higher than physiologic blood flow are required to maintain adequate oxygen delivery. In recirculating systems, blood-containing perfusate is oxygenated and recirculated through the liver at a constant flow rate that is similar to liver blood flow *in vivo*. The hepatic clearance of the drug can be determined from the dose introduced into the reservoir and the AUC in the reservoir. In recirculating systems, the only route of metabolite elimination is via biliary excretion, and metabolites usually accumulate in hepatocytes or in the perfusate, if they are able to flux across the hepatic basolateral membrane. Accumulation of metabolites may be advantageous in mass-balance determination of metabolite formation and kinetic evaluation of hepatic influx of metabolites. However,

potential drug-metabolite interactions may be magnified in the recirculating system compared with the single-pass IPL.

The IPL model can be applied to transporter knock-out animals in combination with chemical inhibitors to investigate the contribution of specific hepatic drug efflux transporters (63, 64). However, these experiments are relatively expensive and low-throughput. Furthermore, species-specific differences between human and rodent transport proteins may significantly limit the clinical applicability of information generated using this approach. Whether or not the results obtained from IPL analyses can be extrapolated to *in vivo* findings in humans remains compound-dependent. The major applications of the IPL models as well as advantages and disadvantages when applied to studying hepatobiliary drug transport are summarized in Table 2.3.

IN VIVO MODELS AND METHODS TO STUDY HEPATOBILIARY DRUG TRANSPORT

In vivo pharmacokinetic/pharmacodynamic studies in humans are the gold standard for investigating the role of hepatic transporters. However, the complexity of the hepatobiliary system and considerable substrate overlap for many of the transporters makes it difficult to identify the function of specific transport proteins based on *in vivo* studies. Genetically-modified animals and patients with polymorphisms in transporter genes are valuable in evaluating the function of transport proteins, but species differences in transport protein function, and compensatory up-regulation of other transport proteins, may confound the translation of *in vivo* data generated in preclinical species to humans.

***In Vivo* Biliary Excretion Studies**

Biliary excretion is an important route of elimination for some drugs and a potential site of drug interactions that may alter hepatic and/or systemic drug exposure. Accurate measurement of biliary clearance and understanding the mechanism(s) of biliary excretion are very important in evaluating the contribution of biliary clearance to total systemic clearance, predicting DDIs, identifying the contribution of enterohepatic recirculation to overall systemic and intestinal exposure, and elucidating potential mechanisms of hepatobiliary toxicity.

Bile Duct-Cannulation Animals, primarily rodents, often are used to determine the extent and the mechanisms of biliary excretion *in vivo*. Complete collection of bile is possible in bile duct-cannulated animals, which generates information about the extent of biliary excretion and the potential involvement of enterohepatic recirculation in overall systemic exposure. Proper study design is critical to obtain useful information from bile-duct cannulated animals. For example, if bile flow is exteriorized for extended periods of time to obtain complete bile collection, intravenous or intestinal supplementation with bile acids should be considered to replenish the bile acid pool. *In vivo* biliary clearance data has been used to assess the accuracy of *in vitro* methods of estimating biliary clearance; reasonable *in vitro-in vivo* correlations have been obtained (49, 51, 52, 65). Genetically modified animals that are deficient in specific transport proteins has improved our understanding of the complex molecular processes involved in excretion of endogenous and exogenous compounds into bile. However, significant interspecies differences in substrate specificity and regulation of transport proteins have been reported, which complicates the direct extrapolation of animal data to humans (66).

Aspiration of Duodenal Fluids Determining the biliary clearance of drugs *in vivo* in humans is challenging because it is difficult to access bile for sample collection from healthy human subjects. Bile samples can be collected in postsurgical patients with underlying hepatobiliary disease via a T-tube or nasobiliary tube (67, 68). However, it is difficult to rule out the effects of underlying hepatobiliary disease (e.g. altered protein expression, function, localization, and/or bile flow) in these patients. In healthy subjects, feces often are used as a surrogate to quantify the amount of drug excreted via non-renal pathways. However, this method cannot distinguish between biliary excretion, intestinal secretion, and unabsorbed drug following oral administration. Moreover, unstable drugs may not be recovered in feces due to the long exposure to the intestinal contents and colonic flora. Furthermore, drugs that are reabsorbed in the intestine and undergo enterohepatic recycling will not be recovered completely in the feces.

Oroenteric Tube Sampling duodenal fluids in healthy volunteers using an oroenteric tube alleviates some of the above mentioned problems. Duodenal bile is representative of gallbladder bile in

terms of bile composition, and collecting bile upon discharge from the biliary tract into the small intestines excludes the contribution of intestinal excretion and minimizes loss associated with metabolism and/or reabsorption. Oroenteric tubes have been commonly used to withdraw pancreatico-biliary secretions from the duodenum in medical practice, and have been used to study the biliary excretion of drugs (69, 70). Use of an occlusive balloon can facilitate more complete bile collection, and incomplete bile collection can be corrected by perfusing nonabsorbable markers. The most challenging part of this method is incomplete and highly variable recovery of compounds excreted into bile. Cholecystokinin 8 (CCK-8) may be administered intravenously to pharmacologically stimulate gall bladder emptying, but inter-individual response is variable. Ghibellini et al. introduced a novel method to evaluate the degree of gallbladder contraction and to detect any leakage of bile due to partial occlusion of the intestine (71). Subjects were administered a hepatobiliary imaging agent (e.g., ^{99m}Tc -mebrofenin), and the gall bladder ejection fraction was calculated from the abdominal gamma images of the study participants during gallbladder contraction. Incorporation of the ejection fraction as a correction factor in the calculation of the amount of drug excreted into the duodenum accounted for the variability in biliary excretion of the drug (72). This type of study provides direct evidence for biliary excretion and more precise quantification of biliary clearance, but is not used widely due to requirements for a gamma camera and personnel with expertise in gamma scintigraphy. The major applications of the *in vivo* biliary excretion models as well as advantages and disadvantages when used to study hepatobiliary drug transport are summarized in Table 2.4.

Hepatobiliary Imaging Techniques

Although techniques are available to study genetic polymorphisms and the expression of drug transporters at the mRNA and protein level, these data do not necessarily correlate with transporter function. Thus, there continues to be considerable interest in studying transporter function non-invasively. Pharmacokinetic analyses based on plasma concentrations in clinical studies provide information on overall hepatic clearance; however, differentiation between influx and canalicular efflux is not possible. While variations in influx activity of transporters might have a profound influence on systemic

concentrations, altered canalicular efflux might significantly affect liver concentrations without having measureable effects upon systemic exposure. This is especially relevant for drugs where the target site for effect or toxicity is within the hepatocyte. Therefore, quantitative estimations of tissue concentrations *in vivo* are necessary to investigate variations in efflux caused by DDIs or transporter polymorphisms. Furthermore, assessing the functional transport activity of P-gp, MRP2, or BCRP in the human liver might benefit the diagnosis of transporter deficiency-related diseases (e.g. PFIC3 and DJS). Several noninvasive imaging techniques such as magnetic-resonance imaging (MRI), single-photon emission computed tomography (SPECT) using ^{99m}Tc -labeled compounds, and positron emission tomography (PET) using short-lived ^{11}C , ^{13}N , ^{15}O or ^{18}F - isotopes have been employed to visualize and measure hepatic transporter activity *in vivo*.

Magnetic-Resonance Imaging The first MRI contrast agents were developed in the early 1980s (e.g. gadopentetate dimeglumine, gadodiamide, gadoteridol). These extremely hydrophilic compounds distributed primarily into the extracellular fluid and were excreted predominantly via the kidney. Because of this distribution pattern, these contrast agents have been used primarily for angiography and to detect lesions in the brain. The development of gadobenate dimeglumine (Gd-BOPTA) and gadolinium-ethoxybenzyl-diethylenetriamine pentaacetic acid (GD-EOB-DPTA, gadoxetic acid) allowed liver imaging and facilitated the distinction between normal and pathological tissue. Using these imaging agents, most hepatic tumors appear as hypointense lesions because they do not possess functional hepatocytes, while positive hepatocyte-enhancement may be observed in patients with tumors of hepatocellular origin (e.g. hepatocellular carcinoma, HCC). Hepatocyte influx of gadolinium compounds is thought to be mediated by OATPs (73, 74), while MRP2 mediates biliary excretion (75). Indeed, studies indicated that the degree of expression and localization of OATP1B1/1B3 and MRP2 affect the degree of hepatocyte-specific enhancement in HCC (73, 76).

SPECT and PET imaging For quantitative determination of drug transporters, the radionucleotide-based molecular imaging techniques SPECT and PET hold great promise. Initially, PET was used to quantify P-gp function in the blood-brain-barrier; several ^{11}C -labeled tracers have been

developed for this purpose (verapamil, carvedilol, N-desmethyl-loperamide, daunorubicin, paclitaxel). However, PET imaging also can be employed to study influx and excretion in other tissues. In 1995, Guhlmann et al. determined the hepatobiliary and renal excretion of N-[¹¹C] acetyl-leukotriene E4 in rats and monkeys by PET analysis. In rats, cholestasis due to bile duct obstruction as well as Mrp2 deficiency (TR⁻ rats) led to prolonged organ storage, metabolism, transport back into the blood and subsequently enhanced renal elimination compared to wild-type rats (77). Currently, compounds are being developed to evaluate hepatobiliary transport (78). In order to be useful clinically, such probes will need to be metabolically stable in humans, and ideally, the probes should be a substrate for a specific hepatic influx and/or efflux transport protein.

Cholescintigraphy studies with ^{99m}Tc-N(2,6-dimethylphenyl carbamoylmethyl) iminodiacetic acid (^{99m}Tc-HIDA) were performed in patients with liver disease in the late 70s/early 80s for diagnostic imaging of hepatobiliary disorders (79). Furthermore, ^{99m}Tc-mebrofenin has been used widely to diagnose cholestasis, gallbladder function, and bile duct leakage. In 2004, Hendrikse et al. proposed that both compounds were useful tools to evaluate the function of Mrp1, Mrp2 and P-gp *in-vivo* (80). Another compound, ^{99m}Tc-sestamibi, has been suggested to be a probe for P-gp function (81). This compound originally was developed for imaging of myocardial ischemia and is a positively charged, lipophilic compound that readily enters cells and accumulates in mitochondria. *In vivo* studies with ^{99m}Tc-sestamibi showed that this substance is retained in the liver and kidneys after P-gp inhibition with PSC833, suggesting that inhibition of P-gp transport in these organs can be imaged with ^{99m}Tc-sestamibi (81). However, ^{99m}Tc-sestamibi is also a substrate for MRP1 (82). The major applications of *in vivo* imaging together with advantages and disadvantages when used to study hepatobiliary drug transport are summarized in Table 2.4.

CONCLUSIONS

Hepatic transport proteins play important roles in the hepatic influx and biliary excretion of drugs and metabolites, thus affecting the therapeutic efficacy and toxicity of many drugs. Therefore, it is

important to understand the roles of hepatic transport proteins in the disposition of drugs and metabolites during the drug development process. Table 2.5 summarizes preferred approaches that can be used to answer specific questions regarding hepatobiliary drug transport. It is relatively straightforward to determine which transport proteins are capable of transporting drugs and metabolites by using membrane vesicle systems or cell lines expressing a single transport protein. However, determining the contribution of each transport protein to the hepatic influx or efflux of a specific compound in the whole cell/intact organ is not as straightforward, and may require the use of several model systems (e.g., transfected cell lines and SCH) and scaling factors (e.g., relative activity factor) (83). Moreover, reference compounds used to obtain the scaling factor between different systems are often not specific to a single transporter, which makes it difficult to determine the precise contribution of a single transporter to overall disposition.

Accurate predictions of clinically relevant drug interactions in hepatobiliary transport [either DDIs, drug-endogenous compound interactions (e.g. competition with bilirubin for influx or excretion) or drug-transporter interactions] are critical in drug development. Direct competitive interactions with a single protein can be predicted from membrane vesicle or transfected cell assays; however, accurate extrapolation to the *in vivo* setting requires an understanding of the unbound concentration at the site of transport. The ability of other transport proteins or drug metabolizing enzymes to compensate for drug interactions cannot be predicted accurately from these simplistic systems, and intact hepatocytes (suspended for influx studies; sandwich-cultured for hepatic efflux and overall hepatobiliary disposition) or whole organ and/or *in vivo* studies are required. More complex drug-transporter interactions involving signaling cascades and/or regulatory mechanisms, or interactions that involve generated drug metabolites require the complex machinery of the intact cell.

Drug-induced liver injury (DILI) is one of the most common reasons for withdrawal of drugs from the market, or failure of new drugs in clinical trials. Inhibition of canalicular BSEP, which leads to elevated hepatic exposure of detergent-like bile acids, has been reported as one mechanism of DILI. Some hepatotoxic drugs also are potent inhibitors of NTCP and/or MRPs. Thus, determining whether drug and/or generated metabolite(s) inhibit(s) bile acid transport would provide key information about the

drug's potential for DILI. High-throughput screening is possible to determine the inhibitory effects of a specific compound on bile acid transport in membrane vesicles expressing a single transporter. However, model systems that enable the generation of metabolites, and allow for direct measurement of bile acids accumulated in hepatocytes (e.g., SCH or IPL) provide more information to determine the potential for DILI. Hepatic exposure of the drug is important in predicting efficacy and toxicity, but this cannot be measured directly *in vivo* in humans nor predicted based on systemic exposure. Human SCH will provide invaluable information about the hepatic accumulation potential of drugs and generated metabolites, and how hepatic exposure changes when the function of transport proteins are altered due to disease states, drug interactions, or changes associated with genetic polymorphisms in transport proteins. Because only unbound drugs are available to interact with transporters, it is important to determine the intracellular unbound concentration. However, our current knowledge about intracellular unbound concentrations is limited, and development of *in vitro* systems to characterize hepatocellular binding/sequestration and the unbound concentration in the intact cell is needed.

Many tools and model systems are available to analyze the role of hepatic transport proteins in drug development. Current efforts are focused on assessing which tools should be appropriately used at defined steps in the drug development process, as well as how the resulting information can be used most efficiently to answer the key questions before the compound reaches the clinic. Important work continues to focus on mathematical modeling and simulation based on data generated from the various *in vitro* and *in vivo* models to accurately predict the role of hepatic transport proteins in drug disposition, and how alterations in hepatic transport could alter efficacy and/or toxicity.

Table 2.1. Human hepatic influx transporter proteins.

Protein/ Trivial Names	Gene	Substrate/References
NTCP	<i>SLC10A1</i>	cholate; E1S; glycochenodeoxycholate; pitavastatin; rosuvastatin; taurocholate; taurochenodeoxycholate [U], BSP; glycocholate; taurochenodeoxycholate (85)
OATP1B1 OATP-C LST-1 OATP2	<i>SLCO1B1</i> (<i>SLC21A6</i>)	atorvastatin; bilirubin; bisglucuronosyl bilirubin; bosentan; BSP; cholate; CGamF; DHEAS; E ₂ 17G; E1S; fluo-3; fluvastatin; glycochenodeoxycholate; methotrexate; monoglucuronosyl bilirubin; olmesartan; pitavastatin; pravastatin; rifampicin; rosuvastatin; taurochenodeoxycholate; valsartan [U], benzylpenicillin (86), BQ-123; DPDPE; LTC ₄ ; PGE ₂ ; T ₃ ; T ₄ (87), caspofungin (88), cerivastatin (89, 90), SN-38 (91), microcystin-LR (92), phalloidin (93), repaglinide (94, 95), simvastatin (90), troglitazone-sulfate (96)
OATP1B3 OATP-8 LST-2	<i>SLCO1B3</i> (<i>SLC21A8</i>)	amantinin; bilirubin; bosentan; BSP; CCK-8; CGamF; digoxin; E ₂ 17G; E1S; fexofenadine; fluo-3; fluvastatin; glycochenodeoxycholate; methotrexate; monoglucuronosyl bilirubin; olmesartan; paclitaxel; pitavastatin; rifampicin; rosuvastatin; taurocholate; taurochenodeoxycholate; telmisartan; telmisartan glucuronide; T ₃ ; valsartan [U], BQ-123; deltorphin II; DHEAS; DPDPE; LTC ₄ ; ouabain; T ₄ (87), CCK-8 (97), microcystin-LR (92), phalloidin (93)
OATP2B1 OATP-B	<i>SLCO2B1</i> (<i>SLC21A9</i>)	atorvastatin; bosentan; BSP; E1S; fexofenadine; fluvastatin; glyburide; pitavastatin; pravastatin; rosuvastatin; taurocholate; telmisartan glucuronide [U], DHEAS (87), pregnenolone sulfate (98)
OAT2	<i>SLC22A7</i>	2'-deoxyguanosine; 5-fluorouracil; bumetanide; cyclic GMP; erythromycin; paclitaxel; PGE ₂ ; PGF _{2α} ; tetracycline; theophylline; zidovudine [U], allopurinol; L-ascorbic acid; DHEAS; E1S; glutarate (99), methotrexate (100), ranitidine (101)
OAT 7	<i>SLC22A9</i>	DHEAS; E1S (9)
OCT1	<i>SLC22A1</i>	DASPMI; acyclovir; furamidine; ganciclovir; metformin; N-methylpyridinium; oxaliplatin; pentamidine; PGE ₂ ; PGF _{2α} ; ranitidine; tetraethylammonium; YM155 [U], ganciclovir (102), azidoprocaïnamide methoiodide; n-methylquinidine; n-methylquinine; tributylmethylammonium (103), choline (104), imatinib (105), MPP ⁺ ; N-methylnicotinamide (106, 107), famotidine (108)
OCT3 EMT	<i>SLC22A3</i>	Epinephrine; etilefrine; histamine; metformin; N-methylpyridinium; norepinephrine [U], adrenaline; noradrenaline; tyramine (109), agmatine; MPP ⁺ ; tetraethylammonium (110-112), atropine (113), histamine (104)
OCTN2	<i>SLC22A5</i>	acetyl-L-carnitine; D-carnitine; ipratropium; L-carnitine; quinidine; verapamil [U], cephaloridine; TEA; choline; purilamine (8)

[U] From UCSF-FDA TransPortal webpage (<http://bts.ucsf.edu/fdatransportal/>); the information about transporter substrates is listed by transporters or compounds under the “Transporter Data Index”.

BSP, bromosulphthalein; BQ-123, cyclo(D-Trp-D-Asp-L-Pro-D-Val-L-Leu); CCK-8, cholecystokinin 8; CGamF, cholyglycyl amido-fluorescein; DASPMI, 4-(4-dimethylamino)styryl-N-methylpyridinium; DHEAS, dehydroepiandrosterone; DPDPE, [D-penicillamine_{2,5}]-enkephalin; E1S, estrone 3-sulfate; E₂17G, estradiol-17 β -D-glucuronide; GMP, guanosine monophosphate; LTC₄, leukotriene C₄; MPP⁺, 1-methyl-4-phenylpyridinium; PGE₂, prostaglandin E₂; PGF_{2 α} , prostaglandin F₂;T₃, triiodothyronine; T₄, thyroxine

Table 2.2. Human hepatic efflux transporter proteins.

Protein/ Trivial Names	Gene	Substrates [Reference]
Hepatic canalicular efflux transport proteins		
MDR1 P-gp	<i>ABCB1</i>	berberine; biotin; colchicine; dexamethasone; digoxin; doxorubicin; etoposide; fexofenadine; indinavir; irinotecan; loperamide; nocardipine; paclitaxel; rhodamine 123; ritonavir; saquinavir; topotecan; valinomycin; verapamil; vinblastine; vincristine [U], amprenavir; nelfinavir (114, 115), aldosterone; corticosterone (116), cyclosporin A; mitoxanthrone (117), debrisoquine; erythromycin; lovastatin; terfenadine (118), quinidine (119), levofloxacin; grepafloxacin (120), losartan (121), tacrolimus (122), talinolol (123), norverapamil (124)
MDR3 Phospholipid flippase MDR2/3	<i>ABCB4</i>	digoxin; paclitaxel; verapamil; vinblastine [U], phospholipids (125)
BSEP Sister P-gp	<i>ABCB11</i>	glycochenodeoxycholate; glycocholate; pravastatin; taurochenodeoxycholate; taurocholate [U]
MRP2 CMOAT cMRP	<i>ABCC2</i>	DHEAS; E ₂ 17G; etoposide; irinotecan; methotrexate; olmesartan; para-aminohippurate; SN-38; SN-38 glucuronide; valsartan; vinblastine [U], LTC ₄ ; bisglucuronosyl bilirubin; monoglucuronosyl bilirubin; ochratoxin A; cholecystokinin peptide; E1S; cholestyramine-L-lysyl-fluorescein (19) acetaminophen glucuronide; carboxydichlorofluorescein (126), camptothecin; doxorubicin (127), cerivastatin (128), cisplatin; vincristine (129), glibenclamide; indomethacin; rifampin (130), pravastatin (33)
BCRP MXR ABCP	<i>ABCG2</i>	4-methylumbelliferone sulfate; daunorubicin; doxorubicin; E ₂ 17G; E1S; hematoporphyrin; imatinib; methotrexate; mitoxanthrone; pitavastatin; rosuvastatin, SN-38; SN-38 glucuronide; sulfasalazine; topotecan [U], mitoxanthrone glucuronides and sulfate conjugates (131), irinotecan (132), prazosin; rhodamine 123 (133), testosterone; tamoxifen; estradiol (134)
MATE1	<i>SLC47A1</i>	acyclovir; cimetidine; E1S; ganciclovir; guanidine; metformin; N-methylpyridinium; paraquat; procainamide; tetraethylammonium; topotecan [U]
Hepatic basolateral efflux transport proteins		
MRP3 MOAT-D MLP1 cMOAT1	<i>ABCC3</i>	E ₂ 17G; ethinylestradiol-glucuronide; fexofenadine; folic acid; glycocholate; hyocholate-glucuronide; hyodeoxycholate-glucuronide; leucovorin; LTC ₄ ; methotrexate; S-(2,4-dinitrophenyl)-glutathione; taurocholate [U], bisglucuronosyl bilirubin; monoglucuronosyl bilirubin; DHEAS (19), acetaminophen glucuronide (18), monovalent and sulfated bile salts (22), etoposide (135)
MRP4 MOAT-B	<i>ABCC4</i>	adefovir; chenodeoxycholyglycine; chenodeoxycholytaurine; cholate; cholyltaurine; cyclic AMP; cyclic GMP; DHEAS; deoxycholyglycine;

E₂17G; folic acid; methotrexate; olmesartan; para-aminohippurate;
PGE₁; PGE₂; tenofovir; topotecan [U], cholyglycine;
ursodeoxycholyglycine; ursodeoxycholyltaurine; urate; ADP; PMEA;
fluo-cAMP (19), azidothymidine (136)

[U] From UCSF-FDA TransPortal webpage (<http://bts.ucsf.edu/fdatransportal/>); the information about transporter substrates is listed by transporters or compounds under the “Transporter Data Index”.
BQ-123, cyclo(D-Trp-D-Asp-L-Pro-D-Val-L-Leu); CCK-8, cholecystokinin 8; DHEAS, dehydroepiandrosterone; E1S, estrone 3-sulfate; E₂17G, estradiol-17β-D-glucuronide; LTC₄, leukotriene C₄; LTD₄, leukotriene D₄; PGE₁, prostaglandin E₁; PGE₂, prostaglandin E₂; PMEA, 9-(2-phosphonomethoxyethyl)adenine

Table 2.3. Summary of advantages and disadvantages of in vitro models used to study hepatobiliary drug transport.

<i>In Vitro</i> Model	Major Applications	Advantages	Disadvantages
Membrane vesicle system			
Plasma membrane vesicles from tissue	<ul style="list-style-type: none"> - Determine the transport of compounds at particular membrane domain 	<ul style="list-style-type: none"> - All relevant transporters expressed - No interference from metabolism 	<ul style="list-style-type: none"> - Isolation of high-purity membranes is labor intensive and technically challenging - Difficult to determine the contribution of a single transporter - Activity of efflux transporters may be confounded by influx transporters
Membrane vesicles prepared from non-mammalian cells (Sf9)	<ul style="list-style-type: none"> - Functional characterization of new transporters for which a stable cell line has not been developed 	<ul style="list-style-type: none"> - Low interference by background activity of endogenous transporters 	<ul style="list-style-type: none"> - Lower levels of glycosylation or phosphorylation of target protein than in mammalian cell lines - Lower cholesterol content in lipid bilayer compared to mammalian cell lines
Membrane vesicles prepared from transfected mammalian cells	<ul style="list-style-type: none"> - High-throughput screening for substrates and inhibitors of a single transporter 	<ul style="list-style-type: none"> - High-throughput 	<ul style="list-style-type: none"> - Interference with background activity of endogenous transporters - Difficult to determine the transport of highly-diffusible compounds - Difficult to assess the relative contribution of multiple transport proteins.
Transfected cells			
Nonpolarized cells	<ul style="list-style-type: none"> - High-throughput screening for substrate and inhibitors. 	<ul style="list-style-type: none"> - High-throughput cell-based model. 	<ul style="list-style-type: none"> - Not optimal for study of efflux transport proteins
Polarized cells	<ul style="list-style-type: none"> - Vectorial transport across whole cells can be investigated. 	<ul style="list-style-type: none"> - Polarized phenotype mimics hepatocyte polarity 	<ul style="list-style-type: none"> - Species or cell type differences in protein trafficking or localization may exist

		<ul style="list-style-type: none"> - Multiple transfections can be conducted 	<ul style="list-style-type: none"> - Difficult to standardize relative expression levels - Difficult to determine the relative contribution of a specific transport protein
Hepatocytes			
Suspended hepatocytes	<ul style="list-style-type: none"> - Investigate kinetics and mechanisms of hepatic influx 	<ul style="list-style-type: none"> - Metabolic enzymes are intact - Applicable to hepatocytes from species of interest, including humans 	<ul style="list-style-type: none"> - Only used for short-time influx studies because hepatocyte viability decreases over time - Canalicular (apical) transport proteins may be internalized - Not suitable for study of canalicular efflux transport
Sandwich-cultured hepatocytes	<ul style="list-style-type: none"> - Mechanistic studies on hepatobiliary disposition, drug interactions, and transporter regulation 	<ul style="list-style-type: none"> - Sandwich culture allows for optimal transporter expression - Most hepatic transport proteins and drug-metabolizing enzymes are expressed and functional 	<ul style="list-style-type: none"> - Static model with respect to blood flow - Inherent variability among donors in protein expression, function, and canalicular network formation
Isolated Perfused Liver			
Single-pass	<ul style="list-style-type: none"> - Study mechanisms of hepatic influx, metabolism, biliary excretion, and basolateral efflux 	<ul style="list-style-type: none"> - Intact organ physiology (retains hepatic architecture and bile flow) - Rodents can be pretreated in vivo prior to liver isolation to examine effects of inducers or inhibitors on hepatobiliary clearance - Direct measurement of steady-state extraction ratio is possible 	<ul style="list-style-type: none"> - Low throughput - Labor- and animal-intensive - Limited to ~3 hours after liver isolation - Most amendable to rodents due to technical difficulties in perfusing livers from larger species
Recirculating	<ul style="list-style-type: none"> - Study mechanisms of hepatic influx, metabolism, and biliary excretion 	<ul style="list-style-type: none"> - Intact organ physiology (retains hepatic architecture and bile flow) - Rodents can be pretreated in vivo prior to liver isolation to examine 	<ul style="list-style-type: none"> - Low throughput - Labor- and animal-intensive - Limited to ~3 hours after liver isolation

-
- effects of inducers or inhibitors on hepatobiliary clearance
 - Metabolites accumulate in perfusate allowing mass-balance determination of metabolite formation and kinetic evaluation of hepatic influx of metabolites
 - Most amendable to rodents due to technical difficulties in perfusing livers from larger species
 - Potential drug-metabolite interaction
-

Table 2.4. Summary of advantages and disadvantages of in vivo models used to study hepatobiliary drug transport.

<i>In vivo</i> Model	Major Applications	Advantages	Disadvantages
<i>In vivo</i> biliary excretion			
Bile duct cannulation	- Direct measure of biliary excretion in animals	- Studies may be conducted in freely moving animals - Most physiologically relevant model	- Low throughput
Oroenteric tube	- Direct measure of biliary excretion in humans - DDI study using probe drug	- Direct measure of biliary excretion - Most physiologically relevant model	- Low throughput - Requires specialized personnel and equipment - Correction for gallbladder ejection fraction is required to accurately quantify biliary excretion
<i>In vivo</i> imaging			
MRI	- Anatomical imaging	- Safer compared to radiation based imaging	- Parent drug and metabolites not differentiated
Cholescintigraphy (HIDA scan)	- Evaluate the function of gallbladder - Investigate the function of transporters or drug interactions at transporter level	- 2D image - Non-invasive, real-time quantitative estimation of tissue concentration of drugs in vivo	- Radionuclide-labeled probe - Parent drug and metabolites not differentiated
SPECT, PET	- Investigate the function of transporters or drug interactions at transporter level	- 3D image - Noninvasive, real-time quantitative estimation of tissue concentration of drugs in vivo	- Radionuclide-labeled probe - Parent drug and metabolites not differentiated

Table 2.5. Preferred approaches to answer specific questions regarding hepatobiliary drug transport.

	Membrane vesicles*	Transfected cells	Suspended hepatocytes	Sandwich-cultured hepatocytes	Isolated perfused liver	<i>In vivo</i> bile collection	<i>In vivo</i> imaging
Which influx transporters are capable of transporting the NCE?	NA	1	2 ^a	2 ^a	2 ^a	NA	2 ^{a, c}
Which efflux transporters are capable of transporting the NCE?	1	2	NA	2 ^a	2 ^a	NA	2 ^{a, c}
What is the Cl _{biliary} of the NCE?	NA	NA	NA	1	2	1	NA
Is the NCE subject to transporter-based DDIs in the liver?	2	2	2	1	1	2	1 ^c
Is the NCE subject to DDIs at a specific transporter?	1	1	2 ^b	2 ^b	2 ^b	NA	2 ^b
Is the NCE likely to inhibit bile acid excretion?	1 ^b	NA	NA	1 ^b	1 ^b	2	NA
Is the NCE likely to accumulate in the liver?	NA	NA	NA	1	1	NA	1
Is the NCE subject to transporter-enzyme interplay?	NA	2	NA	1	1	2	NA

NCE: new chemical entity

*Membrane vesicles overexpressing transporter(s)

1, preferred; 2, possible; NA, not applicable

^a, if used with a specific inhibitor; ^b, if used with a specific probe; ^c, NCE needs to be labeled or fluorescent

Figure 2.1. In vivo architecture of polarized hepatocytes with distinct apical and basolateral domains facing respectively the bile canaliculus and bloodstream.

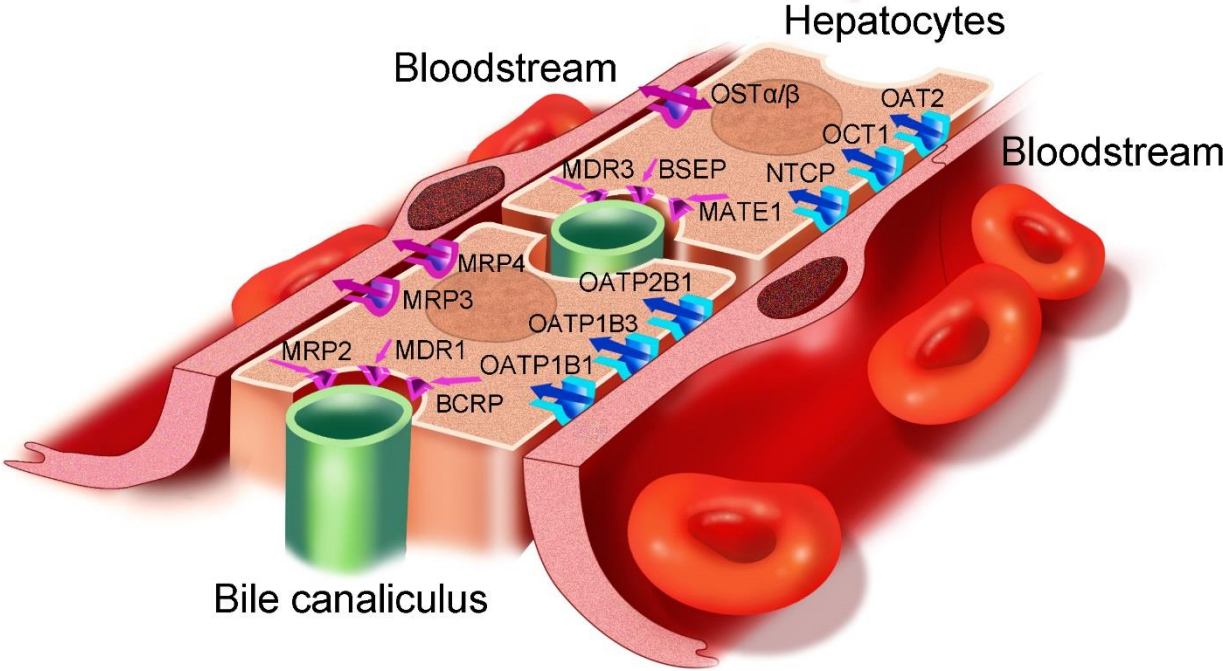
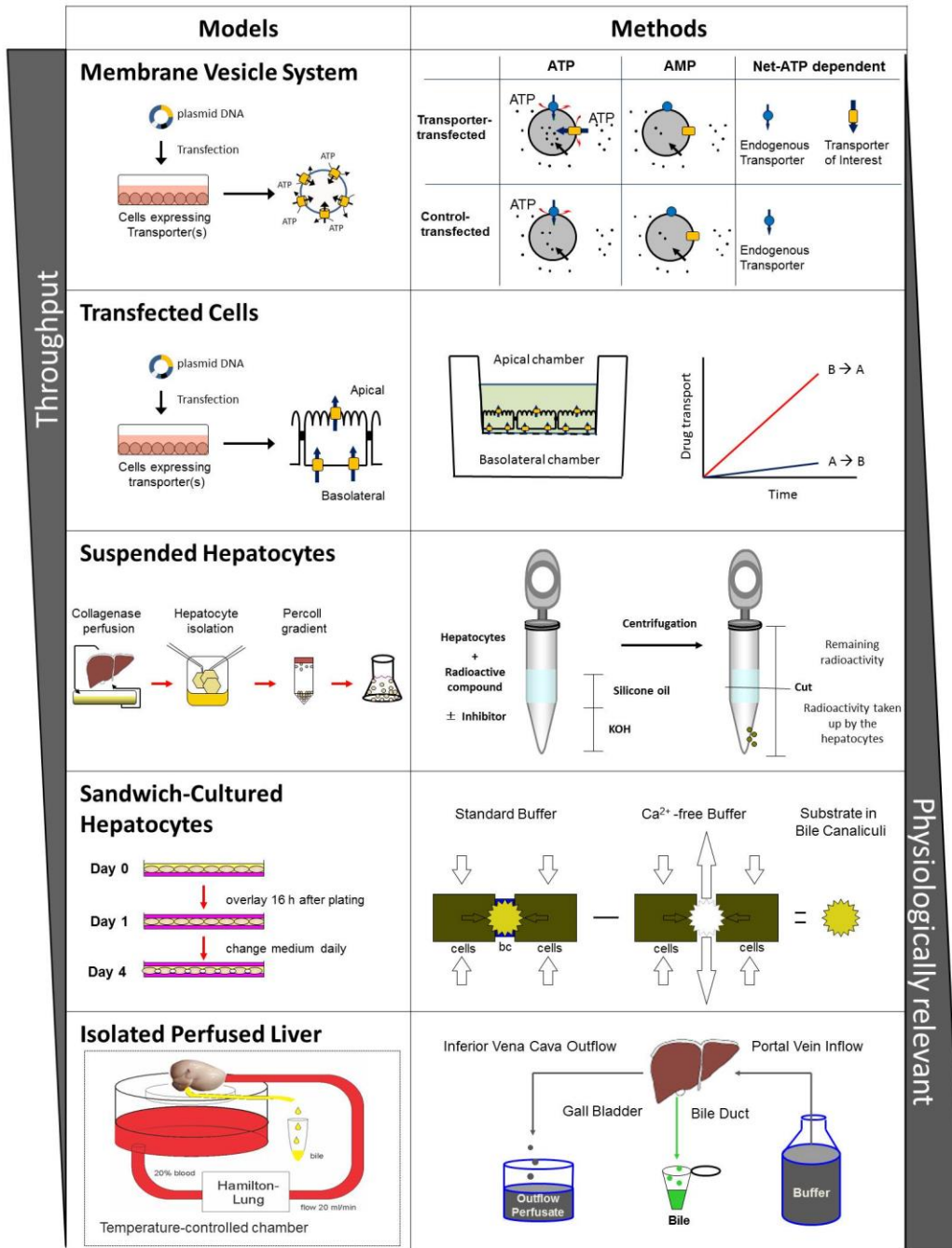


Figure 2.2. In vitro models and the related methods to study hepatobiliary drug transport.



REFERENCES

- (1) Stieger, B. The role of the sodium-taurocholate cotransporting polypeptide (NTCP) and of the bile salt export pump (BSEP) in physiology and pathophysiology of bile formation. *Handb Exp Pharmacol*, 205-59 (2011).
- (2) Gundala, S., Wells, L.D., Milliano, M.T., Talkad, V., Luxon, B.A. & Neuschwander-Tetri, B.A. The hepatocellular bile acid transporter Ntcp facilitates uptake of the lethal mushroom toxin alpha-amanitin. *Arch Toxicol* **78**, 68-73 (2004).
- (3) Briz, O. *et al.* OATP8/1B3-mediated cotransport of bile acids and glutathione: an export pathway for organic anions from hepatocytes? *J Biol Chem* **281**, 30326-35 (2006).
- (4) Li, L., Meier, P.J. & Ballatori, N. Oatp2 mediates bidirectional organic solute transport: a role for intracellular glutathione. *Mol Pharmacol* **58**, 335-40 (2000).
- (5) Satlin, L.M., Amin, V. & Wolkoff, A.W. Organic anion transporting polypeptide mediates organic anion/HCO₃⁻ exchange. *J Biol Chem* **272**, 26340-5 (1997).
- (6) Campbell, S.D., de Morais, S.M. & Xu, J.J. Inhibition of human organic anion transporting polypeptide OATP 1B1 as a mechanism of drug-induced hyperbilirubinemia. *Chem Biol Interact* **150**, 179-87 (2004).
- (7) Link, E. *et al.* SLCO1B1 variants and statin-induced myopathy--a genomewide study. *N Engl J Med* **359**, 789-99 (2008).
- (8) Hagenbuch, B. Drug uptake systems in liver and kidney: a historic perspective. *Clin Pharmacol Ther* **87**, 39-47 (2010).
- (9) Shin, H.J. *et al.* Novel liver-specific organic anion transporter OAT7 that operates the exchange of sulfate conjugates for short chain fatty acid butyrate. *Hepatology* **45**, 1046-55 (2007).
- (10) Soroka, C.J., Ballatori, N. & Boyer, J.L. Organic solute transporter, OSTalpha-OSTbeta: its role in bile acid transport and cholestasis. *Semin Liver Dis* **30**, 178-85 (2010).
- (11) Boyer, J.L. *et al.* Upregulation of a basolateral FXR-dependent bile acid efflux transporter OSTalpha-OSTbeta in cholestasis in humans and rodents. *Am J Physiol Gastrointest Liver Physiol* **290**, G1124-30 (2006).
- (12) Juliano, R.L. & Ling, V. A surface glycoprotein modulating drug permeability in Chinese hamster ovary cell mutants. *Biochim Biophys Acta* **455**, 152-62 (1976).

- (13) Oude Elferink, R.P. & Paulusma, C.C. Function and pathophysiological importance of ABCB4 (MDR3 P-glycoprotein). *Pflugers Arch* **453**, 601-10 (2007).
- (14) Rosmorduc, O., Hermelin, B., Boelle, P.Y., Parc, R., Taboury, J. & Poupon, R. ABCB4 gene mutation-associated cholelithiasis in adults. *Gastroenterology* **125**, 452-9 (2003).
- (15) Hirano, M., Maeda, K., Hayashi, H., Kusuhara, H. & Sugiyama, Y. Bile salt export pump (BSEP/ABCB11) can transport a nonbile acid substrate, pravastatin. *J Pharmacol Exp Ther* **314**, 876-82 (2005).
- (16) Kullak-Ublick, G.A., Stieger, B., Hagenbuch, B. & Meier, P.J. Hepatic transport of bile salts. *Semin Liver Dis* **20**, 273-92 (2000).
- (17) Kullak-Ublick, G.A., Stieger, B. & Meier, P.J. Enterohepatic bile salt transporters in normal physiology and liver disease. *Gastroenterology* **126**, 322-42 (2004).
- (18) Tsujii, H., Konig, J., Rost, D., Stockel, B., Leuschner, U. & Keppler, D. Exon-intron organization of the human multidrug-resistance protein 2 (MRP2) gene mutated in Dubin-Johnson syndrome. *Gastroenterology* **117**, 653-60 (1999).
- (19) Keppler, D. Multidrug resistance proteins (MRPs, ABCCs): importance for pathophysiology and drug therapy. *Handb Exp Pharmacol*, 299-323 (2011).
- (20) Konig, J., Rost, D., Cui, Y. & Keppler, D. Characterization of the human multidrug resistance protein isoform MRP3 localized to the basolateral hepatocyte membrane. *Hepatology* **29**, 1156-63 (1999).
- (21) Wagner, M., Zollner, G. & Trauner, M. New molecular insights into the mechanisms of cholestasis. *J Hepatol* **51**, 565-80 (2009).
- (22) Hirohashi, T., Suzuki, H. & Sugiyama, Y. Characterization of the transport properties of cloned rat multidrug resistance-associated protein 3 (MRP3). *J Biol Chem* **274**, 15181-5 (1999).
- (23) Wang, R., Sheps, J.A. & Ling, V. ABC transporters, bile acids, and inflammatory stress in liver cancer. *Curr Pharm Biotechnol* **12**, 636-46 (2011).
- (24) Rius, M., Nies, A.T., Hummel-Eisenbeiss, J., Jedlitschky, G. & Keppler, D. Cotransport of reduced glutathione with bile salts by MRP4 (ABCC4) localized to the basolateral hepatocyte membrane. *Hepatology* **38**, 374-84 (2003).

- (25) Sampath, J. *et al.* Role of MRP4 and MRP5 in biology and chemotherapy. *AAPS PharmSci* **4**, E14 (2002).
- (26) Barnes, S.N. *et al.* Induction of hepatobiliary efflux transporters in acetaminophen-induced acute liver failure cases. *Drug Metab Dispos* **35**, 1963-9 (2007).
- (27) Meier, P.J., Sztul, E.S., Reuben, A. & Boyer, J.L. Structural and functional polarity of canalicular and basolateral plasma membrane vesicles isolated in high yield from rat liver. *J Cell Biol* **98**, 991-1000 (1984).
- (28) Blitzer, B.L. & Donovan, C.B. A new method for the rapid isolation of basolateral plasma membrane vesicles from rat liver. Characterization, validation, and bile acid transport studies. *J Biol Chem* **259**, 9295-301 (1984).
- (29) Jedlitschky, G., Leier, I., Buchholz, U., Hummel-Eisenbeiss, J., Burchell, B. & Keppler, D. ATP-dependent transport of bilirubin glucuronides by the multidrug resistance protein MRP1 and its hepatocyte canalicular isoform MRP2. *Biochem J* **327** (Pt 1), 305-10 (1997).
- (30) Gerloff, T. *et al.* Differential expression of basolateral and canalicular organic anion transporters during regeneration of rat liver. *Gastroenterology* **117**, 1408-15 (1999).
- (31) Germann, U.A., Willingham, M.C., Pastan, I. & Gottesman, M.M. Expression of the human multidrug transporter in insect cells by a recombinant baculovirus. *Biochemistry* **29**, 2295-303 (1990).
- (32) Pal, A. *et al.* Cholesterol potentiates ABCG2 activity in a heterologous expression system: improved in vitro model to study function of human ABCG2. *J Pharmacol Exp Ther* **321**, 1085-94 (2007).
- (33) Sasaki, M., Suzuki, H., Ito, K., Abe, T. & Sugiyama, Y. Transcellular transport of organic anions across a double-transfected Madin-Darby canine kidney II cell monolayer expressing both human organic anion-transporting polypeptide (OATP2/SLC21A6) and Multidrug resistance-associated protein 2 (MRP2/ABCC2). *J Biol Chem* **277**, 6497-503 (2002).
- (34) Cui, Y., Konig, J. & Keppler, D. Vectorial transport by double-transfected cells expressing the human uptake transporter SLC21A8 and the apical export pump ABCC2. *Mol Pharmacol* **60**, 934-43 (2001).
- (35) Sasaki, M., Suzuki, H., Aoki, J., Ito, K., Meier, P.J. & Sugiyama, Y. Prediction of in vivo biliary clearance from the in vitro transcellular transport of organic anions across a double-transfected Madin-Darby canine kidney II monolayer expressing both rat organic anion transporting polypeptide 4 and multidrug resistance associated protein 2. *Mol Pharmacol* **66**, 450-9 (2004).

- (36) Kopplow, K., Letschert, K., Konig, J., Walter, B. & Keppler, D. Human hepatobiliary transport of organic anions analyzed by quadruple-transfected cells. *Molecular pharmacology* **68**, 1031-8 (2005).
- (37) Hirouchi, M., Kusuvara, H., Onuki, R., Ogilvie, B.W., Parkinson, A. & Sugiyama, Y. Construction of triple-transfected cells [organic anion-transporting polypeptide (OATP) 1B1/multidrug resistance-associated protein (MRP) 2/MRP3 and OATP1B1/MRP2/MRP4] for analysis of the sinusoidal function of MRP3 and MRP4. *Drug metabolism and disposition* **37**, 2103-11 (2009).
- (38) Fahrmayr, C., Konig, J., Auge, D., Mieth, M. & Fromm, M. Identification of drugs and drug metabolites as substrates of MRP2 using triple-transfected MDCK-OATP1B1-UGT1A1-MRP2 cells. *Br J Pharmacol*, (2011).
- (39) Lau, Y.Y., Sapidou, E., Cui, X., White, R.E. & Cheng, K.C. Development of a novel in vitro model to predict hepatic clearance using fresh, cryopreserved, and sandwich-cultured hepatocytes. *Drug Metab Dispos* **30**, 1446-54 (2002).
- (40) Houle, R., Raoul, J., Levesque, J.F., Pang, K.S., Nicoll-Griffith, D.A. & Silva, J.M. Retention of transporter activities in cryopreserved, isolated rat hepatocytes. *Drug Metab Dispos* **31**, 447-51 (2003).
- (41) Shitara, Y. *et al.* Function of uptake transporters for taurocholate and estradiol 17beta-D-glucuronide in cryopreserved human hepatocytes. *Drug Metab Pharmacokinet* **18**, 33-41 (2003).
- (42) De Bruyn, T. *et al.* Determination of OATP-, NTCP- and OCT-mediated substrate uptake activities in individual and pooled batches of cryopreserved human hepatocytes. *Eur J Pharm Sci* **43**, 297-307 (2011).
- (43) Bi, Y.A., Kazolias, D. & Duignan, D.B. Use of cryopreserved human hepatocytes in sandwich culture to measure hepatobiliary transport. *Drug Metab Dispos* **34**, 1658-65 (2006).
- (44) Hoffmaster, K.A., Turncliff, R.Z., LeCluyse, E.L., Kim, R.B., Meier, P.J. & Brouwer, K.L. P-glycoprotein expression, localization, and function in sandwich-cultured primary rat and human hepatocytes: relevance to the hepatobiliary disposition of a model opioid peptide. *Pharm Res* **21**, 1294-302 (2004).
- (45) Swift, B., Pfeifer, N.D. & Brouwer, K.L. Sandwich-cultured hepatocytes: an in vitro model to evaluate hepatobiliary transporter-based drug interactions and hepatotoxicity. *Drug Metab Rev* **42**, 446-71 (2010).

- (46) Liu, X. *et al.* Biliary excretion in primary rat hepatocytes cultured in a collagen-sandwich configuration. *Am J Physiol* **277**, G12-21 (1999).
- (47) Liu, X., LeCluyse, E.L., Brouwer, K.R., Lightfoot, R.M., Lee, J.I. & Brouwer, K.L. Use of Ca²⁺ modulation to evaluate biliary excretion in sandwich-cultured rat hepatocytes. *J Pharmacol Exp Ther* **289**, 1592-9 (1999).
- (48) Abe, K., Bridges, A.S., Yue, W. & Brouwer, K.L. In vitro biliary clearance of angiotensin II receptor blockers and 3-hydroxy-3-methylglutaryl-coenzyme A reductase inhibitors in sandwich-cultured rat hepatocytes: comparison with in vivo biliary clearance. *J Pharmacol Exp Ther* **326**, 983-90 (2008).
- (49) Fukuda, H., Ohashi, R., Tsuda-Tsukimoto, M. & Tamai, I. Effect of plasma protein binding on in vitro-in vivo correlation of biliary excretion of drugs evaluated by sandwich-cultured rat hepatocytes. *Drug Metab Dispos* **36**, 1275-82 (2008).
- (50) Liu, X., Chism, J.P., LeCluyse, E.L., Brouwer, K.R. & Brouwer, K.L. Correlation of biliary excretion in sandwich-cultured rat hepatocytes and in vivo in rats. *Drug Metab Dispos* **27**, 637-44 (1999).
- (51) Li, N., Singh, P., Mandrell, K.M. & Lai, Y. Improved extrapolation of hepatobiliary clearance from in vitro sandwich cultured rat hepatocytes through absolute quantification of hepatobiliary transporters. *Mol Pharm* **7**, 630-41 (2010).
- (52) Abe, K., Bridges, A.S. & Brouwer, K.L. Use of sandwich-cultured human hepatocytes to predict biliary clearance of angiotensin II receptor blockers and HMG-CoA reductase inhibitors. *Drug Metab Dispos* **37**, 447-52 (2009).
- (53) Ghibellini, G. *et al.* In vitro-in vivo correlation of hepatobiliary drug clearance in humans. *Clin Pharmacol Ther* **81**, 406-13 (2007).
- (54) Kouzuki, H., Suzuki, H., Ito, K., Ohashi, R. & Sugiyama, Y. Contribution of organic anion transporting polypeptide to uptake of its possible substrates into rat hepatocytes. *The Journal of pharmacology and experimental therapeutics* **288**, 627-34 (1999).
- (55) Tian, X., Zamek-Gliszczynski, M.J., Zhang, P. & Brouwer, K.L. Modulation of multidrug resistance-associated protein 2 (Mrp2) and Mrp3 expression and function with small interfering RNA in sandwich-cultured rat hepatocytes. *Mol Pharmacol* **66**, 1004-10 (2004).
- (56) Yue, W., Abe, K. & Brouwer, K.L. Knocking down breast cancer resistance protein (Bcrp) by adenoviral vector-mediated RNA interference (RNAi) in sandwich-cultured rat hepatocytes: a

- novel tool to assess the contribution of Bcrp to drug biliary excretion. *Mol Pharm* **6**, 134-43 (2009).
- (57) Liao, M. *et al.* Inhibition of hepatic organic anion-transporting polypeptide by RNA interference in sandwich-cultured human hepatocytes: an in vitro model to assess transporter-mediated drug-drug interactions. *Drug Metab Dispos* **38**, 1612-22 (2010).
- (58) Milkiewicz, P., Roma, M.G., Elias, E. & Coleman, R. Pathobiology and experimental therapeutics in hepatocellular cholestasis: lessons from the hepatocyte couplet model. *Clin Sci (Lond)* **102**, 603-14 (2002).
- (59) Boyer, J.L. Isolated hepatocyte couplets and bile duct units--novel preparations for the in vitro study of bile secretory function. *Cell Biol Toxicol* **13**, 289-300 (1997).
- (60) Coleman, R., Wilton, J.C., Stone, V. & Chipman, J.K. Hepatobiliary function and toxicity in vitro using isolated hepatocyte couplets. *Gen Pharmacol* **26**, 1445-53 (1995).
- (61) Le Vee, M., Jigorel, E., Glaise, D., Gripon, P., Guguen-Guillouzo, C. & Fardel, O. Functional expression of sinusoidal and canalicular hepatic drug transporters in the differentiated human hepatoma HepaRG cell line. *Eur J Pharm Sci* **28**, 109-17 (2006).
- (62) Song, Z. *et al.* Efficient generation of hepatocyte-like cells from human induced pluripotent stem cells. *Cell Res* **19**, 1233-42 (2009).
- (63) Hoffmaster, K.A., Zamek-Gliszczyński, M.J., Pollack, G.M. & Brouwer, K.L. Hepatobiliary disposition of the metabolically stable opioid peptide [D-Pen2, D-Pen5]-enkephalin (DPDPE): pharmacokinetic consequences of the interplay between multiple transport systems. *J Pharmacol Exp Ther* **311**, 1203-10 (2004).
- (64) Zamek-Gliszczyński, M.J. *et al.* Multiple mechanisms are involved in the biliary excretion of acetaminophen sulfate in the rat: role of Mrp2 and Bcrp1. *Drug Metab Dispos* **33**, 1158-65 (2005).
- (65) Nakakariya, M., Ono, M., Amano, N., Moriwaki, T., Maeda, K. & Sugiyama, Y. In Vivo Biliary Clearance Should Be Predicted by Intrinsic Biliary Clearance in Sandwich-Cultured Hepatocytes. *Drug Metab Dispos*, (2011).
- (66) Ishizuka, H. *et al.* Species differences in the transport activity for organic anions across the bile canalicular membrane. *J Pharmacol Exp Ther* **290**, 1324-30 (1999).

- (67) Brune, K., Nuernberg, B. & Schneider, H.T. Biliary elimination of aspirin after oral and intravenous administration in patients. *Agents Actions Suppl* **44**, 51-7 (1993).
- (68) Verho, M., Luck, C., Stelter, W.J., Rangoonwala, B. & Bender, N. Pharmacokinetics, metabolism and biliary and urinary excretion of oral ramipril in man. *Curr Med Res Opin* **13**, 264-73 (1995).
- (69) Galatola, G., Jazrawi, R.P., Bridges, C., Joseph, A.E. & Northfield, T.C. Direct measurement of first-pass ileal clearance of a bile acid in humans. *Gastroenterology* **100**, 1100-5 (1991).
- (70) Northfield, T.C. & Hofmann, A.F. Biliary lipid output during three meals and an overnight fast. I. Relationship to bile acid pool size and cholesterol saturation of bile in gallstone and control subjects. *Gut* **16**, 1-11 (1975).
- (71) Ghibellini, G., Johnson, B.M., Kowalsky, R.J., Heizer, W.D. & Brouwer, K.L. A novel method for the determination of biliary clearance in humans. *AAPS J* **6**, e33 (2004).
- (72) Ghibellini, G., Vasist, L.S., Hill, T.E., Heizer, W.D., Kowalsky, R.J. & Brouwer, K.L. Determination of the biliary excretion of piperacillin in humans using a novel method. *Br J Clin Pharmacol* **62**, 304-8 (2006).
- (73) Narita, M. *et al.* Expression of OATP1B3 determines uptake of Gd-EOB-DTPA in hepatocellular carcinoma. *Journal of gastroenterology* **44**, 793-8 (2009).
- (74) Leonhardt, M. *et al.* Hepatic uptake of the magnetic resonance imaging contrast agent Gd-EOB-DTPA: role of human organic anion transporters. *Drug metabolism and disposition* **38**, 1024-8 (2010).
- (75) Pascolo, L. *et al.* Abc protein transport of MRI contrast agents in canalicular rat liver plasma vesicles and yeast vacuoles. *Biochemical and biophysical research communications* **282**, 60-6 (2001).
- (76) Tsuboyama, T. *et al.* Hepatocellular carcinoma: hepatocyte-selective enhancement at gadoxetic acid-enhanced MR imaging--correlation with expression of sinusoidal and canalicular transporters and bile accumulation. *Radiology* **255**, 824-33 (2010).
- (77) Guhlmann, A. *et al.* Noninvasive assessment of hepatobiliary and renal elimination of cysteinyl leukotrienes by positron emission tomography. *Hepatology* **21**, 1568-75 (1995).
- (78) Takashima, T. *et al.* Positron emission tomography studies using (15R)-16-m-[11C]tolyl-17,18,19,20-tetranorisocarbacyclin methyl ester for the evaluation of hepatobiliary transport. *J Pharmacol Exp Ther* **335**, 314-23 (2010).

- (79) Stadalnik, R.C., Matolo, N.M., Jansholt, A.L. & Vera, D.R. Clinical experience with ^{99m}Tc-disofenin as a cholescintigraphic agent. *Radiology* **140**, 797-800 (1981).
- (80) Hendrikse, N.H. *et al.* In vivo imaging of hepatobiliary transport function mediated by multidrug resistance associated protein and P-glycoprotein. *Cancer Chemother Pharmacol* **54**, 131-8 (2004).
- (81) Luker, G.D., Fracasso, P.M., Dobkin, J. & Piwnica-Worms, D. Modulation of the multidrug resistance P-glycoprotein: detection with technetium-99m-sestamibi in vivo. *Journal of nuclear medicine : official publication, Society of Nuclear Medicine* **38**, 369-72 (1997).
- (82) Gomes, C.M., Abrunhosa, A.J., Pauwels, E.K. & Botelho, M.F. P-glycoprotein versus MRP1 on transport kinetics of cationic lipophilic substrates: a comparative study using [^{99m}Tc]sestamibi and [^{99m}Tc]tetrofosmin. *Cancer Biother Radiopharm* **24**, 215-27 (2009).
- (83) Hirano, M., Maeda, K., Shitara, Y. & Sugiyama, Y. Contribution of OATP2 (OATP1B1) and OATP8 (OATP1B3) to the hepatic uptake of pitavastatin in humans. *J Pharmacol Exp Ther* **311**, 139-46 (2004).
- (84) Kock, K. & Brouwer, K.L. A perspective on efflux transport proteins in the liver. *Clin Pharmacol Ther* **92**, 599-612 (2012).
- (85) Ho, R.H. *et al.* Drug and bile acid transporters in rosuvastatin hepatic uptake: function, expression, and pharmacogenetics. *Gastroenterology* **130**, 1793-806 (2006).
- (86) Tamai, I. *et al.* Molecular identification and characterization of novel members of the human organic anion transporter (OATP) family. *Biochem Biophys Res Commun* **273**, 251-60 (2000).
- (87) Kullak-Ublick, G.A. *et al.* Organic anion-transporting polypeptide B (OATP-B) and its functional comparison with three other OATPs of human liver. *Gastroenterology* **120**, 525-33 (2001).
- (88) Sandhu, P. *et al.* Hepatic uptake of the novel antifungal agent caspofungin. *Drug Metab Dispos* **33**, 676-82 (2005).
- (89) Shitara, Y., Itoh, T., Sato, H., Li, A.P. & Sugiyama, Y. Inhibition of transporter-mediated hepatic uptake as a mechanism for drug-drug interaction between cerivastatin and cyclosporin A. *J Pharmacol Exp Ther* **304**, 610-6 (2003).
- (90) Kameyama, Y., Yamashita, K., Kobayashi, K., Hosokawa, M. & Chiba, K. Functional characterization of SLCO1B1 (OATP-C) variants, SLCO1B1*5, SLCO1B1*15 and

- SLCO1B1*15+C1007G, by using transient expression systems of HeLa and HEK293 cells. *Pharmacogenet Genomics* **15**, 513-22 (2005).
- (91) Nozawa, T., Minami, H., Sugiura, S., Tsuji, A. & Tamai, I. Role of organic anion transporter OATP1B1 (OATP-C) in hepatic uptake of irinotecan and its active metabolite, 7-ethyl-10-hydroxycamptothecin: in vitro evidence and effect of single nucleotide polymorphisms. *Drug Metab Dispos* **33**, 434-9 (2005).
- (92) Fischer, W.J., Altheimer, S., Cattori, V., Meier, P.J., Dietrich, D.R. & Hagenbuch, B. Organic anion transporting polypeptides expressed in liver and brain mediate uptake of microcystin. *Toxicol Appl Pharmacol* **203**, 257-63 (2005).
- (93) Meier-Abt, F., Faulstich, H. & Hagenbuch, B. Identification of phalloidin uptake systems of rat and human liver. *Biochim Biophys Acta* **1664**, 64-9 (2004).
- (94) Kajosaari, L.I., Niemi, M., Neuvonen, M., Laitila, J., Neuvonen, P.J. & Backman, J.T. Cyclosporine markedly raises the plasma concentrations of repaglinide. *Clin Pharmacol Ther* **78**, 388-99 (2005).
- (95) Niemi, M. *et al.* Polymorphic organic anion transporting polypeptide 1B1 is a major determinant of repaglinide pharmacokinetics. *Clin Pharmacol Ther* **77**, 468-78 (2005).
- (96) Nozawa, T. *et al.* Involvement of organic anion transporting polypeptides in the transport of troglitazone sulfate: implications for understanding troglitazone hepatotoxicity. *Drug Metab Dispos* **32**, 291-4 (2004).
- (97) Ismail, M.G. *et al.* Hepatic uptake of cholecystokinin octapeptide by organic anion-transporting polypeptides OATP4 and OATP8 of rat and human liver. *Gastroenterology* **121**, 1185-90 (2001).
- (98) Grube, M. *et al.* Modification of OATP2B1-mediated transport by steroid hormones. *Mol Pharmacol* **70**, 1735-41 (2006).
- (99) Kobayashi, Y., Ohshiro, N., Sakai, R., Ohbayashi, M., Kohyama, N. & Yamamoto, T. Transport mechanism and substrate specificity of human organic anion transporter 2 (hOat2 [SLC22A7]). *J Pharm Pharmacol* **57**, 573-8 (2005).
- (100) Sun, W., Wu, R.R., van Poelje, P.D. & Erion, M.D. Isolation of a family of organic anion transporters from human liver and kidney. *Biochem Biophys Res Commun* **283**, 417-22 (2001).

- (101) Tahara, H. *et al.* A species difference in the transport activities of H₂ receptor antagonists by rat and human renal organic anion and cation transporters. *J Pharmacol Exp Ther* **315**, 337-45 (2005).
- (102) Takeda, M. *et al.* Human organic anion transporters and human organic cation transporters mediate renal antiviral transport. *J Pharmacol Exp Ther* **300**, 918-24 (2002).
- (103) van Montfoort, J.E., Muller, M., Groothuis, G.M., Meijer, D.K., Koepsell, H. & Meier, P.J. Comparison of "type I" and "type II" organic cation transport by organic cation transporters and organic anion-transporting polypeptides. *J Pharmacol Exp Ther* **298**, 110-5 (2001).
- (104) Grundemann, D., Liebich, G., Kiefer, N., Koster, S. & Schomig, E. Selective substrates for non-neuronal monoamine transporters. *Mol Pharmacol* **56**, 1-10 (1999).
- (105) Thomas, J., Wang, L., Clark, R.E. & Pirmohamed, M. Active transport of imatinib into and out of cells: implications for drug resistance. *Blood* **104**, 3739-45 (2004).
- (106) Gorboulev, V. *et al.* Cloning and characterization of two human polyspecific organic cation transporters. *DNA Cell Biol* **16**, 871-81 (1997).
- (107) Zhang, L., Gorset, W., Dresser, M.J. & Giacomini, K.M. The interaction of n-tetraalkylammonium compounds with a human organic cation transporter, hOCT1. *J Pharmacol Exp Ther* **288**, 1192-8 (1999).
- (108) Bourdet, D.L., Pritchard, J.B. & Thakker, D.R. Differential substrate and inhibitory activities of ranitidine and famotidine toward human organic cation transporter 1 (hOCT1; SLC22A1), hOCT2 (SLC22A2), and hOCT3 (SLC22A3). *J Pharmacol Exp Ther* **315**, 1288-97 (2005).
- (109) Grundemann, D., Schechinger, B., Rappold, G.A. & Schomig, E. Molecular identification of the corticosterone-sensitive extraneuronal catecholamine transporter. *Nat Neurosci* **1**, 349-51 (1998).
- (110) Hayer-Zillgen, M., Bruss, M. & Bonisch, H. Expression and pharmacological profile of the human organic cation transporters hOCT1, hOCT2 and hOCT3. *Br J Pharmacol* **136**, 829-36 (2002).
- (111) Grundemann, D., Hahne, C., Berkels, R. & Schomig, E. Agmatine is efficiently transported by non-neuronal monoamine transporters extraneuronal monoamine transporter (EMT) and organic cation transporter 2 (OCT2). *J Pharmacol Exp Ther* **304**, 810-7 (2003).
- (112) Wu, X. *et al.* Structure, function, and regional distribution of the organic cation transporter OCT3 in the kidney. *Am J Physiol Renal Physiol* **279**, F449-58 (2000).

- (113) Muller, J., Lips, K.S., Metzner, L., Neubert, R.H., Koepsell, H. & Brandsch, M. Drug specificity and intestinal membrane localization of human organic cation transporters (OCT). *Biochem Pharmacol* **70**, 1851-60 (2005).
- (114) Kim, R.B. *et al.* The drug transporter P-glycoprotein limits oral absorption and brain entry of HIV-1 protease inhibitors. *J Clin Invest* **101**, 289-94 (1998).
- (115) Polli, J.W. *et al.* Role of P-glycoprotein on the CNS disposition of amprenavir (141W94), an HIV protease inhibitor. *Pharm Res* **16**, 1206-12 (1999).
- (116) Ueda, K. *et al.* Human P-glycoprotein transports cortisol, aldosterone, and dexamethasone, but not progesterone. *J Biol Chem* **267**, 24248-52 (1992).
- (117) Marie, J.P., Helou, C., Thevenin, D., Delmer, A. & Zittoun, R. In vitro effect of P-glycoprotein (P-gp) modulators on drug sensitivity of leukemic progenitors (CFU-L) in acute myelogenous leukemia (AML). *Exp Hematol* **20**, 565-8 (1992).
- (118) Cvetkovic, M., Leake, B., Fromm, M.F., Wilkinson, G.R. & Kim, R.B. OATP and P-glycoprotein transporters mediate the cellular uptake and excretion of fexofenadine. *Drug Metab Dispos* **27**, 866-71 (1999).
- (119) Fromm, M.F., Kim, R.B., Stein, C.M., Wilkinson, G.R. & Roden, D.M. Inhibition of P-glycoprotein-mediated drug transport: A unifying mechanism to explain the interaction between digoxin and quinidine [see comments]. *Circulation* **99**, 552-7 (1999).
- (120) Yamaguchi, H., Yano, I., Hashimoto, Y. & Inui, K.I. Secretory mechanisms of grepafloxacin and levofloxacin in the human intestinal cell line caco-2. *J Pharmacol Exp Ther* **295**, 360-6 (2000).
- (121) Soldner, A., Christians, U., Susanto, M., Wachter, V.J., Silverman, J.A. & Benet, L.Z. Grapefruit juice activates P-glycoprotein-mediated drug transport. *Pharm Res* **16**, 478-85 (1999).
- (122) Floren, L.C. *et al.* Tacrolimus oral bioavailability doubles with coadministration of ketoconazole. *Clin Pharmacol Ther* **62**, 41-9 (1997).
- (123) Spahn-Langguth, H. *et al.* P-glycoprotein transporters and the gastrointestinal tract: evaluation of the potential in vivo relevance of in vitro data employing talinolol as model compound. *Int J Clin Pharmacol Ther* **36**, 16-24 (1998).
- (124) Pauli-Magnus, C. *et al.* Characterization of the major metabolites of verapamil as substrates and inhibitors of P-glycoprotein. *J Pharmacol Exp Ther* **293**, 376-82 (2000).

- (125) Smith, A.J. *et al.* MDR3 P-glycoprotein, a phosphatidylcholine translocase, transports several cytotoxic drugs and directly interacts with drugs as judged by interference with nucleotide trapping. *J Biol Chem* **275**, 23530-9 (2000).
- (126) Xiong, H., Turner, K.C., Ward, E.S., Jansen, P.L. & Brouwer, K.L. Altered hepatobiliary disposition of acetaminophen glucuronide in isolated perfused livers from multidrug resistance-associated protein 2-deficient TR(-) rats. *J Pharmacol Exp Ther* **295**, 512-8 (2000).
- (127) Koike, K. *et al.* A canalicular multispecific organic anion transporter (cMOAT) antisense cDNA enhances drug sensitivity in human hepatic cancer cells. *Cancer Res* **57**, 5475-9 (1997).
- (128) Matsushima, S. *et al.* Identification of the hepatic efflux transporters of organic anions using double-transfected Madin-Darby canine kidney II cells expressing human organic anion-transporting polypeptide 1B1 (OATP1B1)/multidrug resistance-associated protein 2, OATP1B1/multidrug resistance 1, and OATP1B1/breast cancer resistance protein. *J Pharmacol Exp Ther* **314**, 1059-67 (2005).
- (129) Kawabe, T. *et al.* Enhanced transport of anticancer agents and leukotriene C4 by the human canalicular multispecific organic anion transporter (cMOAT/MRP2). *FEBS Lett* **456**, 327-31 (1999).
- (130) Payen, L., Courtois, A., Campion, J.P., Guillouzo, A. & Fardel, O. Characterization and inhibition by a wide range of xenobiotics of organic anion excretion by primary human hepatocytes. *Biochem Pharmacol* **60**, 1967-75 (2000).
- (131) Kawabata, S. *et al.* Breast cancer resistance protein directly confers SN-38 resistance of lung cancer cells. *Biochem Biophys Res Commun* **280**, 1216-23 (2001).
- (132) Maliepaard, M. *et al.* Overexpression of the BCRP/MXR/ABCP gene in a topotecan-selected ovarian tumor cell line. *Cancer Res* **59**, 4559-63 (1999).
- (133) Ozvegy, C. *et al.* Functional characterization of the human multidrug transporter, ABCG2, expressed in insect cells. *Biochem Biophys Res Commun* **285**, 111-7 (2001).
- (134) Janvilisri, T., Venter, H., Shahi, S., Reuter, G., Balakrishnan, L. & van Veen, H.W. Sterol transport by the human breast cancer resistance protein (ABCG2) expressed in *Lactococcus lactis*. *J Biol Chem* **278**, 20645-51 (2003).
- (135) Stieger, B., Fattinger, K., Madon, J., Kullak-Ublick, G.A. & Meier, P.J. Drug- and estrogen-induced cholestasis through inhibition of the hepatocellular bile salt export pump (Bsep) of rat liver. *Gastroenterology* **118**, 422-30 (2000).

- (136) Schuetz, J.D. *et al.* MRP4: A previously unidentified factor in resistance to nucleoside-based antiviral drugs. *Nat Med* **5**, 1048-51 (1999).

CHAPTER 3. Species Differences in Hepatobiliary Disposition of Taurocholic acid in Human and Rat Sandwich-Cultured Hepatocytes; Implications for Drug-Induced Liver Injury¹

INTRODUCTION

Bile acids are important endogenous molecules that are involved in digestion and absorption of fats, and regulation of lipid and glucose homeostasis (1, 2). However, bile acids can exert toxic effects at supra-physiologic concentrations through disruption of mitochondrial ATP synthesis, necrosis, and apoptosis (3, 4); thus, defects in excretion may lead to hepatic accumulation of bile acids and subsequent hepatotoxicity.

Hepatic transporters play important roles in vectorial transport of bile acids. Sodium taurocholate cotransporting polypeptide (NTCP) and organic anion transporting polypeptides (OATPs) are responsible for sodium-dependent and sodium-independent uptake of bile acids from sinusoidal blood into hepatocytes, respectively. Bile acids in hepatocytes are excreted into bile across the canalicular membrane, predominantly via the bile salt export pump (BSEP). Consistent with the important role of BSEP in bile acid excretion, impaired BSEP function due to genetic polymorphisms has been shown to induce liver injury (e.g., progressive familial intrahepatic cholestasis type II) (5). Also, there has been increasing evidence that inhibition of BSEP by drugs is associated with cholestatic/mixed type drug-induced liver injury (DILI) (6-9).

In addition to BSEP-mediated canalicular excretion, bile acids also are transported back into sinusoidal blood via basolateral efflux transporters, including multidrug resistance-associated protein (MRP) 3, MRP4, and organic solute transporter (OST) α -OST β . Expression levels of MRP3 and MRP4

¹This work has been presented, in part, at the 2012 AAPS Annual Meeting and Exposition, Chicago, IL, October 14-18, 2012, and will be submitted to *Journal of Pharmacology and Experimental Therapeutics*.

are up-regulated under cholestatic conditions, suggesting that they function as a compensatory route of bile acid excretion and thereby serve as an important part of adaptive response (10-12). OST α -OST β mediates basolateral efflux of bile acids from enterocytes into the portal circulation by facilitated diffusion (13), but the role of OST α -OST β in hepatic bile acid efflux remains to be further characterized. Recently, Morgan et al. reported that prediction of DILI was improved by considering the inhibitory effect of a drug on MRP2, MRP3 and MRP4, compared to BSEP inhibition alone (8). In addition, studies from our laboratory demonstrated that MRP4 inhibition was associated with cholestatic/mixed DILI among BSEP non-inhibitors, emphasizing the role of MRP4 in DILI (14).

DILI is one of the primary reasons for withdrawal of approved drugs from the market and a major concern during drug development (15). One prominent example is troglitazone (TGZ), the first of the thiazolidinedione class of antidiabetic drugs that was withdrawn from worldwide markets due to severe DILI. (16, 17). Although mechanisms of TGZ-mediated hepatotoxicity remain unclear, *in vitro* vesicular transport assays demonstrated that TGZ and its major metabolite, TGZ sulfate (TS), are potent BSEP inhibitors, suggesting a cholestatic component in TGZ-induced hepatotoxicity (6, 7, 18). TGZ also inhibits NTCP, MRP3, and MRP4 (8, 19); although TS accumulates extensively in hepatocytes (20, 21), the effect of TS on basolateral efflux transporters has not been investigated.

Due to extensive biliary excretion, it generally has been accepted that the contribution of basolateral efflux to hepatocellular bile acid excretion is minimal under normal conditions. However, as proposed in the “hepatocyte hopping” theory of bilirubin glucuronides (22), it is plausible that bile acids may undergo extensive basolateral efflux (through MRP3/4) and re-uptake into downstream hepatocytes (through NTCP/OATP). This would prevent saturation of biliary transporters in upstream hepatocytes and transfer bile acids to downstream hepatocytes, protecting hepatocytes from bile acid toxicity. To our knowledge, the contribution of basolateral efflux vs. biliary excretion to hepatocellular bile acid disposition has not been precisely characterized. Jemnitz et al. (2010) investigated basolateral efflux and biliary excretion of TCA in human and rat sandwich-cultured hepatocytes (SCH) by measuring efflux of TCA from pre-loaded SCH into the standard or Ca²⁺-free buffer (23). However, these investigators did

not account for the “flux” of TCA accumulated within bile networks into the buffer, which results from regular “pulsing” of the bile canaliculi in SCH (24). Regular, ordered contraction of bile canaliculi, has been reported previously in isolated couplets and cultured hepatocytes (25, 26), and also has been shown to facilitate bile flow in vivo in rat liver (27).

The purpose of the present studies was to characterize TCA hepatobiliary disposition (basolateral uptake, basolateral efflux, biliary excretion, flux from canalicular networks) in human and rat SCH using a novel uptake and efflux protocol developed by our laboratory combined with pharmacokinetic modeling (28). Results from the current investigation revealed that species differences exist in cellular TCA efflux pathways in human vs. rat SCH; differential hepatobiliary disposition of TCA in human and rat SCH in the presence of inhibitors of canalicular excretion and/or basolateral efflux was predicted by simulations. This study also investigated the effects of TGZ and its metabolites on the disposition of TCA in human and rat SCH, and the inhibitory effects of TS on MRP4, a basolateral efflux transporter that mediates bile acid transport.

METHODS

Materials

All chemicals were purchased from Sigma-Aldrich (St. Louis, MO) unless otherwise stated. TGZ was purchased from Cayman Chemical Company (Ann Arbor, MI). TS was kindly provided by Daiichi-Sankyo Co, Ltd. (Tokyo, Japan). TS also was synthesized from TGZ in-house as described by Saha et al. (29). [³H]TCA (5 Ci/mmol) and [³H]dehydroepiandrosterone sulfate (DHEAS; 79.5 Ci/mmol) were purchased from Perkin Elmer (Waltham, MA). Dimethyl sulfoxide (DMSO) was obtained from Fisher Scientific (Fairlawn, NJ). GIBCO brand fetal bovine serum, recombinant human insulin, and Dulbecco’s modified Eagle’s medium (DMEM) were purchased from Life Technologies (Carlsbad, CA). Insulin/transferrin/selenium (ITS) culture supplement, BioCoatTM culture plates, and MatrigelTM extracellular matrix were purchased from BD Biosciences Discovery Labware (Bedford, MA).

Sandwich-Cultured Hepatocytes (SCH)

Rat hepatocytes were isolated from male Wistar rats (234–245 g, Charles River Laboratories, Inc., Wilmington, MA) using a two-step collagenase perfusion method as previously described (LeCluyse et al., 1996). Animals had free access to water and food before surgery and were allowed to acclimate for at least five days. All animal procedures complied with the guidelines of the Institutional Animal Care and Use Committee (University of North Carolina, Chapel Hill, NC). Rat hepatocytes were seeded onto 6-well BioCoat™ culture plates at a density of 1.75×10^6 cells/well in seeding medium (DMEM containing 5% fetal bovine serum, 10 μ M insulin, 1 μ M dexamethasone, 2 mM L-glutamine, 1% MEM nonessential amino acids, 100 units of penicillin G sodium, and 100 μ g of streptomycin) as described previously (30). Hepatocytes were incubated for 2 h at 37°C in a humidified incubator (95% O₂, 5% CO₂) and allowed to attach to the collagen substratum, after which time the medium was aspirated to remove unattached cells and replaced with fresh medium. On the next day, cells were overlaid with BD Matrigel™ at a concentration of 0.25 mg/ml in ice-cold feeding medium (DMEM supplemented with 0.1 μ M dexamethasone, 2 mM L-glutamine, 1% MEM nonessential amino acids, 100 units of penicillin G sodium, 100 μ g of streptomycin, and 1% ITS). The culture medium was changed daily until experiments were performed on day 4. Human SCH, seeded onto 24-well BioCoat™ culture plates and overlaid with Matrigel™, were purchased from Triangle Research Labs (Research Triangle Park, NC). Human hepatocytes were obtained from two Caucasian females (31 years old, BMI 29.05 kg/m²; 56 years old, BMI 22.30 kg/m²), and one African American female (48 years old, BMI 24.9 kg/m²). The culture medium (the same feeding medium used for rat SCH) was changed daily until experiments were performed on day 7.

Uptake and Efflux Studies in SCH

Uptake and efflux studies of TCA were performed in human and rat SCH as previously described (28). Briefly, on day 4 (rat) or day 7 (human) of culture, SCH were pre-incubated for 10 min in 0.3 mL/well standard (Ca²⁺-containing) or Ca²⁺-free (Ca²⁺/Mg²⁺-free buffer containing EGTA) HBSS. Incubating SCH in Ca²⁺-free HBSS disrupts the tight junctions that form the bile canalicular networks (B-

CLEAR[®] technology, Qualyst Transporter Solutions, Research Triangle Park, NC). For uptake and efflux studies with TCA, SCH were treated with 1 μM [³H]TCA (400 nCi/mL) in 0.3 mL/well standard HBSS for 20 min at 37°C. After the 20-min uptake phase, buffers containing TCA were removed, cells were washed twice with 0.3 mL/well standard or Ca²⁺-free HBSS buffer at 37°C, and the third application of buffer was added to SCH for the 15-min (rat) or 10-min (human) efflux phase (Figure 3.1). For determination of TGZ effects on TCA disposition, SCH were pre-incubated with 10 μM TGZ for 30 min before 10-min application of standard or Ca²⁺-free HBSS. The rest of experiment (uptake and efflux) was performed as described above. Pre-incubation was selected to minimize the inhibitory effects of TGZ and its metabolites on TCA uptake, and to allow enough time for the formation of TS, a potent BSEP inhibitor. TCA accumulation in cells+bile (standard HBSS) and cells (Ca²⁺-free HBSS) during uptake (2, 5, 10, and 20 min in human SCH; 2, 5, 10, 15, and 20 min in rat SCH) and efflux (2, 3.5, 5, and 10 min in human SCH; 2, 3.5, 5, 10, and 15 min in rat SCH) phases were determined by terminal sampling of n=3 wells at each time point. During the efflux phase, incubation buffer (standard HBSS or Ca²⁺-free HBSS) also was collected at the end of the each incubation period. Cells were washed twice in ice-cold HBSS, and were solubilized in 0.3 mL (24-well; human SCH) or 1 mL (6-well; rat SCH) 0.5% Triton X-100. Radioactivity in cell lysates and buffer samples was quantified by liquid scintillation counting (Packard TriCarb, Perkin-Elmer, Waltham, MA).

Pharmacokinetic Modeling

Pharmacokinetic modeling was employed to evaluate the hepatobiliary disposition of TCA (Control), and to determine the effects of TGZ on TCA disposition (+TGZ) in human and rat SCH. A model scheme incorporating linear parameters governing TCA disposition (Figure 3.2) were fit to mass versus time data from individual SCH experiments (Figure 3.3). The model fitting was performed with Phoenix WinNonlin, v6.1 (Certara, St. Louis, MO) using the stiff estimation method and a power model to account for residual error. The following differential equations, which were developed based on the model scheme depicted in Figure 3.2, were fit simultaneously to data generated in SCH in the presence of intact and disrupted bile canaliculi for each condition (human and rat; Control and +TGZ):

Mass in standard HBSS buffer:

$$\frac{dX_{\text{Buffer}}^+}{dt} = CL_{\text{BL}} \times C_{\text{Cell}}^+ + K_{\text{Flux}} \times X_{\text{Bile}} - CL_{\text{Uptake}} \times C_{\text{Buffer}}^+ - K_{\text{Wash}} \times X_{\text{Buffer}}^+ \quad X_{\text{Buffer}}^+ \circ = X_{\text{dose}}$$

Mass in Ca²⁺-free HBSS buffer:

$$\frac{dX_{\text{Buffer}}^-}{dt} = (CL_{\text{BL}} + CL_{\text{Bile}}) \times C_{\text{Cell}}^- - CL_{\text{Uptake}} \times C_{\text{Buffer}}^- - K_{\text{Wash}} \times X_{\text{Buffer}}^- \quad X_{\text{Buffer}}^- \circ = X_{\text{dose}}$$

Mass in cells:

$$\frac{dX_{\text{Cell}}^{+ \text{ or } -}}{dt} = CL_{\text{Uptake}} \times C_{\text{Buffer}}^{+ \text{ or } -} - (CL_{\text{BL}} + CL_{\text{Bile}}) \times C_{\text{Cell}}^{+ \text{ or } -} \quad X_{\text{Cell}}^{+ \text{ or } -} \circ = 0$$

Mass in bile (standard HBSS):

$$\frac{dX_{\text{Bile}}}{dt} = CL_{\text{Bile}} \times C_{\text{Cell}}^+ - K_{\text{Flux}} \times X_{\text{Bile}} \quad X_{\text{Bile}} \circ = 0$$

Mass in cells+bile (standard HBSS):

$$\frac{dX_{\text{Cells+Bile}}}{dt} = \frac{dX_{\text{Bile}}}{dt} + \frac{dX_{\text{Cell}}^+}{dt} \quad X_{\text{Cells+Bile}} \circ = 0$$

where variables and parameters are defined as in Figure 3.2, and K_{wash} was activated for 1 minute at the end of the 20-min uptake phase and fixed at $1 \times 10^4 \text{ min}^{-1}$ based on simulations to eliminate the TCA dose from the buffer compartment and represent the wash step. C_{Cell} represents the intracellular concentration, calculated as $X_{\text{Cell}}/V_{\text{Cell}}$, where cellular volume (V_{Cell}) was estimated based on the protein content of each preparation, using a value of 7.4 $\mu\text{L}/\text{mg}$ protein (31). C_{Buffer} represents the buffer concentration, calculated as $X_{\text{Buffer}}/V_{\text{Buffer}}$ where the buffer volume (V_{Buffer}) was constant (0.3 mL). Initial parameter estimates were obtained from noncompartmental analysis of SCH data, where CL_{Uptake} was estimated from the initial (2 min) uptake data as follows, $CL_{\text{Uptake}} = (dX_{\text{cells+bile}}/dt)/C_{\text{Buffer}}$. CL_{BL} and CL_{Bile} were estimated from efflux phase data under Ca²⁺-free conditions, where $(CL_{\text{BL}} + CL_{\text{Bile}}) = X_{\text{Buffer},0-15\text{min}}^- / \text{AUC}_{\text{cells},0-15\text{min}}^- \cdot K_{\text{Flux}}$, which represents the flux of substrate out of bile networks in standard HBSS conditions, was estimated initially from simulations using Berkeley-Madonna. The impact of impaired function of canalicular and/or basolateral efflux transporters on hepatic TCA exposure in human and rat SCH was simulated using the TCA model and parameter estimates (Figure 3.2 and Table 3.1); parameters representing transport-

mediated efflux (CL_{BL} and CL_{Bile}) were decreased by 10-fold in isolation, or in combination, in human and rat SCH; the resulting changes in predicted cellular TCA concentrations are plotted in Figure 3.5. To determine the net effect of impaired function of uptake and/or efflux (basolateral and canalicular) transporters on hepatic TCA exposure in human SCH, simulations were performed by decreasing CL_{Uptake} and CL_{Efflux} ($CL_{BL} + CL_{Bile}$) gradually by 10 to 100-fold in combination; it was assumed that both efflux pathways (CL_{BL} and CL_{Bile}) were impaired to the same extent. Simulated cellular TCA concentrations are presented in Figure 3.6. All simulations were performed using Berkeley-Madonna v.8.3.11.

Membrane Vesicles

Human MRP4 plasmid (pcDNA3.1(-)-MRP4) was kindly provided by Dr. Dietrich Keppler (German Cancer Research Center, Heidelberg, Germany). HEK293T cell lines stably transfected with pcDNA3.1(-)-MRP4 or an empty plasmid vector (control) were established as previously described (14). Membrane vesicles were prepared from these cell lines, and transport experiments were carried out by a rapid filtration assay as described previously (32). Briefly, membrane vesicles (5 μ g protein) were incubated at 37°C in Tris-sucrose buffer (TSB; 50 mM Tris-HCl/250 mM sucrose) containing 10 mM $MgCl_2$, 10 mM creatine phosphate, 100 μ g/mL creatine kinase, 4 mM ATP or AMP, and [3H]DHEAS (0.7 μ Ci/mL) in the absence and presence of TS, in a volume of 50 μ L. After incubation for 2 min, the reaction was stopped by the addition of 0.8 mL ice-cold TSB and immediately applied to a glass fiber filter (type A/E, Pall Corp., Port Washington, NY) and washed twice with 2 mL ice-cold TSB. Filters were mixed by vortexing in 5 mL of scintillation fluid and radioactivity was quantified by liquid scintillation counting (Packard TriCarb, Perkin-Elmer, Waltham, MA). The ATP-dependent uptake of substrate was calculated by subtracting substrate uptake in the presence of AMP from substrate uptake in the presence of ATP. The MRP4-dependent uptake of substrate was calculated by subtracting ATP-dependent uptake in MRP4-overexpressing vesicles from that in control vesicles. Initially, the inhibitory effect of TS (10 μ M) on MRP4-dependent transport of [3H]DHEAS (2 μ M) was evaluated in the presence or absence of 3 mM GSH. Further studies were performed using concentration ranges of [3H]DHEAS (0.5 - 20 μ M) and TS (5 - 50 μ M) in the absence of GSH to determine the inhibition constant (K_i). Type of

inhibition and kinetic parameters (K_m , V_{max} , and K_i) were determined by fitting competitive, noncompetitive, and uncompetitive models by nonlinear regression using Phoenix WinNonlin, v6.1. Representative data from $n=2$ independent experiments in triplicate are presented in Figure 3.4.

Data Analysis

TCA accumulation was corrected for nonspecific binding to the BioCoat™ plate without cells, and normalized to protein concentration measured by the BCA protein assay (Pierce Chemical, Rockford, IL). The intracellular concentration of TCA was obtained by dividing TCA accumulation (pmol/mg protein) by the previously reported hepatocyte volume (7.4 μ l/mg protein) (31). Apparent ($CL_{Bile,app}$) and intrinsic ($CL_{Bile,int}$) biliary clearance values were calculated using B-CLEAR® technology (Qualyst Transporter Solutions, LLC, Durham, NC) based on the following equations:

$$CL_{Bile,app} = \frac{\text{Accumulation}_{\text{Cells+Bile}} - \text{Accumulation}_{\text{Cells}}}{AUC_{\text{Buffer},0-t}}$$

$$CL_{Bile,int} = \frac{\text{Accumulation}_{\text{Cells+Bile}} - \text{Accumulation}_{\text{Cells}}}{AUC_{\text{Cells}, 0-t}}$$

Where $AUC_{\text{Buffer},0-t}$ is the area under the TCA buffer concentration – time curve, which is the product of initial TCA buffer concentration (1 μ M) and incubation time (t), assuming that sink conditions of TCA in the buffer are maintained (concentration changes < 10% during the uptake phase). $AUC_{\text{Cell},0-t}$ is the area under the TCA cellular concentration – time curve, which was obtained using the linear trapezoidal rule. Paired Student's t-test was used to compare parameters in the presence or absence of TGZ pre-incubation. In all cases, $P < 0.05$ was considered statistically significant. All statistical analyses were performed using SigmaStat 3.5 (San Jose, CA).

RESULTS

TCA Disposition in Human and Rat SCH with and without TGZ Pre-incubation

TCA uptake and efflux studies were conducted as described in Figure 3.1. The mass-time profiles of TCA in cells+bile and cells (during the uptake and efflux phases), and buffer (during the efflux phase)

in human and rat SCH in the absence (Control) and presence (+TGZ) of TGZ pre-incubation are presented in Figure 3.3. Under all conditions, TCA accumulation in cells+bile and cells increased during the uptake phase and decreased during the efflux phase. Appearance of TCA in the standard and Ca²⁺-free HBSS buffer increased during the efflux phase. TGZ pre-incubation decreased TCA accumulation in cells+bile, cells, and the efflux into buffers in both human and rat SCH. $CL_{Bile,app}$ of TCA during the uptake phase was also significantly decreased after pre-incubation with TGZ compared to the Control group, indicating that TGZ decreased uptake and/or biliary excretion of TCA; in human SCH, $CL_{Bile,app}$ values after 10 min uptake (standard B-CLEAR[®] method) in Control and +TGZ groups were 11.9 ± 3.8 $\mu\text{l}/\text{min}/\text{mg}$ protein and 1.1 ± 0.24 $\mu\text{l}/\text{min}/\text{mg}$ protein, respectively ($P = 0.035$). The corresponding values in rat SCH were 4.3 ± 0.7 $\mu\text{l}/\text{min}/\text{mg}$ protein and 0.7 ± 0.12 $\mu\text{l}/\text{min}/\text{mg}$ protein, respectively ($P = 0.008$). TCA $CL_{Bile,int}$ was also significantly decreased after TGZ pre-incubation, suggesting that TGZ decreased TCA biliary excretion; in human SCH, $CL_{Bile,int}$ values after 10 min uptake in Control and +TGZ groups were 3.4 ± 0.83 $\mu\text{l}/\text{min}/\text{mg}$ protein and 1.7 ± 0.98 $\mu\text{l}/\text{min}/\text{mg}$ protein, respectively ($P = 0.004$). The corresponding values in rat SCH were 5.5 ± 0.95 $\mu\text{l}/\text{min}/\text{mg}$ protein and 2.0 ± 0.68 $\mu\text{l}/\text{min}/\text{mg}$ protein, respectively ($P = 0.049$).

Parameter estimates recovered from fitting differential equations (see Methods) based on the model scheme in Figure 3.2 to TCA accumulation data from independent SCH preparations are presented in Table 3.1. In the absence of TGZ pre-incubation (Control), human SCH showed greater CL_{Uptake} , slightly lower CL_{Bile} and notably lower CL_{BL} relative to rat SCH. This is consistent with greater cellular accumulation of TCA observed in human SCH (Figure 3.3). Interestingly, CL_{Bile} was about 3.3-fold greater than CL_{BL} in human SCH, whereas CL_{Bile} and CL_{BL} showed a similar contribution to the total cellular efflux of TCA in rat SCH in the absence of TGZ. In human SCH, TGZ pre-incubation significantly decreased CL_{Uptake} ($P = 0.017$); there were trends toward decreased CL_{BL} and CL_{Bile} after TGZ pre-incubation compared to the Control groups. In rat SCH, CL_{Bile} was significantly decreased after TGZ pre-incubation ($P = 0.017$); there were trends toward decreased CL_{Uptake} and CL_{BL} after TGZ pre-

incubation compared to the Control groups. However, these differences failed to reach statistical significance due to large variability in mean differences.

Inhibitory Effects of TS on MRP4-Mediated [³H]-DHEAS Transport in Membrane Vesicles

The inhibitory effects of TS on MRP4, a basolateral bile acid efflux transporter, were evaluated using membrane vesicles prepared from HEK293T cells overexpressing MRP4 or control cells. TS (10 μM) inhibited MRP4-mediated transport of [³H]-DHEAS (2 μM) by 78 and 72% in the absence and presence of GSH, respectively (Figure 3.4A). Inhibition of MRP4-mediated [³H]-DHEAS transport by TS was determined in membrane vesicles over a range of substrate concentrations (DHEAS, 0.5 – 20 μM) and inhibitor concentrations (TS, 5 – 50 μM), with a K_i value of 8.0 μM based on a non-competitive inhibition model (Figure 3.4B).

Impact of Impaired Function of Canalicular vs. Basolateral Efflux Transporters on Hepatic TCA Exposure

The altered hepatobiliary disposition of TCA due to impaired function of bile acid efflux transporters was simulated based on the TCA model described in this report (Figure 3.2 and Table 3.1). Simulated hepatic TCA concentrations –up to and including steady-state ($C_{H,ss}$) in human and rat SCH are shown in Figures 3.5A and 3.5B, respectively. CL_{Uptake} of TCA in rat SCH might have been underestimated compared to rats in vivo because it has been reported that TCA uptake clearance was decreased by 5-fold on day 4 compared to day 0 due to decrease in Ntcp protein expression, whereas TCA uptake clearance remained unchanged over time in human SCH (33-35). To account for decreased Ntcp function over days of culture, simulations also were performed with 5-fold higher CL_{Uptake} in rat SCH (Figure 3.5C). TCA $C_{H,ss}$ was higher in human SCH (11.1 μM) compared to rat SCH (1.9 μM) (Figures 3.5A and 3.5B); this is consistent with the observed higher cellular TCA accumulation during uptake and efflux studies compared to rat SCH (Figure 3.3). However, TCA $C_{H,ss}$ in rat SCH with 5-fold greater CL_{Uptake} (9.1 μM) is comparable to that in human SCH (Figures 3.5A and 3.5C). In human SCH, a 10-fold decrease in CL_{Bile} increased TCA $C_{H,ss}$ by 2.9-fold compared to control, whereas there was an 1.3-fold increase in TCA $C_{H,ss}$ relative to control when CL_{BL} was decreased by 10-fold (Figure 3.5A).

Interestingly, a 10-fold decrease in both CL_{Bile} and CL_{BL} increased TCA $C_{H,ss}$ by 7.0-fold compared to control, which is a greater-than proportional increase compared to inhibiting either pathway in isolation. In rat SCH, TCA $C_{H,ss}$ was increased by 2.0- and 1.6-fold when CL_{Bile} and CL_{BL} were decreased by 10-fold, respectively, relative to Control (Figure 3.5B). TCA $C_{H,ss}$ increased by 9.3-fold relative to control when both CL_{Bile} and CL_{BL} were decreased by 10-fold; similar to human SCH simulations, the increase in $C_{H,ss}$ is greater than proportional compared to when either pathway is impaired in isolation. The same trends were observed in rat SCH with 5-fold greater CL_{Uptake} (Figure 3.5C); the fold increase in TCA $C_{H,ss}$ was 1.9, 1.6, and 7.3 relative to control when CL_{Bile} , CL_{BL} , and both CL_{Bile} and CL_{BL} were decreased 10-fold, respectively.

Impact of Impaired Function of Uptake vs. Efflux Transporters on Hepatic TCA Exposure in Human SCH

Hepatic bile acid concentrations are determined by both hepatic uptake and efflux, and drugs that inhibit efflux transporters often also inhibit uptake transporters. To understand the net effects of impaired function of uptake and efflux transporters on hepatic TCA exposure, TCA $C_{H,ss}$ in human SCH was simulated based on various values of CL_{Uptake} and CL_{Efflux} ($CL_{Bile} + CL_{BL}$) (Figure 3.6). When CL_{Uptake} remained unchanged (fractional inhibition of $CL_{Uptake} = 0$), TCA $C_{H,ss}$ increased exponentially as the fractional inhibition of CL_{Efflux} increased. On the other hand, $C_{H,ss}$ decreased proportionally as the fractional inhibition of CL_{Uptake} increased, when CL_{Efflux} remained unchanged (fractional inhibition of $CL_{Efflux} = 0$). When the fractional inhibition of CL_{Uptake} and CL_{Efflux} were the same, TCA $C_{H,ss}$ remained unchanged (fold-change = 1). If the fractional inhibition of $CL_{Uptake} >$ the fractional inhibition of CL_{Efflux} , then TCA $C_{H,ss}$ was decreased (fold-change $<$ 1). If the fractional inhibition of $CL_{Uptake} <$ the fractional inhibition of CL_{Efflux} , then the fold-change in TCA $C_{H,ss}$ was greater than 1; TCA $C_{H,ss}$ increased exponentially with increasing fractional inhibition of CL_{Efflux} , but the fold-increase in TCA $C_{H,ss}$ decreased with increasing fractional inhibition of CL_{Uptake} . Notably, a greater than 10-fold increase in TCA $C_{H,ss}$ was observed only when the fractional inhibition of CL_{Uptake} was less than 0.6.

DISCUSSION

The present study determined the hepatobiliary disposition of TCA in human and rat SCH using a novel uptake and efflux protocol recently developed in our laboratory combined with pharmacokinetic modeling (28). The results demonstrated that species differences exist in the hepatocellular excretion of TCA; in human SCH, biliary excretion predominated, whereas biliary excretion and basolateral efflux contributed equally to hepatocellular TCA excretion in rat SCH (Table 3.1). Jemnitz et al. reported that basolateral and biliary excretion contribute equally to TCA efflux in human SCH, whereas basolateral efflux was the dominant cellular efflux pathway of TCA in rat SCH (23). The likely reason for these discrepancies is that TCA “flux” from the canalicular spaces into the buffer (K_{Flux} in Figures 3.1 and 3.2) was not considered by Jemnitz et al. In their study, basolateral efflux was evaluated by measuring TCA in standard buffer during the efflux phase. However, the amount of TCA that appeared in the buffer during the efflux phase was actually the sum of basolateral efflux and flux from the bile canalicular spaces, which led to an overestimation of basolateral efflux. To circumvent these issues and accurately estimate the relative contributions of CL_{BL} , CL_{Bile} , and K_{Flux} , pharmacokinetic modeling was employed in the current study.

After pre-incubation with TGZ, CL_{Bile} was significantly decreased (rat SCH) or tended to decrease (human SCH) compared to Control (Table 3.1), consistent with reported inhibitory effects of TGZ and TS on BSEP (6, 20). Interestingly, CL_{BL} tended to decrease after TGZ pre-incubation compared to Control, suggesting that TGZ and/or TS might also inhibit basolateral efflux of TCA. TGZ has been reported to inhibit basolateral efflux transporters, MRP3 and MRP4, but with less potency compared to its effects on BSEP (8). However, hepatic concentrations of TGZ are minimal whereas TS accumulates in hepatocytes due to extensive hepatic metabolism of TGZ (20, 21). To test the hypothesis that TS inhibits hepatic efflux transporters, the effects of TS on MRP4-mediated transport were investigated using membrane vesicles prepared from HEK293T cells overexpressing MRP4 or control cells. MRP4 was selected because TCA is transported by human MRP4, but not by human MRP3 (36, 37). Since GSH is co-transported with bile acids by MRP4 (36), the inhibitory effect of TS at a single concentration (10 μM)

was tested initially in the absence and presence of GSH. TS inhibited MRP4-mediated transport of [³H]-DHEAS to a similar extent regardless of GSH, suggesting that the inhibitory effects of TS on MRP4 are independent of GSH (Figure 3.4A). Further studies were performed in the absence of GSH, and revealed that TS inhibited MRP4-mediated [³H]-DHEAS transport by non-competitive inhibition with a K_i value of 8 μ M (Figure 3.4B).

In addition to efflux inhibition, CL_{Uptake} was significantly decreased (human SCH) or showed trends towards a decrease (rat SCH) compared to Control after TGZ pre-incubation (Table 3.1). Although TGZ is a potent inhibitor of NTCP/Ntcp-mediated bile acid uptake (19), TGZ concentrations in the buffer were minimal during the uptake phase because TGZ-containing buffer was removed and replaced with TGZ-free buffer during the 10-min pre-incubation (standard or Ca^{2+} -free buffers) as well as the 20-min uptake phase. These data suggest that TGZ might inhibit NTCP/Ntcp by mechanisms other than direct inhibition; further studies are needed to characterize the precise mechanism(s) of inhibition.

Preclinical animals often are less sensitive to bile acid-mediated DILI compared to humans, and thus, do not reliably predict human hepatotoxicity. Potential reasons include species differences in toxic bile acid composition, substrate and/or inhibitor specificity of bile acid transporters, and metabolism/detoxification pathways of bile acids (38-41). In addition, differential inhibition of hepatocellular excretion pathways, as demonstrated in the current study, may contribute to species differences in bile acid-mediated hepatotoxicity. Simulations revealed that impaired function of canalicular and/or basolateral efflux transporters led to differential hepatobiliary disposition of TCA in human and rat SCH. In human SCH, hepatic TCA concentrations, which are relevant to hepatotoxicity, were increased by 2.9-fold relative to control when canalicular transporter function was impaired, whereas impaired function of basolateral efflux transporters minimally increased hepatic TCA concentration (1.2-fold) (Figure 3.5A). This was expected due to the predominant role of biliary excretion and the minor contribution of basolateral efflux to the overall hepatocellular excretion of TCA in human SCH. Interestingly, impaired function of both canalicular and basolateral efflux transporters further increased hepatic TCA concentrations by 2.4-fold compared to impaired function of canalicular

transport alone (7.3-fold increase compared to control) (Figure 3.5A), suggesting that basolateral efflux, despite serving as a minor route of hepatic excretion under normal conditions, plays an important role as a compensatory efflux pathway when canalicular excretion is impaired in human hepatocytes.

Expression and/or function of Ntcp have been reported to decrease over days of culture in rat SCH, whereas it remains constant in human SCH; in rat SCH, TCA uptake clearance was decreased by 5-fold on day 4 compared to day 0 (33-35). Thus, the CL_{Uptake} of TCA is likely underestimated in rat SCH, but not in human SCH. Although robust functional or quantitative proteomics data for BSEP and MRP3/4 in SCH over time do not exist, available data suggest that protein expression of Bsep in rat SCH, and MRP3/4 in rat and human SCH remain relatively unchanged over days of culture (30, 34). To account for the decreased function of Ntcp in day 4 rat SCH, simulations were performed in rat SCH with a CL_{Uptake} estimate obtained in day 4 rat SCH (1X CL_{Uptake}) as well as a 5-fold greater CL_{Uptake} (5X CL_{Uptake}). When 5X CL_{Uptake} was employed, hepatic TCA concentrations were comparable between rat and human SCH (Figures 3.5B and 3.5C). In both human and rat SCH, an exponential increase in hepatic TCA concentrations was only observed when the function of both efflux pathways was decreased (Figure 3.5). These results are consistent with the mathematical relationship that governs fold-change in cellular exposure: $1/(1 - fe)$, where fe is the total fraction excreted by all pathways (biliary or basolateral) (42). Zamek-Gliszczyński et al. demonstrated that if multiple excretion pathways exist, minor changes in exposure (<2-fold) are expected when a transport pathway that contributes to less than 50% of total excretion is impaired, as noted when biliary excretion (rat) or basolateral efflux (human and rat) pathways alone are decreased in the current study. However, hepatic exposure increases exponentially in response to loss-of-function of transport pathways that contribute to >50% of total excretion, as noted in the current study when both biliary excretion and basolateral efflux transporters are impaired.

Bile acids undergo efficient enterohepatic recirculation; only ~5% of the bile acid pool is synthesized in hepatocytes, while the remaining 95% is re-absorbed from the intestinal lumen after biliary excretion, and taken up into hepatocytes (43). Therefore, in addition to canalicular and basolateral efflux transporters, hepatic bile acid exposure also is regulated by hepatic uptake transporters. Inhibition of bile

acid efflux transporters by drugs is reported to be associated with cholestatic/mixed type DILI, but often, these drugs also inhibit uptake transporters, which may exert protective effects (38); the net effect will be determined by the relative extent (potency) of uptake inhibition vs. efflux inhibition. As might be expected, simulations suggest that hepatic TCA exposure increases only when the extent of efflux inhibition exceeds that of uptake inhibition (Figure 3.6). Notably, fractional inhibition of $CL_{Uptake} > 0.6$ prevents hepatic TCA exposure from increasing by more than 10-fold, thereby confirming the protective effects of uptake inhibition. Simulations in the current study were performed using a constant fractional inhibition of uptake and efflux transporters throughout the simulation, assuming steady-state drug (inhibitor) concentrations in the medium and in the cell. In reality, drug concentrations change over time. Thus, dynamic changes in inhibitor concentrations should be considered by incorporating drug disposition into the model in order to more accurately predict altered bile acid disposition by a drug.

In the current study, species differences in hepatic excretion of TCA in human and rat SCH were identified. In human SCH, biliary excretion predominated, whereas biliary excretion and basolateral efflux contributed equally to TCA efflux in rat SCH. As a result, the hepatic accumulation of TCA in rat SCH due to inhibition of BSEP alone might not be as extensive as that observed in human SCH. In human and rat SCH, inhibition of both excretion pathways led to exponential increases in hepatic TCA exposure, suggesting that inhibition of both excretion pathways might have increased DILI liability. Alternatively, administration of a drug that inhibits one excretion pathway may predispose individuals with impaired transport function (due to disease or genetic polymorphisms) in the alternate pathway to hepatic bile acid accumulation and subsequent DILI. Simulations confirmed that uptake inhibition plays a protective role by helping to minimize hepatic bile acid accumulation. This work emphasizes that the inhibitory effects of a drug on bile acid transporters mediating uptake as well as multiple efflux pathways should be considered when evaluating the hepatotoxic potential of a drug.

Table 3.1. Summary of parameter estimates based on the model scheme depicted in Figure 3.2 describing taurocholic acid (TCA) disposition in human and rat sandwich-cultured hepatocytes (SCH) without (Control) or with 10 μ M Troglitazone (+TGZ) pre-incubation.

Human and rat SCH were treated with 1 μ M TCA (see Figure 3.1 for details of incubation conditions) and the model was fit simultaneously to all data from each preparation.

<i>Conditions:</i>	CL_{Uptake} (mL/min/g liver)	CL_{Bile} (mL/min/g liver)	CL_{BL} (mL/min/g liver)	K_{Flux} (min ⁻¹)
<u>Human SCH</u>				
Control	4.8 \pm 0.94	0.31 \pm 0.09	0.094 \pm 0.042	0.043 \pm 0.015
+TGZ	0.51 \pm 0.08*	0.19 \pm 0.15	0.050 \pm 0.041	0.070 \pm 0.036
<u>Rat SCH</u>				
Control	2.1 \pm 0.83	0.61 \pm 0.13	0.47 \pm 0.13	0.053 \pm 0.015
+TGZ	0.36 \pm 0.07	0.33 \pm 0.09*	0.39 \pm 0.11	0.077 \pm 0.038

Data are presented as mean \pm SD of individual fits from n=3 SCH preparations; *, significantly different from Control ($P < 0.05$)

Figure 3.1. Schemes depicting the uptake and efflux protocol.

(A) Uptake and efflux studies were conducted in the presence of standard (+Ca²⁺) Hanks' balanced salt solution (HBSS). (B) Tight junctions remained open throughout the study period by pre-incubating with Ca²⁺-free HBSS, then performing an uptake phase in standard HBSS to provide relief from the removal of Ca²⁺, followed by a brief wash and efflux in Ca²⁺-free HBSS. Dashed box represents pre-incubation with 10 μM troglitazone (TGZ) for TGZ-treated groups. Gray shading represents inclusion of the substrate, 1 μM taurocholic acid (TCA), in Standard HBSS during the uptake phase. Black shading represents 1 min wash. Cell schemes on the right represent the intended condition of the SCH system during the efflux phase, with arrows depicting the potential pathways leading to substrate efflux from cells + bile (A) and cells (B); CL_{BL}, CL_{Bile}, and K_{Flux} represent basolateral efflux, biliary excretion, and flux from the bile networks (depicted by the dashed arrow), respectively.

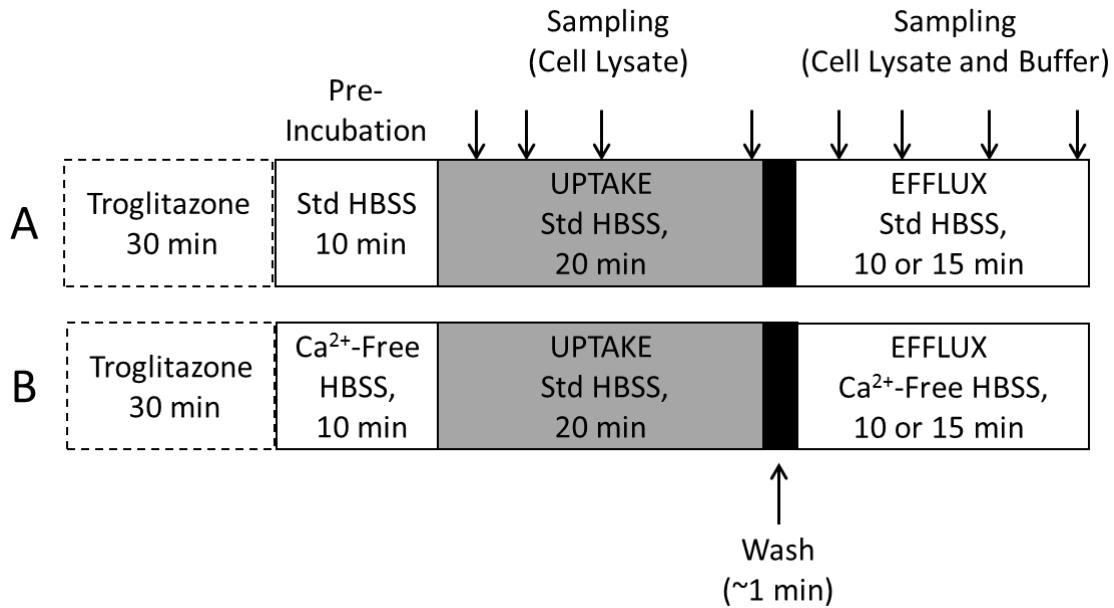
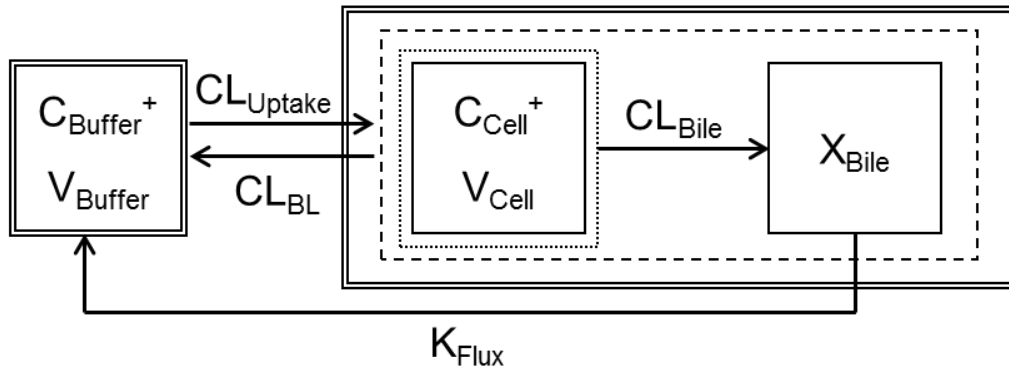


Figure 3.2. Model schemes depicting the disposition of taurocholic acid (TCA) in sandwich-cultured hepatocytes (SCH) studies based on the experimental design depicted in Figure 3.1.

X, V, and C denote mass of TCA, compartmental volume, and compartmental concentration, respectively. Subscripts on mass, volume, and concentration terms denote the corresponding compartment in the model scheme. Superscripts represent the presence (+, intact tight junctions; cells + bile) and absence (-, modulated tight junctions; cells) of Ca^{2+} in the pre-incubation and efflux buffer. $\text{CL}_{\text{uptake}}$, CL_{BL} , and CL_{Bile} represent clearance values for uptake from buffer into hepatocytes, efflux from hepatocytes into buffer, and canalicular excretion from hepatocytes, respectively. K_{Flux} represents the first order rate constant for flux from bile networks into buffer.

Standard HBSS ($X_{\text{Cell+Bile}}$, X_{Buffer^+}):



Ca^{2+} -free HBSS (X_{Cell} , X_{Buffer^-}):

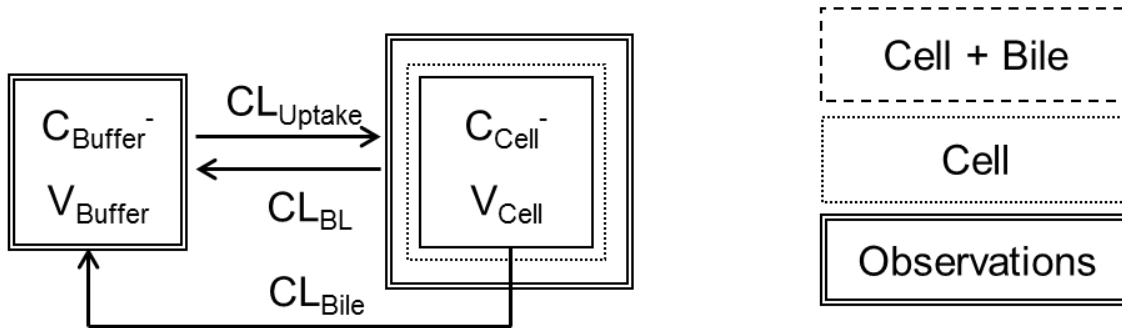


Figure 3.3. Taurocholic acid (TCA) mass versus time data in rat and human sandwich-cultured hepatocytes (SCH) in the absence (Control) or presence of 10 μ M troglitazone (TGZ) pre-incubation.

Closed symbols/solid lines represent TCA in cells + bile (standard HBSS), and open symbols/dashed lines represent TCA in cells (Ca^{2+} -free HBSS). The simulated mass-time profiles were generated from the relevant equations based on the model scheme depicted in Figure 3.2, and the final parameter estimates are reported in Table 3.1. Data (pmol/mg protein) represent mean \pm S.E.M. (n=3 SCH preparations in triplicate per group).

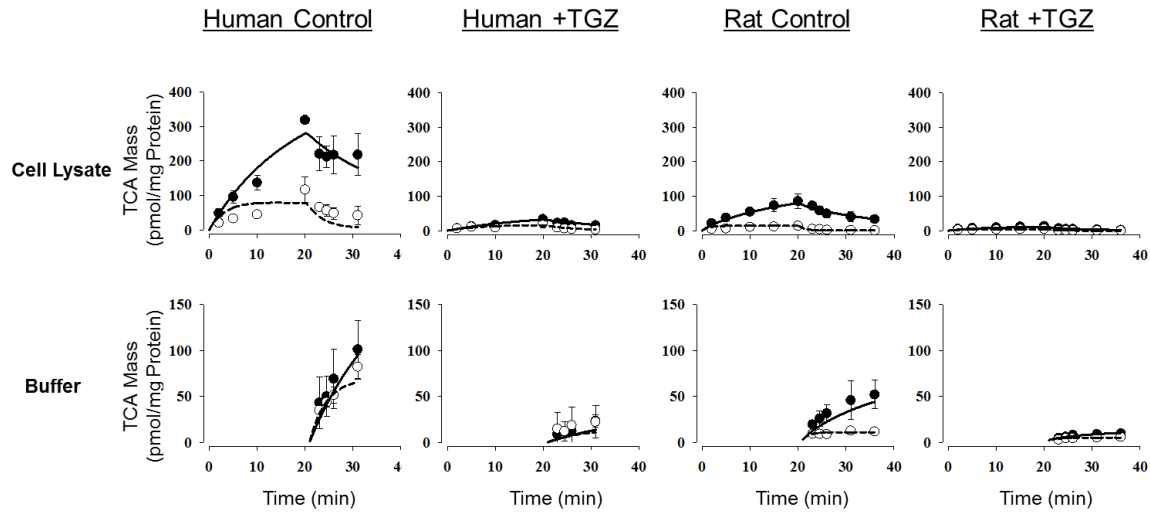


Figure 3.4. Inhibition of multidrug resistance-associated protein 4 (MRP4)-mediated transport of [³H]dehydroepiandrosterone sulfate (DHEAS) by troglitazone sulfate (TS) in membrane vesicles from MRP4-overexpressing and control human embryonic kidney cells.

Effect of GSH (3 mM) on MRP4-mediated transport of 2 μ M DHEAS and inhibition by 10 μ M TS. (B) Effect of increasing concentrations of TS (0, 5, 10, and 50 μ M) on MRP4-mediated DHEAS (2 min, 0.5 - 20 μ M) transport in the absence of GSH. Each point represents mean \pm S.D.

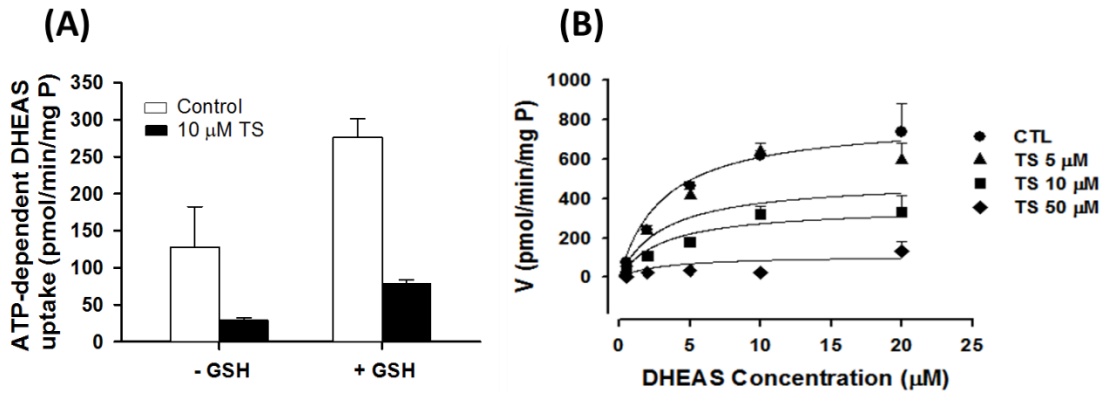


Figure 3.5. Impact of impaired function of canalicular and/or basolateral efflux transporters on hepatic TCA exposure.

Cellular TCA concentrations in human and rat SCH were simulated based on the TCA model scheme depicted in Figure 3.2 and parameter estimates (Table 3.1). Parameters representing transport-mediated efflux (CL_{BL} and CL_{Bile}) were decreased by 10-fold in isolation, or in combination, to represent impaired function of canalicular efflux transporters (solid line with open circle), basolateral efflux transporters (dashed line), and both pathways (dashed line with closed circle). Simulations were performed for 200 minutes to obtain steady-state intracellular concentrations; the time to reach steady-state was longer when efflux pathways were impaired compared to control.

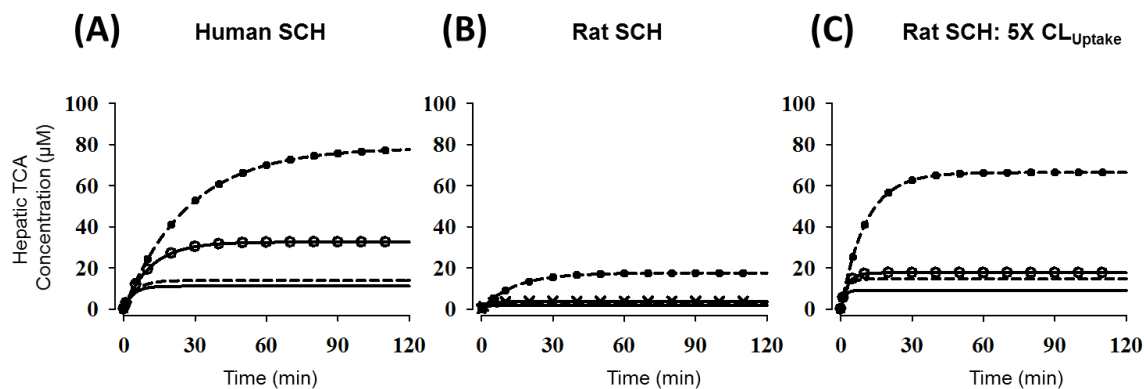
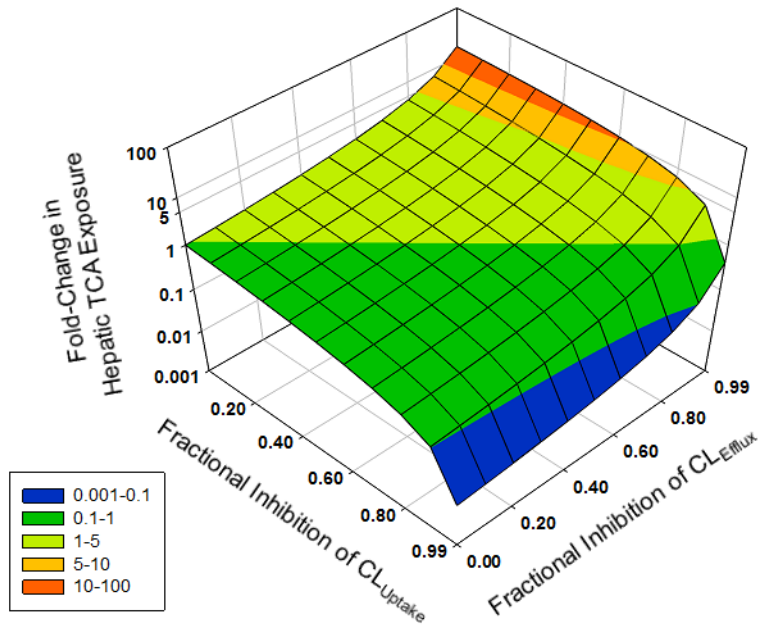


Figure 3.6. Net effects of inhibition of uptake and efflux transporters on hepatic TCA exposure.

Cellular TCA concentrations in human SCH were simulated as a function of decreased (10- to 100-fold) CL_{Uptake} and CL_{Efflux} ($CL_{BL} + CL_{Bile}$); both efflux pathways (CL_{BL} and CL_{Bile}) were assumed to be impaired to the same extent. The Z-axis represents the fold-change in steady-state hepatic TCA concentrations; 10 to 100-fold (orange), 5 to 10-fold (yellow), 1 to 5-fold (light green), 0.1 to 1-fold (dark green), and 0.001 to 0.1-fold (blue).



REFERENCES

- (1) Hofmann, A.F. Bile Acids: The Good, the Bad, and the Ugly. *News Physiol Sci* **14**, 24-9 (1999).
- (2) Nguyen, A. & Bouscarel, B. Bile acids and signal transduction: role in glucose homeostasis. *Cellular signalling* **20**, 2180-97 (2008).
- (3) Maillette de Buy Wenniger, L. & Beuers, U. Bile salts and cholestasis. *Dig Liver Dis* **42**, 409-18 (2010).
- (4) Perez, M.J. & Briz, O. Bile-acid-induced cell injury and protection. *World J Gastroenterol* **15**, 1677-89 (2009).
- (5) Jansen, P.L. *et al.* Hepatocanalicular bile salt export pump deficiency in patients with progressive familial intrahepatic cholestasis. *Gastroenterology* **117**, 1370-9 (1999).
- (6) Dawson, S., Stahl, S., Paul, N., Barber, J. & Kenna, J.G. In vitro inhibition of the bile salt export pump correlates with risk of cholestatic drug-induced liver injury in humans. *Drug Metab Dispos* **40**, 130-8 (2012).
- (7) Morgan, R.E. *et al.* Interference with bile salt export pump function is a susceptibility factor for human liver injury in drug development. *Toxicol Sci* **118**, 485-500 (2010).
- (8) Morgan, R.E. *et al.* A Multifactorial Approach to Hepatobiliary Transporter Assessment Enables Improved Therapeutic Compound Development. *Toxicol Sci*, (2013).
- (9) Pedersen, J.M. *et al.* Early Identification of Clinically Relevant Drug Interactions With the Human Bile Salt Export Pump (BSEP/ABCB11). *Toxicol Sci* **136**, 328-43 (2013).
- (10) Akita, H., Suzuki, H. & Sugiyama, Y. Sinusoidal efflux of taurocholate is enhanced in Mrp2-deficient rat liver. *Pharm Res* **18**, 1119-25 (2001).
- (11) Zollner, G. *et al.* Expression of bile acid synthesis and detoxification enzymes and the alternative bile acid efflux pump MRP4 in patients with primary biliary cirrhosis. *Liver Int* **27**, 920-9 (2007).
- (12) Trauner, M., Wagner, M., Fickert, P. & Zollner, G. Molecular regulation of hepatobiliary transport systems: clinical implications for understanding and treating cholestasis. *J Clin Gastroenterol* **39**, S111-24 (2005).

- (13) Ballatori, N., Li, N., Fang, F., Boyer, J.L., Christian, W.V. & Hammond, C.L. OST alpha-OST beta: a key membrane transporter of bile acids and conjugated steroids. *Front Biosci* **14**, 2829-44 (2009).
- (14) Kock, K. *et al.* Risk Factors for Development of Cholestatic Drug-induced Liver Injury: Inhibition of Hepatic Basolateral Bile Acid Transporters MRP3 and MRP4. *Drug Metab Dispos*, (2013).
- (15) Watkins, P.B. & Seeff, L.B. Drug-induced liver injury: summary of a single topic clinical research conference. *Hepatology* **43**, 618-31 (2006).
- (16) Watkins, P.B. & Whitcomb, R.W. Hepatic dysfunction associated with troglitazone. *N Engl J Med* **338**, 916-7 (1998).
- (17) St Peter, J.V., Neafus, K.L., Khan, M.A., Vessey, J.T. & Lockheart, M.S. Factors associated with the risk of liver enzyme elevation in patients with type 2 diabetes treated with a thiazolidinedione. *Pharmacotherapy* **21**, 183-8 (2001).
- (18) Funk, C. *et al.* Troglitazone-induced intrahepatic cholestasis by an interference with the hepatobiliary export of bile acids in male and female rats. Correlation with the gender difference in troglitazone sulfate formation and the inhibition of the canalicular bile salt export pump (Bsep) by troglitazone and troglitazone sulfate. *Toxicology* **167**, 83-98 (2001).
- (19) Marion, T.L., Leslie, E.M. & Brouwer, K.L. Use of sandwich-cultured hepatocytes to evaluate impaired bile acid transport as a mechanism of drug-induced hepatotoxicity. *Mol Pharm* **4**, 911-8 (2007).
- (20) Funk, C., Ponelle, C., Scheuermann, G. & Pantze, M. Cholestatic potential of troglitazone as a possible factor contributing to troglitazone-induced hepatotoxicity: in vivo and in vitro interaction at the canalicular bile salt export pump (Bsep) in the rat. *Mol Pharmacol* **59**, 627-35 (2001).
- (21) Lee, J.K., Marion, T.L., Abe, K., Lim, C., Pollock, G.M. & Brouwer, K.L. Hepatobiliary disposition of troglitazone and metabolites in rat and human sandwich-cultured hepatocytes: use of Monte Carlo simulations to assess the impact of changes in biliary excretion on troglitazone sulfate accumulation. *J Pharmacol Exp Ther* **332**, 26-34 (2010).
- (22) Iusuf, D., van de Steeg, E. & Schinkel, A.H. Hepatocyte hopping of OATP1B substrates contributes to efficient hepatic detoxification. *Clin Pharmacol Ther* **92**, 559-62 (2012).
- (23) Jemnitz, K., Veres, Z. & Vereczkey, L. Contribution of high basolateral bile salt efflux to the lack of hepatotoxicity in rat in response to drugs inducing cholestasis in human. *Toxicol Sci* **115**, 80-8 (2010).

- (24) Pfeifer, N.D., Hardwick, R.N. & Brouwer, K.L. Role of hepatic efflux transporters in regulating systemic and hepatocyte exposure to xenobiotics. *Annu Rev Pharmacol Toxicol* **54**, 509-35 (2014).
- (25) Oshio, C. & Phillips, M.J. Contractility of bile canaliculi: implications for liver function. *Science* **212**, 1041-2 (1981).
- (26) Phillips, M.J., Oshio, C., Miyairi, M., Katz, H. & Smith, C.R. A study of bile canalicular contractions in isolated hepatocytes. *Hepatology* **2**, 763-8 (1982).
- (27) Watanabe, N., Tsukada, N., Smith, C.R. & Phillips, M.J. Motility of bile canaliculi in the living animal: implications for bile flow. *J Cell Biol* **113**, 1069-80 (1991).
- (28) Pfeifer, N.D., Yang, K. & Brouwer, K.L. Hepatic basolateral efflux contributes significantly to rosuvastatin disposition I: characterization of basolateral versus biliary clearance using a novel protocol in sandwich-cultured hepatocytes. *J Pharmacol Exp Ther* **347**, 727-36 (2013).
- (29) Saha, S., New, L.S., Ho, H.K., Chui, W.K. & Chan, E.C. Direct toxicity effects of sulfo-conjugated troglitazone on human hepatocytes. *Toxicol Lett* **195**, 135-41 (2010).
- (30) Swift, B., Pfeifer, N.D. & Brouwer, K.L. Sandwich-cultured hepatocytes: an in vitro model to evaluate hepatobiliary transporter-based drug interactions and hepatotoxicity. *Drug Metab Rev* **42**, 446-71 (2010).
- (31) Lee, J.K. & Brouwer, K.R. Determination of Intracellular Volume of Rat and Human Sandwich-Cultured Hepatocytes (Abstract ID 1595). *The Toxicologist, Supplement to Toxicological Sciences* **114**, 339 (2010).
- (32) Ghibellini, G., Leslie, E.M., Pollack, G.M. & Brouwer, K.L. Use of tc-99m mebrofenin as a clinical probe to assess altered hepatobiliary transport: integration of in vitro, pharmacokinetic modeling, and simulation studies. *Pharmaceutical research* **25**, 1851-60 (2008).
- (33) Kotani, N. *et al.* Culture period-dependent changes in the uptake of transporter substrates in sandwich-cultured rat and human hepatocytes. *Drug Metab Dispos* **39**, 1503-10 (2011).
- (34) Tchapanian, E.H., Houghton, J.S., Uyeda, C., Grillo, M.P. & Jin, L. Effect of culture time on the basal expression levels of drug transporters in sandwich-cultured primary rat hepatocytes. *Drug Metab Dispos* **39**, 2387-94 (2011).
- (35) Liu, X. *et al.* Partial maintenance of taurocholate uptake by adult rat hepatocytes cultured in a collagen sandwich configuration. *Pharm Res* **15**, 1533-9 (1998).

- (36) Rius, M., Hummel-Eisenbeiss, J., Hofmann, A.F. & Keppler, D. Substrate specificity of human ABCC4 (MRP4)-mediated cotransport of bile acids and reduced glutathione. *Am J Physiol Gastrointest Liver Physiol* **290**, G640-9 (2006).
- (37) Akita, H., Suzuki, H., Hirohashi, T., Takikawa, H. & Sugiyama, Y. Transport activity of human MRP3 expressed in Sf9 cells: comparative studies with rat MRP3. *Pharm Res* **19**, 34-41 (2002).
- (38) Leslie, E.M., Watkins, P.B., Kim, R.B. & Brouwer, K.L. Differential inhibition of rat and human Na⁺-dependent taurocholate cotransporting polypeptide (NTCP/SLC10A1) by bosentan: a mechanism for species differences in hepatotoxicity. *J Pharmacol Exp Ther* **321**, 1170-8 (2007).
- (39) Chiang, J.Y. Bile acids: regulation of synthesis. *J Lipid Res* **50**, 1955-66 (2009).
- (40) Hofmann, A.F. Detoxification of lithocholic acid, a toxic bile acid: relevance to drug hepatotoxicity. *Drug Metab Rev* **36**, 703-22 (2004).
- (41) Setchell, K.D. *et al.* Bile acid concentrations in human and rat liver tissue and in hepatocyte nuclei. *Gastroenterology* **112**, 226-35 (1997).
- (42) Zamek-Gliszczynski, M.J., Kalvass, J.C., Pollack, G.M. & Brouwer, K.L. Relationship between drug/metabolite exposure and impairment of excretory transport function. *Drug Metab Dispos* **37**, 386-90 (2009).
- (43) Hofmann, A.F. The continuing importance of bile acids in liver and intestinal disease. *Arch Intern Med* **159**, 2647-58 (1999).

CHAPTER 4. An Experimental Approach to Evaluate the Impact of Impaired Transport Function on Hepatobiliary Drug Disposition using Mrp2-deficient TR⁻ Rat Sandwich-Cultured Hepatocytes in Combination with Bcrp Knockdown¹

INTRODUCTION

Hepatocytes are polarized cells with distinct apical and basolateral domains. Transport proteins on the apical membrane are responsible for excretion of compounds into the bile canaliculus, whereas basolateral transport proteins mediate influx into hepatocytes and efflux back to sinusoidal blood. Hepatic canalicular and basolateral transport proteins play important roles in regulating the pharmacologic and toxicologic effects of many drugs by modulating hepatocellular exposure. Breast cancer resistance protein (BCRP), a member of the ATP-binding cassette (ABC) transporter family, is a half-transport protein that forms a functional homodimer or oligomer (1, 2). BCRP is highly expressed in the canalicular membrane of hepatocytes as well as in the intestine, breast, and placenta (3). BCRP substrates include glucuronide and sulfate conjugates [e.g., estrone-sulfate, estradiol-17 β -D-glucuronide (E₂17G), SN-38 glucuronide], anticancer drugs (e.g., irinotecan, SN-38, methotrexate, daunorubicin, doxorubicin), and some statins [e.g., pitavastatin, rosuvastatin (RSV)] (4-9). The pharmacokinetics and pharmacodynamics of these drugs may be affected by modulation of BCRP expression and/or function resulting from genetic polymorphisms or drug-drug interactions (DDIs).

Multidrug resistance-associated protein 2 (MRP2), is another member of the ABC transporter family that is expressed in the canalicular membrane of hepatocytes. Many drugs are substrates for both BCRP and MRP2 including RSV, methotrexate, doxorubicin, SN-38, and SN-38 glucuronide.

¹This chapter has been published in *Molecular Pharmaceutics*, and is presented in the style of that Journal: *Mol Pharm* 2014 Jan 30 [Epub ahead of print, doi: 10.1021/mp400471e].

Overlapping substrate specificity can make it challenging to predict the impact of altered function of one or more transport proteins on the hepatic and systemic exposure of substrates. A significant change in drug exposure is expected following loss-of-function of one or more transport pathways when clearance by that particular pathway (apical or basolateral) exceeds 50% of total clearance (10). Moreover, altered drug exposure as a result of impaired transport function depends on the remaining excretion routes, such as complimentary efflux transporters on the same membrane (e.g., canalicular excretion into bile) or alternative efflux transporters on the opposite membrane (e.g., basolateral excretion into sinusoidal blood). Thus, *in vitro* and *in vivo* models to assess changes in hepatocellular accumulation and routes of excretion of compounds in the setting of impaired transport function are greatly needed.

Several model systems have been proposed to assess the role of BCRP and MRP2 in the disposition of a substrate. One approach is the use of specific BCRP and MRP2 inhibitors in hepatocytes. However, inhibitors of BCRP (e.g., GF120918, Ko134, fumitremorgin C, mitoxantrone, novobiocin) and MRP2 (e.g., MK-571, benzbromarone) may not be specific enough to allow assessment of the role of individual proteins (11-13). Similarly, specific substrates have been employed in hepatocytes and transport protein overexpressing cells to evaluate quantitatively the contribution of an individual hepatic uptake transporter [i.e., relative activity factor (RAF) method] (14), but “specific” BCRP and MRP2 substrates are lacking due to the aforementioned overlapping substrate spectrum of these transport proteins. Although the use of transient or stably transfected cell lines expressing one or more transport proteins is a popular approach to assess the role of individual proteins in substrate disposition, this approach may be misleading. Expression levels of transport proteins in these *in vitro* systems may not be representative of the true physiologic state, and metabolic systems as well as other regulatory factors impacting hepatobiliary disposition of substrates may be absent or present at low levels, depending on the *in vitro* system. Thus, transport of substrates by a specific protein in transporter-expressing cells *in vitro* does not guarantee that the transporter will play a key role in substrate disposition *in vivo*.

Another approach is the use of naturally occurring, genetically-deficient rodents or genetically engineered animals lacking a specific transport protein. MRP2-deficient Wistar (TR⁻) rats and

Eisai-hyperbilirubinemic Sprague-Dawley rats have been used to delineate the role of Mrp2 in drug disposition *in vivo* (15, 16). Likewise, Bcrp knockout (*Abcg2*^{-/-}) mice have been used to investigate whether Bcrp is involved in the disposition of drugs such as RSV, methotrexate, mitoxantrone, and pitavastatin (8, 17-19). Recently, Mrp2 knockout rats and Bcrp knockout rats were generated using zinc finger nuclease technology, and knockout phenotypes in these rats were characterized using sulfasalazine and 5-(and 6)-carboxy-2',7'-dichlorofluorescein as probes for Bcrp and Mrp2 function, respectively (20, 21). While *in vivo* pharmacokinetic studies in these models provide insight regarding overall drug distribution and excretion, sandwich-cultured hepatocytes (SCH) prepared from rodents lacking a specific transport protein allow assessment of altered hepatobiliary disposition in isolation from other organs (22-24).

RNA interference (RNAi) is one approach to explore the consequences of impaired protein function, and has been used to knock down transport proteins in the SCH system. Tian et al. transfected rat SCH with synthetic small interfering RNA (siRNA) to specifically knock down protein levels of Mrp2 and Mrp3; approximately 50% knockdown was achieved using this approach (25). Knockdown of mRNA and protein levels of OATP1B1, OATP1B3, and OATP2B1 using siRNA has been reported in human SCH (26). In primary cells, it is technically challenging to reach high transfection efficiency. Delivery of short hairpin (sh) RNA using an adenoviral vector system resulted in high infection efficiency leading to high knockdown efficiency (27). Rat SCH infected with adenoviral vectors expressing shRNA targeting Bcrp exhibited a significant decrease in protein expression and activity of this canalicular transport protein; the disposition of digoxin, a P-gp substrate, and the expression of some other transport proteins was not affected (28).

To date, primary hepatocyte models lacking multiple transport proteins have not been established. Such a model may be of particular importance if it mimics the physiological condition when an administered drug inhibits the function of multiple transporters due to the non-specific nature of transport inhibitors. The purpose of this investigation was to develop an *in vitro* model system to assess the consequences of altered transport function when multiple proteins are involved in hepatic excretion.

Knockdown of Bcrp in SCH from TR⁻ and wild-type (WT) rats was developed as an *in vitro* system to assess the impact of impaired function of Bcrp and/or Mrp2 using probe substrates. RSV, a Bcrp and Mrp2 substrate, and taurocholate (TC), a model bile acid that is not transported by Bcrp and Mrp2, were selected as probe substrates for investigation. This report describes a two-stage statistical analysis strategy for optimizing the knockdown system.

EXPERIMENTAL METHODS

Chemicals

Penicillin-streptomycin solution, dexamethasone, Hanks' balanced salt solution (HBSS; with or without Ca²⁺ and Mg²⁺), collagenase (type IV), and Triton X-100 were purchased from Sigma-Aldrich (St. Louis, MO). Dulbecco's modified Eagle's medium (DMEM) and MEM nonessential amino acids were purchased from Invitrogen (Carlsbad, CA). Insulin/transferrin/selenium culture supplement, BioCoat culture plates, and MatrigelTM extracellular matrix were purchased from BD Biosciences Discovery Labware (Bedford, MA). [³H]TC (5 Ci/mmol; purity >97%) and [³H]E₂17G (50.3 Ci/mmol; purity >97%) were purchased from Perkin Elmer (Waltham, MA). [³H]RSV (10 Ci/mmol; purity >99%) was purchased from American Radiolabeled Chemicals (St. Louis, MO). All other chemicals and reagents were of analytical grade and were readily available from commercial sources.

Packaging of Recombinant shRNA-Expressing Adenoviral Vectors

Adenoviral vectors expressing small hairpin RNA (shRNA) targeting rat Bcrp (Ad-siBcrp), rat Mrp2 (Ad-siMrp2) or a non-targeted control shRNA (Ad-siNT) were packaged as published previously using the Adeno-XTM ViralTrak DsRed-Express Promoterless Expression System 2 (Clontech Laboratories, Mountain View, CA)(28). The titer of adenoviral vectors was measured using Adeno-X Rapid Titer Kit (Clontech Laboratories, Mountain View, CA). siRNA sequences targeting the rat Bcrp gene at positions 288-306 relative to the start codon were published previously(28); siRNA sequences targeting rat MRP2 at positions 4257-4275, and a non-target siRNA (Ad-siNT) control sequence (ATGTATTGGCCTGTATTAG) were obtained from Dharmacon (Chicago, IL).

Isolation and Culture of Rat SCH

Primary rat hepatocytes were isolated from male Wistar (220 – 300 g, Charles River Laboratories, Inc., Wilmington, MA) and TR⁻ (220 – 300 g, bred in-house; breeding stock obtained from Dr. Mary Vore, University of Kentucky, Lexington, KY) rats and seeded onto 24-well collagen-coated plates at a density of 0.35×10^6 cells/well in seeding medium (DMEM containing 5% fetal bovine serum, 10 μ M insulin, 1 μ M dexamethasone, 2 mM L-glutamine, 1% MEM nonessential amino acids, 100 units of penicillin G sodium, and 100 μ g of streptomycin). One hour after seeding, hepatocytes were infected with Ad-siBcrp, Ad-siMrp2, or Ad-siNT at multiplicity of infection (MOI) of 1, 3, 5, and 10 by replacing the seeding medium with fresh seeding medium containing virus. On the next day, medium including viruses was removed, and cells were overlaid with MatrigelTM at a concentration of 0.25 mg/ml in 0.5 ml/well ice-cold culture medium (DMEM supplemented with 0.1 μ M dexamethasone, 2 mM L-glutamine, 1% MEM nonessential amino acids, 100 units of penicillin G sodium, 100 μ g of streptomycin, and 1% insulin/transferrin/selenium). Culture medium was changed every 24 h until experiments were performed on day 4.

Quantitative Real-Time Polymerase Chain Reaction (RT-PCR)

Total RNA was isolated from cell lysates using the ABI RNA isolation system (Applied Biosystems, Foster City, CA). mRNA levels of rat Bcrp and β -actin (internal control) were measured by TaqMan real-time RT-PCR using an ABI Prism 7700 System (Applied Biosystems) as described previously (29). The TaqMan probe and primer sequences (5'-3') used for rat Bcrp were as follows: Forward (TGGATTGCCAGGCGTTCATT), Reverse (GTCCCAGTATGACTGTAACAA), and Probe (CTGCTCGGGAATCCTCAAGCTTCTG). Rat β -actin was detected using the following probe and primer sequences: Forward (TGCCTGACGGTCAGGTCA), Reverse (CAGGAAGGAAGG-CTGGAAG), and Probe (CACTAATCGGCAATGAGCGGTTCCG). Fold changes in mRNA levels of Bcrp were evaluated after normalizing the gene expression levels by those of β -actin ($2^{-\Delta\Delta C_t}$ method) as previously described (30).

Immunoblots

Cells were washed with HBSS and lysis buffer containing 1% NP-40, 0.1% Na⁺-deoxycholate, 1 mM EDTA, and complete protease inhibitor cocktail (Roche Diagnostics, Mannheim, Germany) was applied. Protein concentrations were measured by the BCA assay (Pierce, Rockford, IL). Whole-cell lysates (15 µg) were resolved on NuPAGE 4 to 20% Bis-Tris gel (Invitrogen, Carlsbad, CA), and the proteins were transferred to nitrocellulose membranes. After blocking in 5% non-fat milk in Tris-buffered saline with Tween 20 (TBST) for 30 min, blots were incubated overnight at 4°C with the following antibodies: Bcrp (BXP-53), Mrp2 (M2III-6), Mrp4 (M4I-10), and P-gp (C219) (Alexis Biochemicals, San Diego, CA); Oatp1a1 (AB3570P, Millipore, Billerica, MA); Bsep (K44, kind gift from Drs. Bruno Stieger and Peter Meier); and β-actin (C4, Chemicon, San Francisco, CA). After incubation with HRP-conjugated secondary antibody, signals were detected by chemiluminescent substrate Supersignal West Duro (Pierce, Rockford, IL) with a Bio-Rad VersaDoc imaging system; densitometry analysis was performed using Quantity One V4.1 software (Bio-Rad Laboratories, Hercules, CA).

Accumulation Studies in Rat SCH

Accumulation studies were conducted in SCH on day 4 as described previously (31). Briefly, cells were washed twice with 0.3 mL warm standard (Ca²⁺-containing) or Ca²⁺/Mg²⁺-free HBSS with 0.38 g/L EGTA (hereafter referred to as Ca²⁺-free) and incubated in the same buffer for 10 min at 37°C to maintain or disrupt tight junctions, respectively. Subsequently, cells were incubated at 37°C for 10 min with 0.25 ml standard HBSS containing [³H]TC, [³H]RSV, or [³H]E₂17G at 1 µM (100 nCi/ml). After 10 min, cells were washed 3x with ice-cold standard HBSS and lysed with 0.25 ml 0.5% (v/v) Triton X-100 in phosphate-buffered saline. Samples were quantified by a Tri-Carb 3100 TR liquid scintillation analyzer (Perkin Elmer, Waltham, MA). Transport function was normalized to the protein content of each preparation using the BCA protein assay. The biliary excretion index (BEI; %) was calculated using B-CLEAR[®] technology (Qualyst Transporter Solutions, Research Triangle Park, NC) as follows:

$$\text{BEI (\%)} = \frac{\text{Accumulation}_{\text{cells+bile}} - \text{Accumulation}_{\text{cells}}}{\text{Accumulation}_{\text{cells+bile}}} \times 100$$

Experimental Design

SCH were obtained from n=3 WT rats and n=3 TR⁻ rats. From each rat, sets of 3 SCH samples (“triplicates”) were systematically assigned by plate location to each of the 36 combinations of virus (Ad-siBcrp, Ad-siNT, non-infected), MOI (1, 3, 5, 10), and evaluation procedure (RT-PCR, immunoblots, RSV accumulation, TC accumulation, as noted in Figures 4.1, 4.2, 4.3). For each level of MOI, triplicates were assigned to the three levels of virus (Ad-siBcrp, Ad-siNT, non-infected) in ratios of 1:1:1. For RT-PCR and immunoblot assays, two of the triplicate samples were measured, which provided 2 numerical assay values that were averaged together as a preliminary step for statistical analysis. For the accumulation studies of probe substrates, triplicate samples provided 3 numerical assay values that were averaged together as a preliminary step for statistical analysis. MOI of 1 was intentionally not studied by RT-PCR and immunoblots; otherwise, the experimental design produced complete data (i.e., no missing values for any assays).

Auxiliary Experimental Designs

Preliminary experimentation briefly explored two alternatives to the recommended knockdown system: (1) a system using Ad-siMrp2 for knockdown as an alternative to relying on TR⁻ rat SCH, and (2) a system using Ad-siBcrp with Ad-siMrp2 for double-knockdown. SCH obtained from n=4 WT rats were systematically assigned to selected combinations of three factors: virus (Ad-siMrp2, Ad-siBcrp with Ad-siMrp2, Ad-siNT, non-infected), MOI (5, 10, 15, 20), and evaluation procedure (RT-PCR, immunoblots, probe accumulation). Intentionally, the combinations studied were assigned to either triplicate or duplicate sets of SCH samples from 2, 3, or 4 rats (as noted in Supplement Figures 4.1, 4.2, 4.3); otherwise, the design produced complete data (i.e., no missing values for the assays.)

Two-Stage Statistical Analysis Strategy

The “dose-finding” analyses of stage 1 (Figures 4.1, 4.2, 4.3) explored the dose-response relationship between MOI and measures of the resulting on-target and off-target effects. For the MOI ‘dose’ selected as optimal, stage 2 (Table 4.1) summarized for each of two probes, RSV and TC, the effects of suppressing Bcrp and/or Mrp2 function. Stages 1 and 2 illustrate proposed approaches for

MOI-selection and characterization of the effects of impaired transporter function on the disposition of compounds of interest.

In stage 1, the extent of Bcrp knockdown (Figure 4.1) was evaluated in terms of Bcrp mRNA expression, and separately in terms of Bcrp protein: the primary inferential analysis of Bcrp expression relied on a univariate repeated-measures analysis of variance model (unirep-ANOVA) assuming that mean expression was a function of seven categories defined by virus [Ad-siBcrp, Ad-siNT, and non-infected (MOI=0 only)] and MOI (3, 5, 10 for Ad-siBcrp and Ad-siNT). The model was fit to the TR⁻ rat SCH data, and separately to the WT rat SCH data yielding statistical estimates of mean expression [with 95% confidence intervals (CIs)], residual variance, and within-rat correlation. The extent of Bcrp knockdown was defined by the three mean differences between Ad-siBcrp infected (MOI=3, 5, 10) and non-infected (MOI=0) SCH. The null hypothesis “all three differences are exactly zero” was rejected if any of the three sub-hypotheses were rejected by the (modified-Bonferroni) Hochberg test procedure ($\alpha=0.05$). The same strategy was applied to similar hypothesis tests regarding Ad-siNT. The graphical summary was computed in terms of relative expression; specifically, the values for each rat type (WT or TR⁻) were expressed as a percent of the average that was observed in that non-infected SCH samples.

Continuing stage 1, potential off-target knockdown (Figure 4.2) was explored for a selection of six other proteins (Oatp1a1, Ntcp, Bsep, P-gp, Mrp4, and Mrp2) using the same graphical summary method and the same inferential analysis methods that were applied to Bcrp protein expression. For each protein, the unirep-ANOVA model was used to obtain point and confidence interval estimates of mean expression as a function of five categories defined by virus [Ad-siBcrp, Ad-siNT, and non-infected (MOI=0 only)] and MOI (5, 10 for Ad-siBcrp and Ad-siNT). The hypothesis testing strategy was as described above for Bcrp protein.

Completing stage 1, the dose-response relationship (Figure 4.3) between MOI and disposition of RSV and TC was explored in terms of total substrate accumulation (uptake in pmol/mg protein) and biliary excretion index (BEI %). The analysis relied on a unirep-ANOVA model assuming that the mean was a function of nine categories defined by virus [Ad-siBcrp, Ad-siNT, and non-infected (MOI=0 only)]

and MOI (1, 3, 5, 10 for Ad-siBcrp and Ad-siNT). The model was fit to the TR⁻ rat SCH data, and separately to the WT rat SCH data, yielding statistical estimates of mean levels of response (total accumulation and BEI), residual variance and within-rat correlation. Estimates of mean responses (individual and marginal) and differences among mean marginal responses were all tabulated together with 95% CIs. The off-target effects of Ad-siNT were defined by the four mean differences between Ad-siNT infected (MOI=1, 3, 5, 10) and non-infected (MOI=0) SCH. The null hypothesis “all four differences are exactly zero” was rejected if any of the four sub-hypotheses were rejected by the Hochberg test procedure ($\alpha=0.05$). The targeted effects of siBcrp expression were defined by the four MOI-specific mean differences between Ad-siBcrp and Ad-siNT infected SCH. The null hypothesis “all four differences are zero” was rejected if any of the four sub-hypotheses were rejected by the Hochberg test procedure ($\alpha=0.05$). The results from all eight unirep-ANOVA models are summarized in a graphical illustration (Figure 4.3).

In stage 2, best estimates (Table 4.1) of effects on the disposition of probes attributable to impaired Bcrp function and/or absence of Mrp2 function were obtained for total substrate accumulation (uptake in pmol/mg protein) and BEI (%) using the responses from the SCH samples that were non-infected compared to those administered virus at the MOI level selected as optimal ‘dose’. This stage 2 analyses relied on a unirep-ANOVA model assuming mean response was a function of the six categories of virus (Ad-siBcrp, Ad-siNT, non-infected) and WT or TR⁻ status. For probes RSV and TC, the resulting estimates of category means, marginal means, and contrasts thereof were tabulated with their SEs and 95% CIs. The null hypothesis tested via an F-test procedure ($\alpha=0.05$) included “effects of the viruses do not depend on WT or TR⁻ status”, “no difference between the marginal means for WT and TR⁻ rat SCH”, and “no differences among three virus-specific marginal means”. If and only if virus effects were detected, then an F-test procedure ($\alpha=0.05$) was performed for the two sub-hypotheses regarding marginal means: “off-target effects are zero (siNT vs. non-infected)”, “targeted effects are zero (siBcrp vs. siNT)”. The results from all four unirep-ANOVA models were summarized in Table 4.1.

For stages 1 and 2, auxiliary analyses were performed to more fully explore the data and to evaluate the robustness of the main results to reasonable perturbations of the statistical modeling assumptions and methods. For example, in stage 1, unrep-ANOVA models accounting for all three factors (WT or TR⁻ status, virus, and MOI) were evaluated and interactions were explored.

All statistical computations were performed using SAS software v9.2 (SAS Institute Inc., Cary, NC).

RESULTS

Targeted Knockdown of Bcrp in WT and TR⁻ Rat SCH

Relative to non-infected hepatocytes, mean levels of Bcrp mRNA (Figure 4.1A) decreased with increasing MOI of Ad-siBcrp in both WT and TR⁻ rat SCH. For MOI 10, the mean was only 12% and 6.5% of that in non-infected WT and TR⁻ rat SCH, respectively. In contrast, Ad-siNT infection had negligible impact on mean Bcrp mRNA. Similarly, for Bcrp protein (Figure 4.1B) the mean level decreased with increasing MOI of Ad-siBcrp in both WT and TR⁻ rat SCH relative to non-infected hepatocytes. In WT rat SCH, the mean decreased by 61%, 66%, and 81% with Ad-siBcrp at MOI of 3, 5, and 10, respectively. In TR⁻ rat SCH, the mean decreased by 33%, 65%, and 70%, respectively. In contrast, Ad-siNT infection had much less impact on the mean level of Bcrp protein in TR⁻ and WT rat SCH; however, for MOI of 10 in WT, the mean level was decreased by 47%, suggesting that off-target (non-specific) effects of viral infection can exist at high MOI (≥ 10) under the conditions of the proposed SCH knockdown system.

Off-Target Effects of Bcrp Knockdown on the Levels of Other Transport Proteins

For TR⁻ rat SCH, no off-target effects were detected for Oatp1a1, Ntcp, Bsep, P-gp, Mrp4, and Mrp2 proteins at MOI of 5 and 10 (Figure 4.2). For WT rat SCH, off-target effects (Ad-siNT vs. non-infected) were detected only for Mrp4 and Mrp2 proteins. Mean levels of Mrp4 protein were decreased by 30% and 55% with Ad-siNT at MOI of 5 and 10, and by 55% and 56% with Ad-siBcrp at MOI of 5 and 10, respectively, relative to non-infected SCH samples. For Mrp2 protein, an off-target effect was

statistically significant for Ad-siNT at MOI of 5, but not at MOI of 10, and not for Ad-siBcrp at either MOI level.

Effects of Impaired Transporter Function on Probe Disposition

Based on stage 1 analyses, MOI=5 was selected as the optimal ‘dose’ for stage 2 analyses of probes RSV and TC.

RSV Total Accumulation. Mean total accumulation of RSV was similar in WT and TR⁻ rat SCH, and minimally altered by viral infection. Stage 1 analyses (Figure 4.3A) did not detect off-target effects (siNT vs. non-infected), targeted effects (siBcrp vs. siNT), nor any effects with increasing MOI. In stage 2 analysis (Table 4.1), targeted and non-targeted effects were not detected in samples administered virus at the MOI of 5.

RSV BEI. MOI-dependent effects of virus and WT or TR⁻ status were observed in stage 1 analyses (Figure 4.3B). For WT rat SCH, a mean decrease in BEI due to off-target effects (siNT vs. non-infected) was detected at MOI of 5 and 10 only, and a mean decrease in BEI due to targeted effects (siBcrp vs. siNT) was detected at MOI of 5 and 10 only. For TR⁻ rat SCH, the pattern of response was similar but no effects were statistically significant. Stage 2 analyses (Table 4.1) detected effects for both factors. The marginal mean for TR⁻ was smaller than for WT rat SCH by 28.6% with 95% CI [5.8, 51.3]. The targeted and non-targeted effects were statistically significant: relative to non-infected samples, siNT reduced the marginal mean BEI by 7.8% [3.2, 12.4]; relative to siNT, siBcrp reduced the marginal mean BEI by 13.3% [7.5, 19.1]. The difference in BEI between non-infected and siBcrp was 21% [16.5, 25.7].

TC Total Accumulation. MOI-dependent effects were found in stage 1 analyses (Figure 4.3C): for WT rat SCH, the dose-dependent off-target effects were statistically significant for MOI of 3, 5 and 10. For TR⁻ rat SCH, off-target effects were not detected. For both WT and TR⁻ rat SCH, targeted effects were statistically significant only for MOI of 10. In stage 2 analyses (Table 4.1), focusing on MOI = 5, the marginal means were decreased by non-targeted and targeted effects: relative to non-infected samples, siNT reduced the marginal mean by 4.8 pmol/mg protein [1.9, 7.7]; relative to siNT, siBcrp reduced the

marginal mean by 5.1 pmol/mg protein [1.4, 8.8]. The difference between non-infected and siBcrp was 9.9 pmol/mg protein [7.0, 12.8].

TC BEI. In stage 1 analyses (Figure 4.3D) for TR⁻ rat SCH, off-target effects and targeted effects were statistically significant at an MOI of 10. In stage 2 analyses (Table 4.1), an off-target effect was evident: relative to non-infected samples, siNT reduced the marginal mean BEI by 6.3% [2.5, 10.1]. The targeted effect was not detected, as in comparison to siNT, siBcrp reduced the marginal mean BEI by only 1.2% [-3.7, 6.1]; however, the difference in BEI between non-infected and siBcrp, 7.5% [3.7, 11.3], was statistically significant. The difference in BEI between TR⁻ and WT, 12.6% [-2.1, 27.3], was not statistically significant.

Sensitivity Analyses and Exploratory Analyses. The main results of stage 1 and stage 2 analyses were robust to perturbations of the modeling assumptions (e.g., variance homogeneity across WT and TR⁻ rat SCH). In stage 1, a MOI-by-WT or TR⁻ interaction was observed in 3-factor models for the analyses of TC BEI (p=0.0038) and RSV total accumulation (p=0.0460); however, inclusion or exclusion of interactions and commonality assumptions yielded negligible changes in the main results of interest (data not presented).

Ancillary Study of Knockdown of Mrp2 in WT Rat SCH

Infection with Ad-siMrp2 decreased mean relative levels of Mrp2 protein by 45%, 79%, and 78% at MOI of 5, 10 and 15, respectively, compared to non-infected SCH (Supplement Figure 4.1). Infection with Ad-siNT decreased the mean by 39% at MOI of 10, suggesting that some off-target effects may exist for large MOI. In contrast, Ad-siNT or Ad-siMrp2 at MOI of 5, 10 and 15 had little influence on the mean relative level of Bcrp protein.

Mean total accumulation of E₂17G (Supplement Figure 4.2A) showed little evidence of targeted or off-target effects. Mean BEI values for E₂17G (Supplement Figure 4.2B) appeared to decrease slightly with increasing MOI. Mean total accumulation of TC (Supplement Figure 4.2C) was decreased by Ad-siNT and Ad-Mrp2 at MOI of 10, suggesting again that off-target effects become more prevalent at MOI ≥ 10. Mean BEI values for TC (Supplement Figure 4.2D) were influenced least by viral infection.

Due to the off-target effects on TC total accumulation at an MOI of 10, an MOI of 5 was selected for the double knockdown study.

Ancillary Study of Double Knockdown of Mrp2 and Bcrp in WT Rat SCH

To suppress both Mrp2 and Bcrp (Supplement Figure 4.3), SCH were infected with Ad-siNT at MOI of 10, Ad-siMrp2 and Ad-siBcrp (MOI of 5 each; total MOI=10), or not infected. The targeted effects (double knockdown vs. Ad-siNT) decreased the mean relative levels of Mrp2 protein and Bcrp protein by 67% and 64%, respectively, relative to non-infected control. However, off-target effects also were observed: Ad-siNT infection at MOI of 10 decreased the mean levels of Mrp2 protein and Bcrp protein by 47% and 30%, respectively, relative to non-infected SCH samples. MOI of 10 also induced off-target effects in Bcrp knockdown SCH described elsewhere in this report; at MOI=10, Ad-siNT decreased mean relative levels of Bcrp (Figure 4.1B) and Mrp4 (Figure 4.2) in WT rat SCH, and altered hepatobiliary disposition of probe substrates [i.e. TC total accumulation in WT SCH (Figure 4.3C), RSV BEI in WT SCH (Figure 4.3B), and TC BEI in TR⁻ SCH (Figure 4.3D)].

DISCUSSION

Protein knockdown in cultured primary hepatocytes is challenging because it is difficult to reach high transfection efficiency using conventional transfection reagents. Our laboratory previously had established an efficient and specific Bcrp knockdown system in WT rat SCH in 6-well plates using adenoviral vectors to deliver shRNA into hepatocytes (28). In the present study, that work was extended to establish an *in vitro* system exhibiting impaired function of multiple specific transport proteins in the 24-well plate format. Scaling from 6-well to 24-well plates enabled more efficient use of hepatocytes and other resources required for the study. Initially, double knockdown of both Mrp2 and Bcrp was attempted. However, off-target effects in 24-well rat SCH were noted at the higher MOI required to knock down multiple transport proteins. Because an MOI of 5 was required for efficient knockdown of each transport protein (Mrp2 and Bcrp), the combination of two different shRNA targeting different transport proteins required an MOI of 10, at which off-target effects were prevalent. Use of a tandem plasmid vector that

expresses two different shRNA to facilitate the simultaneous double knockdown of genes has been applied in stable cell lines (32). However, plasmid DNA has low transfection efficiency into primary hepatocytes (27), and adenoviral vectors that similarly express tandem expression shRNA are not commercially available. Therefore, efficient double-knockdown of transport proteins using the adenoviral vector approach necessitated a higher viral load in hepatocytes. In order to circumvent this problem, Mrp2-deficient TR⁻ rat SCH were employed in combination with Bcrp knockdown using adenoviral infection of shRNA targeting Bcrp.

To validate this *in vitro* system, the impact of Bcrp knockdown on the hepatobiliary disposition of RSV and TC was examined in the absence and presence of functional Mrp2. RSV and TC were selected as probe substrates because different mechanisms dominate their hepatocellular uptake and biliary excretion. The results, for a range of MOI ‘doses’ with multiple viral vectors (siNT vs. siBcrp or siMrp2), demonstrated the importance of optimizing the system when an RNAi approach is employed to knock down transport proteins. This approach allows greater confidence in identification of off-target effects and interactions among factors that might otherwise have been dismissed as spurious if evaluated at only one level of MOI. This report demonstrates the use of a two-stage statistical analysis: stage 1 evaluated targeted and off-target effects for a range of MOI in order to identify dose-response relationships and select an optimal MOI ‘dose’ for the system. Stage 2 summarized for each of two probes, RSV and TC, the effects of impaired Bcrp and/or Mrp2 function. Results of stages 1 and 2 analyses demonstrated MOI-selection and characterization of the effects of impaired transporter function on the disposition of compounds of interest. Since changes in protein levels may not always translate to changes in protein activity, use of relevant probe substrates (positive and negative controls; TC and RSV in this study) to assess changes in protein activity is strongly recommended.

The MOI of 5 was chosen as the optimal ‘dose’ for use in stage 2 analyses of the relative contributions of Mrp2 and Bcrp to the hepatobiliary disposition of the probe substrates. The main considerations in choosing the optimal MOI ‘dose’ were the MOI-dependent patterns of targeted and off-target effects observed in stage 1. For example, targeted effects on RSV BEI were observed at MOI of 5

and 10. In analysis of total accumulation of TC, off-target effects were evident at MOI of 3, 5, and 10. At MOI of 10, off-target effects were maintained or increased based on immunoblots and TC BEI. These data suggest that an MOI of 5 is a better choice than an MOI of 3 or 10.

In stage 1 analyses, some evidence of interactions between MOI and WT or TR⁻ status were observed in auxiliary unirep-ANOVA models for TC BEI and RSV total accumulation. Such interactions are biologically plausible because loss of Mrp2 function (as in TR⁻ rats) may alter the regulatory machinery of the cell due to accumulation of endogenous substances such as bilirubin and bile acid conjugates. This study is consistent with the premise that altered function of individual transport proteins does not occur in isolation. Rather, as a result of overlapping substrate specificity and reliance on multiple mechanisms for vectorial transport from blood to bile, a complex network of cellular regulation is perturbed along with transport function, leading to compensatory changes. If so, it is advantageous to use an organ-specific *in vitro* model system, such as SCH, which recapitulates the relevant disposition, regulatory mechanisms and interplay expected *in vivo*.

At MOI of 5, viral infection had minimal effects on RSV total accumulation. The non-targeted effect (siNT vs. non-infected) statistically significantly decreased the mean BEI of RSV, and the targeted effect (siBcrp vs siNT) further reduced mean BEI of RSV, consistent with the statistically significant mean decrease in Bcrp protein attributed to siBcrp. Mean BEI of RSV was decreased further by TR⁻ status, suggesting an additive effect of targeted Bcrp knockdown and loss of Mrp2 function. Since Bcrp expression and function are decreased significantly in TR⁻ rat SCH (33), reduced RSV BEI in Bcrp knockdown TR⁻ rat SCH resulted from the combined effects of lack of Mrp2, an inherent decrease in Bcrp expression, and targeted knockdown of Bcrp. This is consistent with the known role of Bcrp and Mrp2 in the biliary excretion of RSV *in vivo* in rats (17).

For TC, mean total accumulation and mean BEI values were decreased after viral infection relative to non-infected hepatocytes. TC is a bile acid that is not transported by Bcrp and Mrp2. This finding may be attributed to off-target effects of viral infection on uptake and efflux pathways involved in the hepatobiliary disposition of bile acids. If so, Ntcp function or Bsep function might also be altered by

viral infection. Although the immunoblot analysis failed to detect off-target effects for Ntcp and Bsep proteins, this system should be used with caution when testing the hepatobiliary disposition of Ntcp and/or Bsep substrates. Since RSV is transported by human NTCP, but not by rat Ntcp (34), RSV uptake was not influenced by potential off-target effects on Ntcp function in this system.

Viral infection appeared to exert differential off-target effects on individual transport proteins. Mean levels of Mrp4 protein were decreased in siNT- and siBcrp-infected hepatocytes at MOI of 5 and 10. Viral infection also decreased mean levels of Mrp2 protein in siNT-infected rat SCH, whereas off-target effects of viral infection were not detected on other transport proteins. Notably, off-target effects on Mrp4 were observed in WT, but not in TR⁻ SCH. Mrp4 is known to be induced by constitutive androstane receptor (CAR) (35), which is activated by bilirubin and bile acids (36, 37). Thus, it is plausible that accumulation of organic anions such as bilirubin and bile acids in TR⁻ rat hepatocytes due to lack of Mrp2 prevents viral infection-mediated down-regulation of Mrp4 through nuclear receptor regulation. However, further studies are needed to investigate the mechanism(s) of differential down-regulation of Mrp4 in WT and TR⁻ rats. RSV undergoes biliary and basolateral efflux to a quantitatively similar extent; MRP4 contributes to basolateral efflux of RSV (38). However, RSV total accumulation was not altered by decreased Mrp4 protein expression in siNT- and siBcrp-infected WT rat SCH, suggesting minimal changes in Mrp4 function or the presence of other basolateral efflux transport proteins that can compensate for impaired Mrp4 function.

Recombinant adenovirus has been used widely as a gene delivery vector because of its high infection efficiency and high transgene capacity compared to other viral vector systems (i.e. lentivirus, retrovirus) (27). Thus, it provides a useful tool to deliver siRNA to primary cells, for which gene delivery is challenging. Recently, Hollingshead et al., reported a high-throughput gene silencing method in mouse SCH using transfection reagents (39). To increase transfection efficiency, a “reverse” transfection method was employed that initiated the transfection of suspended hepatocytes prior to plating. This approach resulted in a significant decrease in mRNA levels of Cyp3a11/13. Although this approach provides a

high-throughput method for functional studies, the expression and function of proteins-of-interest, as well as potential off-target effects, needs to be investigated further.

There is increasing evidence that membrane transport proteins play an important role in the pharmacokinetics of many drugs. Effects of altered function of uptake transporters often are reflected in systemic drug exposure. However, it is more challenging to assess the consequences of altered function of efflux transporters because changes in cellular (e.g., hepatocyte) exposure, which may be important in predicting efficacy and toxicity, may not lead to changes in systemic exposure (40-42). The SCH model is an experimental tool that retains hepatic transport and metabolic capabilities, and provides information about hepatic exposure (intracellular concentration), systemic exposure (medium concentration), and biliary excretion (BEI, biliary clearance) in isolation from other organs. The current study assessed the utility of RNAi in SCH from hepatocytes lacking specific transport proteins (e.g., Mrp2-deficient TR⁻ rat hepatocytes), as an *in vitro* tool to predict altered accumulation or disposition of drugs when multiple efflux transporters are impaired. This approach requires initial efforts for optimization, but once optimized, it has potential utility for rapid screening of a number of compounds. Concerns regarding possible off-target effects should be addressed further with validation of the system using additional compounds. Recently, Mrp2- and Bcrp-knockout rats have been shown to possess modest compensatory changes in expression of ADME-related genes, providing a useful *in vivo* system to explore the contribution of these transporters to drug disposition (43). However, results obtained from preclinical species may not necessarily translate to humans because of species differences in transport protein expression, regulation and function. To address this question, RNAi also can be applied to human SCH and future technologies in development (e.g., induced pluripotent stem cells, bioengineered culture systems such as HepatoPacTM and the Liver Chip) to assess species differences in transporter function and altered drug disposition. However, for knockdown of multiple transport proteins in human SCH, alternative approaches (e.g., tandem plasmid vector that can express two different siRNA in one vector) should be developed to minimize potential off-target effects.

Table 4.1. Total Accumulation and BEI (mean ± SEM) of probe substrates at MOI=5 vs. non infected control.

Means were estimated via a univariate repeated-measures ANOVA model. Estimates of marginal means are least squares means (LSM) ± SEM.

(A) [³H]Rosuvastatin:

<u>Viral Treatment</u>	Total Accumulation (pmol/mg protein)			Biliary Excretion Index (BEI; %)		
	<u>WT or TR⁻ status</u>			<u>WT or TR⁻ status</u>		
	<i>Wild-Type</i>	<i>TR⁻</i>	<i>LSM</i>	<i>Wild-Type</i>	<i>TR⁻</i>	<i>LSM</i>
<i>Non-infected</i>	181 (25)	182 (29)	181 (13)	54.3 (8.2)	24.6 (11.0)	39.4 (4.1)
<i>Non-targeted (Ad-siNT)</i>	207 (48)	174 (47)	190 (14)	45.4 (6.6)	17.9 (12.7)	31.7 (4.5)*
<i>Ad-siBcrp</i>	184 (30)	171 (45)	177 (14)	30.8 (7.5)	5.9 (3.0)	18.4 (4.5)*†
<i>LSM</i>	187 (18)	180 (18)		44.1 (5.8)	15.5 (5.8)#	

(B) [³H]Taurocholate:

<u>Viral Treatment</u>	Total Accumulation (pmol/mg protein)			Biliary Excretion Index (BEI; %)		
	<u>WT or TR⁻ status</u>			<u>WT or TR⁻ status</u>		
	<i>Wild-Type</i>	<i>TR⁻</i>	<i>LSM</i>	<i>Wild-Type</i>	<i>TR⁻</i>	<i>LSM</i>
<i>Non-infected</i>	27.1 (6.3)	41.7 (11.8)	34.4 (5)	83.1 (5.9)	72.6 (5.5)	77.8 (2.7)
<i>Non-targeted (Ad-siNT)</i>	21.2 (5.7)	38.0 (14.3)	29.6 (5)*	78.6 (8.3)	64.5 (9.0)	71.5 (3.0)*
<i>Ad-siBcrp</i>	18.0 (5.6)	31.0 (8.7)	24.5 (5)*†	80.1 (5.5)	60.6 (3.1)	70.3 (3.0)*
<i>LSM</i>	22.1 (6)	36.9 (6)		79.5 (3.8)	66.9 (3.8)	

*: $p < 0.05$ compared to non-infected

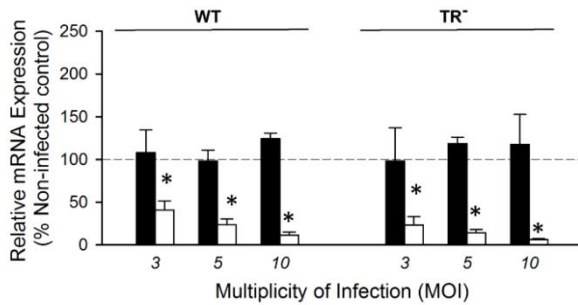
†: $p < 0.05$ compared to non-targeted

#: $p < 0.05$ compared to Wild-Type

Figure 4.1. Efficient knockdown of Bcrp in WT and TR⁻ rat SCH.

(A) Mean relative levels of Bcrp mRNA in SCH samples infected with Ad-siNT (solid bar) or Ad-siBcrp (open bar) at MOI of 3, 5, and 10. Each bar represents mean \pm SEM of n=3 rat livers. Duplicate SCH samples from each liver were analyzed; mRNA levels were expressed as a percent of the mean for non-infected hepatocytes and averaged together as a preliminary step for statistical analysis. The hypothesis testing procedure relied on a univariate repeated-measures ANOVA model for mean response as a function of MOI and virus. The model was fit separately to WT and TR⁻ rat SCH data. (B) Mean relative levels of Bcrp protein in SCH samples infected with Ad-siNT (solid bar) or Ad-siBcrp (open bar) at MOI of 3, 5 and 10. Representative blots from three independent studies are shown. β -actin was used as the loading control for each blot. Each bar represents mean \pm SEM of n=3 rat livers. Duplicate SCH samples from each liver were analyzed; protein levels were expressed as a percent of the mean for non-infected hepatocytes and averaged together as a preliminary step for statistical analysis. The hypothesis testing procedure relied on a univariate repeated-measures ANOVA model for mean response as a function of MOI and virus. The model was fit separately to WT and TR⁻ rat SCH data. *, statistically significantly different from non-infected hepatocytes ($P < 0.05$).

(A)



(B)

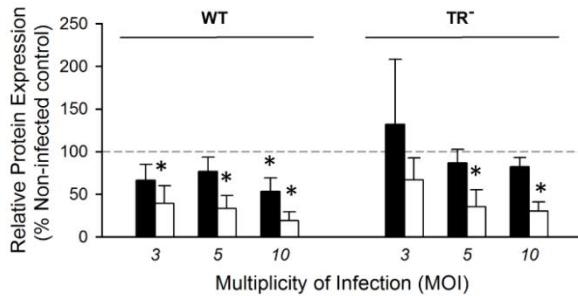
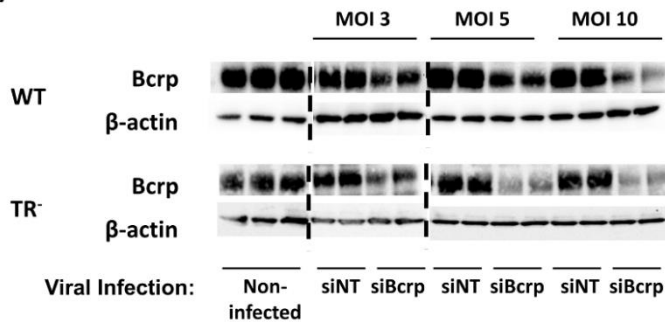


Figure 4.2. Effects of Bcrp knockdown on mean relative levels of Oatp1a1, Ntcp, Bsep, P gp, Mrp4, and Mrp2 proteins in WT and TR⁻ rat SCH infected with Ad siNT Ad siBcrp.

(A) Representative blots from three independent studies are shown. β -actin was used as the loading control for each blot. Mrp2 was evaluated only in WT SCH because it is not expressed in TR⁻ rat SCH. (B) Each bar represents mean \pm SEM of n=3 rat livers. Duplicate SCH samples from each liver were analyzed; protein levels after infection with Ad-siNT (solid bar) or Ad-siBcrp (open bar) at MOI of 5 and 10 were expressed as a percent of the mean for non-infected hepatocytes and averaged together as a preliminary step for statistical analysis. The multiple hypothesis testing procedure relied on a univariate repeated-measures ANOVA model for mean response as a function of MOI and virus. The model was fit separately to WT and TR⁻ rat SCH data.

*, statistically significantly different from non-infected hepatocytes ($P < 0.05$).

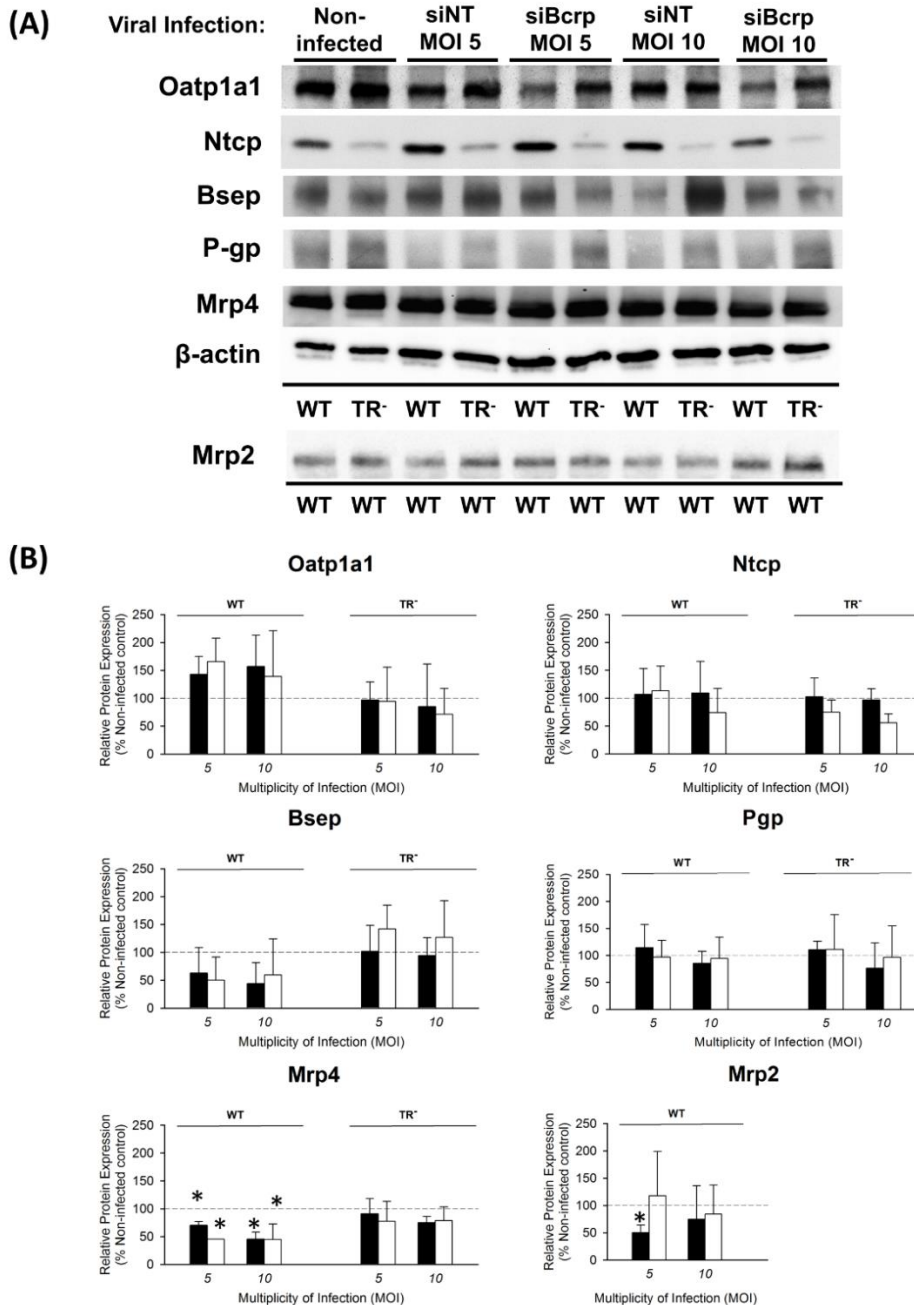
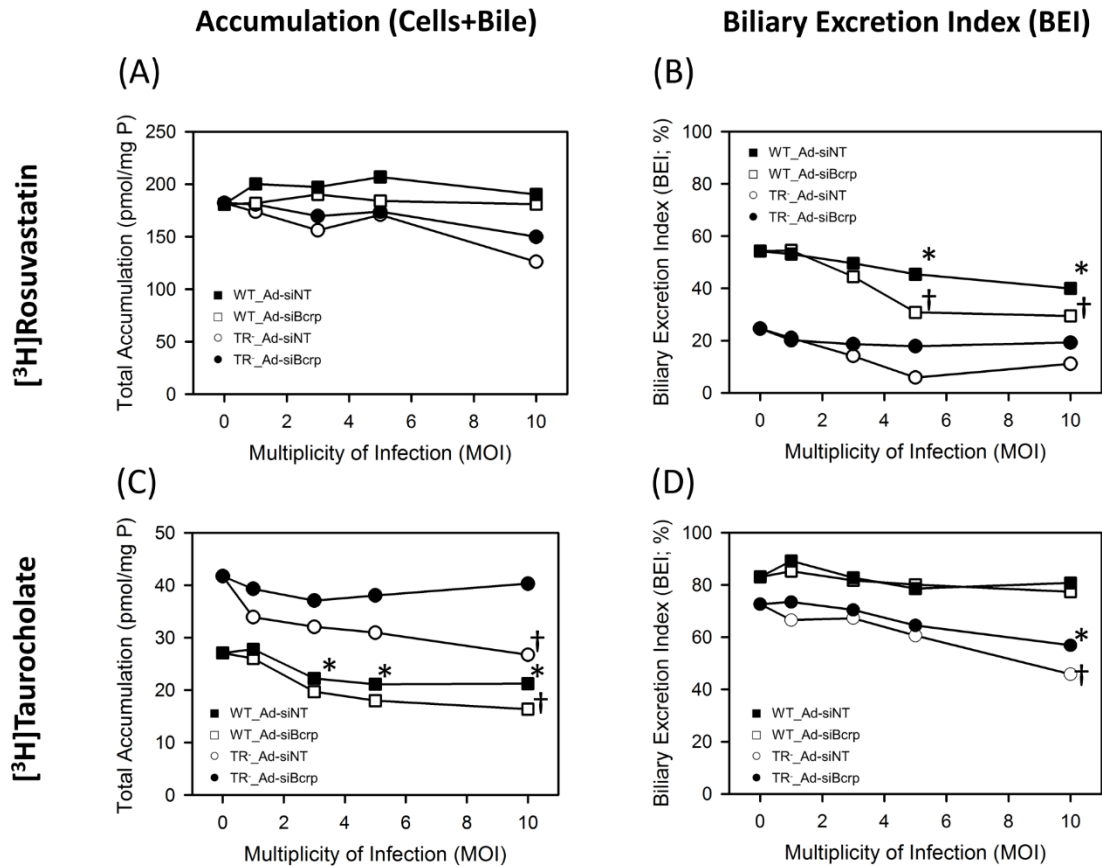


Figure 4.3. Effects of non-targeted and targeted adenoviral infection in WT and TR⁻ SCH at increasing MOI.

(A) Total accumulation and (B) biliary excretion index (BEI) of [³H]rosuvastatin; (C) total accumulation and (D) BEI of [³H]taurocholate. Mean values represent the responses of SCH preparations from n=3 WT (squares) and TR⁻ (circles) rat livers, respectively, infected with non-targeted (Ad-siNT, closed symbols) or targeted (Ad-siBcrp, open symbols) adenoviral vectors. Triplicate SCH samples from each liver were measured and averaged together as a preliminary step for statistical analysis. Estimation of means and differences between means relied on a univariate repeated-measures ANOVA model for mean response as a function of MOI and virus. The model was fit separately to WT and TR⁻ rat SCH data.

*, statistically significant off-target effect [siNT vs. non-infected (MOI of 0)].

†, statistically significant targeted effect (siBcrp vs. siNT).

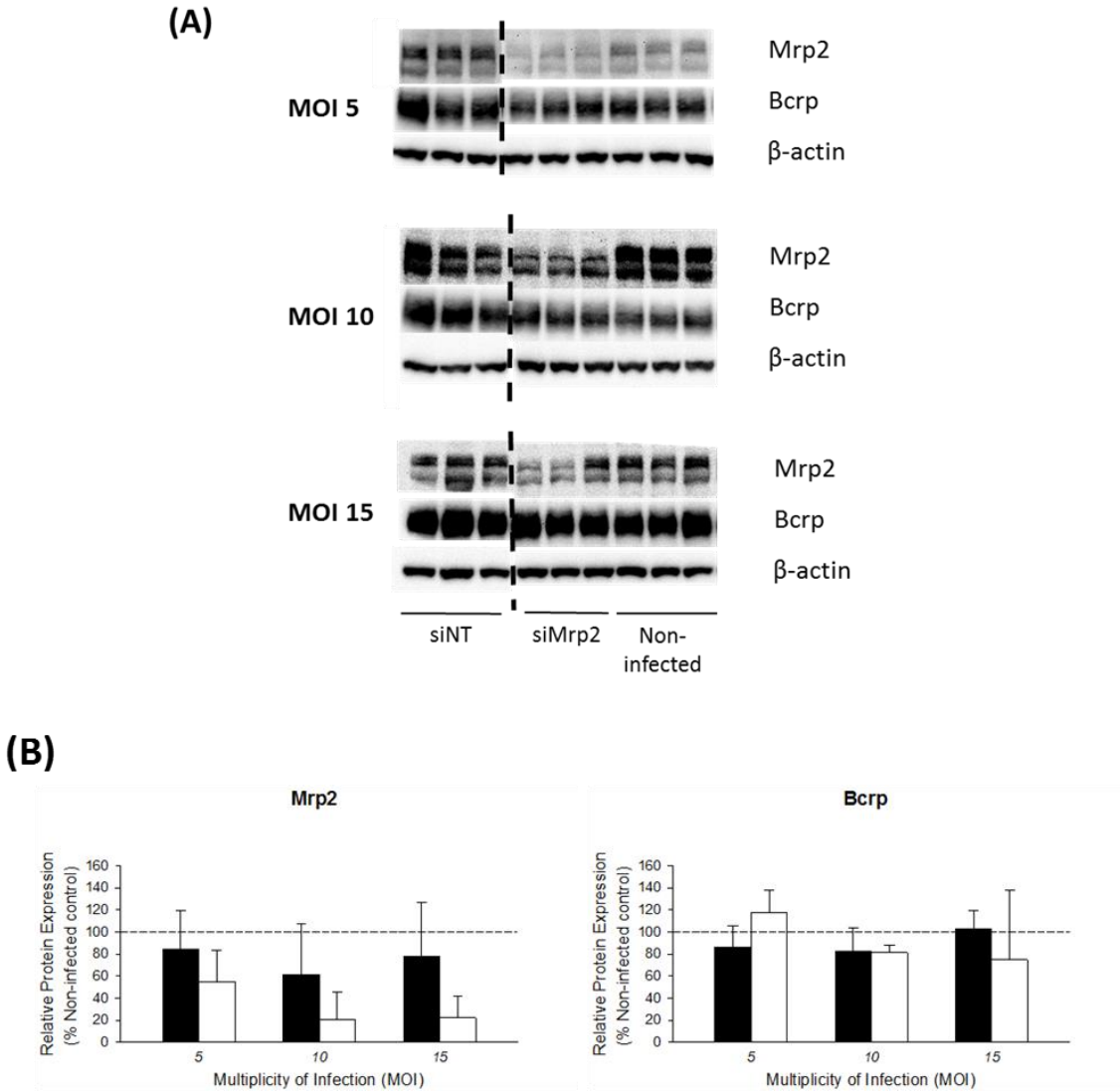


Supporting Information

Supporting figures include 1) Mrp2 and Bcrp protein levels, 2) hepatobiliary disposition of [³H]estradiol-17β-D-glucuronide (E₂17G) and [³H]taurocholate (TC) in Mrp2 knockdown WT rat SCH, and 3) Mrp2 and Bcrp protein levels in Mrp2/Bcrp double knockdown WT rat SCH.

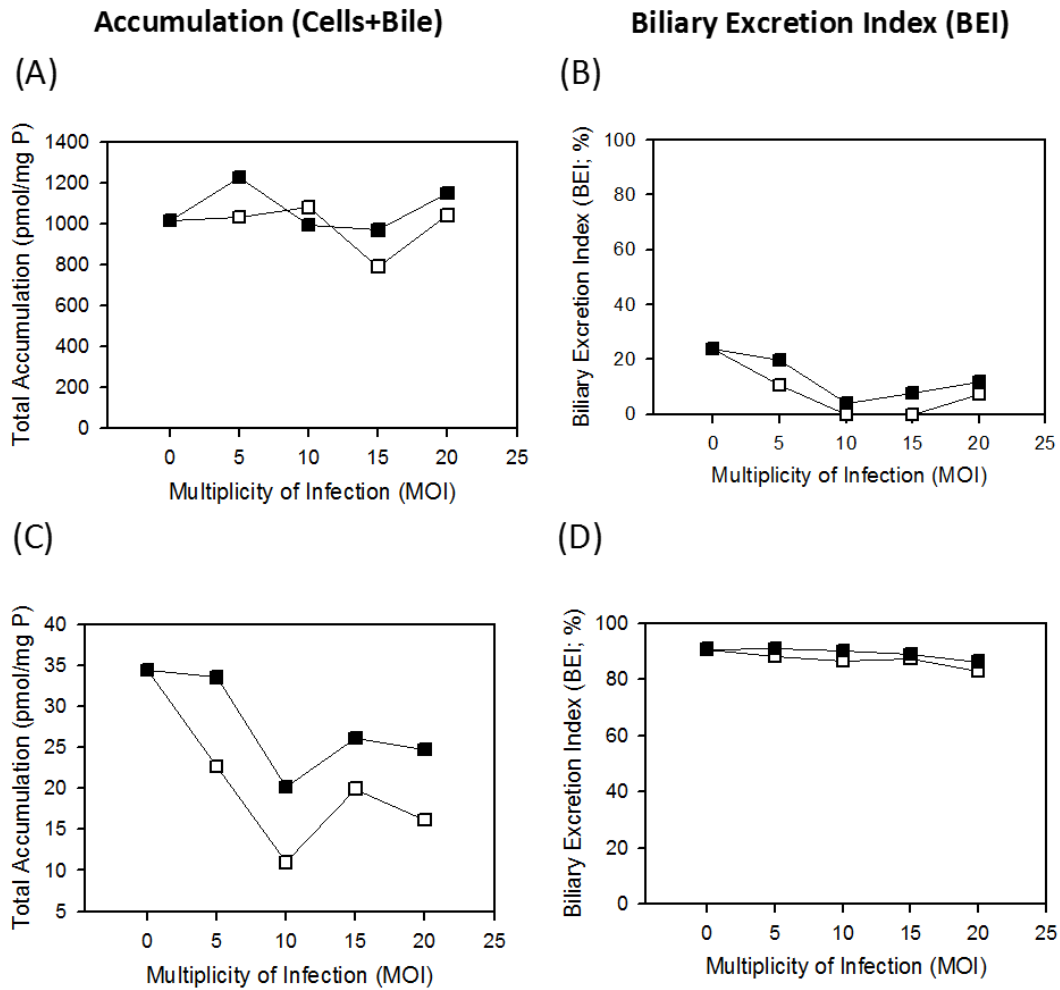
Supplement Figure 4.1. Knockdown of Mrp2 in WT rat SCH by adenoviral vector-mediated RNAi.

Mean relative levels of Mrp2 and Bcrp protein in WT rat SCH infected with Ad-siNT (solid bar) or Ad-siMrp2 (open bar) at MOI of 5, 10, and 15. (A) Representative blots from n=2-4 independent studies are shown. β -actin was used as the loading control for each blot. (B) Each bar represents mean \pm SEM of n=4 (MOI 5) or n=4 (MOI 10) or n=3 (MOI 15) rat livers. Triplicate SCH samples from each liver were analyzed; protein levels were expressed as a percent of the mean for non-infected hepatocytes and averaged.



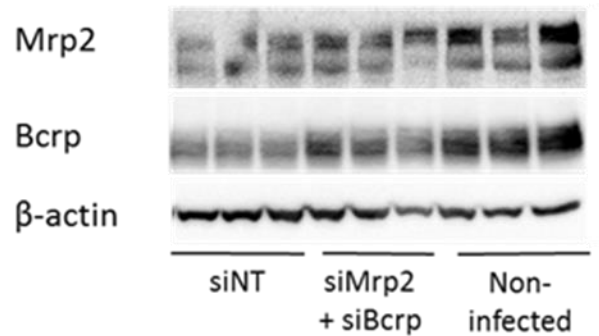
Supplement Figure 4.2. Effect of non-targeted (Ad-siNT, closed symbols) and targeted (Ad-siMrp2, open symbols) adenoviral infection in WT rat SCH at increasing multiplicity-of-infection (MOI).

(A) Total accumulation and (B) biliary excretion index (BEI) of [³H]estradiol-17β-D-glucuronide (E₂17G); (C) Total accumulation and (D) biliary excretion index (BEI) of [³H]taurocholate. Mean values represent the responses of SCH preparations from n=2 rat livers. Triplicate SCH samples from each liver were measured and averaged.

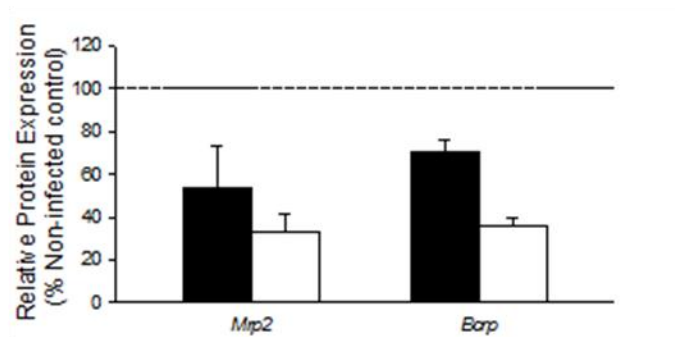


Supplement Figure 4.3. Double-knockdown of Mrp2 and Bcrp by adenoviral vector-mediated RNAi. Mean relative levels of Mrp2 and Bcrp proteins in WT rat SCH infected with Ad-siNT (solid bar, MOI of 10) or Ad-siMrp2 + Ad-siBcrp (open bar, MOI of 5 each). (A) Representative Mrp2 and Bcrp blots from three independent studies are shown. β -actin was used as the loading control for each blot. (B) Each bar represents mean \pm SEM of n=3 rat livers. Duplicate (MOI 5) or triplicate (MOI 10) SCH samples from each liver were analyzed; protein levels were expressed as a percent of the mean for non-infected hepatocytes and averaged.

(A)



(B)



REFERENCES

- (1) Natarajan, K., Xie, Y., Baer, M.R. & Ross, D.D. Role of breast cancer resistance protein (BCRP/ABCG2) in cancer drug resistance. *Biochem Pharmacol* **83**, 1084-103 (2012).
- (2) Doyle, L.A. *et al.* A multidrug resistance transporter from human MCF-7 breast cancer cells. *Proc Natl Acad Sci U S A* **95**, 15665-70 (1998).
- (3) Maliepaard, M. *et al.* Subcellular localization and distribution of the breast cancer resistance protein transporter in normal human tissues. *Cancer Res* **61**, 3458-64 (2001).
- (4) Kawabata, S. *et al.* Breast cancer resistance protein directly confers SN-38 resistance of lung cancer cells. *Biochem Biophys Res Commun* **280**, 1216-23 (2001).
- (5) Maliepaard, M. *et al.* Overexpression of the BCRP/MXR/ABCP gene in a topotecan-selected ovarian tumor cell line. *Cancer Res* **59**, 4559-63 (1999).
- (6) Sargent, J.M., Williamson, C.J., Maliepaard, M., Elgie, A.W., Scheper, R.J. & Taylor, C.G. Breast cancer resistance protein expression and resistance to daunorubicin in blast cells from patients with acute myeloid leukaemia. *Br J Haematol* **115**, 257-62 (2001).
- (7) Huang, L., Wang, Y. & Grimm, S. ATP-dependent transport of rosuvastatin in membrane vesicles expressing breast cancer resistance protein. *Drug metabolism and disposition* **34**, 738-42 (2006).
- (8) Hirano, M., Maeda, K., Matsushima, S., Nozaki, Y., Kusuhara, H. & Sugiyama, Y. Involvement of BCRP (ABCG2) in the biliary excretion of pitavastatin. *Mol Pharmacol* **68**, 800-7 (2005).
- (9) Mao, Q. & Unadkat, J.D. Role of the breast cancer resistance protein (ABCG2) in drug transport. *AAPS J* **7**, E118-33 (2005).
- (10) Zamek-Gliszczyński, M.J., Kalvass, J.C., Pollack, G.M. & Brouwer, K.L. Relationship between drug/metabolite exposure and impairment of excretory transport function. *Drug metabolism and disposition* **37**, 386-90 (2009).
- (11) Matsson, P., Pedersen, J.M., Norinder, U., Bergstrom, C.A. & Artursson, P. Identification of novel specific and general inhibitors of the three major human ATP-binding cassette transporters P-gp, BCRP and MRP2 among registered drugs. *Pharm Res* **26**, 1816-31 (2009).

- (12) Evers, R., Kool, M., Smith, A.J., van Deemter, L., de Haas, M. & Borst, P. Inhibitory effect of the reversal agents V-104, GF120918 and Pluronic L61 on MDR1 Pgp-, MRP1- and MRP2-mediated transport. *Br J Cancer* **83**, 366-74 (2000).
- (13) Duan, P. & You, G. Novobiocin is a potent inhibitor for human organic anion transporters. *Drug metabolism and disposition* **37**, 1203-10 (2009).
- (14) Hirano, M., Maeda, K., Shitara, Y. & Sugiyama, Y. Contribution of OATP2 (OATP1B1) and OATP8 (OATP1B3) to the hepatic uptake of pitavastatin in humans. *J Pharmacol Exp Ther* **311**, 139-46 (2004).
- (15) Nakagomi-Hagihara, R. *et al.* OATP1B1, OATP1B3, and mrp2 are involved in hepatobiliary transport of olmesartan, a novel angiotensin II blocker. *Drug metabolism and disposition*: **34**, 862-9 (2006).
- (16) Zamek-Gliszczyński, M.J., Day, J.S., Hillgren, K.M. & Phillips, D.L. Efflux transport is an important determinant of ethinylestradiol glucuronide and ethinylestradiol sulfate pharmacokinetics. *Drug metabolism and disposition* **39**, 1794-800 (2011).
- (17) Kitamura, S., Maeda, K., Wang, Y. & Sugiyama, Y. Involvement of multiple transporters in the hepatobiliary transport of rosuvastatin. *Drug metabolism and disposition* **36**, 2014-23 (2008).
- (18) Volk, E.L. & Schneider, E. Wild-type breast cancer resistance protein (BCRP/ABCG2) is a methotrexate polyglutamate transporter. *Cancer Res* **63**, 5538-43 (2003).
- (19) Ozvegy, C. *et al.* Functional characterization of the human multidrug transporter, ABCG2, expressed in insect cells. *Biochem Biophys Res Commun* **285**, 111-7 (2001).
- (20) Zamek-Gliszczyński, M.J., Bedwell, D.W., Bao, J.Q. & Higgins, J.W. Characterization of SAGE Mdr1a (P-gp), Bcrp, and Mrp2 knockout rats using loperamide, paclitaxel, sulfasalazine, and carboxydichlorofluorescein pharmacokinetics. *Drug metabolism and disposition* **40**, 1825-33 (2012).
- (21) Huang, L. *et al.* Deletion of Abcg2 has differential effects on excretion and pharmacokinetics of probe substrates in rats. *J Pharmacol Exp Ther* **343**, 316-24 (2012).
- (22) Abe, K., Bridges, A.S., Yue, W. & Brouwer, K.L. In vitro biliary clearance of angiotensin II receptor blockers and 3-hydroxy-3-methylglutaryl-coenzyme A reductase inhibitors in sandwich-cultured rat hepatocytes: comparison with in vivo biliary clearance. *J Pharmacol Exp Ther* **326**, 983-90 (2008).

- (23) Hoffmaster, K.A., Zamek-Gliszczynski, M.J., Pollack, G.M. & Brouwer, K.L. Multiple transport systems mediate the hepatic uptake and biliary excretion of the metabolically stable opioid peptide [D-penicillamine_{2,5}]enkephalin. *Drug metabolism and disposition* **33**, 287-93 (2005).
- (24) Fukuda, H., Ohashi, R., Ohashi, N., Yabuuchi, H. & Tamai, I. Estimation of transporters involved in the hepatobiliary transport of TA-0201CA using sandwich-cultured rat hepatocytes from normal and multidrug resistance-associated protein 2-deficient rats. *Drug metabolism and disposition* **38**, 1505-13 (2010).
- (25) Tian, X., Zamek-Gliszczynski, M.J., Zhang, P. & Brouwer, K.L. Modulation of multidrug resistance-associated protein 2 (Mrp2) and Mrp3 expression and function with small interfering RNA in sandwich-cultured rat hepatocytes. *Mol Pharmacol* **66**, 1004-10 (2004).
- (26) Liao, M. *et al.* Inhibition of hepatic organic anion-transporting polypeptide by RNA interference in sandwich-cultured human hepatocytes: an in vitro model to assess transporter-mediated drug-drug interactions. *Drug Metab Dispos* **38**, 1612-22 (2010).
- (27) Wang, I.I. & Huang, I.I. Adenovirus technology for gene manipulation and functional studies. *Drug Discov Today* **5**, 10-6 (2000).
- (28) Yue, W., Abe, K. & Brouwer, K.L. Knocking down breast cancer resistance protein (Bcrp) by adenoviral vector-mediated RNA interference (RNAi) in sandwich-cultured rat hepatocytes: a novel tool to assess the contribution of Bcrp to drug biliary excretion. *Mol Pharm* **6**, 134-43 (2009).
- (29) Kim, H.S., Lee, G., John, S.W., Maeda, N. & Smithies, O. Molecular phenotyping for analyzing subtle genetic effects in mice: application to an angiotensinogen gene titration. *Proc Natl Acad Sci U S A* **99**, 4602-7 (2002).
- (30) Livak, K.J. & Schmittgen, T.D. Analysis of relative gene expression data using real-time quantitative PCR and the 2⁻(Delta Delta C(T)) Method. *Methods* **25**, 402-8 (2001).
- (31) Swift, B., Pfeifer, N.D. & Brouwer, K.L. Sandwich-cultured hepatocytes: an in vitro model to evaluate hepatobiliary transporter-based drug interactions and hepatotoxicity. *Drug Metab Rev* **42**, 446-71 (2010).
- (32) Imai-Nishiya, H. *et al.* Double knockdown of alpha1,6-fucosyltransferase (FUT8) and GDP-mannose 4,6-dehydratase (GMD) in antibody-producing cells: a new strategy for generating fully non-fucosylated therapeutic antibodies with enhanced ADCC. *BMC Biotechnol* **7**, 84 (2007).

- (33) Yue, W., Lee, J.K., Abe, K., Sugiyama, Y. & Brouwer, K.L. Decreased hepatic breast cancer resistance protein expression and function in multidrug resistance-associated protein 2-deficient (TR(-)) rats. *Drug metabolism and disposition* **39**, 441-7 (2011).
- (34) Ho, R.H. *et al.* Drug and bile acid transporters in rosuvastatin hepatic uptake: function, expression, and pharmacogenetics. *Gastroenterology* **130**, 1793-806 (2006).
- (35) Maher, J.M., Cheng, X., Slitt, A.L., Dieter, M.Z. & Klaassen, C.D. Induction of the multidrug resistance-associated protein family of transporters by chemical activators of receptor-mediated pathways in mouse liver. *Drug metabolism and disposition* **33**, 956-62 (2005).
- (36) Zhang, J., Huang, W., Qatanani, M., Evans, R.M. & Moore, D.D. The constitutive androstane receptor and pregnane X receptor function coordinately to prevent bile acid-induced hepatotoxicity. *J Biol Chem* **279**, 49517-22 (2004).
- (37) Huang, W. *et al.* Induction of bilirubin clearance by the constitutive androstane receptor (CAR). *Proc Natl Acad Sci U S A* **100**, 4156-61 (2003).
- (38) Pfeifer, N.D., Yang, K. & Brouwer, K.L. Hepatic Basolateral Efflux Contributes Significantly to Rosuvastatin Disposition: I. Characterization of Basolateral vs. Biliary Clearance Using a Novel Protocol in Sandwich-Cultured Hepatocytes. *J Pharmacol Exp Ther*, (2013).
- (39) Hollingshead, B.D., Gauthier, L.M. & Burdick, A.D. High-throughput gene silencing and mRNA expression analysis in hepatocyte sandwich cultures. *Curr Protoc Toxicol* **Chapter 14**, Unit 14.1 (2013).
- (40) Watanabe, T., Kusuhara, H., Maeda, K., Shitara, Y. & Sugiyama, Y. Physiologically based pharmacokinetic modeling to predict transporter-mediated clearance and distribution of pravastatin in humans. *J Pharmacol Exp Ther* **328**, 652-62 (2009).
- (41) Chu, X. *et al.* Intracellular Drug Concentrations and Transporters: Measurement, Modeling, and Implications for the Liver. *Clin Pharmacol Ther*, (2013).
- (42) Lee, J.K., Marion, T.L., Abe, K., Lim, C., Pollock, G.M. & Brouwer, K.L. Hepatobiliary disposition of troglitazone and metabolites in rat and human sandwich-cultured hepatocytes: use of Monte Carlo simulations to assess the impact of changes in biliary excretion on troglitazone sulfate accumulation. *J Pharmacol Exp Ther* **332**, 26-34 (2010).
- (43) Zamek-Gliszczynski, M.J., Goldstein, K.M., Paulman, A., Baker, T.K. & Ryan, T.P. Minor compensatory changes in SAGE Mdr1a (P-gp), Bcrp, and Mrp2 knockout rats do not detract from their utility in the study of transporter-mediated pharmacokinetics. *Drug metabolism and disposition* **41**, 1174-8 (2013).

CHAPTER 5. Hepatocellular Exposure of Generated Metabolites, Troglitazone Sulfate and Glucuronide, is Determined by the Interplay between Formation and Excretion in Rat Sandwich-Cultured Hepatocytes Lacking Selected Canalicular Transporters¹

INTRODUCTION

Drug-induced liver injury (DILI) is one of the primary reasons for withdrawal of approved drugs from the market (1); however, the ability to accurately predict a drug's propensity for DILI is limited due to a lack of understanding of the underlying mechanism(s). One important proposed mechanism of DILI is inhibition of bile salt export pump (BSEP)-mediated excretion of bile acids, which may increase hepatic exposure to bile acids, ultimately leading to necrotic and/or apoptotic cell death (2-5). Many drugs that cause either cholestatic or mixed hepatocellular/cholestatic liver injury [e.g., troglitazone (TGZ), bosentan, cyclosporine, rifampin, sulindac, and glibenclamide) inhibit BSEP/Bsep-mediated biliary excretion of bile acids (6-11). However, only a small fraction of patients treated with BSEP inhibitors develop DILI, suggesting that injury is driven by a combination of drug- and patient-specific risk factors. For drugs with a rare incidence of DILI, hepatic exposure to the causative drugs/metabolites may be high in the subset of patients who develop DILI. It is also possible that toxic reactions triggered by drug exposure may develop into severe liver injury in a subset of susceptible patients. Potential patient-specific risk factors that may influence drug disposition and/or toxicity include age, gender, activation of the innate immune system, co-medications, underlying disease, and/or genetic predisposition.

TGZ was the first marketed thiazolidinedione, approved for the treatment of type II non-insulin-dependent diabetes. However, 2% of TGZ-treated patients developed serum ALT elevations more than 3-

¹This work has been presented, in part, at the 2011 AAPS Annual Meeting and Exposition, Washington, DC, October 23-27, 2011, and has been submitted to *Drug Metabolism and Disposition*.

fold greater than the upper limit of normal (12, 13). Subsequent to reports of lethal DILI in humans, TGZ was withdrawn from worldwide markets. Several mechanisms have been proposed to explain TGZ-mediated DILI including formation of reactive metabolites, mitochondrial toxicity, apoptosis, and inhibition of bile acid transport (14, 15). Clinical observations and *in vivo* studies in rats have implicated that a cholestatic mechanism is involved in TGZ-induced hepatotoxicity (9, 16-18). *In vitro* vesicular transport assays demonstrated that TGZ and its major metabolite, TGZ sulfate (TS), are potent inhibitors of bile acid efflux transporters, supporting the involvement of cholestasis in TGZ-induced hepatotoxicity; TGZ inhibits human BSEP- and rat Bsep-mediated bile acid transport with IC₅₀ values of 2.7–5.9 and 3.9–10.6 μM, respectively (2, 3, 9). TS is a 10-fold more potent inhibitor of ATP-dependent transport of taurocholate in rat liver canalicular membrane vesicles compared to TGZ (9). Data from our laboratory demonstrated that TS also inhibits hepatic basolateral efflux transport proteins, multidrug resistance protein 4 (MRP4) (19).

In rats and humans, TGZ is metabolized extensively in the liver, primarily by sulfation, with glucuronidation and oxidation as successively less prominent metabolic pathways; TS exhibited 10-fold higher plasma concentrations than TGZ, and was excreted primarily into bile, suggesting that TGZ metabolism and excretion were similar in humans and male rats (20-22). Previously published data suggested that TS is excreted into bile predominantly via breast cancer resistance protein (Bcrp) and multidrug resistance protein 2 (Mrp2) (23, 24). Extensive hepatic accumulation of TS (20, 25), coupled with the finding that TS potently inhibits bile acid transporters (e.g., BSEP, MRP4), led to the hypothesis that TS is primarily responsible for altered bile acid disposition and subsequent hepatotoxicity; impaired function of Bcrp and Mrp2 (e.g., due to underlying disease, genetic variations, and drug-drug interactions) would increase hepatocellular TS accumulation and enhance inhibition of bile acid transport (Figure 5.1). To test this hypothesis, the hepatobiliary disposition of TGZ and generated metabolites, TS and TG, was examined in rat sandwich-cultured hepatocytes (SCH) using a novel experimental system developed in our laboratory (26) to quantitatively assess the effects of impaired function of Bcrp (using RNA interference technique) and/or Mrp2 (using Mrp2-deficient TR⁻ rats). Differential metabolism of TGZ

also was investigated using S9 fractions prepared from liver tissues of WT and TR⁻ rats. This work highlights the importance of considering both metabolic and transport pathways when predicting hepatocellular exposure to generated metabolites.

METHODS

Materials

TGZ was purchased from Cayman Chemical Company (Ann Arbor, MI). TS, TGZ glucuronide (TG), and TGZ quinone (TQ) were kindly provided by Daiichi-Sankyo Co., Ltd. (Tokyo, Japan). TS also was synthesized from TGZ in-house (27). [³H]Taurocholate (5 Ci/mmol; purity > 97%) was purchased from Perkin Elmer (Waltham, MA). Taurocholate, Triton X-100, Hanks' balanced salt solution (HBSS) premix, HBSS modified (with no calcium chloride, magnesium sulfate, phenol red, and sodium bicarbonate) premix, dexamethasone, penicillin-streptomycin solution, and collagenase (type IV) were purchased from Sigma-Aldrich (St. Louis, MO). Dimethyl sulfoxide (DMSO) was obtained from Fisher Scientific (Fairlawn, NJ). GIBCO brand fetal bovine serum, recombinant human insulin, and Dulbecco's modified Eagle's medium (DMEM), and membrane vesicles prepared from rat Bsep-overexpressing Sf9 cells (Sf9-Bsep) and control Sf9 cells (Sf9-control) were purchased from Life Technologies (Carlsbad, CA). Insulin/transferrin/selenium (ITS) culture supplement, BioCoat™ culture plates, and Matrigel™ extracellular matrix were purchased from BD Biosciences Discovery Labware (Bedford, MA). GF120918 (elacridar) was a generous gift from GlaxoSmithKline (Research Triangle Park, NC). All other chemicals and reagents were of analytical grade and were readily available from commercial sources.

Hepatocyte Isolation and Culture in a Sandwich Configuration

Hepatocytes were isolated from male Wistar rats (270–300 g, Charles River Laboratories, Inc., Wilmington, MA) and TR⁻ rats (220 – 300 g, bred in-house; breeding stock obtained from Dr. Mary Vore, University of Kentucky, Lexington, KY) using a two-step collagenase perfusion method previously described (LeCluyse et al., 1996). Animals had free access to water and food before surgery and were allowed to acclimate for at least five days. All animal procedures complied with the guidelines of the

Institutional Animal Care and Use Committee (University of North Carolina, Chapel Hill, NC).

Hepatocytes were seeded onto 24-well BioCoat™ culture plates at a density of 0.35×10^6 cells/well in seeding medium (DMEM containing 5% fetal bovine serum, 10 μ M insulin, 1 μ M dexamethasone, 2 mM L-glutamine, 1% MEM nonessential amino acids, 100 units of penicillin G sodium, and 100 μ g of streptomycin) as described previously (28). Hepatocytes were incubated for 1 h at 37°C in a humidified incubator (95% O₂, 5% CO₂) and allowed to attach to the collagen substratum, after which time the medium was aspirated to remove unattached cells, and replaced with fresh medium. On the next day, cells were overlaid with BD Matrigel™ at a concentration of 0.25 mg/ml in ice-cold feeding medium (DMEM supplemented with 0.1 μ M dexamethasone, 2 mM L-glutamine, 1% MEM nonessential amino acids, 100 units of penicillin G sodium, 100 μ g of streptomycin, and 1% ITS). The culture medium was changed daily until experiments were performed on day 4.

Knockdown of Bcrp Protein in WT and TR⁻ Rat SCH

Adenoviral vectors expressing short hairpin RNA targeting Bcrp (Ad-siBcrp) or a non-target control (Ad-siNT) were prepared as described previously (29). One hour after seeding on day 0, hepatocytes were infected with Ad-siBcrp or Ad-siNT at multiplicity of infection (MOI) of 5 by replacing the seeding medium with fresh seeding medium containing virus. On the next day, medium including viruses were removed, and cells were overlaid with Matrigel™ as described above.

Accumulation of TGZ and Generated Metabolites in WT and TR⁻ Rat SCH in the Absence or Presence of Bcrp Knockdown

Following 30 min exposure to 0.5 ml feeding medium containing 10 μ M TGZ, 0.2 ml aliquots of medium were collected from day 4 WT and TR⁻ rat SCH in the absence or presence of Bcrp knockdown. The remaining culture medium was completely aspirated, and SCH were rinsed with 0.5 ml/well of warm standard (Ca²⁺-containing) or Ca²⁺-free HBSS buffers. After rinses, HBSS buffers were aspirated, and SCH were incubated with 0.5 ml of HBSS buffers (standard or Ca²⁺-free) at 37°C for 5 min. After incubation, the HBSS buffers were aspirated from all wells. Plates were sealed and stored at -80°C until analysis.

Membrane Vesicle Assay

Membrane vesicles (Sf9-control and Sf9-Bsep, 10 and 25 µg/reaction for taurocholate and TS uptake, respectively) were incubated at 37°C with the substrate (5 µM taurocholate or 100 µM TS) in tris-sucrose buffer (TSB) containing MgCl₂ (10 mM), creatine phosphate (10 mM), creatine kinase (100 µg/ml), adenosine triphosphate (ATP) or adenosine monophosphate (AMP) (4 mM) in a final volume of 50 µl. The assays were performed on three separate experiments in triplicate. After incubation for 5 min, the reaction was stopped by addition of 800 µl ice-cold TSB and immediately filtered using Type A/E glass fiber filter (PALL Corporation, Ann Arbor, MI) presoaked in TSB overnight. Under aspiration, the filters were washed twice with ice-cold TSB using a vacuum filtration system. Glass filters were transferred to glass vials, and 1 ml Bio-Safe II™ (Research Products International, Mount Prospect, IL) was added before counting radioactivity of taurocholate using the Tri-Carb 3100 TR liquid scintillation analyzer (PerkinElmer, Waltham, MA). For liquid chromatography coupled with tandem mass spectrometry (LC-MS/MS) analysis of TS, glass filters were dissolved with 1 ml methanol including 1 nM ethyl warfarin (internal standard). Following vortex mixing and sonication, the supernatant was transferred to microcentrifuge tubes and centrifuged for 20 min at 4°C. After centrifugation, 500 µl of supernatant was transferred to 96-well LC-MS/MS plate, evaporated using SPE Dry 96 (Biotage, Uppsala, Sweden), and reconstituted with 100 µl 1:1 mixture of methanol and DMSO. The ATP-dependent uptake of substrate was calculated by subtracting substrate uptake in the presence of AMP from substrate uptake in the presence of ATP.

Effects of GF120918 on the Biliary Excretion of TS in WT and TR⁻ Rat SCH

WT and TR⁻ rat SCH were pre-incubated with 0.5 µM GF120918 or vehicle control for 10 min followed by 30-min exposure to 0.5 ml feeding medium containing 10 µM TGZ and 0.5 µM GF120918 (or vehicle control). After incubation, the culture medium was completely aspirated, and SCH were rinsed with 0.5 ml/well of warm standard or Ca²⁺-free HBSS buffers. After the second rinse, HBSS buffers were aspirated, and SCH were incubated with 0.5 ml of HBSS buffers (standard or Ca²⁺-free) at 37°C for 5 min.

After incubation, the HBSS buffer was aspirated from all wells. Plates were sealed and stored at -80°C until analysis.

***In Vitro* Metabolism of TGZ in S9 Fraction**

S9 fractions were prepared from liver tissues of WT and TR⁻ rats (n=3, respectively) according to standard procedures and stored at -80°C until used (30). Protein concentration was determined by the BCA protein assay (Pierce Chemical., Rockford, IL) using human serum albumin (standard solution; Sigma) as a standard. Reaction mixture [95 μl of Tris-HCl buffer (pH 7.5, 0.1 M) containing 3'-phosphoadenosine-5'-phosphosulfate (PAPS; final concentration 0.1 mM), uridine 5'-diphosphoglucuronic acid (UDPGA; final concentration 2 mM), nicotinamide adenine dinucleotide phosphate (reduced, NADPH; final concentration 1 mM), alamethicin (final concentration 25 $\mu\text{l}/\text{ml}$), and TGZ (final concentrations of 1 or 10 μM)] was pre-incubated for 5 min at 37°C . TGZ was dissolved in DMSO; the final concentration of DMSO in the reaction mixture was 0.2%. TGZ concentrations of 1 and 10 μM were selected for investigation because they yielded unbound concentrations of TGZ in the S9 fraction that were similar to the unbound concentrations in hepatocytes. Intracellular total concentrations of TGZ ranged from 100 – 250 μM after a 30-min incubation of WT and TR⁻ rat SCH with 10 μM TGZ (25). Assuming that the intracellular unbound fraction (f_u) is equal to the plasma f_u of 0.000921 (31), intracellular concentrations of unbound TGZ would be in the range of 0.9–0.23 μM . TGZ also is highly bound to microsomal and cytosolic protein (TGZ f_u was 0.01 and 0.03 in 2 mg/ml rat liver microsomes and 0.5 mg/ml rat liver cytosol, respectively) (32); therefore, 1 and 10 μM total TGZ in S9 fraction would result in TGZ unbound concentrations of ~ 0.1 –1 μM , which covered the range of intracellular unbound TGZ concentrations in rat SCH. The reaction was started by adding 5 μl of the S9 fraction (final concentration 1 mg/ml). The reaction was stopped after 3 min by mixing with 200 μl ice-cold acetonitrile containing 15 nM ethyl warfarin (analytical internal standard). The 3-min time point was chosen based on the reported linear range to calculate the initial velocity of TS and TG formation (32). The reaction mixture was centrifuged for 20 min at 4°C , and the supernatant was transferred to 96-well LC-MS/MS plates for analysis. To determine desulfation of TS, 5 μl of TS (final concentration of 100 μM) was

incubated with 95 μ l of 0.1M Tris-HCl buffer (pH 7.5) containing S9 fraction (final concentration 1 mg/ml) for 30 min, and the same procedure was followed as detailed above.

LC-MS/MS Analysis

TGZ and generated metabolites were analyzed by LC-MS/MS as described previously (25). Briefly, the medium and cells or cells+ bile lysate samples were centrifuged at 12,000g for 10 min at 4°C, and the supernatant was diluted 1:6 (v/v) with 79%:21% (v/v) methanol/water containing the internal standard (ethyl warfarin). An Applied Biosystems API 4000 triple quadrupole mass spectrometer with a TurboSpray ion source (Applied Biosystems, Foster City, CA) was used for analysis in negative ionization mode. The ranges of the standard curves were extended by adding additional points to the previously reported range (25); eleven point (5 – 10000 nM; TGZ) or ten point (5–5000 nM; TS, TG, and TQ) calibration curves were constructed as composites of TGZ (440.0→397.1), TS (520.2→440.1), TG (616.2→440.1), and TQ (456.1→413.1) by using peak area ratios of analyte and ethyl warfarin (320.8→160.9). All points on the curves back-calculated to within 15% of the nominal value. Care was taken to minimize the light-sensitive degradation of TGZ during all experimental procedures.

Data Analysis and Statistics

TGZ accumulation was corrected for nonspecific binding to the BioCoat™ plate without cells, and normalized to protein concentration measured by the BCA protein assay (Pierce Chemical., Rockford, IL). To account for the incompatibility of the protein assay with methanol, the average protein concentration for standard HBSS or Ca²⁺-free HBSS incubations in a representative plate from the same liver preparation was used to normalize accumulation. The biliary excretion index (BEI; %), defined as the percentage of accumulated substrate residing within the bile canaliculi, was calculated using B-CLEAR® technology (Qualyst, Inc. Durham, NC) according to the following equation (Liu et al., 1999b):

$$\text{BEI (\%)} = \frac{\text{Accumulation}_{\text{Standard HBSS}} - \text{Accumulation}_{\text{Ca}^{2+}\text{-free HBSS}}}{\text{Accumulation}_{\text{Standard HBSS}}} \times 100$$

Effects of viral infection (non-infected vs. Ad-siNT vs. Ad-siBcrp) and rat type (WT vs. TR⁻) on hepatobiliary disposition (accumulation in cells+bile, cellular accumulation, and BEI) and recovery of

TGZ and its metabolites were evaluated using a two-way ANOVA followed by Tukey's post-hoc test. Two-way ANOVA also was used to evaluate the effects of GF120918 and rat type (WT vs. TR⁻) on hepatobiliary disposition of TS and TG. Student's t-test was used to compare ATP-dependent substrate transport in Sf9-Bsep vs. Sf9-control, and the initial velocity of TS/TG formation in S9 fractions prepared from livers of WT and TR⁻ rats. In all cases, $p < 0.05$ was considered statistically significant. All analyses were performed using SigmaStat 3.5 (San Jose, CA).

RESULTS

Hepatobiliary Disposition of TGZ and Generated Metabolites in WT and TR⁻ Rat SCH in the Absence or Presence of Bcrp

Loss-of-function of Mrp2 and Bcrp was validated in this experiment using rosuvastatin, a dual substrate of Mrp2 and Bcrp; rosuvastatin BEI was significantly decreased by impaired function of Mrp2 or Bcrp, and biliary excretion was almost ablated in Bcrp knockdown TR⁻ rat SCH (26). Accumulation of TGZ and generated metabolites in cells + bile, cells, and medium after a 30-min incubation of WT and TR⁻ rat SCH with 10 μ M TGZ is shown in Figures 5.2 and 5.3. BEI values of TS and TG in non-infected WT hepatocytes were 24 and 49 %, respectively (Figures 5.2B and 5.2C); biliary excretion of TGZ (Figure 5.2A) and TQ (data not shown) was negligible, consistent with previously published data (Lee et al., 2010a). The hepatobiliary disposition of TGZ and generated metabolites was not affected by infection of the non-target control adenoviral vector (Ad-siNT), confirming that off-target effects of viral infection were negligible in these studies. Unexpectedly, the BEI of TS was not altered by impaired Mrp2 (TR⁻) and/or Bcrp function (Ad-siBcrp), suggesting that other biliary transporters may compensate for the impaired function of Mrp2 and Bcrp (Figure 5.2B). Interestingly, TS accumulation in cells+bile, cells, and medium was decreased in TR⁻ rat SCH compared to WT rat SCH (Figures 5.2B and 5.3B). Bcrp knockdown did not significantly alter TS accumulation in cells+bile, cells, or medium (Figures 5.2B and 5.3B). The BEI of TG was significantly decreased in TR⁻ rat SCH compared to WT rat SCH, but was not influenced by knockdown of Bcrp (Figure 5.2C). TG cellular accumulation was significantly increased in

TR⁻ rat SCH compared to WT rat SCH, whereas TG accumulation in cells+bile was not altered (Figure 5.2C). In TR⁻ rat SCH, TG medium concentrations were significantly higher compared to WT rat SCH (Figure 5.3C). TG accumulation in cells+bile, cells, and medium was not significantly altered by Bcrp knockdown (Figures 5.2C and 5.3C). TQ accumulation in cells and cells+bile was significantly increased in TR⁻ rat SCH in the absence and presence of Bcrp knockdown compared to WT rat SCH, but medium concentrations were not significantly different (data not shown).

Differential Metabolism of TGZ in WT and TR⁻ Rat SCH

Cumulative recovery of TGZ and generated metabolites from medium, hepatocytes, and bile was comparable among all groups (92.3 – 99.6 %) (Figure 5.4A). After a 30-min incubation, more than 80% of the TGZ dose remained as parent compound in both WT and TR⁻ SCH. Among three generated metabolites, TS was predominant (4.8 % of the dose recovered in cells, bile, and medium), followed by TQ (1.5 % of the dose) and TG (0.9 % of the dose) in non-infected WT rat SCH (Figure 5.4A). In TR⁻ rat SCH, total recovery (medium, hepatocytes, and bile) of TS was significantly lower compared to WT rat SCH (Figure 5.4A). Total recovery of TG was significantly greater in TR⁻ compared to WT rat SCH (Figure 5.4A). TS primarily was recovered from hepatocytes, while TG was recovered primarily from the medium (Figures 5.4B and 5.4C).

Transport of TS in Membrane Vesicles from Bsep-overexpressing Sf9 Cells

To investigate the transport protein(s) involved in the compensatory biliary excretion of TS in the absence of Mrp2 and Bcrp, ATP-dependent uptake of 10 μM taurocholate (positive control) and 100 μM TS was determined in Sf9-control and Sf9-Bsep vesicles. ATP-dependent taurocholate transport was 60-fold greater in Sf9-Bsep vesicles compared to Sf9-control vesicles (Figure 5.5). However, ATP-dependent TS transport was comparable between Sf9-control and Sf9-Bsep vesicles, indicating that TS is not transported by Bsep.

Effects of GF120918 on the Hepatobiliary Disposition of TGZ and Generated Metabolites in WT and TR⁻ Rat SCH

The BEI of TS was not significantly altered by GF120918, a potent inhibitor of Bcrp and P-gp, nor by rat type (WT vs. TR⁻) (Figure 5.6A). The accumulation of TS in cells+bile and cells was significantly decreased in TR⁻ rat SCH compared to WT rat SCH as shown in Figure 5.2B, but was not altered by the presence of GF120918. The BEI of TG was significantly decreased in TR⁻ rat SCH compared to WT rat SCH, consistent with Figure 5.2C, but was not altered by the presence of GF120918 (Figure 5.6B). TG accumulation in cells+bile and cells was not influenced significantly by GF120918 or by rat type, but there was a trend towards an increase in cellular TG accumulation in TR⁻ compared to WT rat SCH (Figure 5.6B).

TGZ Metabolism in S9 Fraction Prepared From Liver Tissues of WT and TR⁻ Rats

To investigate the differential metabolism (i.e. sulfation and glucuronidation) of TGZ in WT and TR⁻ rats, formation of TS and TG was quantified after incubating 1 or 10 μM TGZ with S9 fraction prepared from liver tissues of WT and TR⁻ rats for 3 min. These concentrations were selected for investigation because they yielded unbound concentrations of TGZ in the S9 fraction that were similar to the unbound concentrations in hepatocytes (see **Methods** for details). The initial velocity of TS formation in S9 fraction from WT and TR⁻ rats was comparable after incubation with 1 and 10 μM TGZ, indicating that the activity of sulfotransferases was not altered in TR⁻ rats (Figure 5.7). The initial velocity of TG formation was increased by 1.5- and 6.5-fold in TR⁻ rats after incubation with 1 and 10 μM TGZ, respectively, consistent with the increased recovery of TG in TR⁻ SCH (Figure 5.7). TS did not undergo de-sulfation after incubation of 100 μM TS with S9 fractions over a 30-min period (data not shown).

DISCUSSION

TGZ is metabolized by Phase I and II enzymes and the generated metabolites are eliminated by multiple transport proteins. Consequently, defects in relevant metabolic enzymes and/or transport proteins due to genetic polymorphisms, underlying disease, or co-administered drugs may predispose certain

patients to TGZ-induced hepatotoxicity. Hewitt et al. demonstrated that low CYP3A4 and UGT activity combined with high SULT activity was associated with TGZ toxicity in human hepatocytes (33). Pharmacokinetic modeling and Monte Carlo simulations in rat SCH revealed that intracellular concentrations of TS may increase up to 5.7-fold when biliary excretion of TS is decreased 10-fold (25), but effects of altered function of biliary transporters on TS disposition have not been evaluated experimentally. TS, a potent inhibitor of bile acid efflux transporters, is extensively excreted into bile via Mrp2 and Bcrp (23, 24). Thus, we hypothesized that loss-of-function of Bcrp and/or Mrp2 would result in decreased biliary excretion and increased cellular accumulation of TS, which may lead to further inhibition of bile acid transport and hepatotoxicity. This study examined the effects of impaired function of Bcrp and/or Mrp2 on the hepatobiliary disposition of TGZ and generated metabolites, TS and TG; although TQ was measured, this investigation did not focus on TQ because it is a minor metabolite that also is formed by phototoxidation (34). A recently established novel *in vitro* system, rat SCH lacking Mrp2 (using Mrp2-deficient TR⁻ rat) and Bcrp (using adenoviral vectors expressing shRNA targeting Bcrp), was employed (26).

Unexpectedly, biliary excretion of TS was not altered by loss-of-function of Bcrp and Mrp2, potentially due to the presence of a compensatory canalicular protein that transports TS in the absence of Mrp2 and Bcrp. It is unlikely that residual Bcrp expression played a role in TS transport because loss-of-function of Mrp2 and Bcrp in this experimental system was validated using rosuvastatin, a dual substrate of Mrp2 and Bcrp. Biliary excretion of rosuvastatin was almost ablated in Bcrp knockdown TR⁻ rat SCH. Thus, Bsep and P-gp were investigated as potential compensatory transporters mediating the biliary excretion of TS. Results from membrane vesicle studies demonstrated that TS is not transported by Bsep. P-gp is not likely to be involved in TS biliary excretion because excretion of TS into bile was not altered in the presence of GF120918, a potent inhibitor of P-gp and Bcrp (35, 36), in WT and TR⁻ rat SCH. Other hepatic canalicular transporters such as multidrug and toxin extrusion protein 1 (MATE1) or multidrug resistance protein 2 (Mdr2) might be involved in compensatory TS biliary excretion. MATE1 transports a wide range of chemicals including hydrophilic organic cations with low molecular weight (e.g.,

metformin, tetraethylammonium, 1-methyl-4-phenylpyridinium, oxaliplatin), anionic compounds (e.g., acyclovir, gancyclovir, estrone sulfate), and zwitterions (e.g., cephalexin, cephadrine) (37, 38), so it is plausible that MATE1 contributes to TS biliary excretion. Mdr2 is the rodent ortholog of human MDR3, a phosphatidylcholine flippase, which also transports paclitaxel, digoxin, and verapamil (39). As expected, the biliary excretion of TG was significantly decreased in TR⁻ rat SCH compared to WT rat SCH, but was not altered by Bcrp knockdown, consistent with previous data that Mrp2 plays a major role in the biliary excretion of TG (24).

Even though the BEI of TS remained the same, the total recovery of TS was decreased in TR⁻ compared to WT rat SCH based on decreased TS cellular accumulation and medium concentrations. These data suggest that TGZ sulfation was decreased, or de-sulfation of TS was increased in TR⁻ rat SCH. TGZ is metabolized to TS primarily by SULT1A1 and also by SULT1E1 in humans (40). In rats, TS formation is four times faster in male rats compared to female rats, which is consistent with greater expression of Sult1a1 and Sult1e1 in male rats (41, 42). Interestingly, protein levels of hepatic Sult1a1 and Sult1e1 were comparable between WT and TR⁻ rats (43, 44), and our *in vitro* metabolism study using S9 fractions from livers of WT and TR⁻ rats revealed that TS formation rates were comparable. A decrease in net sulfation of estradiol-17 β -glucuronide (E₂17G) reported in TR⁻ rats was attributed to increased desulfation of estradiol-3-sulfate-17 β -glucuronide (44). However, desulfation of TS to TGZ was not observed in S9 fraction from livers of WT or TR⁻ rats. It is possible that the availability of 3'-phosphoadenosine-5'-phosphosulfate (PAPS) is less in TR⁻ compared to WT rat SCH. In rats and humans, sulfation can be limited by the availability of the cofactor PAPS. PAPS is synthesized rapidly by ATP-sulfurylase and APS-kinase, but its availability is limited by hepatic sulfate concentrations, which are largely dependent on circulating levels of inorganic sulfate (45). TR⁻ rat SCH may have lower levels of PAPS precursors or lower activity of enzymes involved in PAPS synthesis. These differences would not be detected in the current experimental design where adequate PAPS was added exogenously to the *in vitro* metabolism system. TR⁻ rat SCH also may have higher cellular concentrations of endogenous substrates (e.g., bile acids) that deplete PAPS, leading to decreased recovery of TS. Compared to WT rats,

hepatic sulfation activities in TR⁻ rats have been reported to be modestly increased (i.e., acetaminophen, 4-methylumbelliferone), similar (i.e., harmol, E₂17G), or decreased (i.e., resveratrol) in isolated perfused liver (IPL) studies (44, 46-50). However, except for the harmol and E₂17G studies, recovery was measured only in perfusate and bile, and mass balance did not account for recovery in the liver tissue. Further studies are warranted to investigate the mechanisms of altered sulfation in TR⁻ rats and the underlying reason for decreased recovery of TS in TR⁻ rat SCH.

The increase in total recovery of TG in cells, bile, and medium of TR⁻ rat SCH compared to WT rat SCH can be explained by increased activity of UGT enzymes, as shown in the *in vitro* S9 metabolism study. Species differences exist between humans and rats in UGT isozymes responsible for TGZ glucuronidation. TG formation is mediated primarily by UGT1A1 in humans whereas Ugt2b2 is the major isozyme responsible for TGZ glucuronidation in rats (51, 52). Expression of hepatic Ugt1a protein was increased in TR⁻ rats (43). Although expression of hepatic Ugt2b2 in TR⁻ rats has not been characterized, the present *in vitro* S9 metabolism data suggest that expression and/or activity of Ugt2b2 is increased in TR⁻ rats. Overall, decreased biliary excretion combined with increased glucuronidation led to significantly increased cellular accumulation of TG in TR⁻ compared with WT rat SCH. Medium concentrations of TG also were increased in TR⁻ rat SCH, consistent with increased glucuronidation and increased expression of the basolateral efflux transporter Mrp3 (43, 44).

The present study demonstrated that biliary excretion of TS was not altered by loss-of-function of Mrp2 and/or Bcrp, apparently due to a compensatory biliary transporter(s). These data suggest that loss-of-function of Mrp2 and Bcrp is not a risk factor for increased hepatocellular TS accumulation in rats. Interestingly, hepatocellular accumulation of TS was decreased in TR⁻ compared to WT rat SCH due to decreased TGZ sulfation. TR⁻ rats have been employed widely to investigate the contribution of Mrp2 to drug disposition, but loss-of-function of Mrp2 in TR⁻ rats leads to altered expression of several enzymes and transporters (e.g., decreased Bcrp, increased Mrp3, differential expression of CYP isoforms) (43, 53, 54). Results from the present study demonstrated for the first time that in TR⁻ rat SCH, TGZ sulfation was decreased, but these changes were not due to altered sulfotransferase activity. TGZ glucuronidation was

significantly increased, and TG biliary excretion was negligible, leading to increased cellular and medium TG concentrations in SCH from TR⁻ compared to WT rats. Evaluation of hepatocellular exposure of a drug may be important in predicting efficacy and/or toxicity if the liver is the site of action, or the parent drug and/or generated metabolites elicit hepatotoxic effects. These data suggest that altered hepatocellular exposure of hepatically-generated metabolites is determined by both formation and excretion, and that compensatory mechanisms may play important roles when elimination pathways are impaired.

Figure 5.1. Proposed mechanism of troglitazone (TGZ)-mediated hepatotoxicity.

Impaired BCRP and/or MRP2 function (1) causes accumulation of TGZ sulfate (TS; the major TGZ metabolite and a potent inhibitor of bile acid transport proteins) in hepatocytes (2), which inhibits bile acid excretion leading to bile acid accumulation (3) and hepatotoxicity (4).

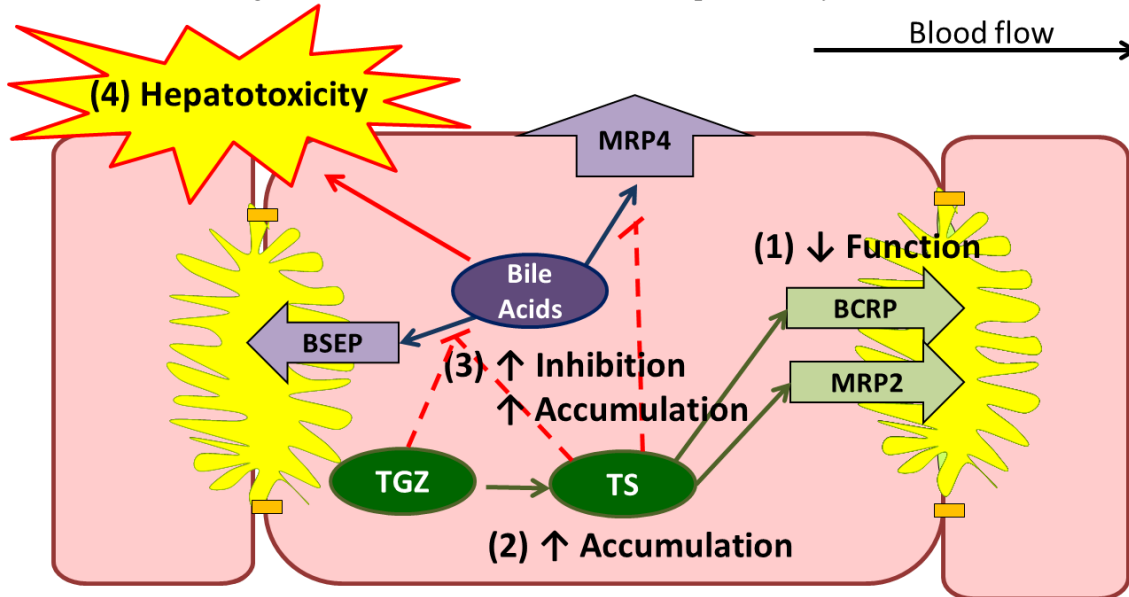


Figure 5.2. Intracellular accumulation of troglitazone (TGZ) and generated metabolites [TGZ sulfate (TS) and TGZ glucuronide (TG)] in WT and TR⁻ rat SCH in the absence or presence of Bcrp Knockdown.

WT and TR⁻ rat SCH were treated with 10 μM TGZ for 30 min in the absence [CTL (non-infected cells) and Ad-siNT (non-target control)] or presence (Ad-siBcrp) of Bcrp knockdown. Hepatobiliary disposition of (A) TGZ, (B) TS, and (C) TG were measured in cells+bile (solid bars) and in cells (open bars). Effects of Bcrp knockdown (CTL vs. Ad-siNT vs. Ad-siBcrp) and rat type (WT vs. TR⁻) on accumulation and biliary excretion index (BEI; diamonds) of TGZ and generated metabolites were evaluated using two-way ANOVA. Data represent mean±S.E.M.; †, *P* < 0.05, significantly different from WT (cells+bile); ‡, *P* < 0.05, significantly different from WT (cell); *, *P* < 0.05, significantly different from WT (BEI).

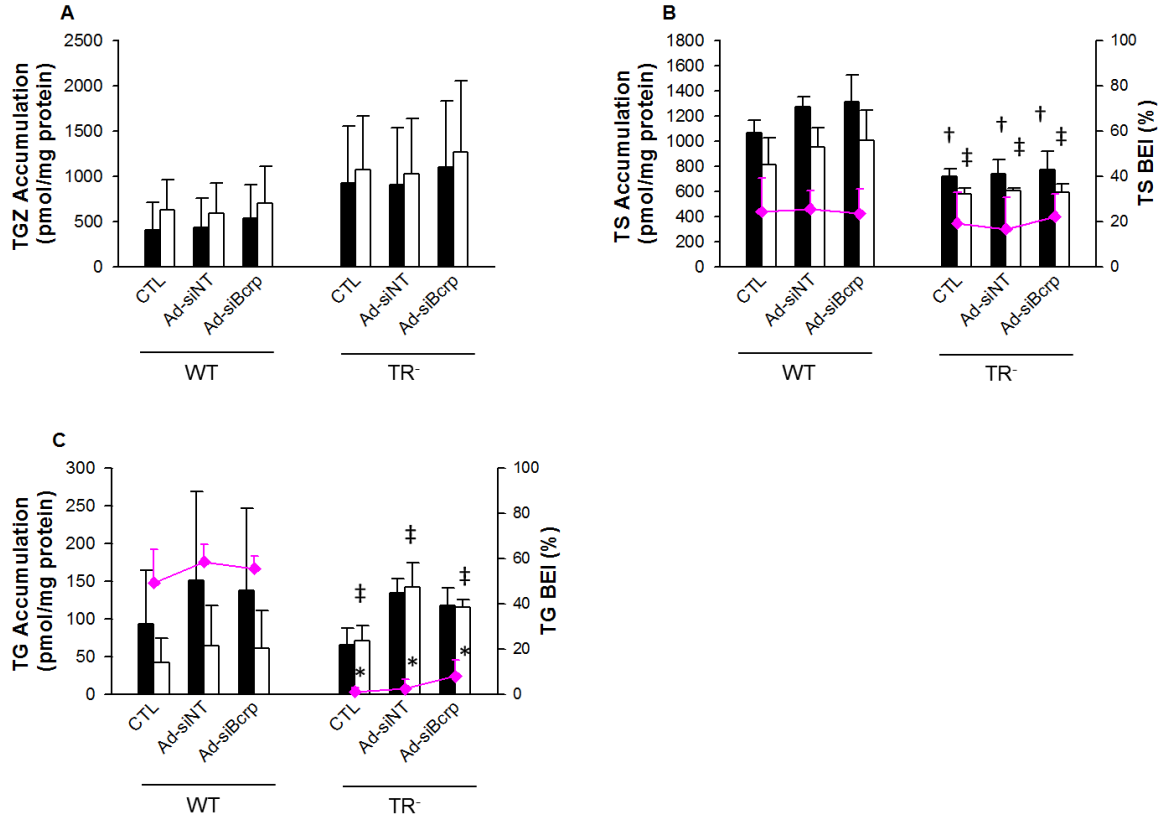


Figure 5.3. Accumulation of troglitazone (TGZ) and generated metabolites [TGZ sulfate (TS) and TGZ glucuronide (TG)] in the medium of WT and TR⁻ rat SCH in the absence or presence of Bcrp Knockdown.

WT and TR⁻ rat SCH were treated with 10 μ M TGZ for 30 min in the absence [CTL (non-infected cells) and Ad-siNT (non-target control)] or presence (Ad-siBcrp) of Bcrp knockdown. Concentrations of (A) TGZ, (B) TS, and (C) TG were measured in medium. Effects of Bcrp knockdown (CTL vs. Ad-siNT vs. Ad-siBcrp) and Mrp2 deficiency (WT vs. TR⁻) on media concentrations of TGZ and generated metabolites were evaluated using two-way ANOVA. Data represent mean \pm S.E.M.; *, $P < 0.05$, significantly different from WT.

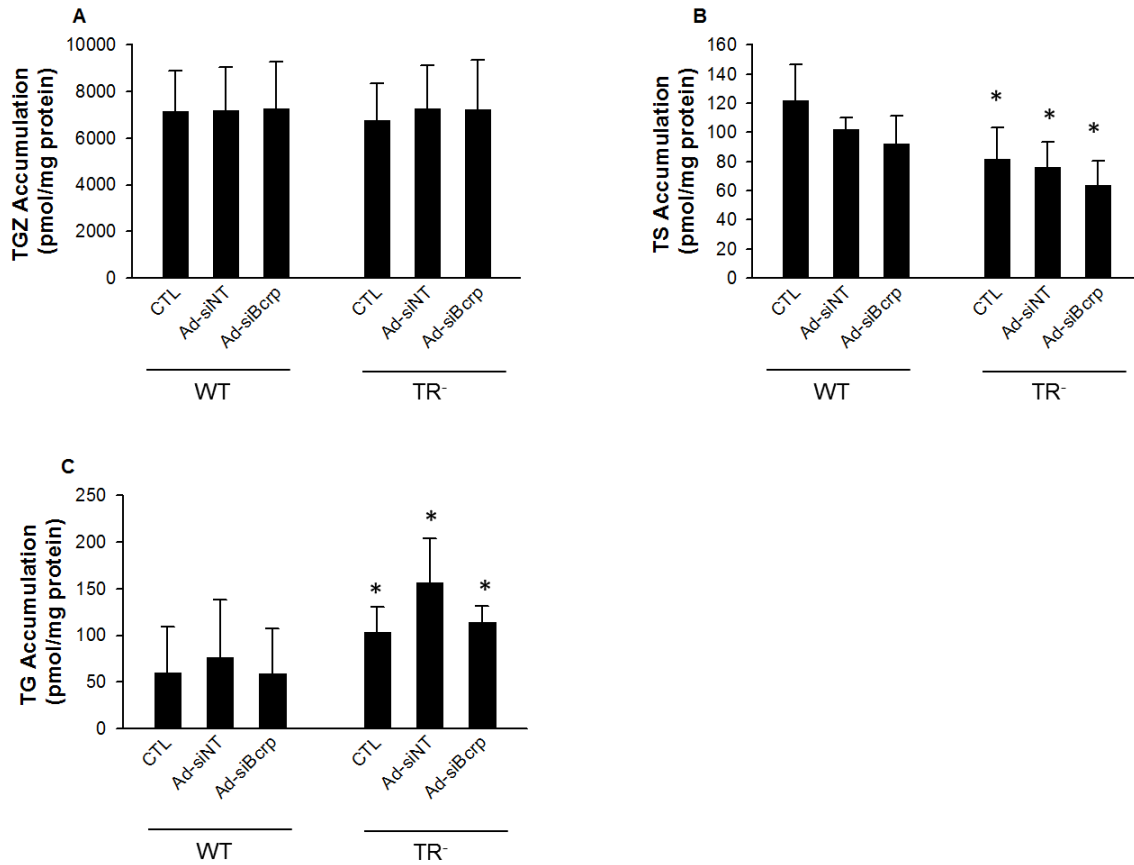


Figure 5.4. Recovery of troglitazone (TGZ) and generated metabolites [TGZ sulfate (TS), TGZ glucuronide (TG), and TGZ quinone (TQ)] in WT and TR^{-/-} rat SCH in the absence or presence of Bcrp Knockdown.

WT and TR^{-/-} rat SCH were treated with 10 μ M TGZ for 30 min in the absence (CTL and Ad-siNT) or presence (Ad-siBcrp) of Bcrp knockdown. Total recovery of TGZ and generated metabolites in cells, bile, and medium are presented as % of the TGZ dose. *, $P < 0.05$, significantly different from WT.

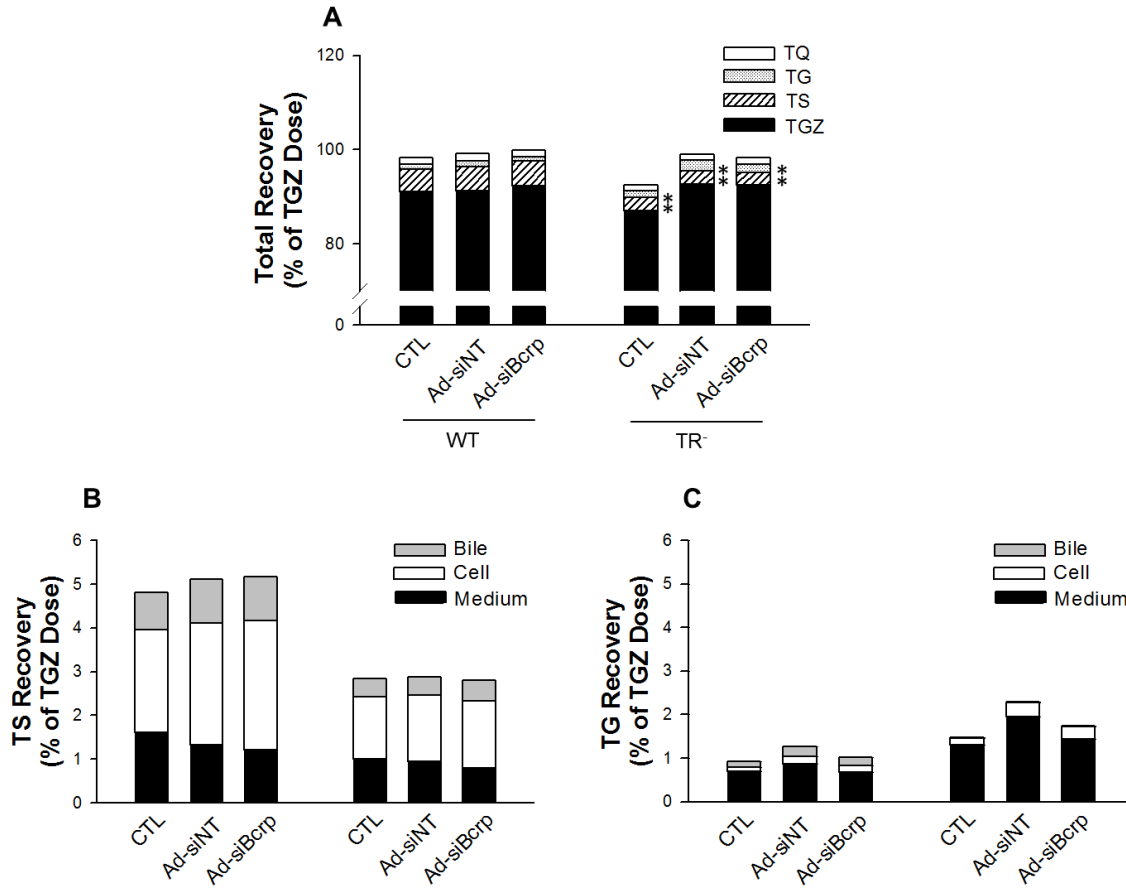


Figure 5.5. Bsep-mediated transport of taurocholate (TC) and troglitazone sulfate (TS) in membrane vesicles.

ATP-dependent transport of taurocholate and TS in membrane vesicles prepared from Sf9 cells overexpressing Bsep (Sf9-Bsep; open bars) or mock controls (Sf9-control; solid bars). The data represent mean±S.E.M. (n=3 in triplicate). *, $P < 0.05$, significantly different from mock controls.

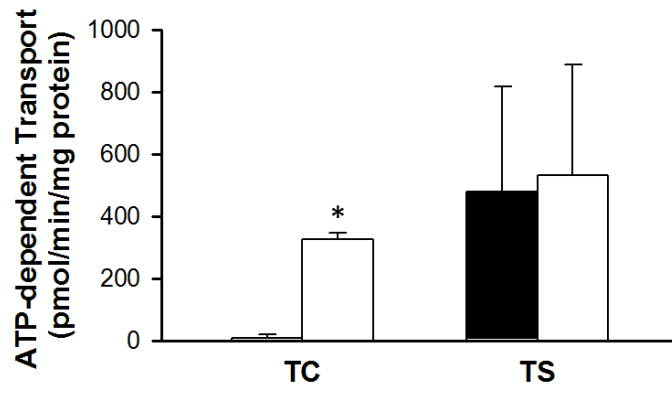


Figure 5.6. Hepatobiliary disposition of troglitazone (TGZ) and generated metabolites [TGZ sulfate (TS) and TGZ glucuronide (TG)] in WT and TR⁻ rat SCH in the absence or presence of GF120918. WT and TR⁻ rat SCH were incubated with 10 μ M TGZ for 30 min in the absence or presence of GF120918. Hepatobiliary disposition of (A) TS and (B) TG were measured in cells+bile (solid bars) and in cells (open bars). Effects of GF120918 and rat type (WT vs. TR⁻) on accumulation and the biliary excretion index (BEI) of TS and TG were evaluated using two-way ANOVA. †, $P < 0.05$, significantly different from WT (cells+bile); ‡, $P < 0.05$, significantly different from WT (cell); *, $P < 0.05$, significantly different from WT (BEI).

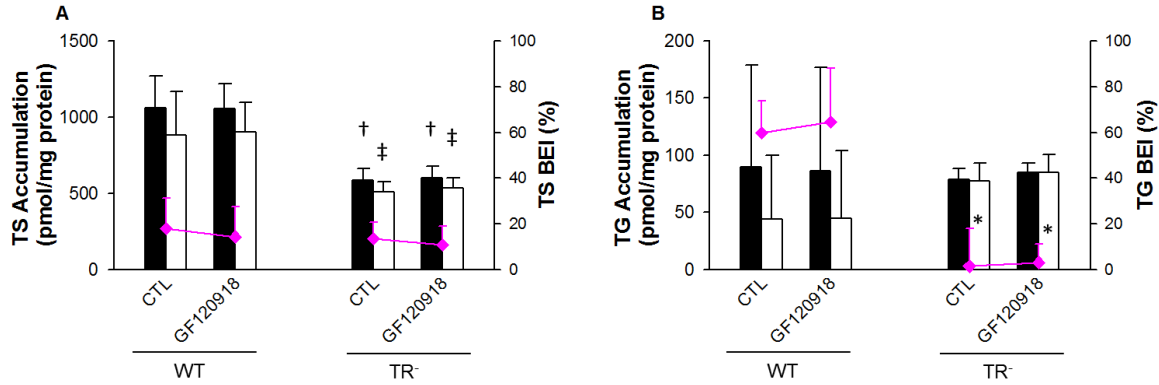
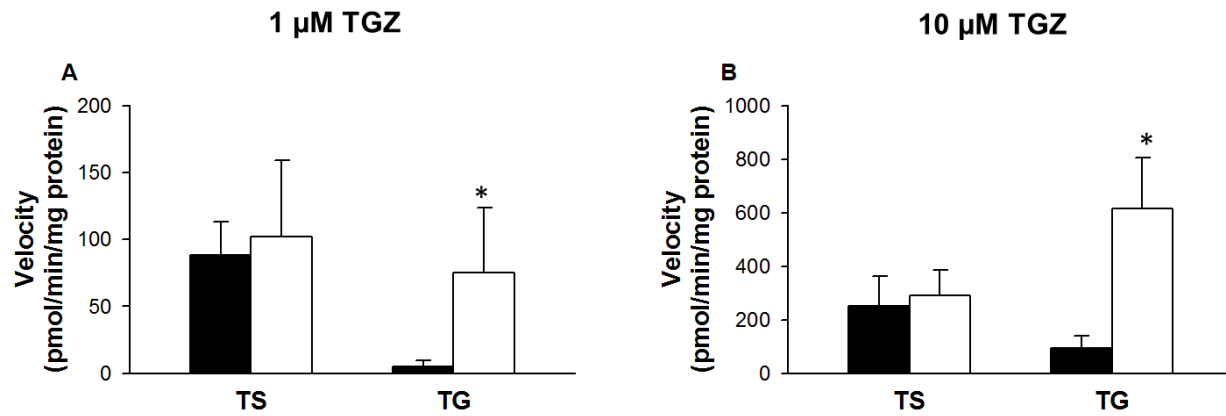


Figure 5.7. Metabolism of troglitazone (TGZ) in S9 fraction prepared from liver tissues of WT and TR^{-/-} rats.

The initial velocity of TGZ sulfate (TS) and TGZ glucuronide (TG) formation was obtained after incubation of 1 and 10 μ M TGZ with S9 fractions prepared from liver tissues of WT (solid bars) and TR^{-/-} (open bars) rats. *, $P < 0.05$, significantly different from WT.



REFERENCES

- (1) Temple, R.J. & Himmel, M.H. Safety of newly approved drugs: implications for prescribing. *JAMA* **287**, 2273-5 (2002).
- (2) Morgan, R.E. *et al.* Interference with bile salt export pump function is a susceptibility factor for human liver injury in drug development. *Toxicol Sci* **118**, 485-500 (2010).
- (3) Dawson, S., Stahl, S., Paul, N., Barber, J. & Kenna, J.G. In vitro inhibition of the bile salt export pump correlates with risk of cholestatic drug-induced liver injury in humans. *Drug Metab Dispos* **40**, 130-8 (2012).
- (4) Perez, M.J. & Briz, O. Bile-acid-induced cell injury and protection. *World J Gastroenterol* **15**, 1677-89 (2009).
- (5) Maillette de Buy Wenniger, L. & Beuers, U. Bile salts and cholestasis. *Dig Liver Dis* **42**, 409-18 (2010).
- (6) Lee, J.K., Paine, M.F. & Brouwer, K.L. Sulindac and its metabolites inhibit multiple transport proteins in rat and human hepatocytes. *J Pharmacol Exp Ther* **334**, 410-8 (2010).
- (7) Fattinger, K. *et al.* The endothelin antagonist bosentan inhibits the canalicular bile salt export pump: a potential mechanism for hepatic adverse reactions. *Clin Pharmacol Ther* **69**, 223-31 (2001).
- (8) Bohme, M., Muller, M., Leier, I., Jedlitschky, G. & Keppler, D. Cholestasis caused by inhibition of the adenosine triphosphate-dependent bile salt transport in rat liver. *Gastroenterology* **107**, 255-65 (1994).
- (9) Funk, C. *et al.* Troglitazone-induced intrahepatic cholestasis by an interference with the hepatobiliary export of bile acids in male and female rats. Correlation with the gender difference in troglitazone sulfate formation and the inhibition of the canalicular bile salt export pump (Bsep) by troglitazone and troglitazone sulfate. *Toxicology* **167**, 83-98 (2001).
- (10) Kis, E., Ioja, E., Nagy, T., Szente, L., Heredi-Szabo, K. & Krajcsi, P. Effect of membrane cholesterol on BSEP/Bsep activity: species specificity studies for substrates and inhibitors. *Drug Metab Dispos* **37**, 1878-86 (2009).
- (11) Mano, Y., Usui, T. & Kamimura, H. Effects of bosentan, an endothelin receptor antagonist, on bile salt export pump and multidrug resistance-associated protein 2. *Biopharm Drug Dispos* **28**, 13-8 (2007).

- (12) Watkins, P.B. & Whitcomb, R.W. Hepatic dysfunction associated with troglitazone. *N Engl J Med* **338**, 916-7 (1998).
- (13) St Peter, J.V., Neafus, K.L., Khan, M.A., Vessey, J.T. & Lockheart, M.S. Factors associated with the risk of liver enzyme elevation in patients with type 2 diabetes treated with a thiazolidinedione. *Pharmacotherapy* **21**, 183-8 (2001).
- (14) Smith, M.T. Mechanisms of troglitazone hepatotoxicity. *Chem Res Toxicol* **16**, 679-87 (2003).
- (15) Chojkier, M. Troglitazone and liver injury: in search of answers. *Hepatology* **41**, 237-46 (2005).
- (16) Gitlin, N., Julie, N.L., Spurr, C.L., Lim, K.N. & Juarbe, H.M. Two cases of severe clinical and histologic hepatotoxicity associated with troglitazone. *Ann Intern Med* **129**, 36-8 (1998).
- (17) Fukano, M. *et al.* Subacute hepatic failure associated with a new antidiabetic agent, troglitazone: a case report with autopsy examination. *Hum Pathol* **31**, 250-3 (2000).
- (18) Funk, C., Ponelle, C., Scheuermann, G. & Pantze, M. Cholestatic potential of troglitazone as a possible factor contributing to troglitazone-induced hepatotoxicity: in vivo and in vitro interaction at the canalicular bile salt export pump (Bsep) in the rat. *Mol Pharmacol* **59**, 627-35 (2001).
- (19) Yang, K., Yue, W., Koeck, K. & Brouwer, K.L.R. Interaction of troglitazone sulfate with hepatic basolateral and canalicular transport proteins. In 2011 AAPS Annual Meeting and Exposition.
- (20) Kawai, K. *et al.* Disposition and metabolism of the new oral antidiabetic drug troglitazone in rats, mice and dogs. *Arzneimittelforschung* **47**, 356-68 (1997).
- (21) Loi, C.M., Alvey, C.W., Vassos, A.B., Randinitis, E.J., Sedman, A.J. & Koup, J.R. Steady-state pharmacokinetics and dose proportionality of troglitazone and its metabolites. *J Clin Pharmacol* **39**, 920-6 (1999).
- (22) Loi, C.M., Alvey, C.W., Randinitis, E.J., Abel, R., Young, M.A. & Koup, J.R. Meta-analysis of steady-state pharmacokinetics of troglitazone and its metabolites. *J Clin Pharmacol* **37**, 1038-47 (1997).
- (23) Enokizono, J., Kusuhara, H. & Sugiyama, Y. Involvement of breast cancer resistance protein (BCRP/ABCG2) in the biliary excretion and intestinal efflux of troglitazone sulfate, the major metabolite of troglitazone with a cholestatic effect. *Drug Metab Dispos* **35**, 209-14 (2007).

- (24) Kostrubsky, V.E. *et al.* The effect of troglitazone biliary excretion on metabolite distribution and cholestasis in transporter-deficient rats. *Drug Metab Dispos* **29**, 1561-6 (2001).
- (25) Lee, J.K., Marion, T.L., Abe, K., Lim, C., Pollock, G.M. & Brouwer, K.L. Hepatobiliary disposition of troglitazone and metabolites in rat and human sandwich-cultured hepatocytes: use of Monte Carlo simulations to assess the impact of changes in biliary excretion on troglitazone sulfate accumulation. *J Pharmacol Exp Ther* **332**, 26-34 (2010).
- (26) Yang, K., Pfeifer, N.D., Hardwick, R.N., Yue, W., Stewart, P.W. & Brouwer, K.L. An Experimental Approach to Evaluate the Impact of Impaired Transport Function on Hepatobiliary Drug Disposition using Mrp2-deficient TR Rat Sandwich-Cultured Hepatocytes in Combination with Bcrp Knockdown. *Mol Pharm*, (2014).
- (27) Saha, S., New, L.S., Ho, H.K., Chui, W.K. & Chan, E.C. Direct toxicity effects of sulfo-conjugated troglitazone on human hepatocytes. *Toxicol Lett* **195**, 135-41 (2010).
- (28) Swift, B., Pfeifer, N.D. & Brouwer, K.L. Sandwich-cultured hepatocytes: an in vitro model to evaluate hepatobiliary transporter-based drug interactions and hepatotoxicity. *Drug Metab Rev* **42**, 446-71 (2010).
- (29) Yue, W., Abe, K. & Brouwer, K.L. Knocking down breast cancer resistance protein (Bcrp) by adenoviral vector-mediated RNA interference (RNAi) in sandwich-cultured rat hepatocytes: a novel tool to assess the contribution of Bcrp to drug biliary excretion. *Mol Pharm* **6**, 134-43 (2009).
- (30) Hill, J.R. In vitro drug metabolism using liver microsomes. *Curr Protoc Pharmacol* **Chapter 7**, Unit7 8 (2004).
- (31) Izumi, T. *et al.* Prediction of the human pharmacokinetics of troglitazone, a new and extensively metabolized antidiabetic agent, after oral administration, with an animal scale-up approach. *J Pharmacol Exp Ther* **277**, 1630-41 (1996).
- (32) Izumi, T., Hosiyama, K., Enomoto, S., Sasahara, K. & Sugiyama, Y. Pharmacokinetics of troglitazone, an antidiabetic agent: prediction of in vivo stereoselective sulfation and glucuronidation from in vitro data. *J Pharmacol Exp Ther* **280**, 1392-400 (1997).
- (33) Hewitt, N.J. *et al.* Correlation between troglitazone cytotoxicity and drug metabolic enzyme activities in cryopreserved human hepatocytes. *Chem Biol Interact* **142**, 73-82 (2002).
- (34) Fu, Y., Sheu, C., Fujita, T. & Foote, C.S. Photooxidation of troglitazone, a new antidiabetic drug. *Photochem Photobiol* **63**, 615-20 (1996).

- (35) Mao, Q. & Unadkat, J.D. Role of the breast cancer resistance protein (ABCG2) in drug transport. *AAPS J* **7**, E118-33 (2005).
- (36) Rautio, J. *et al.* In vitro p-glycoprotein inhibition assays for assessment of clinical drug interaction potential of new drug candidates: a recommendation for probe substrates. *Drug Metab Dispos* **34**, 786-92 (2006).
- (37) Klaassen, C.D. & Aleksunes, L.M. Xenobiotic, bile acid, and cholesterol transporters: function and regulation. *Pharmacol Rev* **62**, 1-96 (2010).
- (38) Hillgren, K.M. *et al.* Emerging transporters of clinical importance: an update from the International Transporter Consortium. *Clin Pharmacol Ther* **94**, 52-63 (2013).
- (39) Smith, A.J. *et al.* MDR3 P-glycoprotein, a phosphatidylcholine translocase, transports several cytotoxic drugs and directly interacts with drugs as judged by interference with nucleotide trapping. *J Biol Chem* **275**, 23530-9 (2000).
- (40) Honma, W. *et al.* Phenol sulfotransferase, ST1A3, as the main enzyme catalyzing sulfation of troglitazone in human liver. *Drug Metab Dispos* **30**, 944-9 (2002).
- (41) Liu, L. & Klaassen, C.D. Ontogeny and hormonal basis of male-dominant rat hepatic sulfotransferases. *Mol Pharmacol* **50**, 565-72 (1996).
- (42) Demyan, W.F. *et al.* Estrogen sulfotransferase of the rat liver: complementary DNA cloning and age- and sex-specific regulation of messenger RNA. *Mol Endocrinol* **6**, 589-97 (1992).
- (43) Johnson, B.M., Zhang, P., Schuetz, J.D. & Brouwer, K.L. Characterization of transport protein expression in multidrug resistance-associated protein (Mrp) 2-deficient rats. *Drug Metab Dispos* **34**, 556-62 (2006).
- (44) Sun, H., Zeng, Y.Y. & Pang, K.S. Interplay of phase II enzymes and transporters in futile cycling: influence of multidrug resistance-associated protein 2-mediated excretion of estradiol 17beta-D-glucuronide and its 3-sulfate metabolite on net sulfation in perfused TR(-) and Wistar rat liver preparations. *Drug Metab Dispos* **38**, 769-80 (2010).
- (45) Klaassen, C.D. & Boles, J.W. Sulfation and sulfotransferases 5: the importance of 3'-phosphoadenosine 5'-phosphosulfate (PAPS) in the regulation of sulfation. *FASEB J* **11**, 404-18 (1997).

- (46) Zamek-Gliszczyński, M.J., Hoffmaster, K.A., Humphreys, J.E., Tian, X., Nezasa, K. & Brouwer, K.L. Differential involvement of Mrp2 (Abcc2) and Bcrp (Abcg2) in biliary excretion of 4-methylumbelliferyl glucuronide and sulfate in the rat. *J Pharmacol Exp Ther* **319**, 459-67 (2006).
- (47) Zamek-Gliszczyński, M.J., Hoffmaster, K.A., Nezasa, K. & Brouwer, K.L. Apparent differences in mechanisms of harmol sulfate biliary excretion in mice and rats. *Drug Metab Dispos* **36**, 2156-8 (2008).
- (48) Zamek-Gliszczyński, M.J. *et al.* Multiple mechanisms are involved in the biliary excretion of acetaminophen sulfate in the rat: role of Mrp2 and Bcrp1. *Drug Metab Dispos* **33**, 1158-65 (2005).
- (49) Xiong, H., Turner, K.C., Ward, E.S., Jansen, P.L. & Brouwer, K.L. Altered hepatobiliary disposition of acetaminophen glucuronide in isolated perfused livers from multidrug resistance-associated protein 2-deficient TR(-) rats. *J Pharmacol Exp Ther* **295**, 512-8 (2000).
- (50) Maier-Salamon, A., Hagenauer, B., Reznicek, G., Szekeres, T., Thalhammer, T. & Jager, W. Metabolism and disposition of resveratrol in the isolated perfused rat liver: role of Mrp2 in the biliary excretion of glucuronides. *J Pharm Sci* **97**, 1615-28 (2008).
- (51) Watanabe, Y., Nakajima, M. & Yokoi, T. Troglitazone glucuronidation in human liver and intestine microsomes: high catalytic activity of UGT1A8 and UGT1A10. *Drug Metab Dispos* **30**, 1462-9 (2002).
- (52) Yoshigae, Y., Konno, K., Takasaki, W. & Ikeda, T. Characterization of UDP-glucuronosyltransferases (UGTs) involved in the metabolism of troglitazone in rats and humans. *J Toxicol Sci* **25**, 433-41 (2000).
- (53) Yue, W., Lee, J.K., Abe, K., Sugiyama, Y. & Brouwer, K.L. Decreased hepatic breast cancer resistance protein expression and function in multidrug resistance-associated protein 2-deficient (TR(-)) rats. *Drug Metab Dispos* **39**, 441-7 (2011).
- (54) Newton, D.J., Wang, R.W. & Evans, D.C. Determination of phase I metabolic enzyme activities in liver microsomes of Mrp2 deficient TR- and EHBR rats. *Life Sci* **77**, 1106-15 (2005).

CHAPTER 6. Quantitative Relationship between Intracellular Lithocholic Acid, Chenodeoxycholic Acid and Toxicity in Sandwich-Cultured Hepatocytes; Incorporation into a Mechanistic Model of Drug-Induced Liver Injury¹

INTRODUCTION

Drug-induced liver injury (DILI) is the most common cause of acute fulminant hepatic failure (1), and is one of the primary reasons for withdrawal of approved drugs from the market. Currently, only 50% of clinical DILI is predicted from standard preclinical testing in rodents (2), and mechanisms underlying interspecies differences have not been fully elucidated. One proposed mechanism of DILI is inhibition of bile acid (BA) efflux in hepatocytes by drugs, which may result in intracellular accumulation of potentially toxic BAs (3, 4). Specifically, there is increasing evidence that inhibition of bile salt export pump (BSEP)-mediated biliary excretion of BAs by drugs is a risk factor for cholestatic or mixed hepatocellular/cholestatic DILI (5, 6). BAs play important roles in the body as key signaling molecules as well as lipid solubilizers, but can be cytotoxic when present at supraphysiologic concentrations in hepatocytes (7). BA toxicity is highly correlated with hydrophobicity; lithocholic acid (LCA), chenodeoxycholic acid (CDCA), and deoxycholic acid (DCA) are more cytotoxic than less hydrophobic BAs, cholic acid (CA) and ursodeoxycholic acid (UDCA) (3, 8, 9). Mechanisms of BA-induced hepatotoxicity include disruption of cell membranes due to their detergent-like properties, disruption of mitochondrial ATP synthesis, necrosis, and apoptosis (3).

In vitro screening for BSEP inhibition demonstrated the importance of BSEP inhibition in cholestatic/mixed type DILI (5, 6), but predictability of hepatotoxic potential of new chemical entities

¹This work has been presented, in part, at the 2013 SOT Annual Meeting and Toxpo, San Antonio, TX, March 10-14, 2013, and will be submitted to *Toxicological Sciences*.

using this isolated transporter system is limited due to the artificial nature of this membrane vesicle system (e.g., lack of metabolic enzymes), the complexity of hepatobiliary BA disposition, and our lack of understanding about the physiology of BA homeostasis. Hepatocellular accumulation of BAs is dependent upon both uptake and efflux (basolateral and canalicular) processes, and thus, data obtained from BSEP membrane vesicles may not represent the drug-BA interaction in the whole cell. For example, inhibition of BSEP-mediated biliary excretion by drugs may not lead to hepatocellular accumulation of BAs if the drug also significantly inhibits hepatic BA uptake (10). In this case, demonstration of BSEP inhibition in membrane vesicles can be a false safety signal because in the whole hepatocyte, BA concentrations may be decreased or unchanged. Therefore, net effects on the whole cell are important to accurately predict drug-induced hepatotoxicity. Furthermore, BA transport inhibition potential should be considered in terms of drug exposure at the site of interaction (e.g., systemic/portal vein exposure for uptake, hepatocellular exposure for canalicular/basolateral efflux). The situation is further complicated because BA homeostasis is tightly regulated by several nuclear receptors including farnesoid X receptor (FXR), pregnane X receptor (PXR), constitutive androstane receptor (CAR), and cell surface BA receptor TGR5 (11-14).

Mechanistic modeling is a useful approach to interpret and extrapolate data obtained from different stages of drug development by integrating knowledge obtained at different scales of biological complexity (e.g., molecules, cells, organs, organisms, and populations) and different species. DILIsym[®] is a predictive, mechanistic, mathematical model based on the physiological processes involved in DILI that is under development as a public-private initiative (<http://dilisy.com/>) (15, 16). The model includes both physiology and drug disposition at multiple scales, ranging from molecular/cellular interactions to organ-tissue level considerations. Data from multiple species including humans, rats, and dogs, are incorporated in the model to explain interspecies differences in susceptibility to DILI and improve prediction of human DILI risk based on preclinical data. The current DILIsym[®] model includes components to predict and further explore reactive metabolite-mediated, mitochondrial, and BA-mediated toxicity. The BA homeostasis sub-model includes hepatobiliary disposition and enterohepatic

recirculation of LCA, CDCA, and respective metabolites, in addition to all other (“bulk”) BAs (17). LCA and CDCA were chosen because they are known to be hydrophobic and potentially toxic BA species; LCA is a secondary BA formed by bacterial metabolism of CDCA in the intestinal lumen (3). CDCA is the most widely implicated BA in cholestatic liver injury (18). An overview of the BA transport inhibition model within DILIsym[®] is presented in Figure 6.1. Altered BA disposition by drugs/metabolites can be simulated by combining physiologically-based pharmacokinetic predictions of hepatocellular drug/metabolite exposure with experimentally-derived estimates of transporter inhibition constants (e.g., IC_{50} or K_i). Accumulation of hepatocellular BAs will lead to decreased hepatocyte ATP, which is an important determinant of necrotic cell death in DILIsym[®]; hepatocyte death will result in increased serum biomarkers of hepatocellular injury and function (e.g., ALT, AST, bilirubin). Loss of hepatocytes will subsequently influence drug and BA disposition, allowing dynamic interaction between kinetics and toxicity mechanisms.

It has been widely accepted that intracellular accumulation of BAs results in hepatotoxicity but, surprisingly, the relationship between hepatocellular BA accumulation and toxicity has not been assessed quantitatively until recently. Chatterjee et al. measured CDCA and DCA toxicity and intracellular accumulation in rat SCH (19), but similar data are not available for humans and other species. To fill this data gap, which is essential to link BA kinetics to toxicity in a BA transport inhibition model within DILIsym[®], studies were undertaken in sandwich-cultured hepatocytes (SCH) from human, rat, mouse, and dog, and quantitative relationships between intracellular LCA and CDCA exposure and toxicity were established. SCH, which maintain metabolic and transporter function as well as regulatory machinery (20-22), were chosen for the current study since direct quantification of intracellular BA and ATP concentrations are possible with this system model. SCH are useful to investigate species differences in hepatobiliary disposition and hepatotoxicity of drugs and endogenous compounds such as BAs. This study also provides insight into species differences in the hepatocellular disposition and toxicity of LCA and CDCA.

METHODS

Chemicals

LCA, CDCA, tauroolithocholic acid (TLCA), taurohyodeoxycholic acid (THDCA), and Triton X-100 were purchased from Sigma-Aldrich (St. Louis, MO). Lactate dehydrogenase (LDH)-Cytotoxicity Detection Kit and CellTiter-Glo[®] Luminescent Cell Viability Assay Kit were purchased from Roche Applied Science (Indianapolis, IN) and Promega (Fitchburg, WI), respectively. Culture medium, standard Hanks balanced salts solution (HBSS), and Ca²⁺-free HBSS (HBSS without Ca²⁺ and Mg²⁺, with 0.38g/L ethylene glycol tetraacetic acid) were provided by Qualyst Transporter Solutions, LLC (Durham, NC). The d₈-taurocholic acid (d₈-TCA) was purchased from Martrex, Inc. (Minnetonka, MN); d₅-TCA, d₅-taurochenodeoxycholic acid (d₅-TCDCA), and d₄-glycochenodeoxycholic acid (d₄-GCDCA) were purchased from Toronto Research Chemicals, Inc. (Toronto, Ontario, Canada). The d₄-glycocholic acid (d₄-GCA), d₄-CDCA, and d₄-CA (cholic acid) were purchased from CDN Isotopes, Inc. (Pointe-Claire, Quebec, Canada), and glycolithocholic acid (GLCA), glycohyodeoxycholic acid (GHDCA), and β-tauromuricholic acid (β-TMCA) were purchased from Steraloids, Inc. (Newport, RI). All other chemicals and reagents were of analytical grade and were readily available from commercial sources.

Cytotoxicity assay and data analysis

Rat, human, mouse, and dog SCH were purchased from Qualyst Transporter Solutions (Durham, NC). Human hepatocytes were obtained from one African American male (51 years old, BMI 30.86kg/m²), one Caucasian male (78 years old, BMI 33.1kg/m²), and one Caucasian female (62 years old, BMI 24kg/m²). Prior studies have reported that the culture days required for SCH to regain polarity varies among species. Thus, cytotoxicity and BA disposition studies were performed on the culture days optimized for each species: days 3–4, 6–8, 2–3, and 3–5, for rat, human, mouse, and dog, respectively (20). On day 3 (rat), 6 (human), 2 (mouse), or 4 (dog) of culture, cells were incubated with LCA (25, 50, 100, 125, 150, and 200μM), 0.1% DMSO (vehicle control), or 2% Triton-X (positive control) for 6, 12, and 24hr. CDCA toxicity was tested only in rat and human SCH; day 3 rat and day 6 human SCH were

incubated with CDCA (50, 100, 250, 375, 500, and 1000 μ M for rat SCH; 250, 375, 500, 650, 800, and 1000 μ M for human SCH), 0.1% DMSO (vehicle control), or 2% Triton-X (positive control) for 6, 12, and 24hr. Cytotoxicity was assessed by LDH release from damaged cells using the LDH-Cytotoxicity Detection Kit according to the manufacturer's protocol. Briefly, after incubation of SCH with BA for designated times, culture medium was collected and aliquots were placed in individual wells of a 96-well plate. The substrate mixture was added to the culture medium and incubated for 15min. During this time, tetrazolium salt 2-(4-iodophenyl)-3-(4-nitrophenyl)-5-phenyl-2H-tetrazolium chloride (INT) in the substrate mixture was reduced to formazan by enzymatic reaction mediated by LDH in the culture medium. Then formazan formation was measured using PowerWaveTM XS Microplate Spectrophotometer (BioTek, Winooski, VT) at 492 nm. Data were corrected for baseline levels in vehicle control (0.1% DMSO-treated SCH) and presented as a percentage of positive control (2% Triton X-100-treated SCH) using the following equation;

$$\text{Cytotoxicity (\%)} = \frac{\text{absorbance of samples} - \text{absorbance of vehicle control}}{\text{absorbance of positive control} - \text{absorbance of vehicle control}} \times 100 \quad (1)$$

The values measured after complete cell lysis using 2% Triton X-100 were considered as maximum cell death (100% cytotoxicity).

Intracellular ATP levels were measured using CellTiter-Glo[®] Luminescent Cell Viability Assay Kit according to the manufacturer's protocol. Briefly, after incubation of SCH with BAs for designated times, culture medium was collected for LDH analysis, and the remaining medium was aspirated from each well twice, and cells were washed with phosphate-buffered saline. Equal volumes of fresh culture medium and CellTiter-Glo reagent (prepared by adding lyophilized CellTiter-Glo substrate to CellTiter-Glo buffer) were added to each well, and plates were placed on an orbital shaker for 2min to induce cell lysis. After incubating plates at room temperature for 10min to allow the luminescent signal to stabilize, luminescence was measured (TopCount NXTTM; Packard, Meriden, CT). Standard samples with known ATP concentrations (0.01–1 μ M ATP) were measured coincident with SCH samples for absolute quantification of ATP concentrations in the hepatocytes. Intracellular ATP concentrations were calculated

by dividing ATP amount (pmol/well) by cellular volume (1.26µl/well) (23), and corrected for cell viability obtained from the LDH assay using the following equations;

$$\text{Cellular ATP concentration of viable cells (mM)} = \frac{\text{ATP amount}}{\text{Cellular volume}} \times \frac{1}{\text{Fraction viable cells}} \quad (2)$$

$$\text{Fraction viable cells} = \frac{100 - \% \text{ cytotoxicity}}{100} \quad (3)$$

The relationship between medium concentrations BA (LCA or CDCA) and intracellular ATP concentrations were evaluated using linear regression analysis. The least-squares estimates for the slope and intercept for the estimated regression lines were obtained using the following model; $Y = \alpha + \beta * X$, where Y represents intracellular ATP concentrations (mM) and X represents medium concentrations of BA (µM). The null hypothesis was $\beta=0$, and the alternative hypothesis was $\beta \neq 0$. The concentration required to kill one-half of the cells, LC_{50} , was estimated by performing non-linear regression analysis on BA medium concentration-LDH leakage data using the following equation:

$$Y = Y_0 + \frac{Y_{inf} - Y_0}{1 + 10^{(\log LC_{50} - \log X) * HillSlope}} \quad (4)$$

where Y represents the measured LDH leakage presented as % of positive control and X represents medium concentrations of BA, Y_0 represents LDH leakage in the absence of exogenous BAs, Y_{inf} represents the LDH leakage at infinite BA medium concentrations, LC_{50} represents the BA medium concentration that gives a response half way between Y_0 and Y_{inf} , and the Hill Slope is the slope at the point of inflection. The data analysis was performed using GraphPad Prism (version 6, La Jolla, CA).

LC-MS/MS analysis of intracellular LCA, CDCA, and their metabolites

After incubation of SCH with LCA and CDCA for designated times, medium was removed and cells were washed with Ca^{2+} -free HBSS. Then hepatocytes were incubated with Ca^{2+} -free HBSS for 5min to open tight junctions using B-CLEAR[®] technology (Qualyst Transporter Solutions, LLC, Durham, NC). Cell lysate samples were prepared and analyzed using liquid chromatography coupled with tandem mass spectrometry (LC-MS/MS) analysis as described previously (Marion 2011). TCA, GCA, TCDCA, GCDCA, CA, and CDCA were measured using calibration curves prepared with stable isotope equivalents to avoid any background contribution from these endogenous BAs. It was not necessary to

use stable isotope equivalents for LCA, TLCA, GLCA, THDCA, and GHDCa. The calibration curve using β -TMCA to measure α/β -TMCA was prepared using a non-rodent analytical plate to avoid background contribution of this endogenous BA in rodents. Under the chromatographic conditions used for this study, the stereoisomers α - and β -TMCA were not separated and were, thus, measured collectively and designated as α/β -TMCA. GMCA values were estimated using TMCA calibration curves and correction factor for the difference in molar response observed between d_8 -TCA and d_4 -GCA. The concentration ranges of the cell lysate calibration curves and the transitions monitored at unit resolution are listed in Supplementary Table 6.1. LC-MS/MS analysis was performed as described previously with the following exceptions; injection volume ranged from 5–20 μ l, depending on the specific analyte; injection rinse solutions were composed of 50:50 methanol:acetonitrile; and chromatographic separation was achieved using a gradient with mobile phase consisting of methanol and 0.5mM ammonium acetate over a 20–25min run time. The transitions monitored at unit resolution are listed in Supplementary Table 6.2. Intracellular BA concentrations were calculated by dividing the amount of BA (pmol/well) by the cellular volume (1.26 μ l/well) (23), and corrected for cell viability obtained from the LDH assay, as described above for intracellular ATP calculations.

LCA and CDCA toxicity modeling

A model incorporating intracellular LCA and CDCA concentrations, which change over time and serve as the toxicity signal, and inhibition of ATP production was constructed using the existing cellular ATP model within DILIsym[®] v1A, which describes ATP production and utilization (Figure 6.1) (15, 16). A continuous function describing the intracellular concentration of the LCA or CDCA over time was generated from the *in vitro* SCH data. This function was used to generate a signal for inhibition of ATP production by the following three equations:

$$\frac{d[\text{TS}]}{dt} = k([\text{BA}] - [\text{TS}]) \quad (5)$$

$$\text{IF} = \frac{V_{\text{max,tox}} * [\text{TS}]^Y}{K_{\text{m,tox}}^Y + [\text{TS}]^Y} \quad (6)$$

$$F_{\text{ATP prod}} = \frac{1}{1+\text{IF}} \quad (7)$$

where [BA] is the intracellular BA concentration, and [TS] is the toxicity signal, which was incorporated in the model to account for the delay between intracellular BA accumulation and the decline in ATP; k represents the time constant for the delayed relationship between the BA concentration and the ATP decline. $V_{\text{max,tox}}$, $K_{\text{m,tox}}$, and γ are the Hill equation parameters for the relationship between [TS] (delayed BA concentrations) and the inhibition factor (IF), and $F_{\text{ATP prod}}$ is the fraction by which ATP production is multiplied to produce the observed toxicity. The parameters $V_{\text{max, tox}}$, $K_{\text{m, tox}}$, γ , and k were fit to the *in vitro* SCH data. These equations were incorporated into the DILIsym[®] model and link hepatocellular BA concentrations and toxicity in DILIsym[®] v2A.

RESULTS

Toxicity and intracellular accumulation of BAs in LCA-treated rat, human, mouse, and dog SCH

In rat SCH treated with LCA, cellular ATP levels decreased in a concentration-dependent manner with respect to LCA concentrations in medium (Figure 6.2A); the linear regression analysis indicated that the slopes were significantly different from zero at 6hr ($p=0.0001$, $r^2=0.59$), 12hr ($p=0.0057$, $r^2=0.70$), and 24hr ($p<0.0001$, $r^2=0.86$). In human SCH, intracellular ATP levels decreased in a concentration-dependent manner with respect to LCA concentrations in medium (Figure 6.2A); the slopes were significantly different from zero at 6hr ($p=0.0001$, $r^2=0.55$), 12hr ($p=0.0057$, $r^2=0.34$), and 24hr ($p<0.0001$, $r^2=0.62$) based on linear regression analysis. In human SCH exposed to LCA, ATP decline >50% was not observed until 24hr, suggesting a delayed response compared to the observed ATP decline in rat SCH by 6hr. In mouse SCH, a significant linear relationship between intracellular ATP levels and LCA medium concentrations was found only at 12hr ($p=0.003$, $r^2=0.37$), and in dog SCH, only at 24hr ($p<0.0001$, $r^2=0.60$) (Figure 6.2A). In rat SCH, LDH leakage was observed at LCA medium concentrations above 100 μM (Figure 6.2A); LC_{50} values were 168, 143, and 130 μM at 6hr, 12hr, and 24hr, respectively. Minimal LDH leakage was observed in human and mouse SCH (Figure 6.2A); in dog

SCH, LDH leakage was observed only at the highest LCA concentration (200 μ M) at 24hr (Figure 6.2A). LCA concentrations greater than 200 μ M were not tested because of the limited solubility of LCA in culture medium.

To establish the quantitative relationship between LCA-induced toxicity and hepatocellular exposure to LCA species, cellular accumulation of LCA and its conjugates were measured in LCA-treated SCH. Because no LDH leakage was observed at all the LCA concentrations tested in human and mouse SCH, and LDH leakage was observed only at the highest LCA concentration in dog SCH, cellular LCA species were measured only in human, mouse, and dog SCH treated with 100–200 μ M of LCA. Unconjugated LCA accumulated extensively (in low mM ranges) in rat, human, mouse, and dog SCH (Figure 6.2B). Cellular LCA concentrations increased in rat SCH with increasing LCA medium concentrations, whereas cellular TLCA and GLCA concentrations decreased at LCA medium concentrations above 100 μ M at which toxicity was observed (Figure 6.2B). Intracellular accumulation of LCA and GLCA in human SCH was comparable to those in rat SCH, whereas TLCA concentrations in human SCH were ~100-fold lower than rat SCH (Figure 6.2B). Unlike rat SCH, intracellular TLCA and GLCA concentrations increased with increasing LCA medium concentrations up to 200 μ M in human SCH. In mouse SCH, intracellular LCA concentrations were modestly lower compared to rat and human SCH (Figure 6.2B). TLCA concentrations were comparable to, or modestly higher than, GLCA concentrations in mouse SCH. In dog SCH, intracellular LCA concentrations were comparable to, or slightly lower than, rat and human SCH, and TLCA concentrations were ~10-fold lower than LCA concentrations; GLCA was below the calibration range at all the LCA medium concentrations analyzed (100–200 μ M) (Figure 6.2B).

In order to explore the metabolism of LCA in SCH, cellular accumulation of other BAs potentially derived from LCA (e.g., conjugates of CA, CDCA, MCA, and HDCA) were measured or estimated (GMCA) in rat, human, mouse, and dog SCH after LCA incubation. In rat SCH, intracellular TCDCA, GCDCA, and GMCA were increased after LCA treatment compared to endogenous levels in vehicle-treated hepatocytes, suggesting that LCA is metabolized to CDCA and MCA (Supplement Figure

6.1A). In human SCH, MCA species were not detected. Instead, GHDCa accumulated extensively in the cells in a concentration-dependent manner with respect to LCA concentrations in medium (Supplement Figure 6.1B). In mouse SCH, TCDCA and GCDCA increased after LCA treatment compared to vehicle-treated hepatocytes, indicating that CDCA species are formed from LCA (Supplement Figure 6.1C). In dog SCH, there were no significant increases in any measured BAs after LCA treatment (Supplement Figure 6.1D).

Toxicity and intracellular accumulation of BAs in CDCA-treated rat and human SCH

In rat SCH treated with 0–1000 μ M CDCA, cellular ATP levels decreased in a concentration-dependent manner with respect to CDCA concentrations in medium (Figure 6.3A); the slopes were significantly different from zero at 6hr ($p<0.0001$, $r^2=0.80$), 12hr ($p<0.0001$, $r^2=0.68$), and 24hr ($p<0.0001$, $r^2=0.82$) based on linear regression analysis. In human SCH, intracellular ATP levels decreased in a concentration-dependent manner with respect to CDCA concentrations in medium (Figure 6.3A); the linear regression analysis indicated that the slopes were significantly different from zero at 6hr ($p<0.0001$, $r^2=0.89$), 12hr ($p<0.0001$, $r^2=0.84$), and 24hr ($p<0.0001$, $r^2=0.85$). In both rat and human SCH, LDH leakage was increased in a concentration-dependent manner with respect to CDCA concentrations in medium (Figure 6.3A); LC_{50} values were lower in rat SCH (383, 258, and 243 μ M at 6hr, 12hr, and 24hr, respectively) compared to human SCH (727 μ M at 24hr; the model did not converge at 6hr and 12hr). In rat SCH, the maximum toxic responses (both ATP and LDH) at each CDCA concentration were achieved after 6–12hr incubation. In human SCH, cellular ATP levels were decreased to a minimum after 6–12hr, but increases in LDH leakage were time-dependent, indicating that the toxic responses were delayed in human compared to rat SCH (Figure 6.3A).

To establish a quantitative relationship between CDCA-induced toxicity and hepatocellular exposure to CDCA species, cellular accumulation of CDCA and its conjugates were measured in CDCA-treated SCH. In both rat and human SCH, unconjugated CDCA accumulated extensively (in low mM ranges), and intracellular GCDCA concentrations were greater by an order of magnitude than TCDCA (Figure 6.3B). In rat SCH, cellular CDCA and TCDCA concentrations increased with increasing CDCA

medium concentrations, whereas cellular GCDCA concentrations decreased at CDCA medium concentrations above 100–250 μ M (Figure 6.3B). Cellular accumulation of unconjugated CDCA increased over time at the highest CDCA medium concentration (1000 μ M) in rat SCH (Figure 6.3B). In human SCH, cellular CDCA and GCDCA concentrations increased with increasing CDCA medium concentrations up to 375 μ M, and then decreased at CDCA medium concentrations above 375 μ M, where toxicity was observed (Figure 6.3B). Cellular TCDCA concentrations were lower than endogenous levels at all CDCA concentrations tested in human SCH (Figure 6.3B).

In order to explore CDCA metabolism in SCH, cellular accumulation of other BAs potentially derived from CDCA (e.g., CA, MCA) and their conjugates also were measured (TMCA) or estimated (GMCA) in CDCA-treated rat and human SCH. In rat SCH, cellular MCA species (MCA, TMCA, and GMCA) increased after CDCA treatment compared to vehicle-treated control, indicating that MCA species are formed from CDCA (Supplement Figure 6.2A). Formation/conjugation of MCA appeared to be saturated at CDCA medium concentrations above 50–375 μ M. Intracellular GCA increased in rat SCH treated with CDCA concentrations of 100-250 μ M compared to vehicle-treated control only at 6hr; CA and TCA were below the calibration range. In CDCA-treated human SCH, unconjugated CA increased, whereas TCA and GCA concentrations decreased compared to vehicle-treated control (Supplement Figure 6.2B).

Parameterization of the relationship between hepatocellular LCA and CDCA concentrations and ATP

Models describing the relationship between intracellular LCA and CDCA, and ATP concentrations in rat and human SCH were constructed using the existing model of cellular ATP within DILIsym[®] (Figure 6.4A). Toxicophores were determined to be unconjugated LCA and CDCA in rat and human SCH. The representative model-generated fit of cellular ATP after LCA exposure in rat SCH is presented in Figure 6.4B. Parameter values ($K_{m,tox}$, $V_{max,tox}$, γ , and k) obtained by fitting the models to the data generated from LCA- and CDCA-treated rat and human SCH are presented in Table 6.1. The $K_{m,tox}$ values represent the approximate concentration at which toxicity begins to occur; a lower $K_{m,tox}$ value

suggests a greater susceptibility to intracellular buildup of that particular BA. This sub-model was incorporated into the BA transport inhibition model within DILIsym[®] to mathematically link hepatocellular BA accumulation (BA Homeostasis Model) and intracellular ATP concentrations (Cellular ATP Model; Figure 6.1).

DISCUSSION

Accumulation of toxic BAs in hepatocytes is involved in the pathogenesis of cholestatic diseases (18, 24, 25). The relative potency of BAs with respect to hepatotoxicity has been investigated using *in vitro* and *in vivo* systems (26, 27), but the relationship between hepatocellular BA concentrations and toxicity has not been determined quantitatively. Recently, Chatterjee et al. reported cytotoxicity and intracellular accumulation of CDCA and DCA in rat SCH (19). However, intracellular BAs were measured at CDCA or DCA medium concentrations up to 100 μ M, where minimal toxicity was observed. Thus, it is difficult to quantify direct relationships between BA accumulation and toxicity using this data. BA concentrations at the site of toxicity (liver or hepatocytes) rarely have been measured because sensitive and specific LC-MS/MS analyses are required. Most studies have reported apparent LC₅₀ values based on the BA concentrations administered to animals and/or medium concentrations for *in vitro* cytotoxicity studies. BAs exist as anions at physiologic pH, and are substrates of hepatic transporters [e.g., sodium-taurocholate cotransporting polypeptide (NTCP), BSEP, and multidrug resistance-associated protein (MRP)3 and 4] (28-30). As a result, medium (plasma) concentrations cannot be assumed to represent actual hepatocellular BA exposure. For example, intracellular LCA concentrations were more than 10-fold higher than medium concentrations in rat SCH incubated with 200 μ M LCA (Figure 6.2B). Given the same medium (plasma) exposure, intracellular accumulation of BA species may vary depending on the expression and/or function of uptake/efflux transporters and metabolic enzymes. For example, mouse SCH accumulated considerably less LCA than other species (Figure 6.2B). In this study, we established a quantitative relationship between intracellular BA concentrations and toxicity

using *in vitro* data obtained from SCH isolated from different species. This is the key information that connects BA kinetics and toxicity in DILIsym[®], a mechanistic model of DILI.

LCA, which is formed by bacterial 7 α -dehydroxylation of CDCA in the gut lumen, has been reported to be the most hydrophobic and toxic BA species, and animals administered LCA have been used as a model of intrahepatic cholestasis (31, 32). In the present study, LCA showed differential toxicity in SCH from different species; treatment with 0–200 μ M LCA exerted a concentration-dependent decrease in ATP in rat SCH, whereas the same medium concentrations showed a delayed decrease in ATP in human and dog SCH, and negligible/minimal toxicity in mouse SCH. In rat SCH exposed to LCA medium concentrations above 100 μ M, ATP levels already were decreased by 6hr compared to the vehicle-treated control, whereas LDH showed a time-dependent increase from 6–24hr, indicating that a delay existed between decreased ATP and LDH leakage (indicator of membrane integrity) in rat SCH. This is consistent with a previous report demonstrating a time delay between ATP depletion and a decrease in hepatocyte viability in rat primary hepatocytes (33). LDH leakage was not observed in human SCH, potentially due to delayed ATP decline and a delay in the time between ATP depletion and loss of cell viability. Toxicity may have been observed if human SCH had been incubated with LCA without daily medium changes. However, this hypothesis was not tested because SCH require daily medium changes to maintain viability due to high metabolic activity. In rat SCH, intracellular unconjugated LCA concentrations correlated with the observed toxicity. Interestingly, TLCA and GLCA cellular concentrations were decreased at LCA medium concentrations greater than 100 μ M, potentially due to altered (e.g., saturation, depletion) glycine- or taurine-conjugation, adaptive increases in hepatic efflux of these conjugates, or further metabolism (e.g., sulfation); similar trends were shown for intracellular TCDCA, GCDCA, and GMCA. Lower intracellular unconjugated LCA concentrations in LCA-treated mouse SCH may explain the lack of toxicity in this species. In human and dog SCH, intracellular unconjugated LCA concentrations were comparable to rat SCH at medium LCA concentrations up to 150 μ M, but no/minimal LDH leakage was observed, suggesting that human and dog SCH are more resistant to LCA-mediated toxicity given the same exposure. Although mechanisms of observed species

differences in the onset and potency of LCA toxicity remain to be investigated, a plausible hypothesis is that intracellular unbound LCA concentrations may differ among different species, potentially due to the differential intracellular binding/disposition/sequestration of LCA. It is also possible that differential accumulation of LCA at the site of toxicity (e.g., mitochondria) exists among different species. In addition to species differences in BA disposition, pathophysiological processes involved in the induction of LCA toxicity (e.g., mitochondrial function, induction of necrosis/apoptosis) downstream of BA exposure may contribute to differential sensitivity/resistance to BA toxicity.

CDCA is the dominant BA in humans, whereas it contributes a smaller proportion of the BA pool in rats and mice. Trihydroxy BAs (e.g., CA) are more abundant in rodents. After incubation with 0–1000 μ M CDCA, medium concentration-dependent toxicity was observed in both rat and human SCH. Human SCH showed delayed toxicity with a higher LC₅₀, suggesting that CDCA-mediated toxicity is less potent compared to rat SCH. In rat SCH, unconjugated CDCA and TCDCA increased with increasing CDCA medium concentrations, consistent with the observed toxicity. Cellular TCDCA was ~100-fold lower compared to CDCA; thus, it is plausible that unconjugated CDCA is associated with the observed toxicity in rat SCH. However, in human SCH, intracellular concentrations of all the measured CDCA species decreased at high CDCA medium concentrations, where toxicity was observed, so it is not clear which BA caused toxicity in human SCH. Further investigation of other CDCA metabolites may provide additional insight.

Results of the present studies demonstrated that rat was the most sensitive species to LCA toxicity in SCH, and CDCA induced toxicity at lower medium concentrations in rat SCH compared to human SCH. The fitted parameters ($K_{m,tox}$) also suggest that LCA and CDCA elicit toxicity at similar intracellular concentrations in rat SCH, and that human SCH are less susceptible to LCA and CDCA toxicity than rat SCH given the similar intracellular exposure. However, this does not necessarily mean that rats are the most sensitive species to DILI *in vivo*. To translate this *in vitro* data to *in vivo*, species differences in the *in vivo* BA profile and hepatocellular accumulation of individual BAs in the setting of drug administration needs to be considered. For example, even if toxicity was observed in rat SCH,

intracellular LCA concentrations that exert toxicity in rat SCH may be difficult to achieve *in vivo* in rats even after administration of a potent BA efflux inhibitor; typical rat hepatocellular LCA concentrations are in the low nM range whereas concentrations in the low mM range were required to elicit toxicity in rat SCH (34, 35). Also, systemic and hepatic CDCA concentrations observed *in vivo* in humans are higher compared to those in rats (34, 36-38). Mechanistic modeling is a useful tool that can incorporate information regarding drug pharmacokinetics and BA physiology/pathophysiology to predict *in vivo* liver injury across species. To build this mechanistic model, a quantitative empirical exposure-toxicity relationship was established using the data obtained from the current *in vitro* study. Toxic effects of BAs were linked to decreases in cellular ATP, which is an important determinant of cellular necrosis in DILI_{sym}[®]; in the current model, reactive metabolite-mediated interference with mitochondrial respiration also is linked to cellular ATP levels.

Several assumptions were made when the present data was incorporated into the mechanistic model. First, unconjugated LCA and CDCA were assumed to be associated with the observed toxicity because cellular unconjugated LCA/CDCA concentrations were correlated with observed toxicity in rat SCH. However, it is possible that conjugated LCA and CDCA might cause toxicity. Conjugation of LCA (amidation, sulfation, and glucuronidation) increases solubility and facilitates biliary/urinary excretion; thus, LCA conjugation generally is considered to be a detoxification pathway. However, LCA conjugates also cause cholestasis (39-41). GCDCA induces apoptosis in primary hepatocytes and mitochondrial permeability transition in isolated mitochondria (42, 43). Additional experiments (e.g., treatment of SCH with conjugates) would be needed to establish the relationship between LCA/CDCA conjugates and toxicity. Also, *in vitro* toxicity was measured after short-term exposure to high concentrations of BAs, assuming that toxicity was associated with direct effects on hepatocytes. A different experimental approach would be necessary to examine the acute effects of BAs on non-parenchymal cells, as well as the effects of long-term exposure to low concentrations of BAs on both parenchymal and non-parenchymal cells.

The present study also demonstrated that the SCH system could reproduce the previously reported species differences in LCA and CDCA hydroxylation. In rats, LCA and CDCA primarily undergo 6 β -hydroxylation to form MDCA and α MCA, respectively (Supplementary Figure 6.3) (44, 45). LCA also is metabolized to a lesser extent to HDCA, CDCA, and UDCA by 6 α -, 7 α -, and 7 β -hydroxylation, respectively (46). In the present study, CDCA formation was observed in LCA-treated rat SCH. Even if HDCA, MDCA, and UDCA were not detected, MCA, which is formed by subsequent hydroxylation of MDCA and CDCA, significantly accumulated in LCA-treated rat SCH. MCA also was found in CDCA-treated rat SCH. In humans, sulfate conjugation is the major LCA detoxification pathway, but LCA also undergoes CYP3A4-mediated hydroxylation (32). Unlike rats, LCA and CDCA are hydroxylated preferentially at the 6 α -position to form HDCA and hyocholic acid (HCA; γ MCA), respectively (Supplementary Figure 6.3) (47-49). HDCA and HCA species are found in small amounts in bile, serum and urine of healthy adult humans, but excretion of these BAs was increased in cholestatic patients (50-52) presumably due to adaptive up-regulation of CYP3A enzymes (Xie 1999). Consistent with these reports, intracellular GHDCAs were increased in LCA-treated human SCH in a concentration-dependent manner with respect to LCA concentrations in medium.

To our knowledge, this is the first investigation that has established quantitative relationships between intracellular LCA and CDCA exposure, and hepatocyte toxicity in multiple species. These relationships were incorporated into DILIsym[®] to link BA homeostasis and ATP dynamic sub-models, and can be used to predict DILI mediated by interruption of BA transport. Species differences in intracellular concentrations and toxic effects of LCA and CDCA after exposure to the same medium concentrations of these BAs were noted in the present studies. Due to species differences in BA metabolism, substrate/inhibitor specificity of BA transporters, BA composition and toxic effects of BAs reported here and elsewhere, preclinical species do not reliably predict BA-mediated DILI in humans (10, 12, 32, 53). Mechanistic modeling incorporating data generated from human-derived *in vitro* systems

including human SCH and membrane vesicles expressing human transporters would be expected to provide a more accurate approach to predict altered hepatic BA disposition and subsequent DILI in humans.

Table 6.1. Parameter values describing the relationship between hepatocellular lithocholic acid (LCA) and chenodeoxycholic acid (CDCA) concentrations, and intracellular ATP.

A model incorporating intracellular LCA and CDCA concentrations, the toxicity signals, and inhibition of ATP production was constructed using the existing cellular ATP model within DILIsym® (Figure 6.4; equations described in the Methods section). Parameter values were generated by fitting this model to hepatocellular bile acid (BA) concentrations and toxicity data obtained from *in vitro* rat and human sandwich-cultured hepatocytes incubated with LCA and CDCA. $V_{\max, \text{tox}}$, $K_{m, \text{tox}}$, and γ are the Hill equation parameters for the relationship between toxicity signal (TS; delayed BA concentration) and the inhibition factor (IF). $K_{m, \text{tox}}$ (μM), the delayed BA concentration producing half-maximal IF; $V_{\max, \text{tox}}$ (dimensionless), the maximal IF generated by TS; γ (dimensionless), Hill coefficient; k (1/hour), the time constant for the delayed relationship between the intracellular BA concentration and the ATP decline.

	LCA		CDCA	
	Rat	Human	Rat	Human
$K_{m, \text{tox}}$ (μM)	1000	2300	1000	4000
$V_{\max, \text{tox}}$ (dimensionless)	2.25	3	8	2
γ (dimensionless)	1.5	1.5	1.5	1.5
k (1/hour)	0.05	0.07	0.5	0.1

Figure 6.1. Schematic overview of the bile acid (BA) transport inhibition model in DILIsym[®].

Hepatic and systemic disposition of drugs/metabolites after intravenous (iv) and oral (po) administration are simulated using a physiologically-based pharmacokinetic (PBPK) model (**Drug PBPK Model**). The **Bile Acid Homeostasis Model** represents hepatobiliary disposition and enterohepatic recirculation of lithocholic acid (LCA) and chenodeoxycholic acid (CDCA) species, and all other (bulk) BAs (17); for simplicity, only the CDCA species are depicted in Figure 6.1. Using BA transport inhibition constants of drugs/metabolites (e.g., K_i , IC_{50}), altered BA disposition is simulated. Increased hepatocellular accumulation of BAs disrupts cellular energy balance and decreases intracellular ATP concentrations (**Cellular ATP Model**), leading to necrotic cell death (**Hepatocyte Life Cycle Model**) and elevations in serum biomarkers of hepatocellular injury and function (e.g., ALT, AST, bilirubin) (**Biomarker Model**) (15, 16).

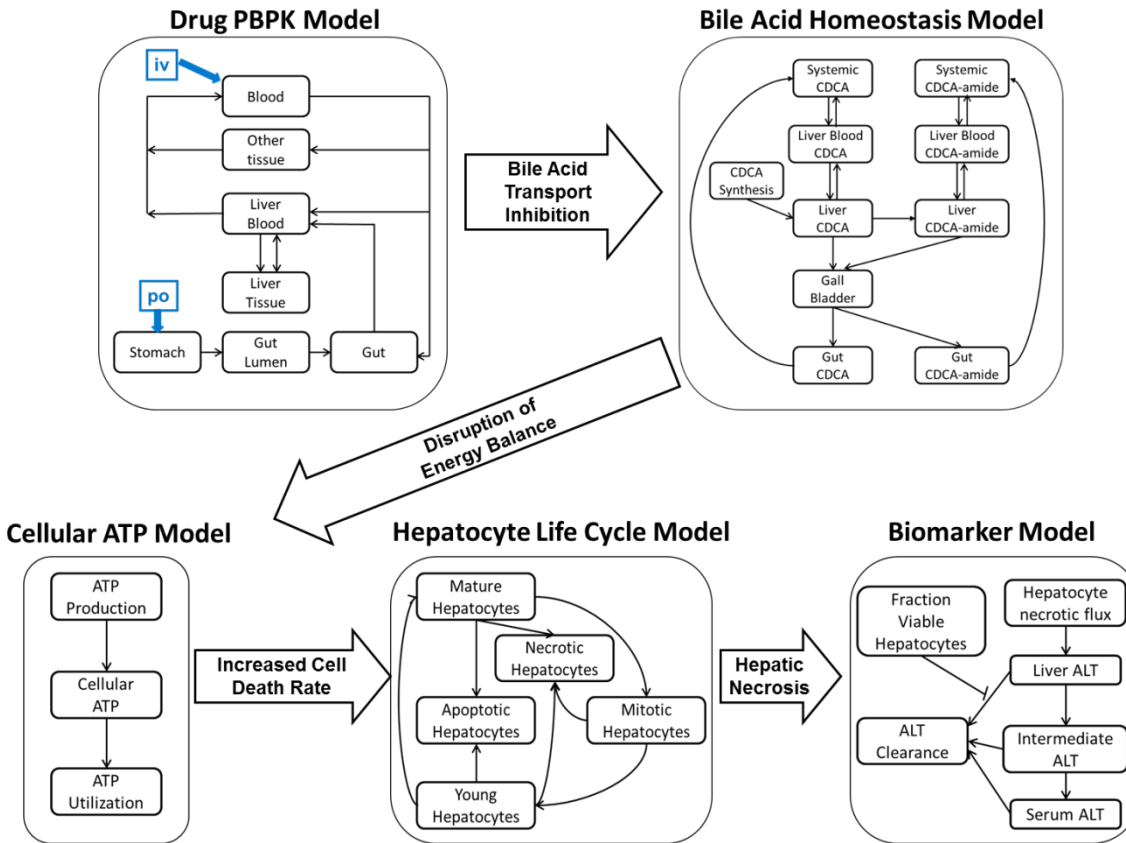


Figure 6.2. Toxicity and bile acid (BA) accumulation in lithocholic acid (LCA)-treated rat, human, mouse, and dog sandwich-cultured hepatocytes (SCH).

(A) Effects of LCA exposure on intracellular ATP and lactate dehydrogenase (LDH) release. Day 3 rat, day 6 human, day 2 mouse, and day 4 dog SCH were incubated with LCA (0–200 μ M) for 6hr (●), 12hr (○), and 24hr (◆). Representative data (mean \pm SD of triplicate determinations) from n=2 (rat, human, and dog) or n=1 (mouse) independent studies. **(B) Intracellular concentrations of LCA and LCA metabolites, glycolithocholic acid (GLCA) and taurolithocholic acid (TLCA).** Day 3 rat, day 6 human, day 2 mouse, and day 4 dog SCH were incubated with LCA (0–200 μ M) for 6hr (●), 12hr (○), and 24hr (◆). Intracellular LCA and LCA metabolites were measured by LC-MS/MS analysis of lysate after hepatocytes were incubated for 5min with Ca⁺²-free HBSS buffer to open tight junctions using B-CLEAR[®]. Representative data (mean \pm SD of triplicate determinations) from n=1 (rat, mouse, and dog) or n=2 (human) independent studies.

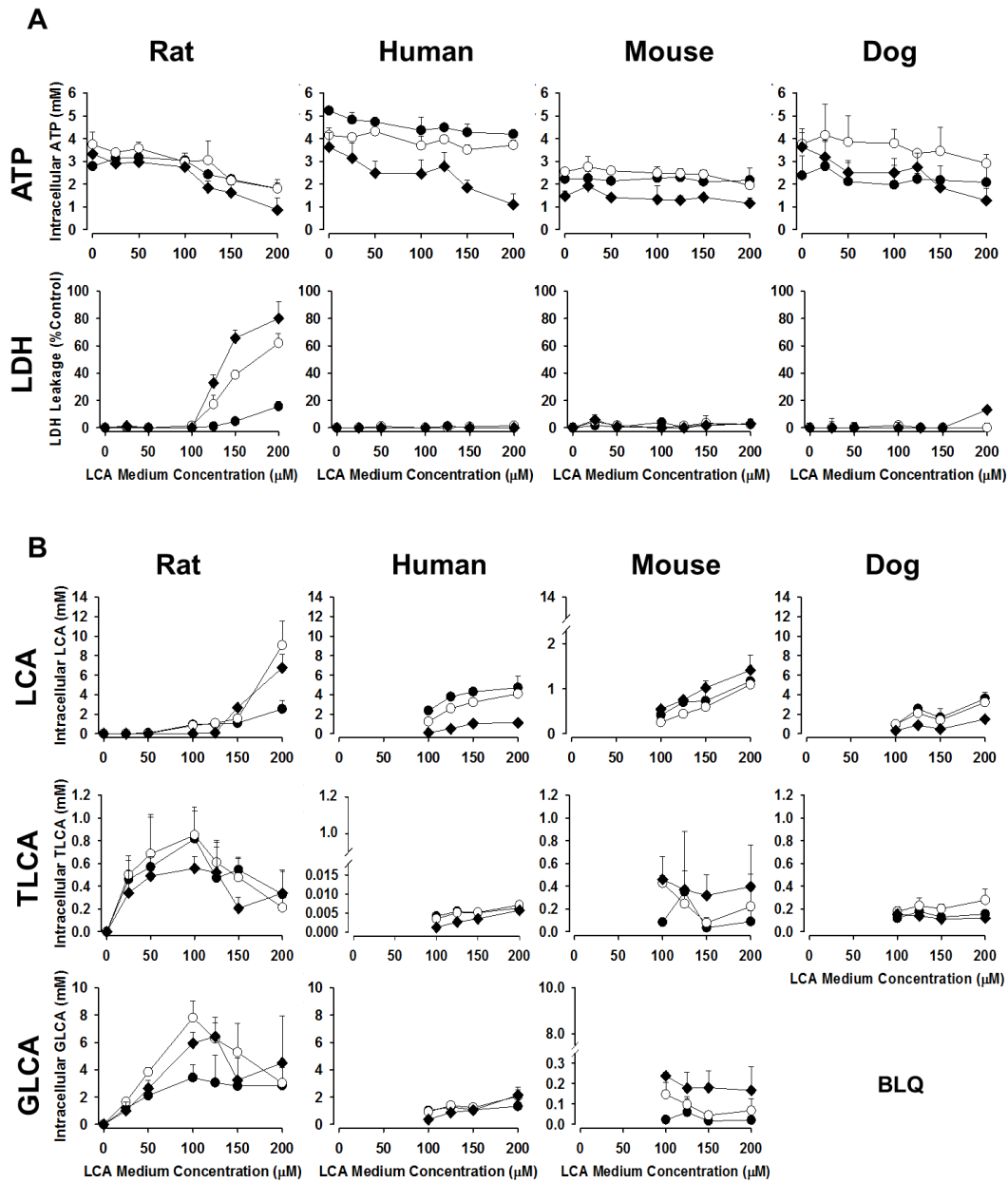


Figure 6.3. Toxicity and bile acid (BA) accumulation in chenodeoxycholic acid (CDCA)-treated rat and human sandwich-cultured hepatocytes (SCH).

Day 3 rat and day 6 human SCH were incubated with CDCA (0–1000 μ M) for 6hr (●), 1hr (○), and 24hr (◆). Representative data (mean \pm SD of triplicate determinations) from n=2 independent studies. **(B)**

Intracellular concentrations of CDCA and CDCA metabolites, glycochenodeoxycholic acid (GCDCA) and taurochenodeoxycholic acid (TLCA). Day 3 rat and day 6 human SCH were incubated with CDCA (0–1000 μ M) for 6hr (●), 12hr (○), and 24hr (◆). Intracellular CDCA and CDCA metabolites were measured by LC-MS/MS analysis of lysate after hepatocytes were incubated for 5min with Ca⁺²-free HBSS buffer to open tight junctions using B-CLEAR[®]. Representative data (mean \pm SD of triplicate determinations) from n=1 (rat) or n=2 (human) independent studies.

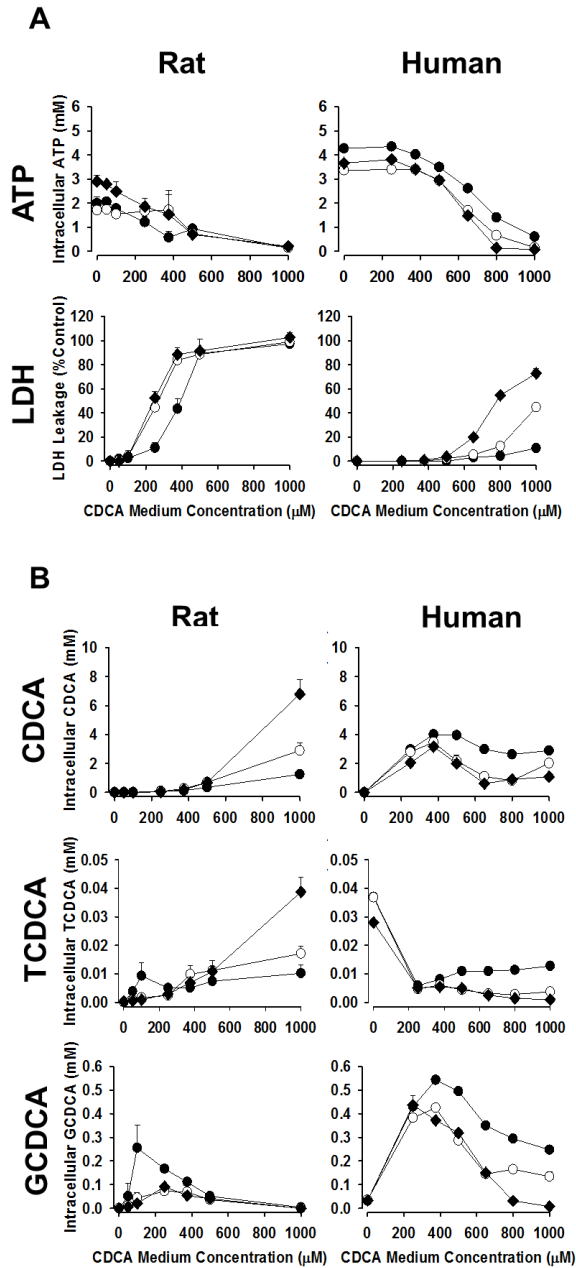
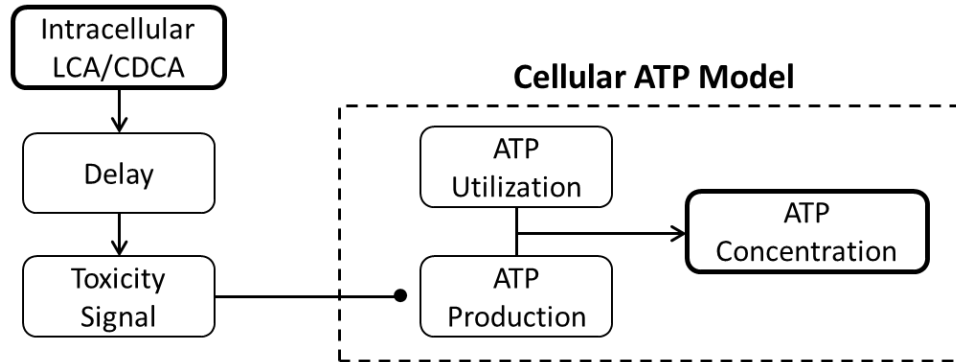


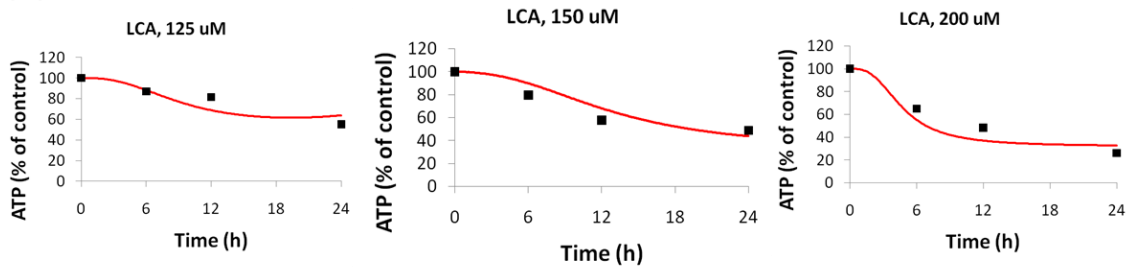
Figure 6.4. Relationship between intracellular lithocholic acid (LCA) and chenodeoxycholic acid (CDCA) concentrations and ATP.

(A) A model incorporating intracellular LCA/CDCA concentrations, the toxicity signals, and inhibition of ATP production was constructed using the existing Cellular ATP Model within DILIsym[®]. The Hill relationship between the toxicity signals (represented by delayed cellular LCA or CDCA concentrations) and inhibition of ATP production was parameterized by fitting the model to the data obtained in LCA and CDCA-treated rat and human SCH. (B) Representative model-generated fit (red curve) and observed (black square) mean cellular ATP levels (expressed as percent of control) as a function of time after LCA exposure in rat SCH.

(A)



(B)



SUPPLEMENTARY MATERIALS

Supplementary Table 6.1. Calibration curve ranges. CA, cholic acid; CDCA, chenodeoxycholic acid; GCA, glycocholic acid; GCDCA, glycochenodeoxycholic acid; GHDCa, glycohyodeoxycholic acid; GLCA, glycolithocholic acid; GMCA, glycomuricholic acid; LCA, lithocholic acid; TCA, taurocholic acid; TCDCA, taurochenodeoxycholic acid; THDCA, taurohyodeoxycholic acid; TLCA, tauroolithocholic acid; TMCA, taumuricholic acid; d₄-/d₅-/d₈-, deuterated.

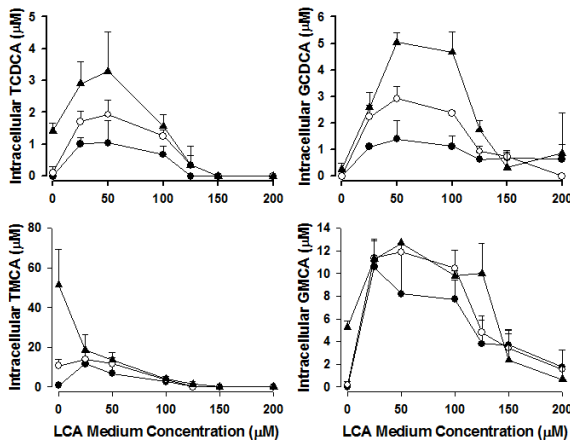
Analyte	Species	Calibration Curve Range (pmol/well)
d ₅ -TCA	All	internal standard
β-TMCA	rat, mouse	0.5 – 500
d ₈ -TCA	All	0.25 - 500
d ₄ -GCA	All	0.25 - 500
d ₄ -TCDCA	All	0.25 - 500
d ₄ -GCDCA	All	0.25 - 500
THDCA	human	0.25 - 100
GHDCa	human	0.25 - 100
d ₄ -CA	human, rat	0.25 - 500
d ₄ -CDCA	human	100 – 10,000
	rat	0.5 - 500
LCA	human, dog, mouse	100 – 10,000
	rat	1000 – 50,000
TLCA	human, rat, dog	1.0 – 1000
	mouse	1 – 1000
GLCA	human	100 – 10,000
	rat	10 – 10,000
	dog, mouse	1 - 1000

Supplementary Table 6.2. Transitions monitored at unit resolution for LC-MS/MS analysis. CA, cholic acid; CDCA, chenodeoxycholic acid; GCA, glycocholic acid; GCDCA, glycochenodeoxycholic acid; GHDCa, glycohyodeoxycholic acid; GLCA, glycolithocholic acid; GMCA, glycomuricholic acid; LCA, lithocholic acid; TCA, taurocholic acid; TCDCA, taurochenodeoxycholic acid; THDCA, taurohyodeoxycholic acid; TLCA, tauroolithocholic acid; TMCA, tauromuricholic acid; d₄-/d₅-/d₈-, deuterated.

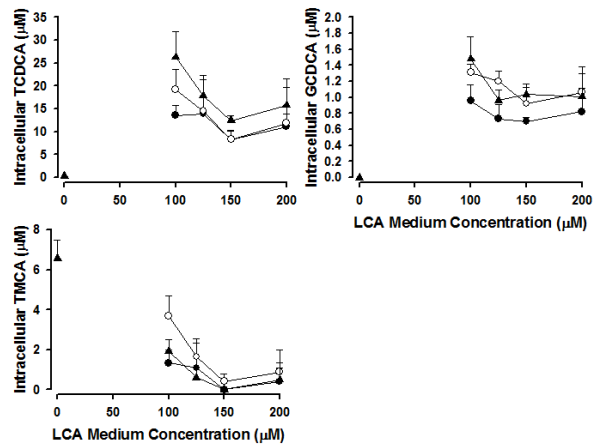
Analyte	Precursor (m/z)	Product (m/z)
TCA	514.3	124.1
α/β -TMCA	514.3	124.1
d ₈ -TCA	522.3	128.1
d ₅ -TCA	519.3	124.1
GCA	464.3	74.1
α/β -GMCA	464.3	74.1
d ₄ -GCA	468.3	74.1
TCDCA	498.3	80.1
THDCA	498.3	80.1
d ₄ -TCDCA	503.3	80.1
GCDCA	448.3	74.1
GHDCa	448.3	74.1
d ₄ -GCDCA	452.3	74.1
CA	407.3	n/a (MS only)
d ₄ -CA	411.3	n/a (MS only)
CDCA	391.3	n/a (MS only)
d ₄ -CDCA	395.3	n/a (MS only)
LCA	375.2	n/a (MS only)
TLCA	482.3	80.1
GLCA	432.2	74.1

Supplementary Figure 6.1. Intracellular concentrations of bile acids (BAs) in lithocholic acid (LCA)-treated rat (A), human (B), mouse (C), and dog (D) sandwich-cultured hepatocytes (SCH). Day 3 rat, day 6 human, day 2 mouse, and day 4 dog SCH were incubated with LCA (0–200 μM) for 6hr (\bullet), 12hr (\circ), and 24hr (\blacktriangle). Intracellular BAs were measured by LC-MS/MS analysis of lysate after hepatocytes were incubated for 5min with Ca^{2+} -free HBSS buffer to open tight junctions using B-CLEAR[®]. Representative data (mean \pm SD of triplicate determinations) from n=1 (rat, mouse, and dog) or n=2 (human) independent studies. TMCA represents α/β -TMCA because the stereoisomers α - and β -TMCA were measured collectively. GMCA, glycocholic acid; GCDCA, glycochenodeoxycholic acid; GHDCa, glycohyodeoxycholic acid; GMCA, glycomuricholic acid; TCA, taurocholic acid; TCDCA, taurochenodeoxycholic acid; TMCA, tauromuricholic acid.

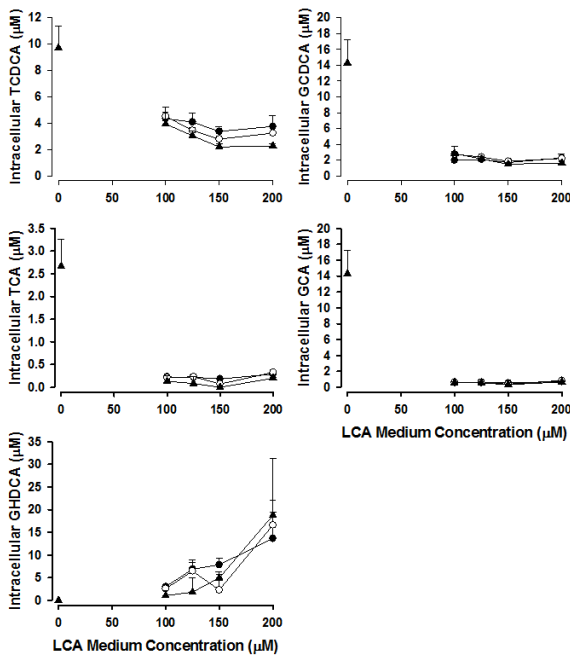
A) Rat



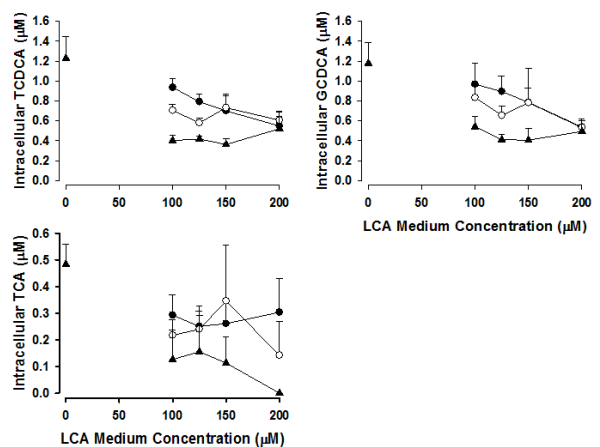
C) Mouse



B) Human

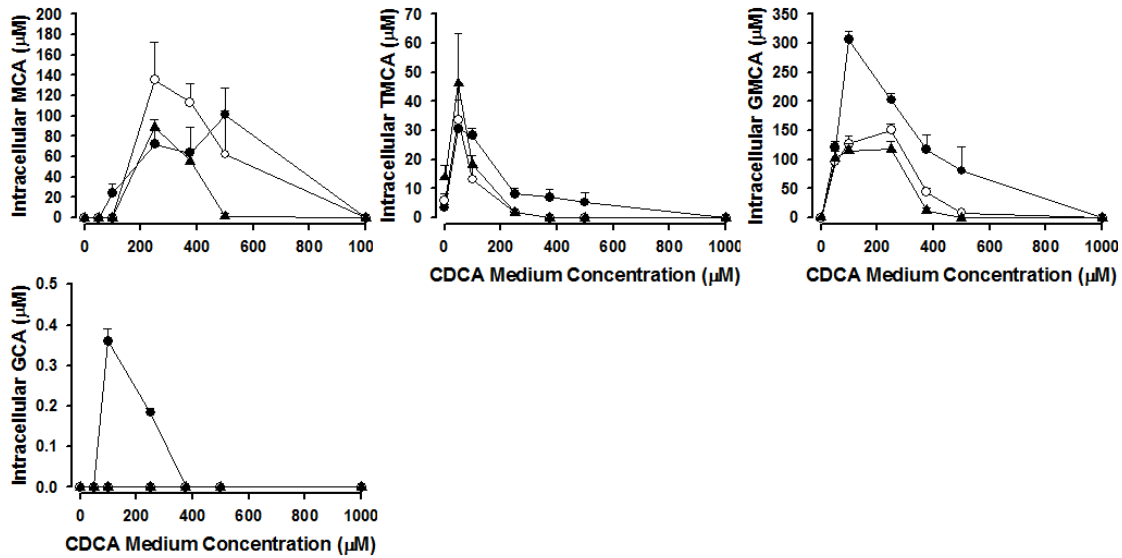


D) Dog

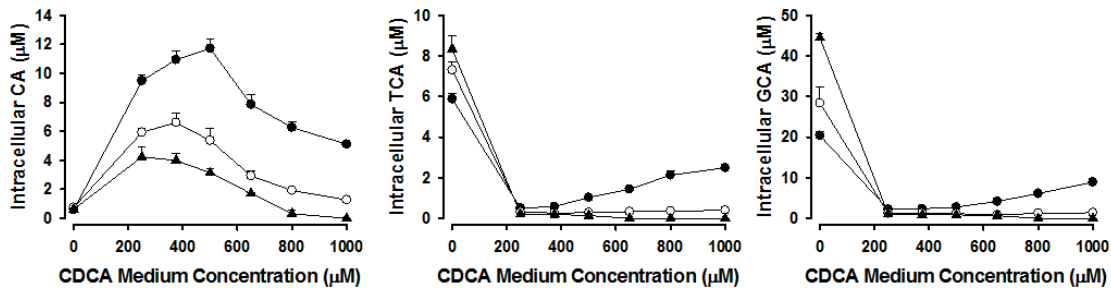


Supplementary Figure 6.2. Intracellular concentrations of bile acids (BAs) in chenodeoxycholic acid (CDCA)-treated rat (A) and human (B) sandwich-cultured hepatocytes (SCH). Day 3 rat and day 6 human SCH were incubated with CDCA (0–1000 μM) for 6hr (●), 12hr (○), and 24hr (▲). Intracellular BAs were measured by LC-MS/MS analysis of lysate after hepatocytes were incubated for 5min with Ca^{2+} -free HBSS buffer to open tight junctions using B-CLEAR[®]. Representative data (mean \pm SD of triplicate determinations) from n=1 (rat) or n=2 (human) independent studies. TMCA represents α/β -TMCA because the stereoisomers α - and β -TMCA were measured collectively. GMCA values are estimates calculated using TMCA calibration curves. CA, cholic acid; GCA, glycocholic acid; GMCA, glycomuricholic acid; MCA, muricholic acid; TCA, taurocholic acid; TMCA, tauromuricholic acid.

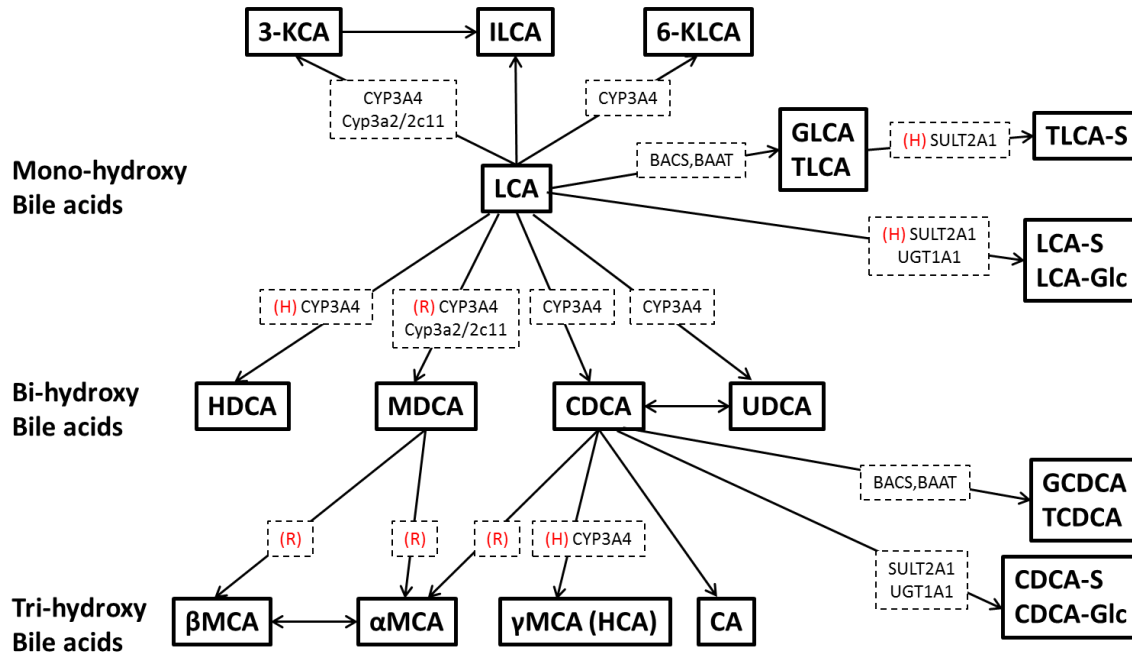
A) Rat



B) Human



Supplementary Figure 6.3. Hepatic metabolic pathways of lithocholic acid (LCA) and chenodeoxycholic acid (CDCA). Schematic overview of previously reported metabolic pathways of LCA and CDCA in the liver. Conjugation pathways are only shown for LCA and CDCA, but other bile acids are also subject to glycine-, taurine-, sulfate-, or glucuronide-conjugation. (H) major pathway in humans; (R) major pathway in rats; 3-KCA, 3-ketocholic acid; 6-KLCA, 6-ketolithocholic acid; BAAT, bile acid:amino acid transferase; BACS, bile acid:coA synthase; CA, cholic acid; CDCA, chenodeoxycholic acid; CDCA-Glc, chenodeoxycholic acid-glucuronide; CDCA-S, chenodeoxycholic acid-sulfate; CYP, cytochrome P450; GCDCA, glycochenodeoxycholic acid; GLCA, glycolithocholic acid; HCA, hyocholic acid; HDCA, hyodeoxycholic acid; ILCA, isolithocholic acid; LCA, lithocholic acid; LCA-Glc, lithocholic acid-glucuronide; LCA-S, lithocholic acid-sulfate; α MCA, α -muricholic acid; β MCA, β -muricholic acid; γ MCA, γ -muricholic acid; MDCA, murideoxycholic acid; SULT, sulfotransferase; TCDCA, taurochenodeoxycholic acid; TLCA, tauroolithocholic acid; TLCA-S, tauroolithocholic acid-sulfate; UDCA, ursodeoxycholic acid; UGT, UDP glucuronosyltransferase.



REFERENCES

- (1) Lee, W.M. Drug-induced hepatotoxicity. *N Engl J Med* **349**, 474-85 (2003).
- (2) Olson, H. *et al.* Concordance of the toxicity of pharmaceuticals in humans and in animals. *Regul Toxicol Pharmacol* **32**, 56-67 (2000).
- (3) Perez, M.J. & Briz, O. Bile-acid-induced cell injury and protection. *World J Gastroenterol* **15**, 1677-89 (2009).
- (4) Maillette de Buy Wenniger, L. & Beuers, U. Bile salts and cholestasis. *Dig Liver Dis* **42**, 409-18 (2010).
- (5) Morgan, R.E. *et al.* Interference with bile salt export pump function is a susceptibility factor for human liver injury in drug development. *Toxicol Sci* **118**, 485-500 (2010).
- (6) Dawson, S., Stahl, S., Paul, N., Barber, J. & Kenna, J.G. In vitro inhibition of the bile salt export pump correlates with risk of cholestatic drug-induced liver injury in humans. *Drug Metab Dispos* **40**, 130-8 (2012).
- (7) Hofmann, A.F. Bile Acids: The Good, the Bad, and the Ugly. *News Physiol Sci* **14**, 24-9 (1999).
- (8) Thomas, C., Pellicciari, R., Pruzanski, M., Auwerx, J. & Schoonjans, K. Targeting bile-acid signalling for metabolic diseases. *Nat Rev Drug Discov* **7**, 678-93 (2008).
- (9) Scholmerich, J. *et al.* Influence of hydroxylation and conjugation of bile salts on their membrane-damaging properties--studies on isolated hepatocytes and lipid membrane vesicles. *Hepatology* **4**, 661-6 (1984).
- (10) Leslie, E.M., Watkins, P.B., Kim, R.B. & Brouwer, K.L. Differential inhibition of rat and human Na⁺-dependent taurocholate cotransporting polypeptide (NTCP/SLC10A1) by bosentan: a mechanism for species differences in hepatotoxicity. *J Pharmacol Exp Ther* **321**, 1170-8 (2007).
- (11) Jonker, J.W., Liddle, C. & Downes, M. FXR and PXR: potential therapeutic targets in cholestasis. *J Steroid Biochem Mol Biol* **130**, 147-58 (2012).
- (12) Chiang, J.Y. Bile acids: regulation of synthesis. *J Lipid Res* **50**, 1955-66 (2009).
- (13) Handschin, C. & Meyer, U.A. Regulatory network of lipid-sensing nuclear receptors: roles for CAR, PXR, LXR, and FXR. *Arch Biochem Biophys* **433**, 387-96 (2005).

- (14) Chen, X., Lou, G., Meng, Z. & Huang, W. TGR5: a novel target for weight maintenance and glucose metabolism. *Exp Diabetes Res* **2011**, 853501 (2011).
- (15) Howell, B.A. *et al.* In vitro to in vivo extrapolation and species response comparisons for drug-induced liver injury (DILI) using DILIsym: a mechanistic, mathematical model of DILI. *J Pharmacokinet Pharmacodyn* **39**, 527-41 (2012).
- (16) Woodhead, J.L. *et al.* An analysis of N-acetylcysteine treatment for acetaminophen overdose using a systems model of drug-induced liver injury. *J Pharmacol Exp Ther* **342**, 529-40 (2012).
- (17) Woodhead, J.L., Yang, K., Brouwer, K.L.R., Watkins, P.B., Siler, S.Q. & Howell, B.A. Mechanistic Modeling Illuminates the Most Important Unknowns in Bile Acid Mediated DILI. *The Toxicologist* **132**, Abstract ID #881 (2013).
- (18) Greim, H. *et al.* Mechanism of cholestasis. 6. Bile acids in human livers with or without biliary obstruction. *Gastroenterology* **63**, 846-50 (1972).
- (19) Chatterjee, S., Bijmans, I.T., van Mil, S.W., Augustijns, P. & Annaert, P. Toxicity and intracellular accumulation of bile acids in sandwich-cultured rat hepatocytes: Role of glycine conjugates. *Toxicol In Vitro*, (2013).
- (20) Swift, B., Pfeifer, N.D. & Brouwer, K.L. Sandwich-cultured hepatocytes: an in vitro model to evaluate hepatobiliary transporter-based drug interactions and hepatotoxicity. *Drug Metab Rev* **42**, 446-71 (2010).
- (21) LeCluyse, E., Madan, A., Hamilton, G., Carroll, K., DeHaan, R. & Parkinson, A. Expression and regulation of cytochrome P450 enzymes in primary cultures of human hepatocytes. *J Biochem Mol Toxicol* **14**, 177-88 (2000).
- (22) Liu, X., LeCluyse, E.L., Brouwer, K.R., Lightfoot, R.M., Lee, J.I. & Brouwer, K.L. Use of Ca²⁺ modulation to evaluate biliary excretion in sandwich-cultured rat hepatocytes. *J Pharmacol Exp Ther* **289**, 1592-9 (1999).
- (23) Lee, J.K. & Brouwer, K.R. Determination of intracellular volume of rat and human sandwich-cultured hepatocytes (Abstract ID 1595). *The Toxicologist, Supplement to Toxicological Sciences* **114**, (2010).
- (24) Fischer, S., Beuers, U., Spengler, U., Zwiebel, F.M. & Koebe, H.G. Hepatic levels of bile acids in end-stage chronic cholestatic liver disease. *Clin Chim Acta* **251**, 173-86 (1996).

- (25) Kaplan, M.M. Primary biliary cirrhosis--a first step in prolonging survival. *N Engl J Med* **330**, 1386-7 (1994).
- (26) Ogimura, E., Sekine, S. & Horie, T. Bile salt export pump inhibitors are associated with bile acid-dependent drug-induced toxicity in sandwich-cultured hepatocytes. *Biochem Biophys Res Commun* **416**, 313-7 (2011).
- (27) Ohta, M., Kanai, S. & Kitani, K. The order of hepatic cytotoxicity of bile salts in vitro does not agree with that examined in vivo in rats. *Life Sci* **46**, 1503-8 (1990).
- (28) Dawson, P.A., Lan, T. & Rao, A. Bile acid transporters. *J Lipid Res* **50**, 2340-57 (2009).
- (29) Alrefai, W.A. & Gill, R.K. Bile acid transporters: structure, function, regulation and pathophysiological implications. *Pharm Res* **24**, 1803-23 (2007).
- (30) Yang, K., Kock, K., Sedykh, A., Tropsha, A. & Brouwer, K.L. An updated review on drug-induced cholestasis: mechanisms and investigation of physicochemical properties and pharmacokinetic parameters. *J Pharm Sci* **102**, 3037-57 (2013).
- (31) Yousef, I.M., Bouchard, G., Tuchweber, B. & Plaa, G.L. Monohydroxy bile acid induced cholestasis: role of biotransformation. *Drug Metab Rev* **29**, 167-81 (1997).
- (32) Hofmann, A.F. Detoxification of lithocholic acid, a toxic bile acid: relevance to drug hepatotoxicity. *Drug Metab Rev* **36**, 703-22 (2004).
- (33) Nieminen, A.L., Saylor, A.K., Herman, B. & Lemasters, J.J. ATP depletion rather than mitochondrial depolarization mediates hepatocyte killing after metabolic inhibition. *Am J Physiol* **267**, C67-74 (1994).
- (34) Garcia-Canaveras, J.C., Donato, M.T., Castell, J.V. & Lahoz, A. Targeted profiling of circulating and hepatic bile acids in human, mouse, and rat using a UPLC-MRM-MS-validated method. *J Lipid Res* **53**, 2231-41 (2012).
- (35) Suzuki, Y. *et al.* Simple and rapid quantitation of 21 bile acids in rat serum and liver by UPLC-MS-MS: effect of high fat diet on glycine conjugates of rat bile acids. *Nagoya J Med Sci* **75**, 57-71 (2013).
- (36) Trottier, J., Caron, P., Straka, R.J. & Barbier, O. Profile of serum bile acids in noncholestatic volunteers: gender-related differences in response to fenofibrate. *Clin Pharmacol Ther* **90**, 279-86 (2011).

- (37) Xiang, X., Backman, J.T., Neuvonen, P.J. & Niemi, M. Gender, but not CYP7A1 or SLCO1B1 polymorphism, affects the fasting plasma concentrations of bile acids in human beings. *Basic Clin Pharmacol Toxicol* **110**, 245-52 (2012).
- (38) Yang, L. *et al.* Bile acids metabonomic study on the CCl₄- and alpha-naphthylisothiocyanate-induced animal models: quantitative analysis of 22 bile acids by ultraperformance liquid chromatography-mass spectrometry. *Chem Res Toxicol* **21**, 2280-8 (2008).
- (39) Kakis, G. & Yousef, I.M. Pathogenesis of lithocholate- and tauroolithocholate-induced intrahepatic cholestasis in rats. *Gastroenterology* **75**, 595-607 (1978).
- (40) Oelberg, D.G., Chari, M.V., Little, J.M., Adcock, E.W. & Lester, R. Lithocholate glucuronide is a cholestatic agent. *J Clin Invest* **73**, 1507-14 (1984).
- (41) Yousef, I.M., Tuchweber, B., Vonk, R.J., Masse, D., Audet, M. & Roy, C.C. Lithocholate cholestasis--sulfated glycolithocholate-induced intrahepatic cholestasis in rats. *Gastroenterology* **80**, 233-41 (1981).
- (42) Sokol, R.J., Dahl, R., Devereaux, M.W., Yerushalmi, B., Kobak, G.E. & Gumpricht, E. Human hepatic mitochondria generate reactive oxygen species and undergo the permeability transition in response to hydrophobic bile acids. *J Pediatr Gastroenterol Nutr* **41**, 235-43 (2005).
- (43) Faubion, W.A. *et al.* Toxic bile salts induce rodent hepatocyte apoptosis via direct activation of Fas. *J Clin Invest* **103**, 137-45 (1999).
- (44) Botham, K.M. & Boyd, G.S. The metabolism of chenodeoxycholic acid to beta-muricholic acid in rat liver. *Eur J Biochem* **134**, 191-6 (1983).
- (45) Deo, A.K. & Bandiera, S.M. Biotransformation of lithocholic acid by rat hepatic microsomes: metabolite analysis by liquid chromatography/mass spectrometry. *Drug Metab Dispos* **36**, 442-51 (2008).
- (46) Zimniak, P., Holsztynska, E.J., Lester, R., Waxman, D.J. & Radomska, A. Detoxification of lithocholic acid. Elucidation of the pathways of oxidative metabolism in rat liver microsomes. *J Lipid Res* **30**, 907-18 (1989).
- (47) Deo, A.K. & Bandiera, S.M. 3-ketocholanoic acid is the major in vitro human hepatic microsomal metabolite of lithocholic acid. *Drug Metab Dispos* **37**, 1938-47 (2009).
- (48) Xie, W. *et al.* An essential role for nuclear receptors SXR/PXR in detoxification of cholestatic bile acids. *Proc Natl Acad Sci U S A* **98**, 3375-80 (2001).

- (49) Araya, Z. & Wikvall, K. 6 α -hydroxylation of taurochenodeoxycholic acid and lithocholic acid by CYP3A4 in human liver microsomes. *Biochim Biophys Acta* **1438**, 47-54 (1999).
- (50) Alme, B., Bremmelgaard, A., Sjøvall, J. & Thomassen, P. Analysis of metabolic profiles of bile acids in urine using a lipophilic anion exchanger and computerized gas-liquid chromatography-mass spectrometry. *J Lipid Res* **18**, 339-62 (1977).
- (51) Summerfield, J.A., Billing, B.H. & Shackleton, C.H. Identification of bile acids in the serum and urine in cholestasis. Evidence for 6 α -hydroxylation of bile acids in man. *Biochem J* **154**, 507-16 (1976).
- (52) Shoda, J. *et al.* Altered metabolism of bile acids in cholestasis: determination of 1 beta- and 6 alpha-hydroxylated metabolites. *J Chromatogr* **488**, 315-28 (1989).
- (53) Setchell, K.D. *et al.* Bile acid concentrations in human and rat liver tissue and in hepatocyte nuclei. *Gastroenterology* **112**, 226-35 (1997).

CHAPTER 7. Mechanistic Modeling of Drug-Induced Liver Injury Predicts Delayed Presentation and Species Differences in Bile Acid -Mediated Troglitazone Hepatotoxicity¹

INTRODUCTION

Drug-induced liver injury (DILI), a frequent cause of liver injury, is manifested as a broad range of illnesses from temporal changes in serum biochemistry to acute hepatitis or cholestasis. DILI is one of the primary reasons for the failure of pharmaceutical agents during drug development as well as withdrawal of approved drugs from the market (1). Unfortunately, current *in vitro* screening approaches or *in vivo* preclinical studies do not adequately predict the DILI liability of new chemical entities. Rare incidences of severe drug-related hepatotoxicity typically are not detected in the Phase III clinical trials that involve a few thousand patients, and may not be detected until the drug has been approved and administered to tens or hundreds of thousands of patients. These unexpected findings have led to blackbox warnings (e.g., bosentan, diclofenac, ketoconazole, isoniazid), or in severe cases, withdrawal of the drug from the market (e.g., troglitazone, bromfenac).

Troglitazone (TGZ) was the first of the thiazolidinedione class drugs approved in worldwide markets for the treatment of insulin resistance occurring in type 2 diabetes. During the clinical trials that led to the approval of TGZ, ALT elevations >3X upper normal limit (ULN) in about 2% of patients and 2 cases of jaundice were reported (2). All of these patients recovered without permanent clinical complications, and the TGZ was approved. However, after the release of TGZ on the market, 2 cases of liver failure related to TGZ were reported, and it was given a blackbox warning status with requirement of monthly monitoring of liver enzymes. Over the next three years, 43 cases of liver failure and 21 deaths

¹This work has been accepted for podium presentation, in part, at the ASCPT 2014 Annual Meeting, Atlanta, GA, March 18-22, 2014, and will be submitted to *Clinical Pharmacology and Therapeutics: Pharmacometrics and Systems Pharmacology*.

related to TGZ therapy were reported (3). With the arrival of rosiglitazone and pioglitazone, drugs from the same class that demonstrated less concerns about hepatotoxicity, TGZ was withdrawn from the market (4).

Fourteen years have passed since the withdrawal of TGZ, but the mechanism(s) of TGZ-mediated hepatotoxicity have not been fully elucidated. Although numerous mechanisms have been postulated, one proposed mechanism is inhibition of bile acid transport inhibition by TGZ and its major metabolite, TGZ sulfate (TS) (5, 6), which may cause accumulation of toxic bile acids in hepatocytes and subsequent toxicity (7, 8). The bile salt export pump (BSEP) is a canalicular transporter that is predominantly responsible for biliary excretion of bile acids. Impaired BSEP function due to genetic polymorphisms induces liver injury (9, 10), and BSEP inhibition mediated by drugs has been associated with cholestatic/mixed type DILI (11, 12). *In vitro* vesicular transport assays revealed that TGZ and TS are potent inhibitors of BSEP and multidrug resistance-associated protein 4 (MRP4), hepatic transporters that mediate biliary and basolateral efflux of bile acids, respectively (11, 13, 14). TGZ is also shown to inhibit NTCP-mediated bile acid uptake (15). However, the involvement of bile acid inhibition in TGZ-mediated hepatotoxicity has not been demonstrated *in vivo* in humans. Also, hepatotoxicity signals were not detected during preclinical testing of TGZ, even though TGZ and TS are potent inhibitors of rat Bsep (13). While it is challenging to translate the results from isolated *in vitro* studies to *in vivo*, and preclinical studies to humans, mechanistic modeling is a useful approach to integrate data from different experimental systems and species, and biological knowledge, to predict human DILI.

In the current study, a mechanistic model of DILI (DILIsym, <http://www.dilisy.com>) was used to investigate the role of bile acid transport inhibition in TGZ hepatotoxicity and underlying mechanisms for species differences. DILIsym includes sub-models representing disposition of drugs and metabolites, physiology and pathophysiology of bile acids, the hepatocyte life cycle, and biomarkers of liver injury (e.g., serum ALT and bilirubin) (Figure 7.1) (16-19). TGZ-mediated DILI responses were simulated in the human and rat populations (SimPops); these simulated populations included variability in key model

parameters describing bile acid and drug disposition. Potential risk factors for TGZ-induced hepatotoxicity in humans in the context of bile acid inhibition also were assessed in human SimPops.

RESULTS

Physiologically-based pharmacokinetic (PBPK) modeling

A PBPK model was developed to describe the disposition of TGZ and TS in humans and male rats (Supplementary Figure 7.2). Simulated TGZ and TS plasma concentration-time profiles in humans following a single oral dose of 400 mg TGZ (Figure 7.2A), and in male rats following a single intravenous dose of 5 mg/kg TGZ (Figure 7.2B) were within 2-fold of the mean observed concentrations measured by high performance liquid chromatography (HPLC) (20-22). In male rats administered a single oral dose of 5 mg/kg TGZ, the simulated TGZ plasma concentration-time profile was within 2.6-fold of the mean observed concentrations measured by HPLC (Figure 7.2B) (21).

Simulations of TGZ hepatotoxicity in human and rat populations (SimPops)

The baseline human simulation did not include population variability; as expected, no DILI responses (i.e., decreased hepatic ATP, decreased viable liver mass, or increased serum ALT) were observed (data not shown) based on the rare incidence of TGZ-mediated hepatotoxicity in the clinic. To explore TGZ hepatotoxicity at the population level, human and rat SimPops that included variability in bile acid and drug disposition were constructed using the parameters listed in Table 7.2. Several TGZ dose levels were employed for the human SimPops (n=331) [once daily oral doses of 200, 400, or 600 mg for 6 months (clinically used doses)] and rat SimPops (n=191) [once daily oral doses of 5 mg/kg (equivalent to the clinical dose) or 25 mg/kg for 6 months]. TGZ-mediated perturbations in bile acid disposition and DILI responses in the human and rat SimPops are presented in Figure 7.3. In the human SimPops, hepatic accumulation of chenodeoxycholic acid (CDCA) and lithocholic acid (LCA) species (sum of LCA, CDCA, and their conjugates) and subsequent DILI responses were dependent on TGZ dose. In the human SimPops, the simulated median (range) maximum hepatic concentrations of CDCA and LCA species post-dose were 203 μM (76–1057), 272 μM (108–1431), and 312 μM (128–1646) at

TGZ doses of 200, 400, and 600 mg/day, respectively, compared to a baseline value of 44 μM . Baseline human hepatic ATP concentration in the current model was 4.2 mM. Hepatic bile acid accumulation led to a decrease in hepatic ATP and a decrease in viable liver mass in a subset of the human SimPops; simulated median (range) values of minimum hepatic ATP concentrations post-dose were 4.14 mM (3.49–4.19), 4.10 mM (3.22–4.18), and 4.07 mM (3.00–4.17) at TGZ doses of 200, 400, and 600 mg/day, respectively. Corresponding values for fractional viable liver mass were 1.00 (0.92–1.00), 1.00 (0.45–1.00), and 1.00 (0.33–1.00). The incidence of elevated serum ALT, serum total bilirubin, and Hy's Law cases (serum ALT >3X ULN and serum bilirubin >2X ULN) in the human SimPops are summarized in Table 7.1; the reported incidence of ALT elevations and jaundice in the clinical trials also are listed (2, 3). In the human SimPops, TGZ doses of 200, 400, and 600 mg/day induced elevations in serum ALT >3X ULN in 0, 2.4, and 4.2% of the population; Hy's Law cases were observed in 0.9 and 3.0% of the population treated with 400 and 600 mg/day TGZ, respectively. This is similar to observations from the clinical trials where TGZ (200–600 mg/day) induced serum ALT elevations >3X ULN in 1.9% of treated patients, and 2 cases of jaundice (0.08%) were reported (2). The time to peak ALT in the human SimPops with ALT elevations >3X ULN was 1.3–6 months at TGZ doses of 400 and 600 mg/day; these are comparable to 3–7 months observed in the clinical trials (Table 7.1) (3). Simulated time-course dynamics of serum ALT and viable liver mass in susceptible individuals (serum ALT >3X ULN) are presented in Figure 7.4.

In the rat SimPops, the simulated median (range) maximum hepatic concentrations of CDCA and LCA species post-dose were 26 μM (11–179) and 41 μM (11–179) at TGZ doses of 5 and 25 mg/kg/day, respectively, compared to baseline values of 8 μM . The baseline rat hepatic ATP concentration was 2.0 mM. Simulated median (range) minimum hepatic ATP concentrations after TGZ doses of 5 mg/kg/day and 25 mg/kg/day were 1.96 mM (1.68–2.00) and 1.93 mM (1.50–1.99), respectively. The corresponding values for fractional viable liver mass were 1.00 (1.00–1.00) and 1.00 (0.92–1.00), respectively. None of the rat SimPops exhibited serum ALT elevations >3X baseline (21 U/L).

Sensitivity analysis

To investigate the sensitivity of DILI responses to transporter inhibition constants, simulations were performed with 10-fold smaller and larger inhibition constants for BSEP, MRP4, and NTCP. Simulated maximum serum ALT levels in human and rat SimPops treated with TGZ (600 mg/day for humans; 5 mg/kg/day for rats) for 1 month are presented in Figure 7.5. In the human SimPops, serum ALT levels were sensitive to the K_i value of TGZ and TS for BSEP inhibition; when BSEP K_i was decreased by 10-fold (assuming 10-fold more potent inhibition), 14.2% of the population exhibited serum ALT >3X compared to only 2.7% of the population with the measured BSEP K_i . None of the individuals showed elevated serum ALT >3X when BSEP K_i was increased 10-fold (assuming 10-fold less potent inhibition). The K_i of TGZ and TS for MRP4 inhibition also influenced serum ALT elevations, but to a smaller extent compared to BSEP K_i ; 3.0% and 1.8% of the population exhibited a serum ALT >3X when the MRP4 K_i was decreased and increased by 10-fold, respectively, compared to an incidence of 2.7% with the measured MRP4 K_i . Modulation of the K_i for NTCP inhibition by TGZ and TS led to opposite effects compared to modulation of BSEP and MRP4 K_i ; a decrease in the NTCP K_i by 10-fold led to a decreased incidence of elevations in serum ALT >3X (1.5% of the population), whereas an increase in the NTCP K_i by 10-fold increased the incidence of elevations in serum ALT >3X (3.6% of the population), compared to an incidence of 2.7% with the measured NTCP K_i . This confirms the suggested protective role of bile acid uptake inhibition in hepatic bile acid accumulation and subsequent DILI. In the rat SimPops, simulated serum ALT levels did not exceed 3X baseline values (21 U/L) even when the K_i for BSEP or MRP4 were decreased by 10-fold, or the K_i for NTCP was increased 10-fold. These results give confidence that TGZ is not expected to be hepatotoxic in rats.

Multiple regression analysis

Hepatotoxicity was not predicted in the baseline human simulation, which did not include population variability, whereas simulations with human SimPops revealed a subset of individuals susceptible to TGZ-mediated hepatotoxicity. To identify the most important parameters in our model in the context of bile acid-mediated DILI, multiple regression analysis was performed with the lowest

hepatic ATP post-dose as the predicted outcome and the 16 parameters used to develop the human SimPops as independent variables. Hepatic ATP was selected because perturbations in cellular ATP synthesis is the first step in the development of bile acid-mediated DILI in the current model (Figure 7.1), and thus is the most sensitive and variable model output compared to other DILI responses (i.e., serum ALT, fractional viable liver mass). Table 7.2 shows the statistical significance (p-values) and standardized coefficients of parameters varied in human SimPops. Among the 16 parameters used to construct human SimPops, seven parameters were statistically significant predictors of hepatic ATP levels; the maximum rate of LCA-sulfate biliary excretion was the most important variable influencing hepatic ATP decline followed by the maximum rate of LCA synthesis in the intestinal lumen, canalicular efflux regulation scaling factor, the maximum rate of CDCA-amide biliary excretion, biliary clearance of TS, body weight, and the maximum velocity of CDCA-amide basolateral efflux.

DISCUSSION

Bile acid transport inhibition by TGZ and its major metabolite, TS, is one proposed mechanism of TGZ-mediated hepatotoxicity. Although TGZ and TS are potent inhibitors of bile acid transporters in isolated membrane vesicle systems, the relationship between bile acid transport inhibition and in vivo hepatotoxicity has not been evaluated. In the current study, a mechanistic model of DILI was used to investigate the hepatotoxic potential of TGZ via bile acid transport inhibition in humans and rats. It is important to consider population variability when predicting bile-acid mediated hepatotoxicity due to large variability in bile acid exposure and the low incidence of hepatotoxicity (2, 23). Lack of TGZ-mediated DILI in the baseline human model in the current study also supports the necessity of population-based analysis. Thus, human and rat SimPops that included variability in key parameters in bile acid disposition, TGZ and TS disposition, body weight, and sensitivity of ATP synthesis to hepatic bile acid accumulation were constructed to investigate the hepatotoxic potential of TGZ at the population level.

In the clinic, TGZ was administered at oral doses of 200, 400, or 600 mg once daily. Thus, each dose level was employed in the human SimPops. The simulated incidences of elevated serum ALT >3X

ULN was 2.4–4.2%, which were similar to 1.9–2.1% that had been observed in clinical trials and a retrospective study of 291 patients with type 2 diabetes (2, 24) (Table 7.1). Hy’s Law cases were observed in 0.9–3.0% of human SimPops, whereas 2 cases of jaundice (0.08%, both Hy’s Law cases) relevant to TGZ treatment were reported in clinical trials (Table 7.1). The incidence of serum bilirubin elevations might have been overestimated in the simulations because TGZ was not discontinued even when serum ALT was increased, in contrast to the clinical situation. Simulations also adequately predicted the delayed time to peak ALT observed in the clinical trials (3–7 months) (Table 7.1). The duration of therapy before ALT elevation in a retrospective study was longer and more variable (413 ± 256 days), which might be explained, in part, by different dosing schemes. In the clinic, patients were administered lower doses and then titrated up to 600 mg/day if they did not respond to TGZ therapy. In the current simulations, a single dose level was administered throughout the simulation, and thus, human SimPops administered 600 mg/day TGZ were exposed from the beginning to the high dose level. Since the incidence of ALT elevations increased with increasing dose in the current simulations, the onset of ALT elevations would have been delayed further if doses had been escalated in the simulations. Also, the estimation of time to peak ALT in the clinic depends on the monitoring frequency. If patients were not monitored routinely, earlier signals may have been missed, resulting in a longer than expected reported time to peak. Although mechanisms underlying delayed presentation of TGZ hepatotoxicity remain unclear, delayed ALT elevations in the present mechanistic model were driven by a delayed build-up of toxic bile acids in hepatocytes. After initiating TGZ administration in the human SimPops, hepatic TS concentrations reached steady-state within 2 weeks (data not shown). However, it took 0.5–3 months before the toxic bile acids accumulated to a high enough concentration in hepatocytes to cause hepatotoxicity because of the dynamic interaction between hepatic bile acid disposition and ATP concentrations in the current model (19); hepatic accumulation of toxic bile acids inhibited ATP synthesis, and ATP depletion in turn decreased function of ATP-dependent bile acid efflux transporters (25, 26), further increasing hepatic bile acid accumulation. The extent of bile acid accumulation and the sensitivity of ATP synthesis to hepatic bile acid accumulation determined the level of hepatic injury (i.e., decreased hepatic ATP and loss of

viable liver mass). In the human SimPops, extensive liver injury led to a marked and early rise in serum ALT, whereas lower level injury resulted in mild and further delayed increases in serum ALT (Figure 7.4).

Currently, only approximately one-half of drugs that cause human DILI exhibit detectable liver injury in preclinical testing (27). Specifically, preclinical animals are less sensitive to bile acid-mediated DILI compared to humans, and thus, do not reliably predict human hepatotoxicity that involves bile acid transport inhibition (28, 29). Toxicity signals for TGZ were not detected during the standard preclinical toxicity testing before approval, and minimal hepatotoxicity was observed in 104 weeks of long-term toxicity studies (30). Potential reasons include species differences in toxic bile acid composition, substrate and/or inhibitor specificity of bile acid transporters, and metabolism/detoxification pathways of bile acids (28, 31-33). For example, bosentan was a more potent inhibitor of rat Ntcp-mediated bile acid uptake compared to human NTCP, which may prevent hepatic accumulation of bile acids despite inhibition of Bsep in rats (12, 28). However, unlike bosentan, TGZ was reported to be a more potent inhibitor of human NTCP relative to rat Ntcp, and inhibition potency was similar for human BSEP and rat Bsep (12, 15). A unifying hypothesis is that differential hepatotoxicity of TGZ could be attributed to species differences in toxic bile acid profiles. Rats have a hydrophilic, and thus less toxic, bile acid pool; CDCA, the most widely implicated bile acid in cholestatic liver injury (34), is one of the dominant bile acids in humans, whereas it contributes a smaller proportion of the bile acid pool in rats and mice (23, 35). Tri-hydroxy bile acids such as cholic acid and muricholic acid are more abundant in rodents (35). LCA, the most hydrophobic and potentially toxic bile acid, is predominantly sulfated in humans, whereas LCA primarily undergoes 6 β -hydroxylation to form murideoxycholic acid in rats (32). Conjugation (i.e., amidation, sulfation, and glucuronidation) increase solubility and facilitate biliary/urinary excretion, and is generally considered as a detoxification pathway. However, LCA conjugates also cause cholestasis (36-38), and the glycine conjugate of CDCA induces mitochondrial permeability transition and apoptosis in isolated mitochondria and primary hepatocytes, respectively (39, 40). In DILIsym, CDCA, LCA, and their conjugates were exclusively modeled as the toxic bile acids. Simulated maximum hepatic

concentrations of CDCA and LCA species in the human SimPops administered 200–600 mg/day TGZ were 74–1646 μM (Figure 7.3A). Although hepatic bile acid concentrations after administration of bile acid transport inhibitors to humans have not been investigated, several investigations revealed that concentrations of hepatic bile acids increased up to $215 \pm 39.1 \mu\text{M}$ and $1960.5 \mu\text{M}$ in patients with end-stage chronic cholestatic liver disease and hepatolithiasis, respectively (41, 42), suggesting that simulated hepatic bile acid concentrations are not physiologically unrealistic. In rat SimPops administered 5–25 mg/kg/day TGZ, simulated maximum hepatic concentrations of CDCA and LCA species ranged 11–179 μM (Figure 7.3B). This is much lower compared to humans due to the hydrophobic bile acid pool and detoxification of LCA by hydroxylation (19), and led to a lack of hepatotoxicity in the rat SimPops. These results demonstrated that a mechanistic model which incorporates species differences in bile acid homeostasis correctly predicted differential hepatotoxicity of TGZ in humans versus rats. Sensitivity analysis also revealed that rat SimPops did not exhibit hepatotoxicity even with 10-fold lower (more potent) inhibition constants for bile acid efflux transporters, suggesting that the differential bile acid profile, rather than inhibitor specificity of drugs, is the main contributor to species difference (Figure 7.5).

Only a small subset of patients treated with TGZ experience elevated serum ALT, suggesting that certain patients are more susceptible to TGZ-mediated toxicity. A multiple linear regression analysis showed that in the current model, decreased biliary excretion of LCA-sulfate and CDCA-amide, decreased TS biliary clearance, decreased hepatic basolateral efflux of CDCA-amide, increased LCA synthesis in the gut, decreased feedback regulation on hepatic efflux transporters, and decreased body weight were key risk factors for TGZ-mediated hepatotoxicity associated with bile acid transport inhibition. Decreased biliary excretion of bile acids and TS represents decreased expression and/or function of hepatic canalicular transporters, which will increase hepatic exposure of toxic bile acids as well as perpetrator drugs/metabolites. Decreased function of basolateral efflux transporters, which serve as an important compensatory pathway for bile acid excretion when biliary excretion is impaired (43), could potentiate hepatic accumulation of toxic bile acids. Thus, impaired expression and/or function of these transporters by concomitant drugs, disease states, or genetic polymorphisms would be expected to

predispose a subset of patients to DILI. Functional variants in BSEP are a known susceptibility factor for the development of estrogen- and fluvastatin-induced cholestasis (44, 45), indicating that patients with impaired BSEP function might be at greater risk of DILI. Hepatocyte exposure to bile acids and perpetrator drugs/metabolites as well as hepatocyte susceptibility to bile acids (e.g., mitochondrial function) also might be altered in liver disease (e.g., non-alcoholic steatohepatitis, cirrhosis), which often are associated with diabetes (46). However, quantitative data relating the extent of functional impairment to the progress and severity of disease are needed to support this. LCA is synthesized in the intestine by bacterial modification of CDCA, which is known to be affected by environmental factors such as diet. However, the rate and variability of LCA synthesis have not been well characterized, and thus further data are needed to evaluate the effects of environmental factors on bile acid-mediated hepatotoxicity using mechanistic modeling. Adaptive response to hepatic bile acid accumulation (e.g., altered bile acid synthesis, metabolism, and transport) is another important unknown for which quantitative data are lacking (47). Predictability of the model will be improved further with advances in our knowledge about bile acid physiology, patient- and disease-specific risk factors.

Increasing evidence supports the hypothesis that drug-mediated functional disturbances in hepatic bile acid transporters leads to intracellular accumulation of potentially harmful bile acids and subsequent development of hepatic injury. Systematic investigation of a panel of drugs for their inhibitory effects on bile acid efflux transporters using isolated membrane vesicles and hepatotoxic potential demonstrated that inhibition of bile acid efflux transporters is associated with DILI (11, 12, 48, 49). More sophisticated model systems such as sandwich-cultured hepatocytes have been used to assess effects of drugs and generated metabolites on hepatic accumulation of bile acids (49-51). However, bile acid-drug interactions may be more complicated due to vectorial transport and enterohepatic recirculation of bile acids, dynamic changes in the systemic as well as hepatic exposure of drugs/metabolites and bile acids, and feedback regulation of bile acid synthesis and transport as an adaptive response to hepatic bile acid accumulation (52). It is of note that knowledge gaps exist in bile acid homeostasis as discussed above and elsewhere (19), which may limit accurate, quantitative prediction of bile acid-mediated DILI. Nonetheless,

mechanistic modeling incorporating 1) physiology and pathophysiology of bile acids in humans and rats, 2) systemic and hepatic disposition of TGZ and TS, and 3) in vitro inhibition potency data reasonably predicted altered bile acid disposition in rats administered glibenclamide (19), and also adequately predicted delayed presentation and species differences in TGZ hepatotoxicity. These findings suggest that mechanistic modeling combined with population analysis may provide a useful tool to integrate our current knowledge about physiological and experimental data obtained during the drug development process, and prospectively predict hepatotoxic potential of new chemical entities that are in the drug development pipeline.

METHODS

Physiologically-based pharmacokinetic (PBPK) model development

A PBPK model was developed to describe the distribution of TGZ and TS in humans and male rats (Figure 7.2) after intravenous (rat) and oral (human and rat) administration. Only male rat data were employed in the current study because gender differences were observed in TGZ and TS pharmacokinetics in rats, but not in humans; plasma TS concentrations in female rats were ~3-fold lower compared to male rats, and female rats did not mimic TGZ and TS disposition observed in humans (53, 54). Details regarding the construction and final structure of the PBPK model are provided in the supplementary material (Supplementary Figure 7.2). Briefly, the TGZ PBPK model consisted of a central compartment representing the blood, as well as hepatic and extrahepatic tissues (e.g., muscle, intestine) linked to the central compartment by blood flow. It was assumed that TGZ metabolism occurred mainly in the liver by sulfation and glucuronidation; the quinone metabolite was not included because this is a minor pathway of metabolism and the current investigation was not focused on quinone-mediated toxicity (53, 55). Disposition of TS was described using a semi-PBPK model, which consisted of a central compartment representing the blood, hepatic tissue, and extrahepatic tissues lumped into one compartment. Chemical-specific kinetic parameters (e.g., tissue partition coefficients, rate of metabolite formation, fraction unbound in plasma, biliary and renal clearances) were obtained from the literature or

optimized using TGZ and TS plasma concentration versus time data obtained from the in vivo experiments (Supplementary Table 7.1).

Construction of human and rat population samples (SimPops)

To account for inter-individual variability in the model parameters governing bile acid and drug disposition, human and rat SimPops were constructed previously within DILIsym using the genetic algorithm in MATLAB (19). Human (n=331) and rat (n=192) population samples (SimPops) were generated by varying parameters 10 (human) or 11 (rat) parameters, as listed in Table 7.2, in the bile acid homeostasis sub-model; these bile acid SimPops are “system-specific” and were used to simulate hepatotoxic potential of different compounds. In the current study, parameters governing TGZ and TS disposition (human and rat), body weight (human), and sensitivity of hepatic ATP decline to hepatic bile acid accumulation (human) also were varied using the probability distribution of each parameter obtained from the literature. Details related to construction of the SimPops can be found in the supplementary material.

Simulation of DILI responses

Perturbation of bile acid disposition and DILI responses after TGZ administration in human (200, 400, or 600 mg/day for 6 months) and rat (5 or 25 mg/kg/day for 1 month) SimPops were simulated using PBPK model predictions of TGZ and TS disposition, a previously developed bile acid homeostasis sub-model (19), and bile acid transport inhibition constants for TGZ and TS (i.e., K_i , IC_{50}) measured in isolated membrane vesicle transport systems (supplemental Table 7.2). To assess the sensitivity of DILI responses to inhibition constants, simulations were performed with 10-fold smaller or greater inhibition constants for BSEP, MRP4, and NTCP in human and rat SimPops administered 600 mg/day (highest dose used in the clinic) and 5 mg/kg/day (equivalent to the clinical dose) TGZ, respectively. Simulations for the sensitivity analysis studies were performed for only 1 month due to the extensive computational time required for long-term (6 month) simulations, and also because even for the individuals with delayed presentation of hepatotoxicity, slight increases (<3X ULN) in serum ALT could be detected within 1 month of simulation. To identify the most important parameters in the context of bile acid-mediated DILI,

a multiple regression analysis was performed with minimum hepatic ATP as the predicted outcome; 16 parameters were used to develop human SimPops as independent variables. Because the units of independent variables were different by orders of magnitude, standardized coefficients were calculated to determine which of the independent variables have a greater effect on the minimum hepatic ATP. Statistical analyses were performed using JMP 10 (SAS, Cary, NC).

Table 7.1. Summary of troglitazone-mediated hepatotoxicity in human SimPops and clinical trials.

	Simulations ^a			Clinical Trials (2, 3)	
	TGZ 200 mg (n=331)	TGZ 400 mg (n=331)	TGZ 600 mg (n=331)	TGZ 200 – 600 mg (n=2510)	Placebo (n=475)
ALT > 3X ULN (%) ^b	0 ^c	2.4	4.2	1.9	0.6
ALT > 5X ULN (%) ^b	0	1.2	3.0	1.7	N/A
ALT > 8X ULN (%) ^b	0	0.9	2.4	0.9	0
ALT > 30X ULN (%) ^b	0	0	0.3	0.2	0
Time to peak ALT (Days) ^d	N/A	128 ± 61	110 ± 62	147 ± 86	N/A
Total Bilirubin > 2X (%) ^e	0	0.9	3.0	N/A	N/A
Hy's Law cases (%)	0	0.9	3.0	0.08	N/A
Jaundice (%)	N/A	N/A	N/A	0.08	0

^a Each dose level was simulated for 6 months.

^b ULN (upper limit of normal) was 34 U/L in the clinical trials. Baseline serum ALT in human SimPops was 30 U/L.

^c 1 individual with ALT >2X ULN.

^d Mean ± S.D.

^e Baseline serum total bilirubin in human SimPops was 0.55 mg/dL. N/A, not available.

Table 7.2. List of parameters varied in the human and rat SimPops and results of multiple regression analysis in human SimPops administered 600 mg/day troglitazone (TGZ) for 6 months. Human and rat population samples incorporating variability in parameters governing bile acid homeostasis (Bile Acid Homeostasis Sub-model) have been constructed previously (19). Four parameters in the Drug PBPK Sub-model and two system-specific parameters also were varied. (See supplementary material for methods and data used for construction of SimPops). In the human SimPops, a multiple regression analysis was performed to identify the most important parameters in TGZ-mediated hepatotoxicity using 16 varied parameters as independent variables and minimum hepatic ATP as the predicted outcome. Statistical significance and standardized coefficients were calculated using JMP 10.

Parameter Name	Parameter Description	Significance	Standardized Coefficient ^a
Bile Acid Homeostasis Sub-model			
LCA-sulfate uptake V_{\max}	Maximum velocity of hepatic uptake of LCA-sulfate	N/S	-0.07
LCA-sulfate canalicular efflux V_{\max}	Maximum velocity of biliary excretion of LCA-sulfate	$P < 0.001$	0.43
CDCA-amide uptake V_{\max}	Maximum velocity of hepatic uptake of CDCA-amide	N/S	0.00
CDCA-amide canalicular efflux V_{\max}	Maximum velocity of biliary excretion of CDCA-amide	$P < 0.001$	0.21
CDCA-amide basolateral efflux V_{\max}	Maximum velocity of hepatic basolateral efflux of CDCA-amide	$P < 0.05$	0.08
CDCA amidation V_{\max}	Maximum velocity of CDCA amidation in hepatocytes	N/S	0.04
LCA-amide sulfation V_{\max}	Maximum velocity of LCA-amide sulfation in hepatocytes	N/S	-0.03
LCA synthesis V_{\max}	Maximum velocity of LCA synthesis in the intestinal lumen	$P < 0.001$	-0.26
Uptake regulation scaling factor	Scaling factor governing the magnitude of feedback regulation of hepatic uptake transporter function by hepatic bile acid accumulation	N/S	0.04
Canalicular efflux regulation scaling factor	Scaling factor governing the magnitude of feedback regulation of hepatic canalicular transporter function by hepatic bile acid accumulation	$P < 0.001$	0.24
LCA hydroxylation V_{\max}^b	Maximum velocity of LCA hydroxylation in hepatocytes	N/A	N/A
Drug PBPK Sub-model			
TGZ intestinal absorption K_{ab}	First-order rate constant for TGZ absorption from intestine	N/S	-0.01
TGZ hepatic uptake V_{\max}	Maximum velocity of TGZ hepatic uptake	N/S	-0.04

TGZ sulfation V_{\max}	Formation rate of TGZ-sulfate (TS)	N/S	-0.06
TS biliary clearance	Biliary clearance of TS	$P < 0.001$	0.18
Other system-specific parameters			
Body weight ^c	Body weight	$P < 0.001$	0.15
Toxicity K_m for CDCA and LCA species ^c	Intracellular bile acid concentrations that induce half-maximal inhibition of ATP synthesis	N/S	0.02

^a Parameter estimates that would have resulted from the regression if all of the variables had been standardized to a mean of 0 and a variance of 1. The greater the absolute value of the standardized coefficient, the greater the effects of the independent variable on the model output.

^b Used in rat SimPops only.

^c Used in human SimPops only.

N/S, not significant.

N/A, not available.

Figure 7.1. Schematic overview of the bile acid transport inhibition module in DILIsym.

Hepatic and systemic disposition of drugs/metabolites are simulated using a physiologically-based pharmacokinetic (PBPK) model (**Drug PBPK Model**). The **Bile Acid Homeostasis Model** represents hepatobiliary disposition and enterohepatic recirculation of lithocholic acid (LCA) and chenodeoxycholic acid (CDCA) species, and all other (bulk) bile acids (19). Using bile acid transport inhibition constants of drugs/metabolites (e.g., K_i , IC_{50}), altered bile acid disposition is simulated. Increased hepatocellular accumulation of bile acids inhibits hepatic ATP synthesis and decreases intracellular ATP concentrations (**Cellular ATP Model**), leading to necrotic cell death (**Hepatocyte Life Cycle Model**) and elevations in serum biomarkers of hepatocellular injury and function (e.g., ALT, AST, bilirubin) (**Biomarker Model**). Loss of hepatocytes will subsequently influence drug and bile acid disposition (dashed lines), allowing dynamic interaction between kinetics and toxicity mechanisms. Details regarding the construction and structures of sub-models can be found in the supplementary materials.

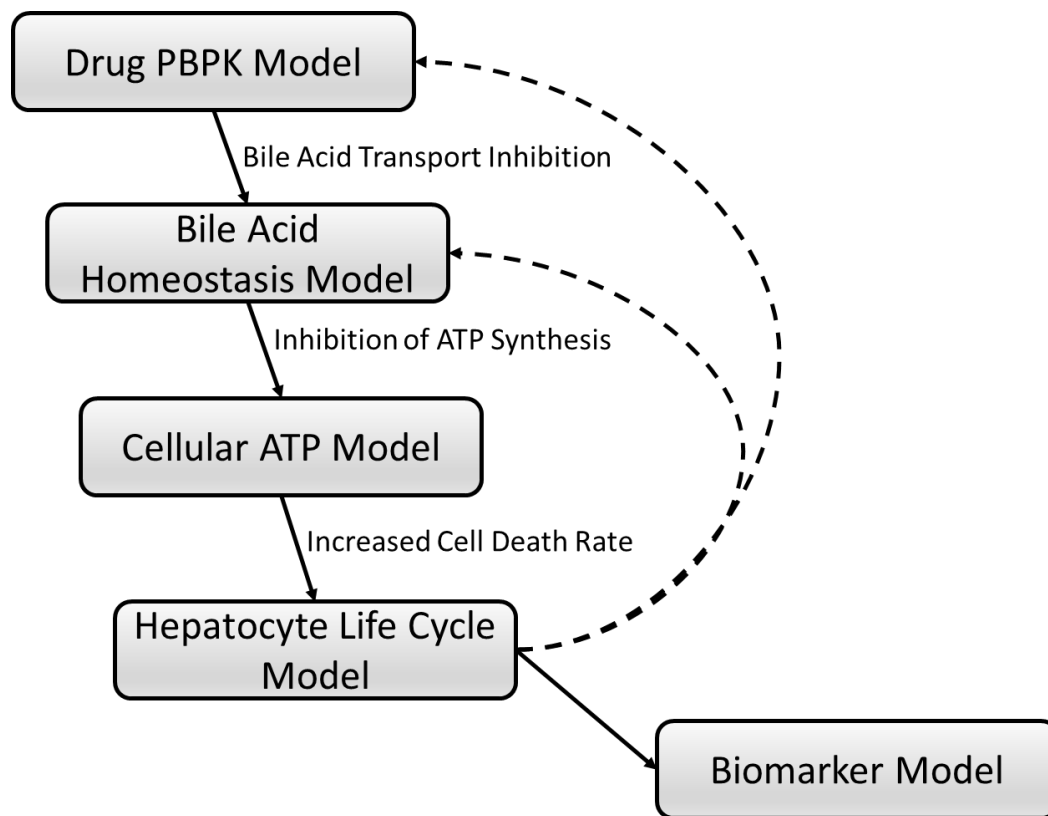


Figure 7.2. Predicted and observed plasma concentration of troglitazone (TGZ) and TGZ sulfate (TS) in humans and rats.

Solid and dashed lines represented plasma concentrations of TGZ and TS, respectively, predicted based on a PBPK model (Supplementary Figure 7.2). Closed and open symbols represent observed plasma concentrations of TGZ and TS, respectively, in (A) humans (triangles) administered 400 mg oral TGZ (20), and (B) male rats administered 5 mg/kg intravenous (circles) or oral (triangles) TGZ (21, 22).

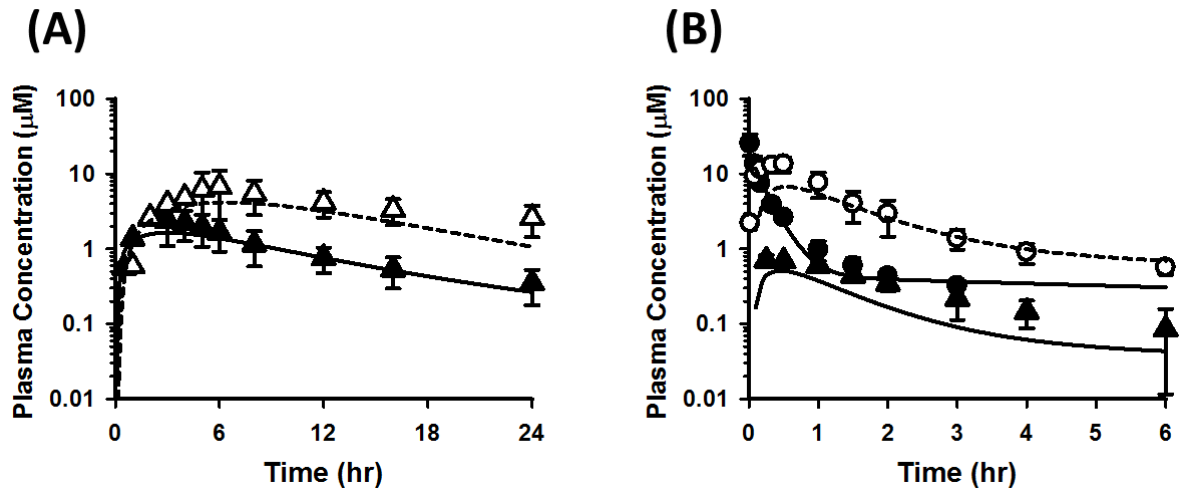
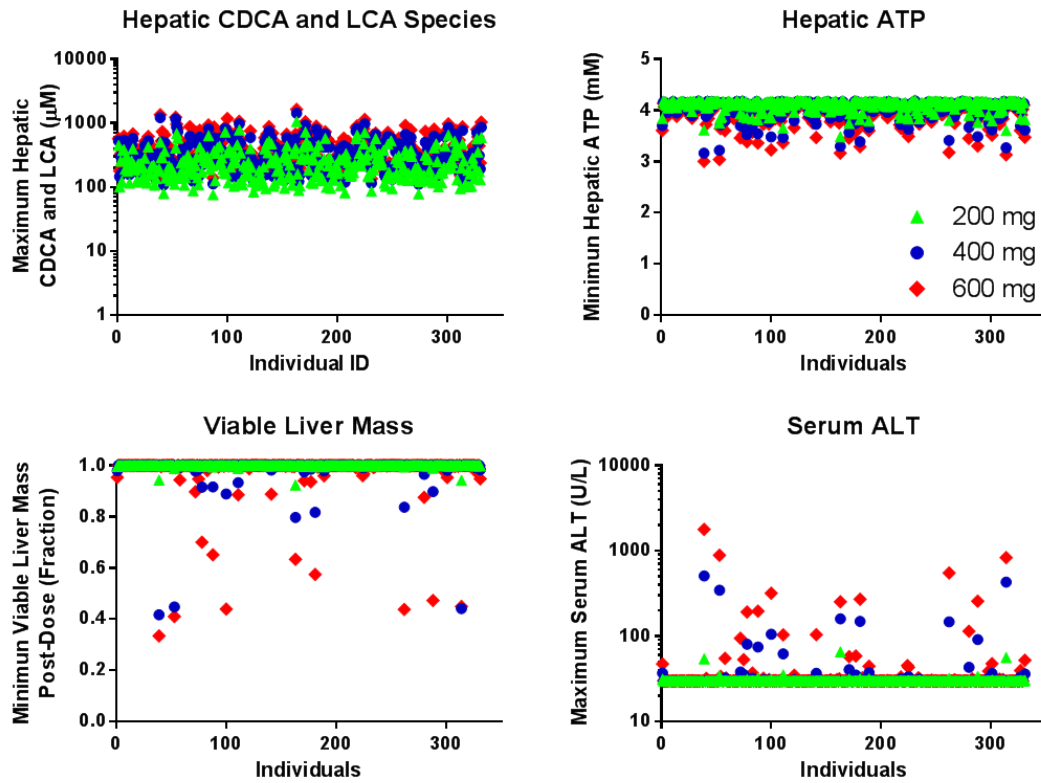


Figure 7.3. Simulated DILI responses in human and rat populations (SimPops) at specified troglitazone (TGZ) dose levels.

Predicted maximum hepatic accumulation of CDCA and LCA species and DILI responses (i.e., minimum hepatic ATP, minimum viable liver mass, maximum serum ALT) post-dose in human SimPops at oral doses of 200 (green triangle), 400 (blue circle), or 600 (red diamond) mg/day TGZ for 6 months (A), and rat SimPops at oral doses of 5 (blue circle) or 25 (red diamond) mg/kg/day for 6 months (B).

(A)



(B)

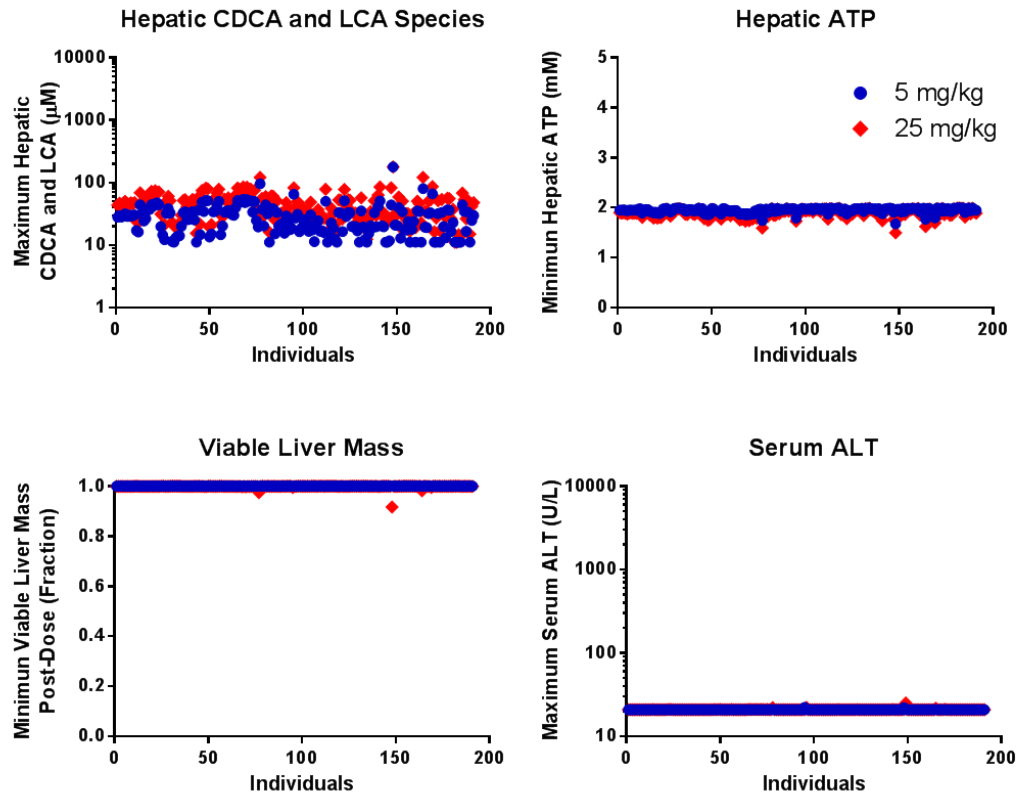
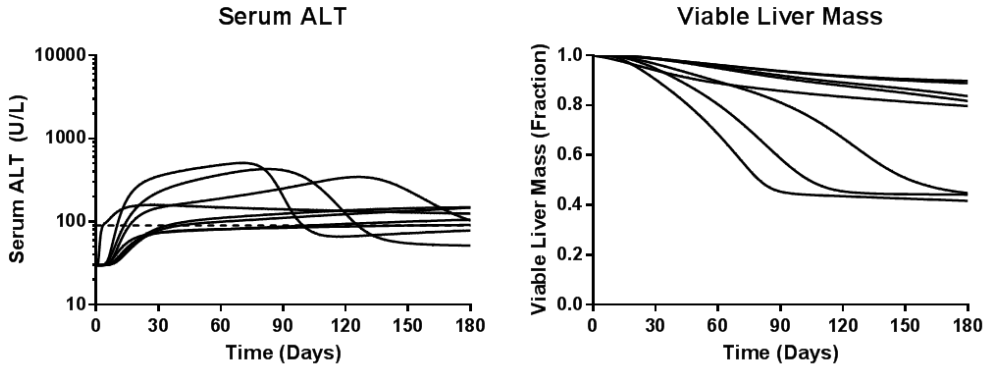


Figure 7.4. Simulated serum ALT and viable liver mass in susceptible individuals.

In human SimPops administered 400 (A) or 600 (B) mg/day troglitazone for 6 months, individuals with serum ALT elevations > 3X (n=8 at 400 mg/day; n=14 at 600 mg/day) are presented.

(A)



(B)

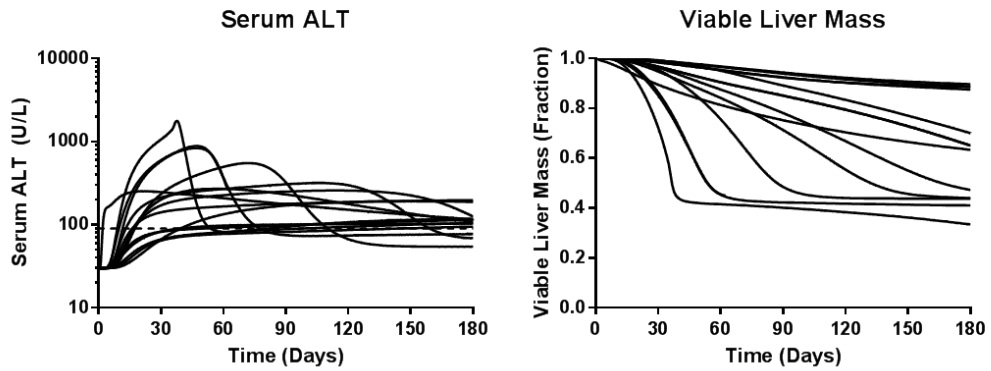
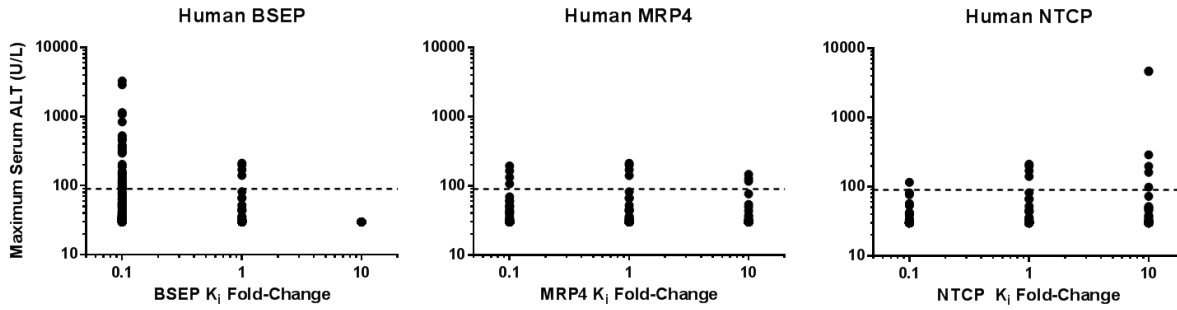


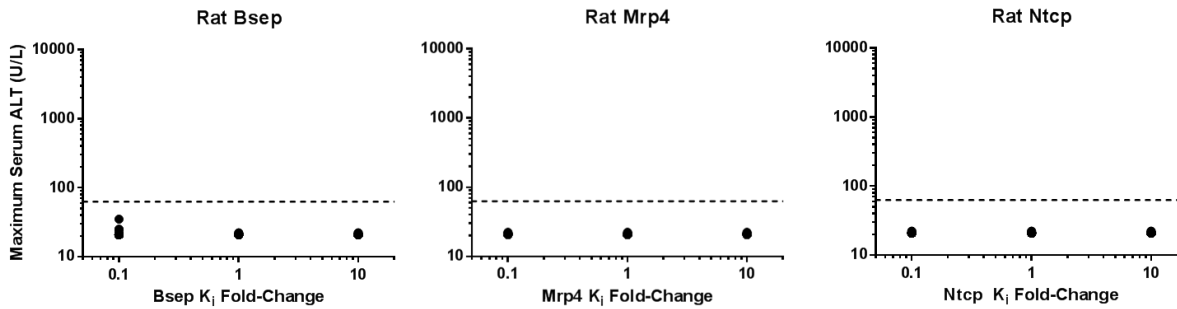
Figure 7.5. Sensitivity analysis of transporter inhibition constants.

Inhibition constants for BSEP, MRP4, and NTCP were altered 10-fold in either direction of the values measured in isolated transport systems (Supplementary Table 7.3). Predicted maximum serum ALT concentrations in human and rat SimPops after an oral dose of 600 mg/day and 5 mg/kg/day TGZ, respectively, for 1 month are presented. Dashed lines represent 3X baseline ALT in human (90 U/L) and rat (63 U/L) SimPops.

(A)



(B)



SUPPLEMENTARY MATERIAL

DILIsym v2

DILIsym is a mechanistic, mathematical model of DILI, which is organized into various sub-models that represent physiological processes involved in DILI and drug disposition (16) (<http://www.dilisyms.com>). These sub-models are mathematically integrated to simulate response in the intact organism. Data from multiple species including humans, rats, mouse, and dogs, are incorporated in the model to explore species differences in DILI susceptibility and interpret preclinical data to improve prediction of human DILI risk. Currently, DILIsym includes components to predict reactive metabolite-mediated, mitochondrial, and bile acid-mediated toxicity.

Physiologically-based Pharmacokinetic (PBPK) Sub-model

The structure of the PBPK model depicting disposition of troglitazone (TGZ) and TGZ sulfate (TS) is presented in Supplementary Figure 7.2. The PBPK model of TGZ consisted of a central compartment representing the blood, as well as hepatic and extrahepatic tissues (e.g., muscle, intestine) linked to the central compartment by blood flow. The size of the liver and the volume of blood are subject to change from baseline values based on the amount of cellular necrosis. Hepatic uptake of TGZ was represented using saturable Michaelis-Menten kinetics representing transport-mediated processes (56). Biliary excretion of TGZ was reported to be negligible (53, 57, 58). Distribution of TGZ to extra-hepatic tissues was assumed to be perfusion-limited and was represented by tissue partition coefficients. TGZ metabolism, represented by Michaelis-Menten kinetics, was assumed to occur primarily in the liver by sulfation and glucuronidation (22). The quinone metabolite was not included due to its minimal (<10%) contribution to total systemic exposure in humans, and total recovery in feces and urine in rats (53, 55). The possibility that systemic and hepatic concentrations of TGZ quinone *in vivo* might have been lower than measured due to photooxidation of TGZ to TGZ quinone during analysis cannot be excluded (59). TGZ quinone also has been shown to induce hepatotoxicity, but quinone-mediated hepatotoxicity is not the focus of the current investigation (6). TGZ glucuronide is formed in the liver, but disposition of TGZ glucuronide was not modeled because TGZ glucuronide does not inhibit bile acid transport. TS moved

from the periportal zone into the midlobular zone, then into the centrilobular zone, and then into the central (blood) compartment, in the direction of blood flow. TS disposition was described using a semi-PBPK model, which consisted of a central compartment representing the blood, hepatic tissue, and extrahepatic tissues lumped into one compartment. TS was reported to be a substrate of hepatic uptake and biliary transporters, but hepatic TS disposition was represented by liver partition coefficients because 1) the semi-PBPK model structure of the metabolites in the current DILIsym does not include active transport of metabolites, and 2) existing data suggest that the ratio of hepatic and plasma concentrations of TS remained constant over time and could thus be represented by a partition coefficient (53). Biliary excretion of TS also was accounted for in the model. Drug-specific parameters, attained from the literature or estimated using available plasma TGZ/TS concentration versus time data, are listed in Supplementary Table 7.1. Physiological parameters for tissue volumes and blood flows in the PBPK module of DILIsym can be found in the supplementary materials of Howell et al. (17).

Bile Acid Homeostasis Sub-model

The sub-model of bile acid homeostasis in humans and rats has been constructed within DILIsym (19). This sub-model includes 1) the synthesis and metabolism of bile acids in hepatocytes, 2) the biliary excretion and basolateral efflux of bile acids via hepatic transporters, 3) the release of bile acids from the gallbladder (humans and dogs only), 4) the synthesis of secondary bile acids and deconjugation of conjugated bile acids in the gut lumen, 5) reabsorption of bile acids from the gut and subsequent uptake into the liver, and 6) the regulatory effects of bile acids on the expression of hepatic transporters and bile acid synthesis (19). Hepatic uptake, basolateral efflux, and biliary excretion of bile acids are transporter-mediated processes which might be interrupted by drugs and/or metabolites. Inhibition constants of TGZ and TS for bile acid transport proteins used in the current investigation are listed in Supplementary Table 7.2. The model represents LCA, CDCA, and respective metabolites, in addition to all other (“bulk”) bile acids. LCA and CDCA were chosen because they are hydrophobic and known to be potentially toxic bile acids. The quantitative relationship between hepatocellular unconjugated LCA and/or CDCA concentrations and ATP concentrations was constructed using the data obtained from human and rat

sandwich-cultured hepatocytes (60). Conjugates of LCA and CDCA were assumed to be equally as toxic as their unconjugated counterpart.

Cellular ATP Sub-model

The cellular ATP model has been constructed previously in DILIsym (17) (Supplementary Figure 7.4). Briefly, basal ATP turnover was designed to include zero order production and first order utilization. The steady-state ATP turnover rate was calculated based on the measured whole body basal metabolic rate (61-64), the fraction of the basal metabolic rate from the liver (65), the mass of the liver, and the weighted average of the energetic cost of synthesizing ATP from fatty acids, carbohydrates, and amino acids (66, 67). Baseline hepatic ATP levels in the DILIsym model were based on Ghosh 2010 (68) and Kaminsky 1984 (69) for the rat, and Noren 2005 (70) and Meyerhoff 1990 (71) for the human.

Hepatocyte Life Cycle Sub-model

The hepatocyte life cycle sub-model has been constructed previously in DILIsym (17) (Supplementary Figure 7.5). Hepatocytes can undergo death by apoptosis or necrosis; both are components of DILI. A variety of determinants push a stressed cell towards apoptosis or necrosis; one of the predominant factors is the energy state of the cell. Without sufficient ATP, the cell cannot support energy-requiring reactions (including apoptosis), and necrosis will result. Apoptosis can be initiated by signals originating in mitochondria or elsewhere. Mitochondrial signals arise when the permeability of the outer mitochondrial membrane and/or the number of open inner mitochondrial pores (due to the mitochondrial permeability transition-mPT) are increased. Extra-mitochondrial apoptotic signals come from “death receptors” and/or ER stress. In addition to the cellular energy state, other factors contribute to necrosis. Increased levels of oxidative species, such as reactive metabolites of drugs or endogenous compounds, can compromise the integrity of the plasma membrane and cause hepatocytes to rupture. Proteases released by Kupffer cells and neutrophils also can elicit necrosis.

Explicit tracking of individual hepatocyte pools (necrotic, apoptotic and mitotic) is done with DILIsym, as it enables comparisons with histological data. Mature and young hepatocytes may have different rates of necrosis and apoptosis, and non-viable cells are cleared with specified half-lives. With

appropriate internal and external cues, mature hepatocytes can commit to mitosis and divide into young hepatocytes. Cell division can be slowed by crowding signals resulting in cell cycle arrest. Oval cells contribute to hepatocyte populations in the periportal zone and hepatocytes may 'stream' (i.e., migrate over time) from periportal to midlobular and then to centrilobular zones. The contributing rates of cell turnover are regulated by mediators (described below in the 'Mediator Production and Regulation' and 'Regulation of Hepatocyte Rates' sections).

All zones are assumed to have the same density of hepatocytes, and hepatocytes have the same volume. In all species, centrilobular (CL) is 1/9, midlobular (ML) is 3/9 and periportal (PP) is 5/9 of total liver volume, based on a 'cake-slice' like three dimensional configuration of the average acinus (72-74). The CL zone is perfused by the venous blood and a decreasing oxygen gradient exists from PP to CL. However in practice, some of the 'inter-septal' hepatocytes in the PP zone also may be poorly perfused and have slightly different properties (75). While inter-septal morphology is not explicitly modeled, a fraction of poorly perfused PP hepatocytes is factored in when interpreting histological data.

The baseline homeostasis rates associated with the hepatocyte life cycle are calculated such that the fraction of hepatocytes that should be young, mature, mitotic, and apoptotic at baseline are consistent with the user defined inputs for these values. Hepatocytes have a long life cycle in the baseline, homeostatic state, living 180-365 days or 6-12 months (76). The default values used in the DILIsym model for these fractions are from the references listed below.

1. The fraction of mitotic and apoptotic hepatocytes at homeostasis was based on Grisham 1962 (77). Necrosis is assumed not to occur at homeostasis.
2. The rate of removal of apoptotic cells was based on Bursch 1990 (78) in rats. This rate is not available for other species. In the current version of the model, the cell removal rates do not further affect rates of necrosis, apoptosis, and/or proliferation. Future versions may include this type of feedback, however.

3. The rate constant for removal of necrotic cells is calibrated in the rat based on time-series data of necrotic hepatocytes after acetaminophen treatment (79). Similar data were not available for other species, so the same rate constant was used for other species.
4. The rate of cell cycle progression is based on Chanda 1996 (80).
5. At baseline, the rate of maturation to go from young to mature hepatocytes is rapid compared to other rates. The differences in the model between young and mature hepatocytes are in their rates of necrosis and apoptosis in each zone. This effect can be explored further with the model.

Biomarker Sub-model

The biomarker sub-model previously has been constructed in DILIsym (17). Several clinical biomarkers are included in the model including alanine aminotransferase (ALT), aspartate aminotransferase (AST), prothrombin time, total plasma bilirubin, keratin 18, and high mobility box group 1 protein (HMGB1). The ALT and bilirubin sub-models are discussed in more detail below, since data from these sub-models is included in this manuscript.

ALT is an intracellular enzyme responsible for amino acid metabolism and gluconeogenesis in the liver and other tissues. In DILI, circulating ALT serves as a marker of hepatocellular injury. An increase in ALT is thought to represent compromised hepatocellular membrane integrity due to necrosis. Care must be taken when using ALT as a biomarker for DILI, however, because increases in ALT have been observed in situations unrelated to DILI. For example, ALT levels may be increased due to release from muscle following high intensity exercise (81).

ALT levels in DILIsym are driven primarily by the rate of hepatocyte necrotic flux (Supplementary Figure 7.6). The intermediate ALT compartment was required to adequately describe observed ALT profiles in response to other hepatotoxic drugs (e.g., acetaminophen), and may represent interstitial space, the Space of Disse, or liver sinusoids. The clearance of ALT has a specified half-life. The half-life of ALT is altered by reductions in the number of viable hepatocytes, i.e. less hepatocytes lead to a longer ALT half-life. Cellular ALT levels were calculated from the literature and used to

estimate the amount of ALT released per necrotic cell (82, 83). More details can be found in the supplementary material of Howell et al. (17).

Combined monitoring of ALT and bilirubin levels often is used as a diagnostic test for DILI. Hy's law, for example, includes the combination of ALT (or AST) increases > 3 -fold the upper limit of normal (ULN) with increases of serum total bilirubin > 2 -fold ULN. For this reason, and because total plasma bilirubin is an important clinical marker for liver function, a bilirubin sub-model was included in DILIsym.

Bilirubin is a byproduct of red blood cell lysis and serves as a marker of hepatocellular function. Bilirubin is derived from the heme molecule, which is abundant in red blood cells. Bilirubin is released to the circulation with red blood cell lysis and is cleared by hepatocytes. Once inside the hepatocyte, bilirubin is conjugated (to glucuronide, primarily) and exported to bile for excretion, which is an ATP-dependent process. Bilirubin levels correlate well with the change in hepatic glutathione (84, 85). Moreover, hepatic glutathione correlates well with hepatic ATP levels (86, 87). ATP reductions are the likely mechanistic link underlying the correlation between bilirubin and glutathione levels. Increases in unconjugated or total bilirubin are used in DILI as a marker of compromised hepatic function. Like ALT, caution must be taken when using bilirubin as a diagnostic test for DILI, because bilirubin levels may increase due to increases in red blood cell lysis or competition for uptake by OATPs instead of decreased hepatocellular function (88).

Bilirubin levels in the model are regulated by changes in clearance, as the input is constant and determined by literature values. The primary regulator of hepatocellular bilirubin uptake is the number of viable hepatocytes (current hepatocyte number as a fraction of baseline) (89). Glucuronidation and transport of bilirubin out of hepatocytes is regulated by cellular ATP levels; this regulation mechanism correlates well with changes in bilirubin prior to cell loss. Conjugated bilirubin is not currently included in the model, but is likely to be integrated into the bile acid transport model in future versions of DILIsym. A schematic of the bilirubin model is shown in Supplementary Figure 7.7.

Construction of human and rat simulated Populations (SimPops)

Human and rat population samples incorporating variability in the most sensitive parameters (n=10 in human, n=11 in rat; Bile Acid Homeostasis Sub-model parameters in Table 7.2) governing bile acid homeostasis were constructed previously in DILIsym using a genetic algorithm in MATLAB (Bile Acid SimPops). The data and genetic algorithm methods used for construction of the Bile Acid SimPops are described in Woodhead et al., and Howell et al., (17, 19). In the human and rat SimPops used in the current study, additional variability was incorporated in four drug-specific parameters (the first-order rate constant for TGZ absorption from intestine, maximum velocity of TGZ hepatic uptake, formation rate of TGZ-sulfate, and biliary clearance of TS). Two system-specific parameters (body weight and sensitivity of mitochondrial toxicity to hepatic bile acid accumulation) also were incorporated in the human SimPops. A list of parameters varied in human and rat SimPops is presented in Table 7.2. Data used for six additional parameters in human and rat SimPops are presented in Supplementary Table 7.3.

Supplementary Table 7.1. Troglitazone (drug-dependent) parameters used for the construction of the physiologically-based pharmacokinetic model.

Parameter	Values	Methods/references
Troglitazone		
Molecular weight (g/mol)	441.5	ChEMBL
Log P	4.69	ChEMBL
pKa	6.35	ChEMBL
Blood to plasma total concentration ratio	0.55 (Human) 0.60 (rat)	(21)
fu _p (plasma unbound fraction)	0.2	Parameter estimation*
K _{liver} (liver to blood partition coefficient)	1	Parameter estimation*
K _{gut} (gut to blood partition coefficient)	0.47	Predicted based on pKa and logP (90)
K _{muscle} (muscle to blood partition coefficient)	0.15	Predicted based on pKa and logP (90)
K _{other} (other tissues to blood partition coefficient)	0.61	Predicted based on pKa and logP (90)
Hepatic uptake V _{max} (mg/hr)	50.1	Parameter estimation*
Hepatic uptake K _m (mg/ml)	0.0035	(56)
Hepatic permeability (ml/hr)	1590	Assumed to be 10% of total hepatic uptake (91)
TS formation V _{max} (mol/hr/kg ^{0.75}) (maximum velocity of TGZ sulfation)	3.34E-05	(22)
TS formation K _{m,u} (mol/ml) (unbound Michaelis Menten constant of TGZ sulfation)	1.66E-11	(22)
TG formation V _{max} (mol/hr/kg ^{0.75}) (maximum velocity of TGZ glucuronidation)	7.60E-05	(22)
TG formation K _{m,u} (mol/ml) (unbound Michaelis Menten constant of TGZ glucuronidation)	7.00E-10	(22)
CL _{bile} (ml/hr/kg ^{0.75})	0	(53, 57, 58)
CL _{renal} (ml/hr/kg ^{0.75})	0	(55, 58)
K _{ab} (1/hr) (the first order rate constant for intestinal absorption)	0.08 (hu)	Parameter estimation*
K _{out_gut} (1/hr) (the first order rate constant for elimination from intestinal lumen to feces)	0.033 (hu)	Parameter estimation*
Troglitazone Sulfate		
Molecular weight (g/mol)	521.6	ChEMBL
Blood to plasma total concentration ratio	0.55 (Human) 0.60 (rat)	Assumed to be the same as TGZ
fu _p	0.2	Parameter estimation*
K _{liver} (liver to blood partition coefficient)	15	(53)

V _{d,wt} (mg/kg) (volume of distribution per kg weight)	380	Parameter estimation*
CL _{bile} (ml/hr/kg ^{0.75})	19.5	(57)
CL _{renal} (ml/hr/kg ^{0.75})	0	(55, 58)

*Optimized using TGZ and/or TS plasma concentration versus time data (20-22, 53, 92).

Supplementary Table 7.2. Inhibition constants of TGZ and TS for bile acid transport proteins.

	Rat Inhibition Constant (μM)		Human Inhibition Constant (μM)	
	TGZ	TS	TGZ	TS
BSEP	1.3 ^a	0.23 ^a	1.3 ^b	0.23 ^b
MRP4	21 (IC_{50}) ^c	8 ^c	31 (IC_{50}) ^d	8 ^e
NTCP	2.3 (IC_{50}) ^f	2.3 (IC_{50}) ^g	0.33 (IC_{50}) ^f	0.33 (IC_{50}) ^g

K_i unless indicated.

^a, (13)

^b, assumed to be the same as rat because IC_{50} values of TGZ for human BSEP and rat Bsep are similar (12).

^c, assumed to be the same as human

^d, (11)

^e, Yang et al., in preparation

^f, (15)

^g, assumed to be the same as TGZ

Supplementary Table 7.3. DILIsym model parameters used to generate human (A) and rat (B) simulated populations (SimPops) to explore troglitazone (TGZ)-mediated hepatotoxicity.

Human SimPops			
Parameter Name	Parameter description	Lower/upper bounds (%)	References
Body weight (kg)	Body weight	64/141	(93)
Toxicity K_m for CDCA and LCA species	Intracellular bile acid concentrations that induce half-maximal inhibition of ATP synthesis	50/150	Nadanaciva et al., unpublished
TGZ intestinal absorption K_{ab}	First-order rate constant for TGZ absorption from intestine	50/150	
TGZ hepatic uptake V_{max} (mg/hr)	Maximum velocity of TGZ hepatic uptake mediated by OATP1B1	13/454*	(94)
TGZ sulfation V_{max} (mol/hr/kg ^{0.75})	Formation rate of TGZ-sulfate (TS) mediated by SULT1A1/1E1	35/248*	(95)
TS biliary clearance (mL/hr/kg ^{0.75})	Biliary clearance of TS mediated by canalicular transport proteins, BCRP and MRP2	29/281*	(94)
Rat SimPops			
Parameter Name	Parameter description	Lower/upper bounds (%)	References
TGZ intestinal absorption K_{ab}	First-order rate constant for TGZ absorption from intestine	50/150	
TGZ hepatic uptake V_{max} (mg/hr)	Maximum velocity of TGZ hepatic uptake mediated by Oatp1b1	51/184*	(96)
TGZ sulfation V_{max} (mol/hr/kg ^{0.75})	Formation rate of TS mediated by Sult1a1/1e1	51/183*	(97)
TS biliary clearance (mL/hr/kg ^{0.75})	Biliary clearance of TS mediated by canalicular transport proteins, Bcrp and Mrp2	51/184*	(96)

The lower and upper bounds give the maximum and minimum values used for the SimPops generation relative to baseline parameter values of 100%. The baseline values were taken from the literature or obtained through optimization using in vivo data (See Methods).

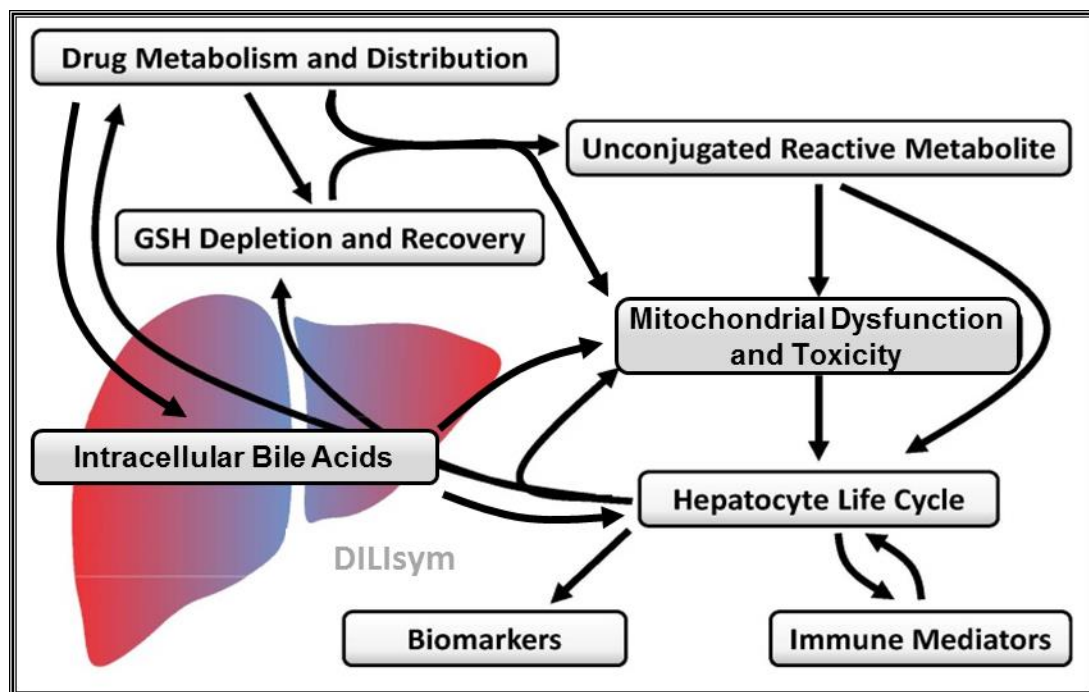
Unless specified, a normal distribution was assumed. The standard deviation of the parameters used to generate the population samples were assumed to be the differences between the upper or lower bound and the baseline value divided by a factor of 2.5. Under this assumption with normal distribution, the above bounds include 98.8% of the population.

*Log-normal distribution was assumed. Mu (μ) and sigma (σ) (mean and standard deviation of log-transformed data) were obtained from mean (m) and variance (v) of non-transformed distribution data

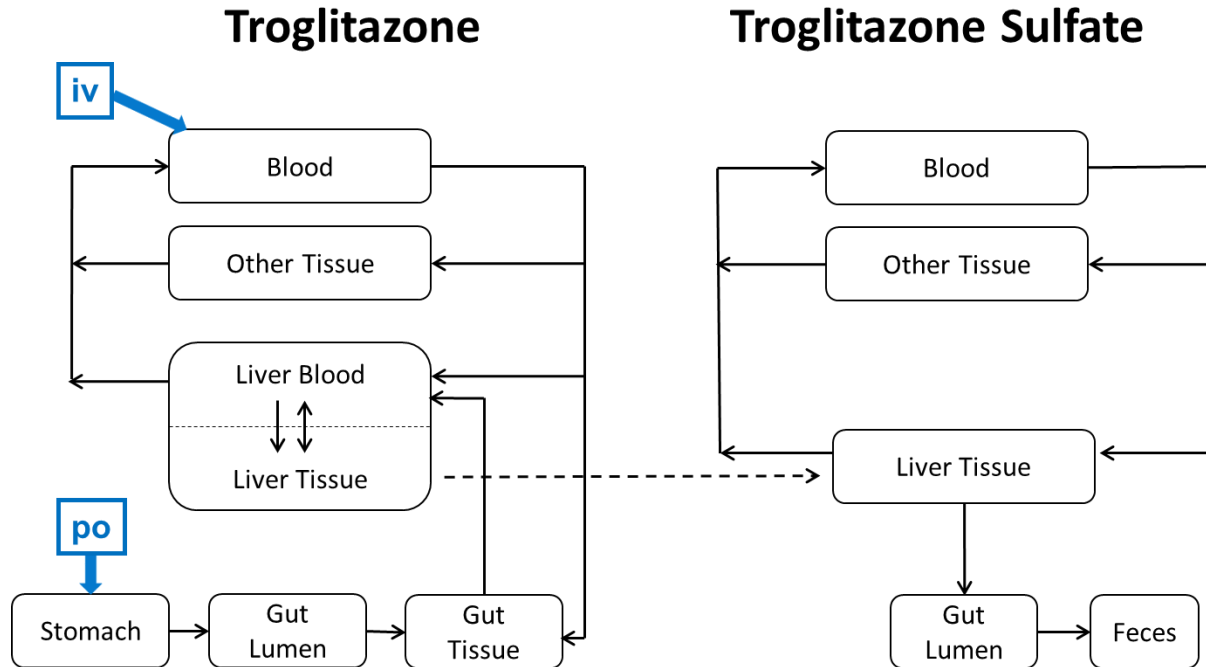
using the following equations: $\mu = \log\left(\frac{m^2}{\sqrt{v+m^2}}\right)$, $\sigma = \sqrt{\log\left(\frac{v}{m^2+1}\right)}$

Upper and lower bounds were assumed to be the exponential of $\mu \pm 2.5 \times \sigma$. Under this assumption with log-normal distribution, the above bounds include 98.8% of the population.

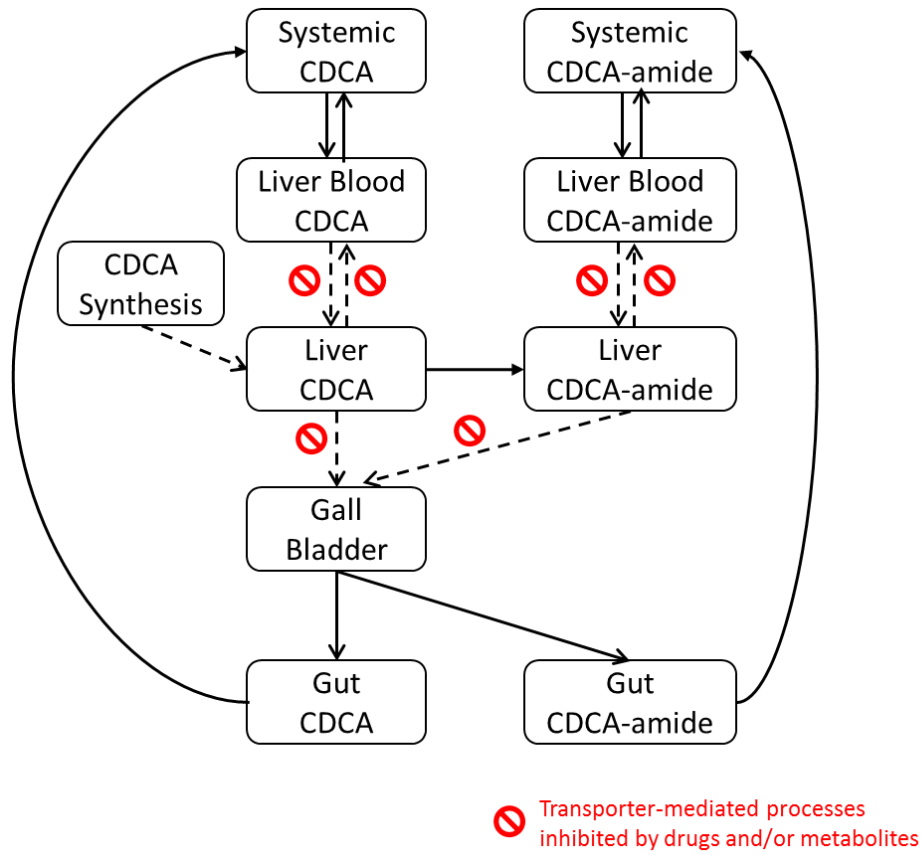
Supplementary Figure 7.1. Diagram of the overall structure of DILI_{sym}.



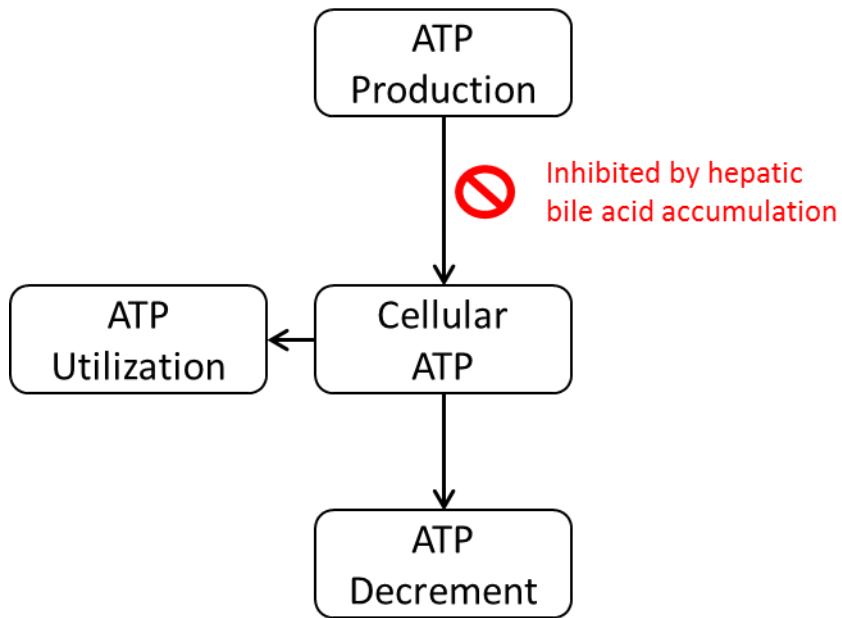
Supplementary Figure 7.2. Diagram of PBPK sub-model. The PBPK model of TGZ consisted of a central compartment representing the blood, as well as liver and extrahepatic tissues (e.g., muscle, intestine) linked to the central compartment by blood flow. Metabolism of TGZ occurred exclusively in the liver. Disposition of TS was described using a semi-PBPK model, which consisted of a central compartment representing the blood, extrahepatic tissues, which were lumped into one compartment, and liver tissue.



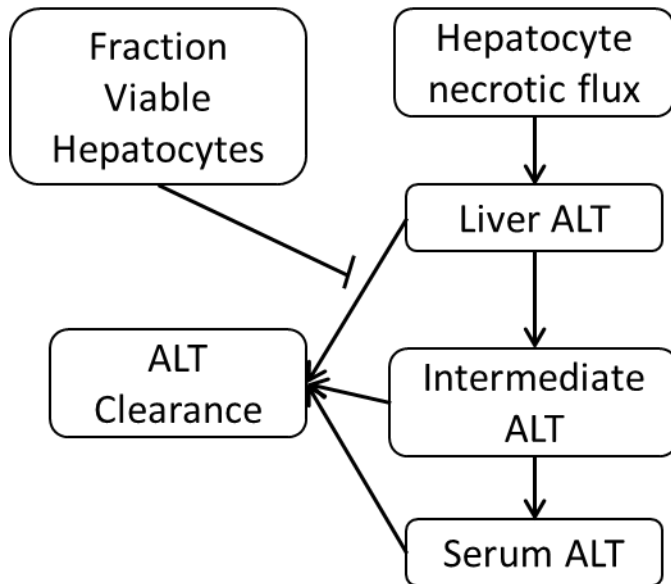
Supplementary Figure 7.3. Diagram of bile acid homeostasis sub-model. The model represents LCA, CDCA, and respective metabolites, in addition to all other (“bulk”) bile acids. For simplicity, only the CDCA species in the periportal zone are depicted here. Pathways represented as dashed lines are subject to feedback regulation mediated by nuclear receptors such as farnesoid X receptor.



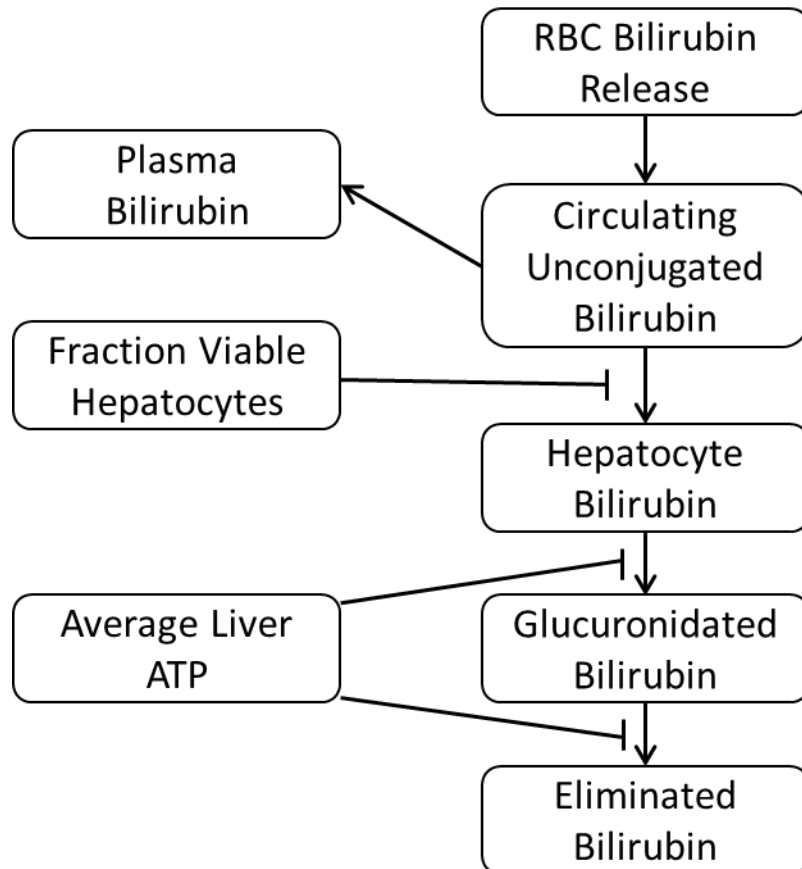
Supplementary Figure 7.4. Diagram of cellular ATP sub-model. ATP is modeled with a simple production and utilization balance, with hepatic bile acid accumulation causing a disruption in ATP production.



Supplementary Figure 7.6. Diagram of ALT sub-model. ALT levels in the model are driven largely by the rate of hepatocyte necrotic flux. The intermediate ALT compartment represents extrahepatic space including interstitial space, the Space of Disse, and liver sinusoids, and was incorporated to adequately describe observed serum ALT profiles in response to other model hepatotoxic drugs (e.g., acetaminophen). The clearance of ALT is driven by the specified half-life. The half-life of ALT is altered by reductions in the number of viable hepatocytes, i.e. less hepatocytes leads to a longer ALT half-life.



Supplementary Figure 7.7. Diagram of bilirubin sub-model. Bilirubin levels in the model are regulated by changes in clearance, as the source of bilirubin is constant and determined from published data (see the text above for details). The primary regulator of hepatocellular bilirubin uptake is the number of viable hepatocytes. Glucuronidation and transport of bilirubin out of hepatocytes is regulated by cellular ATP levels; this regulation mechanism correlates well with changes in bilirubin prior to cell loss.



REFERENCES

- (1) Temple, R.J. & Himmel, M.H. Safety of newly approved drugs: implications for prescribing. *JAMA* **287**, 2273-5 (2002).
- (2) Watkins, P.B. & Whitcomb, R.W. Hepatic dysfunction associated with troglitazone. *N Engl J Med* **338**, 916-7 (1998).
- (3) Presented at the Endocrinologic and Metabolic Drugs Advisory Committee Meeting. April 26, 1999. Available from the US Food and Drug Administration (<http://www.fda.gov/ohrms/dockets/ac/99/transcpt/3499t1a.pdf>). Accessed January 25, 2014.
- (4) Isley, W.L. Hepatotoxicity of thiazolidinediones. *Expert Opin Drug Saf* **2**, 581-6 (2003).
- (5) Smith, M.T. Mechanisms of troglitazone hepatotoxicity. *Chem Res Toxicol* **16**, 679-87 (2003).
- (6) Chojkier, M. Troglitazone and liver injury: in search of answers. *Hepatology* **41**, 237-46 (2005).
- (7) Perez, M.J. & Briz, O. Bile-acid-induced cell injury and protection. *World J Gastroenterol* **15**, 1677-89 (2009).
- (8) Maillette de Buy Wenniger, L. & Beuers, U. Bile salts and cholestasis. *Dig Liver Dis* **42**, 409-18 (2010).
- (9) Jansen, P.L. *et al.* Hepatocanicular bile salt export pump deficiency in patients with progressive familial intrahepatic cholestasis. *Gastroenterology* **117**, 1370-9 (1999).
- (10) van Mil, S.W. *et al.* Benign recurrent intrahepatic cholestasis type 2 is caused by mutations in ABCB11. *Gastroenterology* **127**, 379-84 (2004).
- (11) Morgan, R.E. *et al.* A Multifactorial Approach to Hepatobiliary Transporter Assessment Enables Improved Therapeutic Compound Development. *Toxicol Sci*, (2013).
- (12) Dawson, S., Stahl, S., Paul, N., Barber, J. & Kenna, J.G. In vitro inhibition of the bile salt export pump correlates with risk of cholestatic drug-induced liver injury in humans. *Drug Metab Dispos* **40**, 130-8 (2012).
- (13) Funk, C., Ponelle, C., Scheuermann, G. & Pantze, M. Cholestatic potential of troglitazone as a possible factor contributing to troglitazone-induced hepatotoxicity: in vivo and in vitro interaction at the canalicular bile salt export pump (Bsep) in the rat. *Mol Pharmacol* **59**, 627-35 (2001).

- (14) Yang, K., Yue, W., Koeck, K. & Brouwer, K.L.R. Interaction of troglitazone sulfate with hepatic basolateral and canalicular transport proteins. In 2011 AAPS Annual Meeting and Exposition.
- (15) Marion, T.L., Leslie, E.M. & Brouwer, K.L. Use of sandwich-cultured hepatocytes to evaluate impaired bile acid transport as a mechanism of drug-induced hepatotoxicity. *Mol Pharm* **4**, 911-8 (2007).
- (16) Shoda, L.K., Woodhead, J.L., Siler, S.Q., Watkins, P.B. & Howell, B.A. Linking physiology to toxicity using DILSym((R)), a mechanistic mathematical model of drug-induced liver injury. *Biopharm Drug Dispos* **35**, 33-49 (2014).
- (17) Howell, B.A. *et al.* In vitro to in vivo extrapolation and species response comparisons for drug-induced liver injury (DILI) using DILSym: a mechanistic, mathematical model of DILI. *J Pharmacokinet Pharmacodyn* **39**, 527-41 (2012).
- (18) Woodhead, J.L. *et al.* An analysis of N-acetylcysteine treatment for acetaminophen overdose using a systems model of drug-induced liver injury. *J Pharmacol Exp Ther* **342**, 529-40 (2012).
- (19) Woodhead, J.L. *et al.* Mechanistic modeling reveals the critical knowledge gaps in bile acid-mediated DILI. *CPT:PSP In revision*, (2013).
- (20) Loi, C.M., Randinitis, E.J., Vassos, A.B., Kazierad, D.J., Koup, J.R. & Sedman, A.J. Lack of effect of type II diabetes on the pharmacokinetics of troglitazone in a multiple-dose study. *J Clin Pharmacol* **37**, 1114-20 (1997).
- (21) Izumi, T. *et al.* Prediction of the human pharmacokinetics of troglitazone, a new and extensively metabolized antidiabetic agent, after oral administration, with an animal scale-up approach. *J Pharmacol Exp Ther* **277**, 1630-41 (1996).
- (22) Izumi, T., Hosiyama, K., Enomoto, S., Sasahara, K. & Sugiyama, Y. Pharmacokinetics of troglitazone, an antidiabetic agent: prediction of in vivo stereoselective sulfation and glucuronidation from in vitro data. *J Pharmacol Exp Ther* **280**, 1392-400 (1997).
- (23) Trottier, J., Caron, P., Straka, R.J. & Barbier, O. Profile of serum bile acids in noncholestatic volunteers: gender-related differences in response to fenofibrate. *Clin Pharmacol Ther* **90**, 279-86 (2011).
- (24) St Peter, J.V., Neafus, K.L., Khan, M.A., Vessey, J.T. & Lockheart, M.S. Factors associated with the risk of liver enzyme elevation in patients with type 2 diabetes treated with a thiazolidinedione. *Pharmacotherapy* **21**, 183-8 (2001).

- (25) Muller, M. *et al.* ATP-dependent transport of taurocholate across the hepatocyte canalicular membrane mediated by a 110-kDa glycoprotein binding ATP and bile salt. *J Biol Chem* **266**, 18920-6 (1991).
- (26) Hirohashi, T., Suzuki, H., Takikawa, H. & Sugiyama, Y. ATP-dependent transport of bile salts by rat multidrug resistance-associated protein 3 (Mrp3). *J Biol Chem* **275**, 2905-10 (2000).
- (27) Olson, H. *et al.* Concordance of the toxicity of pharmaceuticals in humans and in animals. *Regul Toxicol Pharmacol* **32**, 56-67 (2000).
- (28) Leslie, E.M., Watkins, P.B., Kim, R.B. & Brouwer, K.L. Differential inhibition of rat and human Na⁺-dependent taurocholate cotransporting polypeptide (NTCP/SLC10A1) by bosentan: a mechanism for species differences in hepatotoxicity. *J Pharmacol Exp Ther* **321**, 1170-8 (2007).
- (29) Watkins, P.B. Idiosyncratic liver injury: challenges and approaches. *Toxicologic pathology* **33**, 1-5 (2005).
- (30) Herman, J.R. *et al.* Rodent carcinogenicity with the thiazolidinedione antidiabetic agent troglitazone. *Toxicol Sci* **68**, 226-36 (2002).
- (31) Chiang, J.Y. Bile acids: regulation of synthesis. *J Lipid Res* **50**, 1955-66 (2009).
- (32) Hofmann, A.F. Detoxification of lithocholic acid, a toxic bile acid: relevance to drug hepatotoxicity. *Drug Metab Rev* **36**, 703-22 (2004).
- (33) Setchell, K.D. *et al.* Bile acid concentrations in human and rat liver tissue and in hepatocyte nuclei. *Gastroenterology* **112**, 226-35 (1997).
- (34) Greim, H. *et al.* Mechanism of cholestasis. 6. Bile acids in human livers with or without biliary obstruction. *Gastroenterology* **63**, 846-50 (1972).
- (35) Garcia-Canaveras, J.C., Donato, M.T., Castell, J.V. & Lahoz, A. Targeted profiling of circulating and hepatic bile acids in human, mouse, and rat using a UPLC-MRM-MS-validated method. *J Lipid Res* **53**, 2231-41 (2012).
- (36) Kakis, G. & Yousef, I.M. Pathogenesis of lithocholate- and taurocholate-induced intrahepatic cholestasis in rats. *Gastroenterology* **75**, 595-607 (1978).
- (37) Oelberg, D.G., Chari, M.V., Little, J.M., Adcock, E.W. & Lester, R. Lithocholate glucuronide is a cholestatic agent. *J Clin Invest* **73**, 1507-14 (1984).

- (38) Yousef, I.M., Tuchweber, B., Vonk, R.J., Masse, D., Audet, M. & Roy, C.C. Lithocholate cholestasis--sulfated glycolithocholate-induced intrahepatic cholestasis in rats. *Gastroenterology* **80**, 233-41 (1981).
- (39) Sokol, R.J., Dahl, R., Devereaux, M.W., Yerushalmi, B., Kobak, G.E. & Gumpricht, E. Human hepatic mitochondria generate reactive oxygen species and undergo the permeability transition in response to hydrophobic bile acids. *J Pediatr Gastroenterol Nutr* **41**, 235-43 (2005).
- (40) Faubion, W.A. *et al.* Toxic bile salts induce rodent hepatocyte apoptosis via direct activation of Fas. *J Clin Invest* **103**, 137-45 (1999).
- (41) Shoda, J., Tanaka, N., He, B.F., Matsuzaki, Y., Osuga, T. & Miyazaki, H. Alterations of bile acid composition in gallstones, bile, and liver of patients with hepatolithiasis, and their etiological significance. *Dig Dis Sci* **38**, 2130-41 (1993).
- (42) Fischer, S., Beuers, U., Spengler, U., Zwiebel, F.M. & Koebe, H.G. Hepatic levels of bile acids in end-stage chronic cholestatic liver disease. *Clin Chim Acta* **251**, 173-86 (1996).
- (43) Trauner, M., Wagner, M., Fickert, P. & Zollner, G. Molecular regulation of hepatobiliary transport systems: clinical implications for understanding and treating cholestasis. *J Clin Gastroenterol* **39**, S111-24 (2005).
- (44) Lang, C. *et al.* Mutations and polymorphisms in the bile salt export pump and the multidrug resistance protein 3 associated with drug-induced liver injury. *Pharmacogenetics and genomics* **17**, 47-60 (2007).
- (45) Meier, Y. *et al.* Increased susceptibility for intrahepatic cholestasis of pregnancy and contraceptive-induced cholestasis in carriers of the 1331T>C polymorphism in the bile salt export pump. *World J Gastroenterol* **14**, 38-45 (2008).
- (46) Wang, T., Shankar, K., Ronis, M.J. & Mehendale, H.M. Mechanisms and outcomes of drug- and toxicant-induced liver toxicity in diabetes. *Crit Rev Toxicol* **37**, 413-59 (2007).
- (47) Jonker, J.W., Liddle, C. & Downes, M. FXR and PXR: potential therapeutic targets in cholestasis. *J Steroid Biochem Mol Biol* **130**, 147-58 (2012).
- (48) Kock, K. *et al.* Risk Factors for Development of Cholestatic Drug-induced Liver Injury: Inhibition of Hepatic Basolateral Bile Acid Transporters MRP3 and MRP4. *Drug Metab Dispos*, (2013).

- (49) Pedersen, J.M. *et al.* Early Identification of Clinically Relevant Drug Interactions With the Human Bile Salt Export Pump (BSEP/ABCB11). *Toxicol Sci* **136**, 328-43 (2013).
- (50) Marion, T.L., Perry, C.H., St Claire, R.L., 3rd & Brouwer, K.L. Endogenous bile acid disposition in rat and human sandwich-cultured hepatocytes. *Toxicol Appl Pharmacol* **261**, 1-9 (2012).
- (51) Ansedè, J.H., Smith, W.R., Perry, C.H., St Claire, R.L., 3rd & Brouwer, K.R. An in vitro assay to assess transporter-based cholestatic hepatotoxicity using sandwich-cultured rat hepatocytes. *Drug Metab Dispos* **38**, 276-80 (2010).
- (52) Yang, K., Kock, K., Sedykh, A., Tropsha, A. & Brouwer, K.L. An updated review on drug-induced cholestasis: mechanisms and investigation of physicochemical properties and pharmacokinetic parameters. *J Pharm Sci* **102**, 3037-57 (2013).
- (53) Kawai, K. *et al.* Disposition and metabolism of the new oral antidiabetic drug troglitazone in rats, mice and dogs. *Arzneimittelforschung* **47**, 356-68 (1997).
- (54) Loi, C.M., Alvey, C.W., Randinitis, E.J., Abel, R., Young, M.A. & Koup, J.R. Meta-analysis of steady-state pharmacokinetics of troglitazone and its metabolites. *J Clin Pharmacol* **37**, 1038-47 (1997).
- (55) Loi, C.M., Alvey, C.W., Vassos, A.B., Randinitis, E.J., Sedman, A.J. & Koup, J.R. Steady-state pharmacokinetics and dose proportionality of troglitazone and its metabolites. *J Clin Pharmacol* **39**, 920-6 (1999).
- (56) Chang, C., Pang, K.S., Swaan, P.W. & Ekins, S. Comparative pharmacophore modeling of organic anion transporting polypeptides: a meta-analysis of rat Oatp1a1 and human OATP1B1. *J Pharmacol Exp Ther* **314**, 533-41 (2005).
- (57) Lee, J.K., Marion, T.L., Abe, K., Lim, C., Pollock, G.M. & Brouwer, K.L. Hepatobiliary disposition of troglitazone and metabolites in rat and human sandwich-cultured hepatocytes: use of Monte Carlo simulations to assess the impact of changes in biliary excretion on troglitazone sulfate accumulation. *J Pharmacol Exp Ther* **332**, 26-34 (2010).
- (58) Kostrubsky, V.E. *et al.* The effect of troglitazone biliary excretion on metabolite distribution and cholestasis in transporter-deficient rats. *Drug Metab Dispos* **29**, 1561-6 (2001).
- (59) Fu, Y., Sheu, C., Fujita, T. & Foote, C.S. Photooxidation of troglitazone, a new antidiabetic drug. *Photochem Photobiol* **63**, 615-20 (1996).

- (60) Yang, K. *et al.* The quantitative relationship between intracellular lithocholic acid and hepatotoxicity in rat; incorporation into a mechanistic model of drug-induced liver injury. *The Toxicologist* **132**, Abstract ID #1059 (2013).
- (61) Balmagiya, T. & Rozovski, S.J. Thermoregulation in young adult rats during short- and long-term protein malnutrition. *The Journal of nutrition* **113**, 228-38 (1983).
- (62) Ussher, J.R. *et al.* Inhibition of de novo ceramide synthesis reverses diet-induced insulin resistance and enhances whole-body oxygen consumption. *Diabetes* **59**, 2453-64 (2010).
- (63) Gonzales-Pacheco, D.M., Buss, W.C., Koehler, K.M., Woodside, W.F. & Alpert, S.S. Energy restriction reduces metabolic rate in adult male Fisher-344 rats. *The Journal of nutrition* **123**, 90-7 (1993).
- (64) Lazzer, S. *et al.* Relationship between basal metabolic rate, gender, age, and body composition in 8,780 white obese subjects. *Obesity* **18**, 71-8 (2010).
- (65) Wang, Z. *et al.* Evaluation of specific metabolic rates of major organs and tissues: comparison between men and women. *American journal of human biology : the official journal of the Human Biology Council* **23**, 333-8 (2011).
- (66) Schulz, A.R. Computer-based method for calculation of the available energy of proteins. *The Journal of nutrition* **105**, 200-7 (1975).
- (67) Muller, M.J. Hepatic fuel selection. *The Proceedings of the Nutrition Society* **54**, 139-50 (1995).
- (68) Ghosh, J., Das, J., Manna, P. & Sil, P.C. Arjunolic acid, a triterpenoid saponin, prevents acetaminophen (APAP)-induced liver and hepatocyte injury via the inhibition of APAP bioactivation and JNK-mediated mitochondrial protection. *Free radical biology & medicine* **48**, 535-53 (2010).
- (69) Kaminsky, Y.G., Kosenko, E.A. & Kondrashova, M.N. Analysis of the circadian rhythm in energy metabolism of rat liver. *The International journal of biochemistry* **16**, 629-39 (1984).
- (70) Noren, B., Lundberg, P., Ressner, M., Wirell, S., Almer, S. & Smedby, O. Absolute quantification of human liver metabolite concentrations by localized in vivo ³¹P NMR spectroscopy in diffuse liver disease. *European radiology* **15**, 148-57 (2005).
- (71) Meyerhoff, D.J., Karczmar, G.S., Matson, G.B., Boska, M.D. & Weiner, M.W. Non-invasive quantitation of human liver metabolites using image-guided ³¹P magnetic resonance spectroscopy. *NMR in biomedicine* **3**, 17-22 (1990).

- (72) Teutsch, H.F. Regionality of glucose-6-phosphate hydrolysis in the liver lobule of the rat: metabolic heterogeneity of "portal" and "septal" sinusoids. *Hepatology* **8**, 311-7 (1988).
- (73) Teutsch, H.F., Schuerfeld, D. & Groezinger, E. Three-dimensional reconstruction of parenchymal units in the liver of the rat. *Hepatology* **29**, 494-505 (1999).
- (74) Rani, H.P., Sheu, T.W., Chang, T.M. & Liang, P.C. Numerical investigation of non-Newtonian microcirculatory blood flow in hepatic lobule. *Journal of biomechanics* **39**, 551-63 (2006).
- (75) Andersen, M.E., Eklund, C.R., Mills, J.J., Barton, H.A. & Birnbaum, L.S. A multicompartiment geometric model of the liver in relation to regional induction of cytochrome P450s. *Toxicol Appl Pharmacol* **144**, 135-44 (1997).
- (76) Bruss, M.D., Thompson, A.C., Aggarwal, I., Khambatta, C.F. & Hellerstein, M.K. The effects of physiological adaptations to calorie restriction on global cell proliferation rates. *American journal of physiology Endocrinology and metabolism* **300**, E735-45 (2011).
- (77) Grisham, J.W. A morphologic study of deoxyribonucleic acid synthesis and cell proliferation in regenerating rat liver; autoradiography with thymidine-H3. *Cancer Res* **22**, 842-9 (1962).
- (78) Bursch, W., Paffe, S., Putz, B., Barthel, G. & Schulte-Hermann, R. Determination of the length of the histological stages of apoptosis in normal liver and in altered hepatic foci of rats. *Carcinogenesis* **11**, 847-53 (1990).
- (79) Zieve, L., Anderson, W.R., Dozeman, R., Draves, K. & Lyftogt, C. Acetaminophen liver injury: sequential changes in two biochemical indices of regeneration and their relationship to histologic alterations. *J Lab Clin Med* **105**, 619-24 (1985).
- (80) Chanda, S. & Mehendale, H.M. Hepatic cell division and tissue repair: a key to survival after liver injury. *Molecular medicine today* **2**, 82-9 (1996).
- (81) Pettersson, J. *et al.* Muscular exercise can cause highly pathological liver function tests in healthy men. *Br J Clin Pharmacol* **65**, 253-9 (2008).
- (82) Lindblom, P. *et al.* Isoforms of alanine aminotransferases in human tissues and serum-- differential tissue expression using novel antibodies. *Arch Biochem Biophys* **466**, 66-77 (2007).
- (83) Sohlenius-Sternbeck, A.K. Determination of the hepatocellularity number for human, dog, rabbit, rat and mouse livers from protein concentration measurements. *Toxicol In Vitro* **20**, 1582-6 (2006).

- (84) Sawant, S.P., Dnyanmote, A.V., Shankar, K., Limaye, P.B., Latendresse, J.R. & Mehendale, H.M. Potentiation of carbon tetrachloride hepatotoxicity and lethality in type 2 diabetic rats. *J Pharmacol Exp Ther* **308**, 694-704 (2004).
- (85) Pooranaperundevi, M., Sumiyabanu, M.S., Viswanathan, P., Sundarapandiyan, R. & Anuradha, C.V. Insulin resistance induced by high-fructose diet potentiates carbon tetrachloride hepatotoxicity. *Toxicology and industrial health* **26**, 89-104 (2010).
- (86) Corbin, I.R., Buist, R., Volotovskyy, V., Peeling, J., Zhang, M. & Minuk, G.Y. Regenerative activity and liver function following partial hepatectomy in the rat using (31)P-MR spectroscopy. *Hepatology* **36**, 345-53 (2002).
- (87) Jenner, A.M. & Timbrell, J.A. Influence of inducers and inhibitors of cytochrome P450 on the hepatotoxicity of hydrazine in vivo. *Archives of toxicology* **68**, 349-57 (1994).
- (88) Limdi, J.K. & Hyde, G.M. Evaluation of abnormal liver function tests. *Postgrad Med J* **79**, 307-12 (2003).
- (89) Davidson, A.R., Rojas-Bueno, A., Thompson, R.P. & Williams, R. Early unconjugated hyperbilirubinaemia after paracetamol overdose. *Scand J Gastroenterol* **11**, 623-8 (1976).
- (90) Rodgers, T. & Rowland, M. Physiologically based pharmacokinetic modelling 2: predicting the tissue distribution of acids, very weak bases, neutrals and zwitterions. *J Pharm Sci* **95**, 1238-57 (2006).
- (91) Menochet, K., Kenworthy, K.E., Houston, J.B. & Galetin, A. Simultaneous assessment of uptake and metabolism in rat hepatocytes: a comprehensive mechanistic model. *J Pharmacol Exp Ther* **341**, 2-15 (2012).
- (92) Ott, P., Ranek, L. & Young, M.A. Pharmacokinetics of troglitazone, a PPAR-gamma agonist, in patients with hepatic insufficiency. *European journal of clinical pharmacology* **54**, 567-71 (1998).
- (93) NHANES 2003-2004 database (www.denofinquiry.com/nahanes/source/choose.php).
- (94) Ohtsuki, S. *et al.* Simultaneous absolute protein quantification of transporters, cytochromes P450, and UDP-glucuronosyltransferases as a novel approach for the characterization of individual human liver: comparison with mRNA levels and activities. *Drug Metab Dispos* **40**, 83-92 (2012).

- (95) Riches, Z., Stanley, E.L., Bloomer, J.C. & Coughtrie, M.W. Quantitative evaluation of the expression and activity of five major sulfotransferases (SULTs) in human tissues: the SULT "pie". *Drug Metab Dispos* **37**, 2255-61 (2009).
- (96) Johnson, D.R., Guo, G.L. & Klaassen, C.D. Expression of rat Multidrug Resistance Protein 2 (Mrp2) in male and female rats during normal and pregnenolone-16alpha-carbonitrile (PCN)-induced postnatal ontogeny. *Toxicology* **178**, 209-19 (2002).
- (97) Dunn, R.T., 2nd & Klaassen, C.D. Tissue-specific expression of rat sulfotransferase messenger RNAs. *Drug Metab Dispos* **26**, 598-604 (1998).

CHAPTER 8. Summary and Future Directions

The objectives of this dissertation research were to characterize the mechanisms of drug-induced liver injury (DILI) that involve bile acid transport inhibition, and to develop a novel strategy to predict liability of drugs for human DILI. DILI is of paramount concern in drug development, but is not well predicted from in vitro assay or standard preclinical testing (1, 2). The rare incidence of DILI, and the fact that DILI may not be detected during clinical trials, suggests that in addition to drug-specific risk factors, patient-specific risk factors also exist that make a subset of patients more susceptible to DILI. To improve our understanding of species differences and patient specific risk factors for bile acid-mediated DILI, a variety of model systems [e.g., membrane vesicles, sandwich-cultured hepatocytes (SCH) isolated from multiple species] and methods (e.g., RNA interference, pharmacokinetic and mechanistic modeling and simulation) were employed in this dissertation project. This research project focused on the model bile acids taurocholic acid (TCA), chenodeoxycholic acid (CDCA), and lithocholic acid (LCA). Troglitazone (TGZ), an antidiabetic drug that was withdrawn from worldwide markets due to severe DILI, was employed as a model hepatotoxic drug. Although numerous mechanisms of TGZ-mediated hepatotoxicity have been postulated, one proposed mechanism is inhibition of bile acid transport by TGZ and its major metabolite, TGZ sulfate (TS) (3, 4). Inhibition of hepatic bile acid efflux might result in hepatic accumulation of harmful bile acids and subsequent hepatotoxicity (5).

In **Aim #1** of this dissertation research, species differences in humans and rats were characterized with respect to the hepatobiliary disposition of bile acids and the interaction of hepatotoxic drugs with bile acids at hepatic transport proteins. TCA is a prototypical bile acid that has been used widely as a probe substrate in transporter inhibition assays (4, 6-8). There exists a wealth of data regarding TCA

kinetics and the interaction of TCA with drugs and/or metabolites, which is a great advantage of using TCA as a model bile acid. In this aim, hepatic uptake, biliary excretion, and basolateral efflux of TCA were characterized using data obtained from human and rat SCH combined with pharmacokinetic modeling. Inhibitory effects of TGZ and TS on hepatobiliary disposition of TCA were also investigated using SCH and isolated membrane vesicles (**Chapter 3**).

Aim #2 investigated the patient-specific risk factors for DILI, focusing on the altered hepatobiliary disposition of drugs/metabolites in the setting of impaired function of canalicular transporters. Only about 2% of the patient treated with TGZ developed hepatotoxicity, suggesting that liver injury was driven by a combination of drug- and patient-specific risk factors. TS, a potent inhibitor of bile acid transporters, is predominantly excreted into by Breast cancer resistance protein (Bcrp) and multidrug resistance-associated protein 2 (Mrp2). Thus, impaired function of these canalicular transporters may cause hepatocellular TS accumulation and lead to hepatotoxicity. To test this hypothesis, an in vitro model system lacking specific Bcrp and Mrp2 was established using SCH (**Chapter 4**), and altered hepatic exposure to TGZ and generated metabolites was assessed in this system (**Chapter 5**).

Lastly, a mechanistic model of DILI was developed in **Aim #3** to improve our understanding about, and predictability of, DILI that involves inhibition of bile acid transport. Experiments were performed to define the quantitative relationship between intracellular bile acid concentrations and hepatotoxicity, which is essential for model development (**Chapter 6**). Although TCA is commonly used as a model bile acid, it is a hydrophilic, less toxic bile acid (5, 9) that is not predominant in humans, and may not be suitable as the sole bile acid to investigate toxicity studies. Therefore, CDCA and LCA, which are hydrophobic and potentially toxic bile acids (10, 11), were chosen for toxicity studies and were modeled exclusively in the mechanistic DILI model. This mechanistic model was used to assess the contribution of bile acid transport inhibition associated with TGZ-mediated hepatotoxicity in humans and to investigate the mechanism(s) for differential hepatotoxicity of TGZ in humans and rats (**Chapter 7**).

The results of this comprehensive dissertation project improved the current understanding about mechanisms, species differences, and patient-specific risk factors in bile acid-mediated DILI, and

developed a mechanistic model to provide a novel framework to predict human DILI. The following is a summary of the findings of the current project and opportunities for future investigation that were identified as a result of this research.

Species Differences in Hepatobiliary Disposition of Taurocholic acid in Human and Rat Sandwich-Cultured Hepatocytes; Implications for Drug-Induced Liver Injury (Chapter 3)

The bile salt export pump (BSEP) plays an important role in biliary excretion of bile acids. Liver diseases caused by functional defects in BSEP due to genetic polymorphisms (e.g., progressive familial intrahepatic cholestasis type 2, benign recurrent intrahepatic cholestasis type 2) emphasize the importance of BSEP in bile acid excretion and demonstrate toxic consequences of bile acid retention in hepatocytes (3, 5, 12). In addition to biliary excretion, bile acids also undergo basolateral efflux via MRP3, MRP4, and potentially organic solute transporter (OST) α – OST β (13-15). The contribution of basolateral efflux to hepatocellular bile acid excretion has been thought to be minimal under normal conditions due to extensive biliary excretion of bile acids. However, as proposed in the “hepatocyte hopping” theory of bilirubin glucuronides (16), it is possible that bile acids may undergo extensive basolateral efflux, and then be taken up into downstream hepatocytes, until they are eventually excreted into bile. So far, the relative contributions of biliary versus basolateral efflux clearances to hepatocellular bile acid excretion have not been determined precisely.

In the present study, the hepatobiliary disposition (basolateral uptake and efflux, biliary excretion) of TCA was characterized using the uptake and efflux data in human and rat SCH combined with pharmacokinetic modeling. The results from this study revealed for the first time that species differences exist in hepatocellular efflux pathways of TCA in human versus rat SCH; biliary excretion of TCA predominated in human SCH, whereas biliary excretion and basolateral efflux contributed equally to hepatocellular TCA excretion. This has important implications in DILI mediated by interruption of bile acid transport. Simulations demonstrated that BSEP inhibition alone led to greater hepatic TCA accumulation in human SCH compared to rat SCH. This explains, in part, why rats are less sensitive to

bile acid-mediated DILI compared to humans after administration of BSEP inhibitors. Additionally, inhibition of both basolateral and biliary excretion pathways led to exponential increases in hepatic TCA exposure in both human and rat SCH, suggesting that a drug that inhibits both excretion pathways will have greater DILI liability. This also implies that impaired function of the alternate pathway due to co-administered drugs, genetic polymorphisms, and/or disease may predispose patients to DILI when administered a drug that inhibits only one pathway.

Bile acids undergo extensive enterohepatic recirculation (17), and thus, hepatic bile acid exposure is modulated by hepatic uptake transporters as well as canalicular and basolateral efflux transporters. While inhibition of bile acid efflux transporters are known to be associated with cholestatic/mixed type DILI (4, 8), inhibition of bile acid uptake has been suggested to exert protective effects (1). If a drug inhibits both hepatic uptake and efflux of bile acids, hepatic bile acid accumulation will be determined by the relative potency of uptake inhibition versus efflux inhibition. Simulations in the present study showed that inhibition of TCA uptake clearance by greater than 60% prevents hepatic TCA exposure from increasing by more than 10-fold in human SCH, thereby confirming the protective effects of uptake inhibition. It is of note that simulations in the current study were performed using a hypothetical inhibitor, of which concentrations in the medium and in the cells were assumed to be at steady-state. Based on this assumption, a constant fractional inhibition of uptake and efflux transporters was employed throughout the simulation. In reality, drug concentrations in the hepatocytes and medium might change over time due to metabolism and transport. Incorporation of a model describing drugs/metabolites disposition will allow prediction of dynamic interactions between drugs/metabolites and bile acids; thus, this would be the natural next step to accurately predict altered bile acid disposition by a specific drug.

The present study was the first investigation to establish that TS is an inhibitor of basolateral bile acid efflux in addition to biliary bile acid excretion. Parameter estimates recovered from the pharmacokinetic modeling revealed that pre-incubation with TGZ tended to decrease basolateral efflux clearance of TCA in human and rat SCH. TGZ has been reported to inhibit basolateral efflux transporters, MRP3 and MRP4 (4). However, hepatic concentrations of TGZ were minimal, whereas TS accumulated

extensively in hepatocytes (18, 19). TS was reported to be a more potent inhibitor of BSEP compared to TGZ (18), suggesting that TS is likely to inhibit basolateral efflux of TCA. To test this hypothesis, in vitro transporter inhibition studies were performed using membrane vesicles prepared from HEK293T cells overexpressing MRP4; TS was found to be a noncompetitive inhibitor of MRP4 with a K_i value of 8 μM . Uptake clearance also was significantly decreased (in human SCH) or showed trends towards a decrease (in rat SCH) compared to control after TGZ pre-incubation. Although TGZ is a potent inhibitor of NTCP/Ntcp-mediated bile acid uptake (20), TGZ concentrations in the buffer during the uptake phase were minimal because TGZ-containing buffer was replaced with TGZ-free buffer during the 10-min pre-incubation (with standard or Ca^{2+} -free standard buffers) as well as during the 20-min uptake phase. This suggests that TGZ might inhibit NTCP/Ntcp by mechanisms other than direct inhibition. For example, intracellular TGZ and/or TS may interact with the intracellular domain of NTCP/Ntcp thereby inhibiting TCA uptake similar to trans-inhibition of BSEP by estradiol-17 β -D-glucuronide (21). It is also possible that intracellular accumulation of TGZ and/or TS leads to retrieval of NTCP/Ntcp from the basolateral plasma membrane by modulation of intracellular signaling pathways (i.e., short-term regulation) (22). Another hypothesis is that irreversible binding of TGZ and/or its metabolites to NTCP/Ntcp might exert long-lasting inhibitory effects. Indirect inhibitory mechanisms for transporters are not well understood currently, and further studies are needed to elucidate the mechanism(s) for long-lasting inhibition of TCA uptake by TGZ observed in the current study.

Mathematical modeling often requires simplification of biological systems, and thus, several assumptions were made during model development. In this modeling project, the hepatocyte compartment was assumed to be a homogenous, well-stirred compartment, which clearly is an over-simplification of the complex subcellular structure of hepatocytes. Although the current model reasonably explained the observed data in human and rat SCH, a slight overestimation of cellular TCA concentrations at earlier time points during the uptake phase was noted. Vectorial transport of bile acids from sinusoidal blood to bile canaliculi suggests that intracellular trafficking of bile acids may be mediated by vesicular transport or carrier-mediated transport rather than simple diffusion of bile acids in the cytosol (23). Intracellular

trafficking of BSEP-containing vesicular structures has been shown by confocal imaging using yellow fluorescent protein-tagged BSEP (24). Bile acids also can be distributed into and sequestered within subcellular organelles. For example, bile acids are ligands of nuclear receptors such as farnesoid X receptor and pregnane X receptor, which translocate into the nucleus after activation (25); a time-dependent increase in nuclear fluorescence was shown after treatment of rat hepatocyte couplets with fluorescent bile acids (26). However, the current body of information is not enough to fully understand intracellular transport of bile acids, and the quantitative data necessary for mathematical model development are lacking. Characterization of the intracellular disposition and transport of bile acids and how drugs modulate these processes would be an important next step to improve our understanding of bile acid-drug interactions.

This research demonstrated the utility of pharmacokinetic modeling and simulation in understanding differential drug-bile acid interactions in humans and rats, and predicting altered hepatobiliary bile acid disposition in the setting of drug-bile acid interactions at multiple hepatic transporters. This approach can be used to predict dynamic interactions when combined with pharmacokinetic data for drugs and metabolites. The current study provided a framework to investigate hepatobiliary disposition of bile acids using TCA, a non-toxic, prototypical bile acid that has been employed widely in investigations of drug effects on bile acid transport. The present work needs to be expanded to cytotoxic bile acids such as CDCA, LCA, and deoxycholic acid (DCA) in order to improve our understanding and predictability of bile acid-mediated DILI.

An Experimental Approach to Evaluate the Impact of Impaired Transport Function on Hepatobiliary Drug Disposition using Mrp2-deficient TR^{-/-} Rat Sandwich-Cultured Hepatocytes in Combination with Bcrp Knockdown (Chapter 4)

Predicting drug disposition in the setting of altered transport function has important clinical significance in terms of drug efficacy and safety. BCRP and MRP2 are members of the ATP-binding cassette transporter family located in the canalicular membrane of hepatocytes; these hepatic efflux

transporters have overlapping substrate specificity. Modulation of expression and/or function of these transporters due to genetic polymorphisms, drug-drug interactions, or disease may alter the pharmacokinetics and pharmacodynamics of substrates. However, it is challenging to predict the impact of altered function of one or more transporters on the hepatic and systemic exposure of substrates due to overlapping substrate specificity. In this project, an in vitro model system was established to evaluate the impact of impaired Mrp2 and Bcrp function on hepatobiliary drug disposition; Bcrp knockdown was achieved by using RNA interference (RNAi) technique, and SCH from Mrp2-deficient (TR⁻) rats were employed to mimic the loss-of-function of Mrp2. To our knowledge, this was the first investigation that established an approach to develop a primary hepatocyte model lacking multiple specific transporters.

This work also emphasized the importance of optimizing the system using a range of multiplicity of infection (MOI) when knocking down a protein by RNAi in hepatocytes, and established a strategy for optimization of the knockdown system. A two-stage statistical analysis approach was employed in this study that included 1) selection of an optimal MOI by identification of a dose (MOI) – response relationship based on the targeted and off-target effects over a range of MOI, and 2) characterization of the impact of impaired transporter function at selected MOI. This two-stage analysis approach allowed a thorough characterization of the system including off-target effects and interactions among factors that might not be revealed by testing only one level of MOI. It is important to note that optimization and characterization in the current study were based on functional changes in the transporter using the probe substrates rosuvastatin (RSV) and TCA. RSV (a dual substrate of Bcrp and Mrp2) and TCA (a model bile acid that is not transported by Bcrp and Mrp2) represented positive and negative controls, respectively, to evaluate the functional changes in the transporter knockdown system. Changes in mRNA or protein levels may not always translate to functional changes, and altered localization of transporters may not be reflected in protein expression levels in the whole cells lysate. Thus, use of relevant probe substrates to evaluate changes in protein activity is strongly recommended when establishing a knockdown system.

It is challenging to knock down proteins in primary cultured hepatocytes because high transfection efficiency is difficult to achieve using conventional transfection reagents. To attain efficient

knockdown, adenoviral vectors were employed to deliver shRNA into hepatocytes in the present study. Recombinant adenovirus had demonstrated high infection efficiency and high transgene capacity, and has been used widely as a gene deliver vector (27). Previous work had revealed that adenoviral vectors expressing shRNA targeting Bcrp exhibited a significant decrease in protein expression and activity of Bcrp in SCH (28). In the current study, double knockdown of Bcrp and Mrp2 using RNAi was attempted initially. However, off-target effects on other transporters were noted at the higher MOI required to knock down both transporters; an MOI of 5 was required for efficient knockdown of Bcrp and Mrp2, respectively, and thus, a combination of shRNA targeting two different transporters required an MOI of 10, at which off-target effects were predominant. To circumvent this issue, SCH from TR⁻ rats were employed in combination with Bcrp knockdown using adenoviral infections of shRNA targeting Bcrp. Alternatively, tandem plasmid vectors that express multiple different siRNA in one vector can be used to achieve double knockdown with minimal off-target effects. This might be of great importance when RNAi is applied to human-derived cells such as human SCH or other technologies in development (e.g., induced pluripotent stems cells, bioengineered culture systems) because it is difficult to obtain human cells naturally lacking specific transporters (e.g., hepatocytes from patients with Dubin-Johnson syndrome). Often, preclinical data do not translate to humans due to species differences in transporter expression and regulation, and substrate/inhibitor specificity and affinity. Therefore, development of a human-derived system lacking multiple transporters would be the next step necessary to reliably predict drug disposition in patients with altered hepatobiliary transporter function. The current study established a strategy for optimization of the knockdown system, and demonstrated the potential use of RNAi in SCH as an *in vitro* tool to predict altered hepatobiliary drug disposition when transporter function is impaired. This research with rat SCH provides a stepping stone for development of a transporter knockdown system in human-derived cells.

Hepatocellular Exposure of Generated Metabolites, Troglitazone Sulfate and Glucuronide, is Determined by the Interplay between Formation and Excretion in Rat Sandwich-Cultured Hepatocytes Lacking Selected Canalicular Transporters (Chapter 5)

TGZ caused hepatotoxicity only in a small fraction of treated patients, suggesting that injury was driven by a combination of drug- and patient-specific risk factors. In hepatocytes, TGZ is extensively metabolized to TS, which is excreted into bile predominantly via Bcrp and Mrp2 (29, 30). TS accumulates extensively in hepatocytes (19, 31), and also is a potent inhibitor of bile acid efflux transporters such as BSEP and MRP4 (18). This suggests that TS may be an important mediator of altered bile acid disposition and subsequent hepatotoxicity. The impaired function of Bcrp and Mrp2 would be expected to increase hepatocellular TS accumulation and enhance inhibition of bile acid efflux, which might predispose a subset of patients to TGZ-mediated hepatotoxicity. To test this hypothesis, the hepatobiliary disposition of TGZ and generated metabolites, TS and TGZ glucuronide (TG), was examined in rat SCH lacking Bcrp and/or Mrp2, as established in the previous chapter. The results from the present study revealed that biliary excretion of generated TS was not significantly altered by impaired Bcrp and/or Mrp2 function, suggesting that loss-of function of Bcrp and/or Mrp2 would not be a risk factor for increased hepatocellular TS accumulation in rats. This might be due to a compensatory transporter(s) that can excrete TS into bile in the absence of Mrp2 and Bcrp. Bsep and P-glycoprotein (P-gp) were investigated as potential compensatory transporters using membrane vesicles overexpressing Bsep, and GF120918, which is a potent inhibitor of P-gp and Bcrp, in rat SCH, respectively. However, results suggested that Bsep and P-gp were not likely to be involved in TS biliary excretion. Other hepatic canalicular transporters such as multidrug and toxic extrusion protein 1 (MATE1) or multidrug resistance protein 2 (Mdr2) might contribute to TS biliary excretion. Further investigations are needed to elucidate the compensatory transporter(s) responsible for TS biliary excretion.

Although TS biliary excretion was not altered, hepatocellular TS accumulation was significantly decreased in TR⁻ rat SCH compared to WT rat SCH. A decrease in the total recovery of TS (in cells, bile, and media) indicated that sulfation was decreased, or de-sulfation was increased, in TR⁻ rat SCH

compared to WT rat SCH. TS de-sulfation was not observed in the S9 fraction from WT or TR⁻ rat livers, suggesting that decreased hepatocellular TS accumulation might be due to decreased sulfation rather than increased de-sulfation. Interestingly, TS formation rates were comparable in S9 fractions from WT and TR⁻ rat livers. The expression levels of sulfotransferase (Sult) 1a1 and Sult1e1 were comparable in livers from WT and TR⁻ rats (32, 33). One hypothesis to explain decreased total TS recovery is that the availability of 3'-phosphoadenosine-5'-phosphosulfate (PAPS), an important cofactor for sulfation, is less in TR⁻ compared to WT rat SCH. In vitro metabolism experiments using S9 fractions were performed with adequate amount of PAPS added exogenously, but sulfation might have been limited by the availability of PAPS in TR⁻ hepatocytes. It is possible that TR⁻ rat SCH may have lower levels of PAPS precursors or lower activity of enzymes involved in PAPS synthesis. This could be tested in future studies by quantifying PAPS biosynthesis from inorganic [³⁵S]sulfate in hepatocytes using a high-performance liquid chromatography (HPLC) radiometric procedure (34). Alternatively, TR⁻ rat SCH may have higher cellular concentrations of endogenous substrates that deplete PAPS, resulting in decreased sulfation of TGZ. Although the mechanisms still remain to be elucidated, the present data demonstrated for the first time that sulfation of TGZ was decreased in TR⁻ rat SCH. TR⁻ rats have been employed widely to investigate the contribution of Mrp2 to drug disposition, but altered expression of several enzymes and transporters in TR⁻ rats has been noted (32, 35, 36). Thus, accurate characterization of altered function of enzymes and transporters in TR⁻ rats is required to correctly interpret the results from TR⁻ rats. The results from the present study suggest that further investigation of mechanisms underlying altered sulfation of TGZ in TR⁻ rat SCH, and the potential impact on sulfation of other compounds, is warranted.

Altered disposition of TS and TG revealed in the present study also confirms that hepatocellular exposure of hepatically-generated metabolites is determined by both formation and excretion. Even though TS biliary excretion was not altered, hepatocellular TS accumulation was decreased in TR⁻ rat SCH as a result of decreased sulfation of TGZ. In contrast, hepatocellular TG accumulation was significantly increased in TR⁻ compared to WT rat SCH as a result of increased glucuronidation of TGZ combined with negligible TG biliary excretion. Loss-of-function of Mrp2 in TR⁻ rats led to altered

expression of several enzymes and transporters as a compensatory mechanism (32, 35, 36). Likewise, changes in function of one pathway might lead to altered function of other enzymes and/or transporters. Therefore, to accurately predict changes in the hepatic exposure of metabolites, altered formation as well as excretion of metabolites needs to be considered. This is important in predicting efficacy and/or toxicity of metabolites if the liver is the site of action or the generated metabolites elicit hepatotoxic effects.

The present study demonstrated that biliary excretion of TS was not altered by loss-of-function of Mrp2 and/or Bcrp, suggesting that loss-of-function of these hepatic efflux proteins is not a risk factor for increased hepatocellular TS accumulation in rats. However, these data might not be directly translated to humans due to species differences in abundance, substrate specificity and/or affinity for canalicular transporters. To characterize risk factors for human DILI, the results from the current study need to be evaluated in primary human hepatocytes or human-derived cell systems. As discussed in the previous chapter, this would require double knock-down of transporters in human systems using tandem vectors, or more advanced technology to minimize the off-target effects on other transporters.

Quantitative Relationship between Intracellular Lithocholic Acid, Chenodeoxycholic Acid and Toxicity in Sandwich-Cultured Hepatocytes; Incorporation into a Mechanistic Model of Drug-Induced Liver Injury (Chapter 6)

Increasing evidence supports the hypothesis that drug-mediated functional disturbances in hepatic bile acid transporters can induce hepatotoxicity by hepatocellular accumulation of harmful bile acids. Inhibition of bile acid efflux transporters by drugs has been demonstrated to be associated with DILI based on the systematic investigation of a panel of drugs for their inhibitory effects on bile acid efflux transporters using isolated membrane vesicle systems (4, 6, 8). However, results from the isolated transporter system cannot be translated directly to in vivo hepatotoxicity due to the complexity of bile acid homeostasis (i.e., vectorial transport, enterohepatic recirculation), dynamic changes in the systemic as well as hepatic exposure of drugs/metabolites and bile acids, and feedback regulation of bile acid synthesis and transport as an adaptive response to hepatic bile acid accumulation. While in vivo

preclinical models predictive of bile acid-mediated DILI are lacking, mechanistic modeling that incorporates biological processes involved in DILI as well as the disposition of drugs and metabolites is a useful approach to translate in vitro data to in vivo and make predictions about human DILI.

The objective of Aim 3 was to develop a mechanistic model of DILI that involves interruption of bile acid transport by drugs. It has been widely accepted that intracellular accumulation of bile acids results in hepatotoxicity. However, the relationship between hepatocellular bile acid accumulation and toxicity, which is essential to link bile acid kinetics to toxicity in the mechanistic model of DILI, has not been assessed quantitatively. In the present study, we established for the first time the relationship between intracellular bile acid concentrations and toxicity in multiple species. Quantification of intracellular concentrations of bile acids and ATP, which is difficult to measure in vivo especially in humans, was possible by using SCH. SCH maintain metabolic and transporter function as well as regulatory machinery, and thus mimic bile acid metabolism and transport in vivo (37-39). The results revealed that unconjugated LCA and CDCA were correlated with observed toxicity (i.e., depletion of intracellular ATP, LDH leakage). Based on these results, LCA and CDCA were selected as the toxicophores for subsequent investigations. Using the in vitro data obtained from SCH, mathematical models describing the relationship between intracellular unconjugated LCA and CDCA, and ATP concentrations were constructed.

This study also provided insight into species differences in toxicity of LCA and CDCA. After incubation with LCA, differential toxicity was noted in SCH from different species. LCA exerted a concentration-dependent decrease in hepatocellular ATP in rat SCH, whereas human and dog SCH were more resistant to LCA-mediated toxicity given the same hepatocellular exposure. Minimal toxicity was observed in mouse SCH treated with LCA, potentially due to lower intracellular unconjugated LCA concentrations compared to other species treated with the same LCA medium concentrations. CDCA induced medium concentration-dependent toxicity in both rat and human SCH. However, human SCH showed delayed toxicity with a higher LC₅₀ value compared to rat SCH, suggesting that CDCA-mediated toxicity is less potent in humans compared to rats. Although mechanisms of observed species differences

remain to be investigated, a plausible hypothesis is that intracellular unbound bile acid concentrations may differ among different species, potentially due to the differential intracellular binding, disposition, and/or sequestration of bile acids. It is also possible that differential accumulation of toxic bile acids at the site of toxicity exists among different species. For example, bile acids are known to induce mitochondrial toxicity by inducing mitochondrial permeability transition (40, 41). Thus, mitochondrial accumulation of toxic bile acids might be different in humans and rats, leading to the observed species difference.

However, little is known about intracellular distribution and transport of bile acids, and further studies are warranted. One approach would be isolation of subcellular fractions after incubation of human and rat hepatocytes with bile acids. However, isolation of subcellular fractions of membrane-bound organelles using differential centrifugation has limitations due to potential redistribution of compounds during fractionation (42). Use of fluorescent bile acids would allow real-time imaging of intracellular localization of bile acids (43, 44). However, such data should be interpreted with caution because tagging bile acids with a fluorophore might alter the intracellular distribution of bile acids. In addition to species differences in bile acid disposition, pathophysiological processes involved in the induction of bile acid toxicity (e.g., mitochondrial function, induction of necrosis/apoptosis) downstream of bile acid exposure may contribute to differential sensitivity/resistance to bile acid toxicity, and further investigations are warranted to fully characterize the underlying mechanisms.

Interestingly, cellular concentrations of LCA conjugates were decreased at LCA medium concentrations greater than 100 μM in rat SCH. Similar trends were observed for intracellular TCDCA, GCDCA, TMCA, and GMCA in rat SCH treated with CDCA, and GCDCA in human SCH incubated with CDCA. This is potentially due to saturation of enzymes involved in bile acid amidation (i.e., bile acid-CoA synthase, bile acid-CoA:amino acid N-acyltransferase) and/or depletion of co-substrates (i.e., glycine, taurine). However, concentration-dependent formation of conjugates alone would be expected to cause intracellular concentrations of conjugates to plateau, rather than decrease as observed, as unconjugated bile acid concentrations in the medium increased. Observed decreases in intracellular conjugate concentrations at higher concentrations of unconjugated bile acids suggests that other changes

are occurring, such as adaptive increases in hepatic efflux and/or further metabolism (e.g., sulfation) of these conjugates. Short-term regulation of efflux transporters due to cytokine-mediated insertion and retrieval of transporters into and from plasma membranes might be involved because incubation times of 6 to 24 hr was not long enough to cause transcriptional changes in transporter expression levels. It is also possible that sulfation of glycine and taurine conjugates of LCA might have been increased at higher medium concentrations of unconjugated LCA, but testing this would require quantification of sulfate conjugates.

In the present study, unconjugated LCA and CDCA were assumed to be associated with the observed toxicity in SCH because cellular unconjugated LCA and CDCA concentrations were correlated with observed toxicity. However, it is possible that conjugated LCA and CDCA might also cause toxicity. For example, LCA conjugates have been shown to cause cholestasis (45-47). GCDCA induces apoptosis in primary hepatocytes and mitochondrial permeability transition in isolated mitochondria (40, 41, 48). In addition, other hydrophobic bile acid species such as DCA might also contribute to bile acid-mediated DILI. Measurement of intracellular bile acid concentrations and toxicity in SCH incubated with concentration ranges of CDCA conjugates, LCA conjugates, or other potentially toxic bile acids would help elucidate the contribution of other bile acids to DILI and improve the predictability of the mechanistic model. Also, toxicity measured in the current study was the direct effect of bile acids on hepatocytes after short-term (6 to 24 hr) exposure to high concentrations of bile acids. Different experimental approaches would be necessary to examine the contribution of non-parenchymal cells to bile acid-mediated toxicity, as well as the toxic effects of long-term exposure to low concentrations of bile acids.

Results from the present study revealed that rat was the most sensitive species to LCA toxicity in SCH, and that CDCA induced toxicity at lower medium concentrations in rat SCH compared to human SCH. However, this does not indicate that rats are more susceptible to bile acid-mediated hepatotoxicity compared to other species. Actually, rats are less sensitive to hepatotoxicity induced by bile acid transport inhibitors (1, 2). To accurately translate the *in vitro* toxicity data generated in the present study to *in vivo*,

species differences in the in vivo bile acid profile, bile acid disposition and regulation, as well as hepatocellular accumulation of toxic bile acids in the setting of drug administration needs to be considered. This can be accomplished by developing a mechanistic model of DILI that incorporates the physiology and pathophysiology of bile acids and the disposition of drugs and metabolites, which will be discussed in the next chapter. The relationships between intracellular bile acid exposure and hepatocyte toxicity in humans and rats established in this chapter were incorporated into the mechanistic model to link bile acid homeostasis and cellular ATP dynamic sub-models, and predict DILI mediated by interruption of bile acid transport.

Mechanistic Modeling of Drug-Induced Liver Injury Predicts Delayed Presentation and Species Differences in Bile Acid -Mediated Troglitazone Hepatotoxicity (Chapter 7)

In this chapter, a mechanistic model of DILI (DILIsym[®]) that involves drug-bile acid interactions was developed to incorporate current knowledge about the biological system and in vitro data to improve the predictability of human DILI. DILIsym[®] incorporates sub-models representing drug and metabolite disposition, the physiology and pathophysiology of bile acids, cellular ATP dynamics, the hepatocyte life cycle, and biomarkers of liver injury (e.g., serum ALT and bilirubin). The quantitative relationships between intracellular bile acid concentrations and toxicity established in the previous chapter were employed to link the bile acid homeostasis model and hepatotoxicity. Population variability also was incorporated into model predictions because of the large variability that exists in bile acid exposure and because incidence rates of bile acid-mediated hepatotoxicity are low (49, 50). DILIsym[®] was used to investigate the role of bile acid transport inhibition in TGZ-mediated hepatotoxicity in humans, and to explore the mechanisms for species differences in hepatotoxicity in humans and rats administered TGZ.

Although TGZ and TS were identified as potent inhibitors of bile acid transporters in isolated membrane vesicle systems (4, 7, 20), the implications of these finding with respect to in vivo hepatotoxicity have not been evaluated. Results from the current study demonstrated for the first time that bile acid transport inhibition alone, without other mechanisms of toxicity (e.g., reactive metabolite,

mitochondrial toxicity), can explain species differences and the lag time in TGZ-mediated hepatotoxicity. In the simulated human population (SimPops) administered 400 – 600 mg/day TGZ for 6 months, 2.4 – 4.2% of individuals exhibited elevations in serum ALT >3X ULN, and Hy's Law cases were identified in 0.9 – 3.0% of the population. This is similar to observations during the clinical trials, where 2% of treated patients experienced elevated serum ALT >3X ULN, and two patients presented with jaundice (50). Simulations also adequately predicted the delayed time to peak ALT elevations observed in the clinic (50). Although the underlying mechanism(s) remain unclear, the mechanistic modeling suggested that delayed bile acid accumulation due to the dynamic interaction between hepatobiliary bile acid disposition and hepatic ATP concentrations might contribute to the delayed presentation of TGZ-mediated toxicity.

DILIsym[®], which incorporates species differences in bile acid homeostasis, correctly predicted the differential hepatotoxicity of TGZ in humans versus rats. Rats have a more hydrophilic, less toxic bile acid pool compared to humans. For example, CDCA, the most widely implicated bile acid in cholestatic liver injury (10), is one of the dominant bile acids in humans, whereas it contributes a smaller proportion to the total bile acid pool in rats and mice (49, 51). LCA, the most hydrophobic bile acid, is primarily sulfated in humans, but undergoes extensive hydroxylation in rats (11). The DILIsym[®] bile acid homeostasis sub-model incorporated these species differences in the bile acid profile, which led to lower hepatic accumulation of toxic bile acids in rats compared to humans, and thus, no apparent toxicity in rats. Sensitivity analysis demonstrated that rat SimPops did not exhibit hepatotoxicity even for compounds with 10-fold lower (more potent) inhibition constants for bile acid efflux transporters, suggesting that the differential bile acid profile, rather than inhibitor specificity and/or potency of drugs, is the main contributor to species differences in DILI.

As shown in the clinic and simulated results, only a small subset of patients treated with TGZ experienced serum ALT elevations, suggesting that certain patients are more susceptible to TGZ-mediated hepatotoxicity (50). Multiple linear regression analysis of DILI responses in the human SimPops enabled identification of potential risk factors; the results suggested that impaired function of hepatic efflux transporters responsible for excretion of bile acids (LCA-sulfate, CDCA-amide) as well as

perpetrator drugs/metabolites (TS) might predispose a subset of patients to DILI. It is possible that diseases (type 2 diabetes and associated conditions such as non-alcoholic steatohepatitis and cirrhosis) might make a subset of patients more susceptible to hepatotoxicity due to functional changes in enzymes and/or transporters, underlying liver injury, and compromised compensatory hepatocyte proliferation and tissue repair (52). However, mechanistic and quantitative assessment of functional impairment of enzymes and/or transporters as well as impaired tissue injury with regard to the progress/severity of disease will be required. Increased LCA synthesis in the intestinal lumen as also identified as a risk factor for DILI. LCA is synthesized in the intestine by bacterial modification of CDCA, which is known to be affected by environmental factors such as diet. However, the rate and interindividual variability of LCA synthesis have not been well characterized, and thus further studies are needed to evaluate the effects of environmental factors on bile acid-mediated hepatotoxicity using the mechanistic modeling.

The current mechanistic model combined with population analysis was able to reasonably predict altered bile acid disposition in rats administered glibenclamide (53), and also correctly predicted species differences in TGZ-mediated hepatotoxicity. This suggests that the mechanistic model can be used to qualitatively predict a drug's propensity to cause bile acid-mediated hepatotoxicity. However, it is of note that there exist knowledge gaps in bile acid homeostasis and bile acid-drug interactions that limit the accurate prediction of bile acid-mediated DILI. For example, quantitative data regarding feedback regulation of bile acid synthesis and/or transport currently are lacking. Intestinal transporters that mediate bile acid reabsorption recently have been characterized, and there has been increasing evidence that enterocytes play important roles in feedback regulation of bile acid synthesis, metabolism, and transport (54). However, this is an emerging area of research, and more information (both qualitative and quantitative) needs to be generated to fully characterize intestinal bile acid transport and regulation. Other important unknowns include hepatocyte drug and bile acid concentrations that are relevant to drug-bile acid interactions at the hepatic efflux transporters. Total hepatic concentrations may not accurately represent the concentrations of drug and/or metabolite available to inhibit transporters. Alternatively, unbound cytosolic concentrations might represent the drug and/or metabolite(s) concentrations that are

capable of exerting inhibitory effects based on the free-drug hypothesis (55). However, if bile acids undergo carrier- or vesicle-mediated intracellular transport, unbound cytosolic drug concentrations might not be relevant. Therefore, intracellular transport and localization of bile acids needs to be elucidated first, and then development of experimental methods to reliably measure the relevant concentrations should follow in order to accurately characterize relevant hepatocyte drug concentrations for inhibition of bile acid efflux.

Although the current model reasonably predicted incidence rates and delayed presentation of serum ALT elevations induced by TGZ treatment, “adaptation” to liver injury was not predicted. Once the injury is initiated (e.g., by drug-mediated hepatic bile acid accumulation), the prognosis of liver injury is determined by biochemical mechanisms that lead to progression or regression of injury and compensatory liver repair. In most patients who experienced TGZ-mediated elevations in serum ALT, enzyme levels returned to normal after discontinuation of the drug or even with the continuing use of TGZ (50), and only a small percentage of patients developed liver failure that led to encephalopathy, transplant or death (56). This suggests that most of the patients who experienced serum ALT elevations were able to adapt to the liver injury, whereas patients who did not adapt progressed to severe hepatotoxicity (2). Although mechanisms underlying adaptation are poorly understood, several studies suggest that regulation of multiple genes including drug metabolizing enzymes and transporters are critical. For example, hepatic basolateral efflux transporters are upregulated under cholestatic conditions when biliary bile acid excretion is impaired, serving as a compensatory elimination pathway of bile acids (57). Genetic defects in this regulatory pathway might make a subset of population more sensitive to bile acid-mediated DILI. Secondary inflammation, oxidative damage, and enzymatic degradation via proteases also are postulated to be involved in the progression of hepatotoxicity (52). Idiosyncratic toxicities are not driven solely by drug exposure, but rather depend on several drug- and patient-related risk factors. Lack of a mechanistic understanding of the adaptation process, a paucity of existing animal models, and the absence of specific and sensitive biomarkers impedes the identification of susceptible patients to idiosyncratic severe liver injury. Validity and predictability of the mechanistic model depend largely on existing data and

knowledge. However, even in the absence of data, mechanistic modeling can be used to test different hypotheses regarding susceptibility factors associated with different biological processes that contribute to severe liver injury beyond serum ALT elevations.

In the present study, a mechanistic model was developed to predict DILI that involves inhibition of hepatic bile acid transport. Results from the current study demonstrated for the first time that bile acid transport inhibition alone could predict the delayed hepatotoxicity observed after TGZ treatment. Also, the mechanistic model incorporating physiology and pathophysiology of bile acids in humans and rats correctly predicted differential TGZ hepatotoxicity in humans and rats. Although development of a mechanistic model is limited by currently available data and knowledge, modeling can define knowledge gaps, prioritize identified knowledge gaps, and guide study design. In the process of model development, a missing link was found between intracellular bile acid concentrations and toxicity, and experiments were performed (LCA and CDCA toxicity studies, as discussed in the previous chapter) to fill this data gap. Data generated from these experiments served as model input, and then the developed model was used to simulate DILI responses in populations. Simulation results were validated against the existing clinical data, and at the same time, used to identify risk factors for DILI, which generated new hypotheses that can be tested by experiments. The current study demonstrated that mechanistic models can be useful to predict hepatotoxic potential of compounds and aid in decision-making throughout drug development. Initially, predictions are based on in vitro and preclinical data. The mechanistic models can be refined iteratively to incorporate additional information generated during the drug development process (e.g., drug disposition and safety data in healthy volunteers during phase I clinical trials) as it becomes available. Refined models can be used to inform the safety profile of drugs in larger populations and/or patients, and identify patients who may be susceptible to toxicity.

CONCLUSION

This dissertation research focused on DILI that involves drug-bile acid interactions at hepatic transport proteins. Various experimental systems and approaches were employed to answer important

questions regarding species differences and patient specific risk factors for bile acid-mediated DILI. A mechanistic, multi-scale model that incorporates information about biological processes involved in DILI was developed to translate experimental data from in vitro systems and preclinical species to humans to improve predictability of human DILI. Although many fundamental questions remain to be answered, the integrative approach employed in these studies established a framework to incorporate knowledge about physiology and experimental data obtained during the drug development process to prospectively predict hepatotoxic potential of chemical entities.

REFERENCES

- (1) Leslie, E.M., Watkins, P.B., Kim, R.B. & Brouwer, K.L. Differential inhibition of rat and human Na⁺-dependent taurocholate cotransporting polypeptide (NTCP/SLC10A1) by bosentan: a mechanism for species differences in hepatotoxicity. *J Pharmacol Exp Ther* **321**, 1170-8 (2007).
- (2) Watkins, P.B. Idiosyncratic liver injury: challenges and approaches. *Toxicologic pathology* **33**, 1-5 (2005).
- (3) Jansen, P.L. *et al.* Hepatocanicular bile salt export pump deficiency in patients with progressive familial intrahepatic cholestasis. *Gastroenterology* **117**, 1370-9 (1999).
- (4) Morgan, R.E. *et al.* A Multifactorial Approach to Hepatobiliary Transporter Assessment Enables Improved Therapeutic Compound Development. *Toxicol Sci*, (2013).
- (5) Perez, M.J. & Briz, O. Bile-acid-induced cell injury and protection. *World J Gastroenterol* **15**, 1677-89 (2009).
- (6) Kock, K. *et al.* Risk Factors for Development of Cholestatic Drug-induced Liver Injury: Inhibition of Hepatic Basolateral Bile Acid Transporters MRP3 and MRP4. *Drug Metab Dispos*, (2013).
- (7) Yang, K., Yue, W., Koeck, K., Pfeifer, N.D. & Brouwer, K.L.R. Interaction of Troglitazone Sulfate with Hepatic Basolateral and Canalicular Transport Proteins. In 2011 AAPS Annual Meeting and Exposition M1301.
- (8) Dawson, S., Stahl, S., Paul, N., Barber, J. & Kenna, J.G. In vitro inhibition of the bile salt export pump correlates with risk of cholestatic drug-induced liver injury in humans. *Drug Metab Dispos* **40**, 130-8 (2012).
- (9) Scholmerich, J. *et al.* Influence of hydroxylation and conjugation of bile salts on their membrane-damaging properties--studies on isolated hepatocytes and lipid membrane vesicles. *Hepatology* **4**, 661-6 (1984).
- (10) Greim, H. *et al.* Mechanism of cholestasis. 6. Bile acids in human livers with or without biliary obstruction. *Gastroenterology* **63**, 846-50 (1972).
- (11) Hofmann, A.F. Detoxification of lithocholic acid, a toxic bile acid: relevance to drug hepatotoxicity. *Drug Metab Rev* **36**, 703-22 (2004).

- (12) van Mil, S.W. *et al.* Benign recurrent intrahepatic cholestasis type 2 is caused by mutations in ABCB11. *Gastroenterology* **127**, 379-84 (2004).
- (13) Rius, M., Hummel-Eisenbeiss, J., Hofmann, A.F. & Keppler, D. Substrate specificity of human ABCC4 (MRP4)-mediated cotransport of bile acids and reduced glutathione. *Am J Physiol Gastrointest Liver Physiol* **290**, G640-9 (2006).
- (14) Ballatori, N., Li, N., Fang, F., Boyer, J.L., Christian, W.V. & Hammond, C.L. OST alpha-OST beta: a key membrane transporter of bile acids and conjugated steroids. *Front Biosci* **14**, 2829-44 (2009).
- (15) Akita, H., Suzuki, H., Hirohashi, T., Takikawa, H. & Sugiyama, Y. Transport activity of human MRP3 expressed in Sf9 cells: comparative studies with rat MRP3. *Pharm Res* **19**, 34-41 (2002).
- (16) Iusuf, D., van de Steeg, E. & Schinkel, A.H. Hepatocyte hopping of OATP1B substrates contributes to efficient hepatic detoxification. *Clin Pharmacol Ther* **92**, 559-62 (2012).
- (17) Hofmann, A.F. The continuing importance of bile acids in liver and intestinal disease. *Arch Intern Med* **159**, 2647-58 (1999).
- (18) Funk, C., Ponelle, C., Scheuermann, G. & Pantze, M. Cholestatic potential of troglitazone as a possible factor contributing to troglitazone-induced hepatotoxicity: in vivo and in vitro interaction at the canalicular bile salt export pump (Bsep) in the rat. *Mol Pharmacol* **59**, 627-35 (2001).
- (19) Lee, J.K., Marion, T.L., Abe, K., Lim, C., Pollock, G.M. & Brouwer, K.L. Hepatobiliary disposition of troglitazone and metabolites in rat and human sandwich-cultured hepatocytes: use of Monte Carlo simulations to assess the impact of changes in biliary excretion on troglitazone sulfate accumulation. *J Pharmacol Exp Ther* **332**, 26-34 (2010).
- (20) Marion, T.L., Leslie, E.M. & Brouwer, K.L. Use of sandwich-cultured hepatocytes to evaluate impaired bile acid transport as a mechanism of drug-induced hepatotoxicity. *Mol Pharm* **4**, 911-8 (2007).
- (21) Stieger, B., Fattinger, K., Madon, J., Kullak-Ublick, G.A. & Meier, P.J. Drug- and estrogen-induced cholestasis through inhibition of the hepatocellular bile salt export pump (Bsep) of rat liver. *Gastroenterology* **118**, 422-30 (2000).
- (22) Muhlfeld, S. *et al.* Short-term feedback regulation of bile salt uptake by bile salts in rodent liver. *Hepatology* **56**, 2387-97 (2012).

- (23) Agellon, L.B. & Torchia, E.C. Intracellular transport of bile acids. *Biochim Biophys Acta* **1486**, 198-209 (2000).
- (24) Wakabayashi, Y., Lippincott-Schwartz, J. & Arias, I.M. Intracellular trafficking of bile salt export pump (ABCB11) in polarized hepatic cells: constitutive cycling between the canalicular membrane and rab11-positive endosomes. *Mol Biol Cell* **15**, 3485-96 (2004).
- (25) Jonker, J.W., Liddle, C. & Downes, M. FXR and PXR: potential therapeutic targets in cholestasis. *J Steroid Biochem Mol Biol* **130**, 147-58 (2012).
- (26) El-Seaidy, A.Z., Mills, C.O., Elias, E. & Crawford, J.M. Lack of evidence for vesicle trafficking of fluorescent bile salts in rat hepatocyte couplets. *Am J Physiol* **272**, G298-309 (1997).
- (27) Wang, I.I. & Huang, I.I. Adenovirus technology for gene manipulation and functional studies. *Drug Discov Today* **5**, 10-6 (2000).
- (28) Yue, W., Abe, K. & Brouwer, K.L. Knocking down breast cancer resistance protein (Bcrp) by adenoviral vector-mediated RNA interference (RNAi) in sandwich-cultured rat hepatocytes: a novel tool to assess the contribution of Bcrp to drug biliary excretion. *Mol Pharm* **6**, 134-43 (2009).
- (29) Kostrubsky, V.E. *et al.* The effect of troglitazone biliary excretion on metabolite distribution and cholestasis in transporter-deficient rats. *Drug Metab Dispos* **29**, 1561-6 (2001).
- (30) Enokizono, J., Kusuhara, H. & Sugiyama, Y. Involvement of breast cancer resistance protein (BCRP/ABCG2) in the biliary excretion and intestinal efflux of troglitazone sulfate, the major metabolite of troglitazone with a cholestatic effect. *Drug Metab Dispos* **35**, 209-14 (2007).
- (31) Kawai, K. *et al.* Disposition and metabolism of the new oral antidiabetic drug troglitazone in rats, mice and dogs. *Arzneimittelforschung* **47**, 356-68 (1997).
- (32) Johnson, B.M., Zhang, P., Schuetz, J.D. & Brouwer, K.L. Characterization of transport protein expression in multidrug resistance-associated protein (Mrp) 2-deficient rats. *Drug Metab Dispos* **34**, 556-62 (2006).
- (33) Sun, H., Zeng, Y.Y. & Pang, K.S. Interplay of phase II enzymes and transporters in futile cycling: influence of multidrug resistance-associated protein 2-mediated excretion of estradiol 17beta-D-glucuronide and its 3-sulfate metabolite on net sulfation in perfused TR(-) and Wistar rat liver preparations. *Drug Metab Dispos* **38**, 769-80 (2010).

- (34) Wong, K.O. & Wong, K.P. Direct measurement and regulation of 3'-phosphoadenosine 5'-phosphosulfate (PAPS) generation in vitro. *Biochem Pharmacol* **52**, 1187-94 (1996).
- (35) Newton, D.J., Wang, R.W. & Evans, D.C. Determination of phase I metabolic enzyme activities in liver microsomes of Mrp2 deficient TR- and EHBR rats. *Life Sci* **77**, 1106-15 (2005).
- (36) Yue, W., Lee, J.K., Abe, K., Sugiyama, Y. & Brouwer, K.L. Decreased hepatic breast cancer resistance protein expression and function in multidrug resistance-associated protein 2-deficient (TR(-)) rats. *Drug Metab Dispos* **39**, 441-7 (2011).
- (37) Swift, B., Pfeifer, N.D. & Brouwer, K.L. Sandwich-cultured hepatocytes: an in vitro model to evaluate hepatobiliary transporter-based drug interactions and hepatotoxicity. *Drug Metab Rev* **42**, 446-71 (2010).
- (38) LeCluyse, E., Madan, A., Hamilton, G., Carroll, K., DeHaan, R. & Parkinson, A. Expression and regulation of cytochrome P450 enzymes in primary cultures of human hepatocytes. *J Biochem Mol Toxicol* **14**, 177-88 (2000).
- (39) Liu, X., LeCluyse, E.L., Brouwer, K.R., Lightfoot, R.M., Lee, J.I. & Brouwer, K.L. Use of Ca²⁺ modulation to evaluate biliary excretion in sandwich-cultured rat hepatocytes. *J Pharmacol Exp Ther* **289**, 1592-9 (1999).
- (40) Sokol, R.J., Dahl, R., Devereaux, M.W., Yerushalmi, B., Kobak, G.E. & Gumprich, E. Human hepatic mitochondria generate reactive oxygen species and undergo the permeability transition in response to hydrophobic bile acids. *J Pediatr Gastroenterol Nutr* **41**, 235-43 (2005).
- (41) Schulz, S. *et al.* Progressive stages of mitochondrial destruction caused by cell toxic bile salts. *Biochim Biophys Acta* **1828**, 2121-33 (2013).
- (42) Pfeifer, N.D., Harris, K.B., Yan, G.Z. & Brouwer, K.L. Determination of Intracellular Unbound Concentrations and Subcellular Localization of Drugs in Rat Sandwich-Cultured Hepatocytes Compared to Liver Tissue. *Drug Metab Dispos*, (2013).
- (43) Murray, J.W., Thosani, A.J., Wang, P. & Wolkoff, A.W. Heterogeneous accumulation of fluorescent bile acids in primary rat hepatocytes does not correlate with their homogenous expression of ntcp. *Am J Physiol Gastrointest Liver Physiol* **301**, G60-8 (2011).
- (44) Yamaguchi, H. *et al.* Transport of fluorescent chenodeoxycholic acid via the human organic anion transporters OATP1B1 and OATP1B3. *J Lipid Res* **47**, 1196-202 (2006).

- (45) Kakis, G. & Yousef, I.M. Pathogenesis of lithocholate- and tauroolithocholate-induced intrahepatic cholestasis in rats. *Gastroenterology* **75**, 595-607 (1978).
- (46) Oelberg, D.G., Chari, M.V., Little, J.M., Adcock, E.W. & Lester, R. Lithocholate glucuronide is a cholestatic agent. *J Clin Invest* **73**, 1507-14 (1984).
- (47) Yousef, I.M., Tuchweber, B., Vonk, R.J., Masse, D., Audet, M. & Roy, C.C. Lithocholate cholestasis--sulfated glycolithocholate-induced intrahepatic cholestasis in rats. *Gastroenterology* **80**, 233-41 (1981).
- (48) Faubion, W.A. *et al.* Toxic bile salts induce rodent hepatocyte apoptosis via direct activation of Fas. *J Clin Invest* **103**, 137-45 (1999).
- (49) Trottier, J., Caron, P., Straka, R.J. & Barbier, O. Profile of serum bile acids in noncholestatic volunteers: gender-related differences in response to fenofibrate. *Clin Pharmacol Ther* **90**, 279-86 (2011).
- (50) Watkins, P.B. & Whitcomb, R.W. Hepatic dysfunction associated with troglitazone. *N Engl J Med* **338**, 916-7 (1998).
- (51) Garcia-Canaveras, J.C., Donato, M.T., Castell, J.V. & Lahoz, A. Targeted profiling of circulating and hepatic bile acids in human, mouse, and rat using a UPLC-MRM-MS-validated method. *J Lipid Res* **53**, 2231-41 (2012).
- (52) Wang, T., Shankar, K., Ronis, M.J. & Mehendale, H.M. Mechanisms and outcomes of drug- and toxicant-induced liver toxicity in diabetes. *Crit Rev Toxicol* **37**, 413-59 (2007).
- (53) Woodhead, J.L. *et al.* Mechanistic modeling reveals the critical knowledge gaps in bile acid-mediated DILI. *CPT:PSP In revision*, (2013).
- (54) Dawson, P.A. Role of the intestinal bile acid transporters in bile acid and drug disposition. *Handbook of experimental pharmacology*, 169-203 (2011).
- (55) Smith, D.A., Di, L. & Kerns, E.H. The effect of plasma protein binding on in vivo efficacy: misconceptions in drug discovery. *Nat Rev Drug Discov* **9**, 929-39 (2010).
- (56) Presented at the Endocrinologic and Metabolic Drugs Advisory Committee Meeting. April 26, 1999. Available from the US Food and Drug Administration (<http://www.fda.gov/ohrms/dockets/ac/99/transcpt/3499t1a.pdf>). Accessed January 25, 2014.

- (57) Zollner, G. *et al.* Expression of bile acid synthesis and detoxification enzymes and the alternative bile acid efflux pump MRP4 in patients with primary biliary cirrhosis. *Liver Int* **27**, 920-9 (2007).

APPENDIX

Data Appendix

Figure 3.3.

Human Control

Study Phase		Taurocholic Acid Accumulation (pmol/mg protein)								
		Time (minute)		Lysate				Buffer		
				Standard HBSS		Ca ²⁺ -free HBSS		Standard HBSS		Ca ²⁺ -free HBSS
(in phase)	(cumulative)	Mean	SEM	Mean	SEM	Mean	SEM	Mean	SEM	
Uptake	2	2	48.0	14.8	20.5	7.2				
	5	5	95.4	18.6	32.9	8.0				
	10	10	136.9	20.8	44.6	6.5				
	20	20	318.6	6.1	116.7	37.2				
Efflux	2	23	220.4	49.3	65.7	9.6	42.9	28.2	34.8	7.1
	3.5	24.5	211.9	31.1	56.4	16.2	49.8	21.7	43.6	5.1
	5	26	217.5	55.9	48.3	16.7	69.0	32.2	51.4	8.5
	10	31	218.1	61.0	41.9	26.0	101.0	31.8	82.0	13.5

Human +TGZ

			Taurocholic Acid Accumulation (pmol/mg protein)							
			Lysate				Buffer			
Study Phase	Time (minute)		Standard HBSS		Ca ²⁺ -free HBSS		Standard HBSS		Ca ²⁺ -free HBSS	
	(in phase)	(cumulative)	Mean	SEM	Mean	SEM	Mean	SEM	Mean	SEM
Uptake	2	2	6.8	0.6	6.3	4.4				
	5	5	12.4	0.8	11.0	8.0				
	10	10	15.9	0.7	8.5	4.9				
	20	20	33.3	4.0	22.1	14.1				
Efflux	2	23	22.4	2.8	8.6	3.9	8.3	3.7	14.7	17.4
	3.5	24.5	22.7	0.9	6.0	3.0	11.1	3.2	11.9	10.3
	5	26	15.3	3.1	4.7	2.9	12.2	4.4	18.5	19.9
	10	31	15.3	0.6	3.2	1.9	23.1	7.0	22.3	17.7

288

Rat Control

			Taurocholic Acid Accumulation (pmol/mg protein)							
			Lysate				Buffer			
Study Phase	Time (minute)		Standard HBSS		Ca ²⁺ -free HBSS		Standard HBSS		Ca ²⁺ -free HBSS	
	(in phase)	(cumulative)	Mean	SEM	Mean	SEM	Mean	SEM	Mean	SEM
Uptake	2	2	21.8	4.7	4.9	0.8				
	5	5	37.5	10.2	5.9	2.6				
	10	10	54.7	9.6	10.5	3.0				
	15	15	73.1	19.1	11.5	1.5				
	20	20	85.3	21.5	13.8	0.9				
Efflux	2	23	72.2	10.6	4.5	1.2	19.3	4.9	9.1	3.7
	3.5	24.5	57.8	12.6	3.9	2.0	25.7	8.4	9.0	3.7
	5	26	49.3	11.3	1.9	0.8	31.4	9.2	8.7	2.5
	10	31	40.3	14.0	1.3	0.6	45.7	21.3	12.5	4.0
	15	36	33.0	6.0	0.5	0.1	51.8	15.5	11.6	0.6

Rat + TGZ

Study Phase			Taurocholic Acid Accumulation (pmol/mg protein)							
			Lysate				Buffer			
			Time (minute)		Standard HBSS		Ca ²⁺ -free HBSS		Standard HBSS	
(in phase)	(cumulative)	Mean	SEM	Mean	SEM	Mean	SEM	Mean	SEM	
Uptake	2	2	5.0	1.8	2.5	0.5				
	5	5	7.5	0.6	2.7	1.0				
	10	10	9.2	0.8	3.2	0.8				
	15	15	11.5	0.6	4.2	0.7				
	20	20	12.9	0.9	5.0	1.1				
Efflux	2	23	6.5	1.6	0.9	0.1	4.7	0.5	2.9	0.1
	3.5	24.5	4.6	1.0	0.7	0.2	5.9	0.3	4.3	1.4
	5	26	4.4	1.1	0.5	0.2	8.0	0.6	4.4	0.3
	10	31	2.6	0.9	0.2	0.1	8.7	1.3	5.1	2.0
	15	36	1.7	0.3	0.1	0.1	9.5	0.5	5.7	2.3

Figure 3.4.(A) 2 μ M DHEAS

	ATP-dependent DHEAS transport (pmol/min/mg protein)			
	- GSH		+ GSH	
	Mean	SD	Mean	SD
Control	127.3	55.3	276.0	25.0
50 μ M TS	29.3	3.1	79.0	4.5

(B) Concentration-dependent transport of DHEAS

DHEAS Concentration (μ M)	ATP-dependent DHEAS transport (pmol/min/mg protein)							
	Control		5 μ M TS		10 μ M TS		50 μ M TS	
	Mean	SD	Mean	SD	Mean	SD	Mean	SD
0.5	79.6	3.6	72.1	2.5	28.0	1.3	3.2	3.3
2	240.2	21.4	233.8	7.0	105.5	6.6	21.7	5.3
5	462.4	24.6	415.3	34.5	176.7	28.4	32.2	8.5
10	614.6	28.7	634.6	47.1	318.4	40.5	21.5	7.5
20	737.3	143.6	593.9	88.3	330.3	82.9	133.9	45.9

Figure 4.1.

(A) Bcrp mRNA

MOI	Bcrp mRNA (% non-infected control)							
	WT				TR ⁻			
	Ad-siNT		Ad-siBcrp		Ad-siNT		Ad-siBcrp	
	Mean	SEM	Mean	SEM	Mean	SEM	Mean	SEM
3	108.1	26.6	41.0	10.4	98.2	38.9	23.4	10.0
5	98.3	12.6	23.5	6.8	118.5	7.7	14.2	4.0
10	124.2	6.5	11.6	3.5	117.7	35.0	6.5	0.9

(B) Bcrp protein

MOI	Bcrp protein (% non-infected control)							
	WT				TR ⁻			
	Ad-siNT		Ad-siBcrp		Ad-siNT		Ad-siBcrp	
	Mean	SEM	Mean	SEM	Mean	SEM	Mean	SEM
3	66.6	18.8	39.4	20.6	131.8	76.4	66.7	26.0
5	76.9	16.5	33.6	15.0	86.8	15.8	35.3	19.9
10	53.3	16.0	19.4	10.1	82.4	10.8	30.1	11.0

Figure 4.2.

(B) Transport protein expression

		Protein (% non-infected control)							
Protein	MOI	WT				TR ⁻			
		Ad-siNT		Ad-siBcrp		Ad-siNT		Ad-siBcrp	
		Mean	SEM	Mean	SEM	Mean	SEM	Mean	SEM
Oatp1a1	5	142.5	32.3	165.8	41.8	97.0	32.5	94.2	61.4
	10	157.0	55.9	139.0	82.0	85.0	76.3	71.3	46.4
Ntcp	5	106.6	46.2	113.4	44.2	102.4	33.5	74.7	22.0
	10	109.3	56.8	73.9	43.5	96.7	20.4	55.9	15.5
Bsep	5	62.9	45.8	50.2	41.3	101.8	46.5	142.0	42.4
	10	43.8	37.6	59.6	64.5	94.2	32.4	126.7	65.9
Pgp	5	114.3	42.5	96.6	31.1	110.3	15.9	111.0	64.2
	10	85.2	22.2	94.2	39.2	76.0	46.8	96.4	57.9
Mrp4	5	70.2	6.9	45.2	0.0	90.8	27.1	77.5	35.7
	10	45.2	12.9	44.7	27.6	75.0	10.8	78.6	24.8
Mrp2	5	50.5	13.7	117.6	81.4				
	10	74.6	61.5	84.3	53.0				

Figure 4.3.**(A) Rosuvastatin accumulation (Cells+Bile)**

MOI	Accumulation in Cells+Bile (pmol/mg protein)			
	WT		TR ⁻	
	Ad-siNT	Ad-siBcrp	Ad-siNT	Ad-siBcrp
0	180.9		182.2	
1	200.2	181.9	180.7	173.7
3	197.3	190.3	169.6	156.1
5	206.9	184.0	173.7	170.9
10	190.3	181.0	149.8	126.1

(B) Rosuvastatin BEI

MOI	BEI (%)			
	WT		TR ⁻	
	Ad-siNT	Ad-siBcrp	Ad-siNT	Ad-siBcrp
0	54.3		24.6	
1	53.1	54.5	20.1	21.0
3	49.6	44.5	18.7	14.1
5	45.4	30.8	17.8	5.9
10	40.0	29.4	19.2	7.7

(C) Taurocholic acid accumulation (Cells+Bile)

MOI	Accumulation in Cells+Bile (pmol/mg protein)			
	WT		TR ⁻	
	Ad-siNT	Ad-siBcrp	Ad-siNT	Ad-siBcrp
0	27.1		41.7	
1	27.8	26.0	39.3	33.9
3	22.3	19.7	37.1	32.1
5	21.1	18.0	38.1	30.9
10	21.3	16.4	40.3	26.7

(D) Taurocholic acid BEI

MOI	BEI (%)			
	WT		TR ⁻	
	Ad-siNT	Ad-siBcrp	Ad-siNT	Ad-siBcrp
0	83.0		72.6	
1	89.2	85.2	73.4	66.5
3	82.7	81.7	70.4	67.2
5	78.6	80.1	64.5	60.6
10	80.8	77.4	56.8	45.8

Supplement Figure 4.1.

(B) Mrp2 and Bcrp protein

MOI	Mrp2 protein (% non-infected control)				Bcrp protein (% non-infected control)			
	Ad-siNT		Ad-siBcrp		Ad-siNT		Ad-siBcrp	
	Mean	SEM	Mean	SEM	Mean	SEM	Mean	SEM
5	109.1	42.1	60.4	30.0	97.9	14.2	114.0	22.1
10	59.7	49.5	17.1	13.6	102.6	27.9	88.2	10.5
15	106.1	0.0	32.7	0.0	104.7	0.0	104.7	0.0

Supplement Figure 4.2.(A) Estradiol-17 β -D-glucuronide accumulation (Cells+Bile)

MOI	Accumulation in Cells+Bile (pmol/mg protein)	
	Ad-siNT	Ad-siMrp2
0	1015.1	
5	1224.1	1031.8
10	992.4	1078.7
15	967.5	788.5
20	1146.6	1039.2

(B) Estradiol-17 β -D-glucuronide BEI

MOI	BEI (%)	
	Ad-siNT	Ad-siMrp2
0	23.8	
5	19.6	10.5
10	4.1	0.0
15	7.6	0.0
20	11.7	7.3

(C) Taurocholic acid accumulation (Cells+Bile)

MOI	Accumulation in Cells+Bile (pmol/mg protein)	
	Ad-siNT	Ad-siMrp2
0	34.4	
5	33.5	22.7
10	20.2	11.0
15	26.1	19.9
20	24.7	16.2

(D) Taurocholic acid BEI

MOI	BEI (%)	
	Ad-siNT	Ad-siMrp2
0	90.8	
5	91.1	88.4
10	90.2	86.5
15	88.9	87.5
20	86.3	83.0

Supplement Figure 4.3.

(B) Mrp2 and Bcrp protein expression

	Protein (% non-infected control)			
	Ad-siNT		Ad-siBcrp + Ad-siMrp2	
	Mean	SEM	Mean	SEM
Mrp2	53.4	19.8	32.9	8.8
Bcrp	70.5	5.6	36.0	4.0

Figure 5.2.

(A) TGZ

Rat	Viral Infection	Cells+Bile (pmol/mg protein)		Cells (pmol/mg protein)	
		Mean	SEM	Mean	SEM
WT	CTL	406.0	301.0	629.1	330.6
	Ad-siNT	431.5	324.6	585.8	335.1
	Ad-siBcrp	529.6	375.3	704.7	405.1
TR-	CTL	927.2	624.2	1069.7	593.9
	Ad-siNT	902.1	630.3	1026.2	607.1
	Ad-siBcrp	1096.0	737.4	1261.0	795.7

(B) TS

Rat	Viral Infection	Cells+Bile (pmol/mg protein)		Cells (pmol/mg protein)		BEI (%)	
		Mean	SEM	Mean	SEM	Mean	SEM
WT	CTL	1067.4	95.3	812.8	212.7	24.3	14.9
	Ad-siNT	1270.0	83.5	949.9	156.5	25.5	8.1
	Ad-siBcrp	1311.7	214.3	1005.6	236.3	23.4	10.9
TR-	CTL	717.5	60.8	575.0	51.4	19.1	13.5
	Ad-siNT	739.9	112.0	606.6	17.3	16.6	14.0
	Ad-siBcrp	771.1	143.6	593.2	65.5	22.1	10.0

(C) TG

Rat	Viral Infection	Cells+Bile (pmol/mg protein)		Cells (pmol/mg protein)		BEI (%)	
		Mean	SEM	Mean	SEM	Mean	SEM
WT	CTL	92.6	71.3	41.8	32.0	49.3	14.7
	Ad-siNT	151.1	117.7	64.3	53.2	58.5	7.7
	Ad-siBcrp	137.1	109.1	60.5	50.8	55.6	5.3
TR-	CTL	64.8	22.5	70.8	19.6	1.0	1.7
	Ad-siNT	134.4	18.4	141.7	32.0	2.3	4.0
	Ad-siBcrp	117.4	23.2	115.3	9.9	7.9	7.2

Figure 5.3.

(A) TGZ

Rat	Viral Infection	Medium (pmol/mg protein)	
		Mean	SEM
WT	CTL	7163.3	1740.0
	Ad-siNT	7206.7	1855.8
	Ad-siBcrp	7260.0	2014.3
TR	CTL	6776.7	1585.9
	Ad-siNT	7256.7	1856.1
	Ad-siBcrp	7233.3	2140.0

(B) TS

Rat	Viral Infection	Medium (pmol/mg protein)	
		Mean	SEM
WT	CTL	121.9	24.6
	Ad-siNT	101.8	8.5
	Ad-siBcrp	92.3	19.0
TR	CTL	81.6	21.8
	Ad-siNT	76.0	17.4
	Ad-siBcrp	63.6	16.8

(C) TG

Rat	Viral Infection	Medium (pmol/mg protein)	
		Mean	SEM
WT	CTL	60.3	49.0
	Ad-siNT	76.3	62.3
	Ad-siBcrp	58.9	48.8
TR	CTL	103.9	26.9
	Ad-siNT	157.1	47.3
	Ad-siBcrp	113.8	17.5

Figure 5.4.

(A) Total recovery

Rat	Viral Infection	Total recovery (% of TGZ Dose)			
		TGZ	TS	TG	TQ
WT	CTL	91.1	4.8	0.9	1.5
	Ad-siNT	91.3	5.1	1.3	1.5
	Ad-siBcrp	92.3	5.2	1.0	1.3
TR	CTL	86.9	2.8	1.5	1.2
	Ad-siNT	92.6	2.9	2.3	1.3
	Ad-siBcrp	92.4	2.8	1.7	1.4

(B) TS Recovery

Rat	Viral Infection	TS recovery (% of TGZ Dose)		
		Medium	Cells	Bile
WT	CTL	1.61	2.36	0.85
	Ad-siNT	1.32	2.78	1.01
	Ad-siBcrp	1.22	2.94	1.01
TR	CTL	1.01	1.42	0.42
	Ad-siNT	0.95	1.52	0.41
	Ad-siBcrp	0.80	1.52	0.47

(C) TG Recovery

Rat	Viral Infection	TG recovery (% of TGZ Dose)		
		Medium	Cells	Bile
WT	CTL	0.69	0.11	0.13
	Ad-siNT	0.87	0.16	0.22
	Ad-siBcrp	0.68	0.15	0.20
TR	CTL	1.30	0.17	0.00
	Ad-siNT	1.94	0.34	0.01
	Ad-siBcrp	1.43	0.28	0.03

Figure 5.5.

	ATP-dependent transport (pmol/min/mg protein)			
Compound	Control		Bsep	
	Mean	SEM	Mean	SEM
TC	7.8	13.0	326.6	18.4
TS	479.8	336.4	532.1	355.0

Figure 5.6.

(A) TS

Rat	Viral Infection	Cells+Bile (pmol/mg protein)		Cells (pmol/mg protein)		BEI (%)	
		Mean	SEM	Mean	SEM	Mean	SEM
WT	CTL	1059.6	212.7	880.2	288.2	18.1	13.1
	GF120918	1058.0	163.5	903.0	191.4	14.4	13.2
TR ⁻	CTL	588.8	73.7	508.8	68.2	13.5	7.3
	GF120918	602.9	77.7	535.9	64.5	10.7	8.4

(B) TG

Rat	Viral Infection	Cells+Bile (pmol/mg protein)		Cells (pmol/mg protein)		BEI (%)	
		Mean	SEM	Mean	SEM	Mean	SEM
WT	CTL	89.6	89.4	43.9	56.2	59.9	13.9
	GF120918	86.6	90.4	44.7	59.7	64.5	23.5
TR ⁻	CTL	78.8	9.9	77.5	15.8	1.5	16.3
	GF120918	84.9	8.1	85.1	15.4	3.2	8.1

Figure 5.7.

1 μ M TGZ

Compound	Velocity (pmol/min/mg protein)			
	WT		TR ⁻	
	Mean	SD	Mean	SD
TS	88.6	24.4	101.8	57.5
TG	4.9	4.8	75.0	48.7

10 μ M TGZ

Compound	Velocity (pmol/min/mg protein)			
	WT		TR ⁻	
	Mean	SD	Mean	SD
TS	251.6	109.8	291.6	93.8
TG	95.6	44.6	616.7	190.6

Figure 6.2.

(A) ATP

LCA Medium Concentration (μM)	Rat ATP (mM)						Human ATP (mM)					
	6 hr		12 hr		24 hr		6 hr		12 hr		24 hr	
	Mean	SD	Mean	SD	Mean	SD	Mean	SD	Mean	SD	Mean	SD
0	2.79	0.13	3.74	0.54	3.33	0.04	5.23	0.07	4.15	0.31	3.63	0.63
25	3.13	0.29	3.39	0.05	2.91	0.21	4.83	0.33	4.06	0.18	3.14	0.67
50	3.17	0.24	3.57	0.27	2.96	0.20	4.73	0.12	4.31	0.27	2.49	0.53
100	3.04	0.33	2.98	0.07	2.75	0.15	4.36	0.57	3.69	0.41	2.46	0.61
125	2.43	0.13	3.05	0.84	1.84	0.29	4.49	0.08	3.97	0.17	2.78	0.61
150	2.22	0.21	2.16	0.23	1.63	0.34	4.28	0.38	3.51	0.23	1.85	0.33
200	1.81	0.23	1.81	0.40	0.87	0.52	4.20	0.14	3.71	0.23	1.11	0.46

LCA Medium Concentration (μM)	Mouse ATP (mM)						Dog ATP (mM)					
	6 hr		12 hr		24 hr		6 hr		12 hr		24 hr	
	Mean	SD	Mean	SD	Mean	SD	Mean	SD	Mean	SD	Mean	SD
0	2.22	0.12	2.55	0.20	1.48	0.22	2.38	0.87	3.76	0.67	3.63	0.63
25	2.25	0.19	2.76	0.46	1.91	0.66	2.78	1.15	4.15	1.36	3.19	0.68
50	2.14	0.18	2.59	0.13	1.42	0.15	2.11	0.85	3.85	1.16	2.51	0.53
100	2.27	0.29	2.49	0.28	1.33	0.61	1.97	0.87	3.79	0.62	2.50	0.62
125	2.30	0.40	2.46	0.16	1.29	0.21	2.22	0.26	3.36	0.10	2.75	0.60
150	2.10	0.25	2.43	0.20	1.42	0.06	2.18	0.63	3.45	1.04	1.84	0.33
200	2.17	0.53	1.95	0.06	1.16	0.25	2.08	0.72	2.91	0.40	1.29	0.53

LDH

LCA Medium Concentration (μM)	Rat LDH (% Control)						Human (% Control)					
	6 hr		12 hr		24 hr		6 hr		12 hr		24 hr	
	Mean	SD	Mean	SD	Mean	SD	Mean	SD	Mean	SD	Mean	SD
0	0.00	0.73	0.00	1.95	0.00	0.83	0.00	0.62	0.00	0.77	0.00	0.62
25	0.00	0.56	0.71	0.84	1.37	0.81	0.00	1.28	0.00	1.67	0.00	1.28
50	0.00	0.43	0.00	0.83	0.00	0.19	0.00	0.99	1.01	0.74	0.00	0.99
100	0.00	0.68	1.46	0.74	0.09	0.62	0.00	1.71	0.00	0.89	0.00	1.71
125	1.05	0.97	17.23	6.70	32.85	5.87	1.10	3.06	0.00	0.70	1.10	3.06
150	4.68	1.48	38.65	3.58	65.62	5.98	0.08	2.05	0.80	2.29	0.08	2.05
200	15.65	3.66	61.93	7.07	80.05	12.41	0.00	0.39	1.46	1.17	0.00	0.39

LCA Medium Concentration (μM)	Mouse (% Control)						Dog (% Control)					
	6 hr		12 hr		24 hr		6 hr		12 hr		24 hr	
	Mean	SD	Mean	SD	Mean	SD	Mean	SD	Mean	SD	Mean	SD
0	0.00	0.78	0.00	1.37	0.00	3.52	0.00	2.08	0.00	2.66	0.00	3.47
25	1.65	0.83	4.56	2.55	5.81	3.56	0.00	4.35	0.00	2.42	0.00	6.85
50	0.70	0.49	1.72	2.55	0.74	1.71	0.00	3.48	0.21	3.35	0.00	3.98
100	4.01	1.10	0.00	1.89	0.00	3.57	0.00	3.59	1.79	2.23	0.00	3.96
125	0.35	1.36	1.42	1.00	0.00	1.97	0.00	0.41	0.00	0.57	0.00	0.53
150	2.83	0.47	3.38	2.98	1.68	7.08	0.00	2.01	0.04	3.12	0.00	1.73
200	2.42	1.35	2.43	3.35	3.00	3.36	0.00	3.57	0.00	1.46	13.23	1.19

(B) LCA

LCA Medium Concentration (μM)	Rat LCA (mM)						Human LCA (mM)					
	6 hr		12 hr		24 hr		6 hr		12 hr		24 hr	
	Mean	SD	Mean	SD	Mean	SD	Mean	SD	Mean	SD	Mean	SD
0	0.00	0.00	0.00	0.00	0.00	0.00						
25	0.01	0.00	0.01	0.00	0.00	0.00						
50	0.07	0.04	0.03	0.00	0.01	0.00						
100	0.93	0.06	0.84	0.01	0.03	0.00	2.36	0.16	1.24	0.08	0.11	0.02
125	0.99	0.14	1.08	0.02	0.11	0.05	3.79	0.18	2.59	0.17	0.51	0.19
150	1.08	0.15	1.54	0.06	2.67	0.15	4.29	0.31	3.22	0.10	1.05	0.23
200	2.53	0.87	9.07	2.46	6.76	1.36	4.72	1.21	4.09	0.17	1.11	0.16

LCA Medium Concentration (μM)	Mouse LCA (mM)						Dog LCA (mM)					
	6 hr		12 hr		24 hr		6 hr		12 hr		24 hr	
	Mean	SD	Mean	SD	Mean	SD	Mean	SD	Mean	SD	Mean	SD
100	0.41	0.05	0.26	0.02	0.55	0.03	0.94	0.29	0.97	0.07	0.33	0.04
125	0.70	0.12	0.44	0.03	0.75	0.06	2.55	0.44	2.10	0.55	0.88	0.10
150	0.73	0.22	0.59	0.17	1.02	0.15	1.66	0.92	1.39	0.30	0.48	0.07
200	1.17	0.19	1.09	0.16	1.41	0.33	3.60	0.67	3.21	0.08	1.49	0.06

TLCA

LCA Medium Concentration (µM)	Rat TLCA (mM)						Human TLCA (mM)					
	6 hr		12 hr		24 hr		6 hr		12 hr		24 hr	
	Mean	SD	Mean	SD	Mean	SD	Mean	SD	Mean	SD	Mean	SD
0	0.00	0.00	0.00	0.00	0.00	0.00						
25	0.46	0.17	0.50	0.16	0.34	0.20						
50	0.57	0.46	0.68	0.32	0.49	0.17						
100	0.82	0.24	0.85	0.25	0.56	0.10	0.0042	0.0005	0.0035	0.0002	0.0013	0.0003
125	0.47	0.33	0.61	0.18	0.52	0.22	0.0054	0.0001	0.0051	0.0002	0.0027	0.0002
150	0.54	0.11	0.48	0.16	0.21	0.10	0.0051	0.0007	0.0052	0.0003	0.0035	0.0004
200	0.33	0.20	0.21	0.12	0.34	0.20	0.0063	0.0008	0.0071	0.0004	0.0057	0.0008

LCA Medium Concentration (µM)	Mouse TLCA (mM)						Dog TLCA (mM)					
	6 hr		12 hr		24 hr		6 hr		12 hr		24 hr	
	Mean	SD	Mean	SD	Mean	SD	Mean	SD	Mean	SD	Mean	SD
100	0.08	0.02	0.43	0.23	0.46	0.03	0.12	0.04	0.18	0.04	0.15	0.04
125	0.35	0.53	0.25	0.11	0.37	0.17	0.18	0.04	0.23	0.07	0.14	0.04
150	0.04	0.01	0.08	0.05	0.32	0.18	0.13	0.08	0.20	0.04	0.11	0.05
200	0.09	0.10	0.22	0.28	0.40	0.36	0.15	0.03	0.28	0.09	0.12	0.03

GLCA

LCA Medium Concentration (µM)	Rat GLCA (mM)						Human GLCA (mM)					
	6 hr		12 hr		24 hr		6 hr		12 hr		24 hr	
	Mean	SD	Mean	SD	Mean	SD	Mean	SD	Mean	SD	Mean	SD
0	0.00	0.00	0.00	0.00	0.00	0.00						
25	1.17	0.29	1.65	0.08	1.00	0.62						
50	2.11	0.38	3.83	0.34	2.64	0.57						
100	3.42	0.94	7.80	1.21	5.94	0.82	1.00	0.04	0.93	0.09	0.36	0.14
125	3.06	1.99	6.26	1.58	6.43	1.00	1.28	0.30	1.38	0.21	0.87	0.13
150	2.81	0.15	5.28	2.10	3.24	1.61	1.07	0.13	1.23	0.11	1.05	0.08
200	2.84	1.66	3.02	1.16	4.50	3.45	1.33	0.31	2.06	0.66	2.14	0.39

LCA Medium Concentration (µM)	Mouse GLCA (mM)					
	6 hr		12 hr		24 hr	
	Mean	SD	Mean	SD	Mean	SD
100	0.02	0.00	0.15	0.06	0.24	0.02
125	0.06	0.08	0.10	0.03	0.18	0.08
150	0.02	0.00	0.04	0.02	0.18	0.08
200	0.02	0.01	0.07	0.06	0.17	0.12

Figure 6.3.

(A) ATP

Rat ATP (mM)							Human ATP (mM)						
CDCA Medium Concentration (μM)	6 hr		12 hr		24 hr		CDCA Medium Concentration (μM)	6 hr		12 hr		24 hr	
	Mean	SD	Mean	SD	Mean	SD		Mean	SD	Mean	SD	Mean	SD
0	2.00	0.26	1.71	0.22	2.90	0.26	0	4.27	0.02	3.36	0.07	3.66	0.13
50	2.06	0.18	1.74	0.15	2.79	0.13	250	4.35	0.08	3.39	0.03	3.81	0.07
100	1.78	0.07	1.54	0.06	2.49	0.40	375	4.02	0.18	3.40	0.04	3.41	0.04
250	1.21	0.25	1.67	0.35	1.86	0.33	500	3.50	0.14	2.94	0.05	2.95	0.06
375	0.58	0.27	1.72	0.80	1.53	0.84	650	2.61	0.17	1.70	0.04	1.48	0.03
500	0.94	0.12	0.73	0.10	0.70	0.03	800	1.41	0.06	0.67	0.07	0.14	0.01
1000	0.15	0.02	0.15	0.05	0.21	0.01	1000	0.61	0.07	0.16	0.02	0.08	0.00

LDH

Rat LDH (% Control)							Human LDH (% Control)						
CDCA Medium Concentration (μM)	6 hr		12 hr		24 hr		CDCA Medium Concentration (μM)	6 hr		12 hr		24 hr	
	Mean	SD	Mean	SD	Mean	SD		Mean	SD	Mean	SD	Mean	SD
0	0.00	1.55	0.00	2.67	0.00	2.73	0	0.00	0.57	0.00	1.36	0.00	0.10
50	1.85	1.02	0.44	1.80	0.00	2.52	250	0.07	0.61	0.00	0.71	0.30	0.95
100	2.49	0.98	3.84	0.69	3.71	4.92	375	0.00	0.60	0.00	0.27	0.81	0.15
250	11.09	4.29	44.56	3.08	52.53	5.41	500	0.00	2.74	2.11	0.38	3.77	0.80
375	43.45	8.07	83.79	4.43	88.50	5.55	650	3.13	1.44	5.35	0.73	19.89	1.10
500	89.34	1.49	88.60	4.65	91.52	10.00	800	4.44	0.32	12.33	1.28	54.69	0.77
1000	97.28	4.77	99.01	6.50	102.69	4.20	1000	10.82	1.66	44.70	3.09	72.80	4.26

(B) CDCA

Rat CDCA (mM)							Human CDCA (mM)						
CDCA Medium Concentration (μM)	6 hr		12 hr		24 hr		CDCA Medium Concentration (μM)	6 hr		12 hr		24 hr	
	Mean	SD	Mean	SD	Mean	SD		Mean	SD	Mean	SD	Mean	SD
0	0.00	0.00	0.00	0.00	0.00	0.00	0	0.00	0.00	0.00	0.00	0.00	0.00
50	0.00096	0.00044	0.00040	0.00038	0.00009	0.00015	250	2.96	0.05	2.80	0.06	2.05	0.27
100	0.00565	0.00242	0.00	0.00	0.00	0.00	375	4.00	0.09	3.47	0.28	3.16	0.08
250	0.10	0.01	0.06	0.01	0.04	0.00	500	3.95	0.10	2.18	0.38	1.99	0.27
375	0.12	0.04	0.26	0.02	0.19	0.01	650	2.98	0.22	1.10	0.09	0.61	0.09
500	0.35	0.04	0.70	0.16	0.68	0.16	800	2.62	0.18	0.82	0.04	0.90	0.04
1000	1.25	0.17	2.89	0.52	6.80	0.98	1000	2.90	0.22	2.02	0.19	1.08	0.16

TCDCA

Rat TCDCA (mM)							Human TCDCA (mM)						
CDCA Medium Concentration (μM)	6 hr		12 hr		24 hr		CDCA Medium Concentration (μM)	6 hr		12 hr		24 hr	
	Mean	SD	Mean	SD	Mean	SD		Mean	SD	Mean	SD	Mean	SD
0	0.0000	0.0000	0.0001	0.0001	0.0003	0.0001	0	0.0369	0.0004	0.0368	0.0006	0.0280	0.0005
50	0.0038	0.0008	0.0008	0.0002	0.0005	0.0001	250	0.0058	0.0006	0.0047	0.0003	0.0051	0.0006
100	0.0093	0.0046	0.0017	0.0004	0.0009	0.0001	375	0.0081	0.0005	0.0061	0.0005	0.0054	0.0005
250	0.0050	0.0014	0.0024	0.0002	0.0029	0.0004	500	0.0109	0.0011	0.0044	0.0004	0.0050	0.0002
375	0.0051	0.0009	0.0099	0.0029	0.0069	0.0020	650	0.0110	0.0007	0.0031	0.0003	0.0025	0.0000
500	0.0074	0.0010	0.0112	0.0035	0.0109	0.0017	800	0.0113	0.0008	0.0028	0.0001	0.0014	0.0001
1000	0.0102	0.0029	0.0171	0.0027	0.0387	0.0051	1000	0.0128	0.0016	0.0037	0.0005	0.0009	0.0002

GCDCA

Rat GCDCA (mM)							Human GCDCA (mM)						
CDCA Medium Concentration (μ M)	6 hr		12 hr		24 hr		CDCA Medium Concentration (μ M)	6 hr		12 hr		24 hr	
	Mean	SD	Mean	SD	Mean	SD		Mean	SD	Mean	SD	Mean	SD
0	0.00	0.00	0.00	0.00	0.00	0.00	0	0.032	0.001	0.035	0.002	0.033	0.000
50	0.0010	0.0004	0.0004	0.0004	0.0001	0.0001	250	0.43	0.02	0.38	0.01	0.44	0.04
100	0.0057	0.0024	0.00	0.00	0.00	0.00	375	0.54	0.02	0.42	0.01	0.37	0.01
250	0.0961	0.0077	0.0633	0.0139	0.0397	0.0035	500	0.50	0.00	0.29	0.03	0.32	0.01
375	0.12	0.04	0.26	0.02	0.19	0.01	650	0.35	0.01	0.14	0.01	0.15	0.01
500	0.35	0.04	0.70	0.16	0.68	0.16	800	0.29	0.01	0.17	0.01	0.03	0.01
1000	1.25	0.17	2.89	0.52	6.80	0.98	1000	0.25	0.01	0.13	0.02	0.01	0.00

Supplementary Figure 6.1.

(A) Rat

LCA Medium Concentration (μM)	TCDCA (μM)						GCDCA (μM)					
	6 hr		12 hr		24 hr		6 hr		12 hr		24 hr	
	Mean	SD	Mean	SD	Mean	SD	Mean	SD	Mean	SD	Mean	SD
0	0.00	0.00	0.11	0.19	1.41	0.25	0.00	0.00	0.00	0.00	0.25	0.22
25	1.02	0.19	1.71	0.34	2.91	0.68	1.11	0.04	2.23	0.45	2.59	0.58
50	1.05	0.70	1.93	0.45	3.28	1.23	1.39	0.72	2.92	0.46	5.05	0.36
100	0.67	0.27	1.25	0.21	1.56	0.38	1.12	0.41	2.37	0.08	4.67	0.78
125	0.00	0.00	0.34	0.30	0.35	0.60	0.63	0.26	0.94	0.21	1.75	0.36
150	0.00	0.00	0.00	0.00	0.00	0.00	0.69	0.17	0.73	0.23	0.33	0.57
200	0.00	0.00	0.00	0.00	0.00	0.00	0.64	0.56	0.00	0.00	0.88	1.52

LCA Medium Concentration (μM)	TMCA (μM)						GMCA (μM)					
	6 hr		12 hr		24 hr		6 hr		12 hr		24 hr	
	Mean	SD	Mean	SD	Mean	SD	Mean	SD	Mean	SD	Mean	SD
0	0.69	0.94	10.62	3.27	51.45	17.96	0.00	0.00	0.19	0.32	5.26	0.54
25	11.64	2.01	13.91	3.58	18.68	7.56	10.58	0.46	11.38	1.65	11.27	1.61
50	6.84	4.72	11.63	3.13	13.56	3.99	8.20	3.67	11.90	0.79	12.70	0.00
100	2.58	1.46	3.55	1.05	4.16	1.30	7.72	1.68	10.47	1.61	9.80	0.46
125	0.00	0.00	0.00	0.00	1.42	1.43	3.80	2.14	4.79	1.45	10.01	2.64
150	0.00	0.00	0.00	0.00	0.00	0.00	3.69	1.01	3.41	1.60	2.39	2.70
200	0.00	0.00	0.00	0.00	0.00	0.00	1.76	1.52	1.53	0.32	0.66	1.15

(B) Human

LCA Medium Concentration (μM)	TCDCA (μM)						GCDCA (μM)					
	6 hr		12 hr		24 hr		6 hr		12 hr		24 hr	
	Mean	SD	Mean	SD	Mean	SD	Mean	SD	Mean	SD	Mean	SD
0					9.70	1.69					14.28	2.93
100	4.35	0.03	4.53	0.30	3.95	1.30	1.98	0.15	2.76	0.20	2.83	0.89
125	4.09	0.67	3.44	0.26	3.05	0.36	2.10	0.16	2.38	0.16	2.16	0.31
150	3.38	0.36	2.80	0.10	2.20	0.21	1.71	0.20	1.86	0.25	1.50	0.22
200	3.76	0.83	3.25	0.09	2.29	0.16	2.28	0.51	2.22	0.14	1.66	0.14

LCA Medium Concentration (μM)	TCA (μM)						GCA (μM)					
	6 hr		12 hr		24 hr		6 hr		12 hr		24 hr	
	Mean	SD	Mean	SD	Mean	SD	Mean	SD	Mean	SD	Mean	SD
0					2.67	0.59					14.28	2.93
100	0.23	0.04	0.21	0.03	0.13	0.12	0.60	0.10	0.63	0.03	0.61	0.15
125	0.22	0.06	0.23	0.04	0.08	0.15	0.63	0.31	0.59	0.09	0.55	0.19
150	0.19	0.01	0.07	0.13	0.00	0.00	0.54	0.14	0.41	0.12	0.34	0.05
200	0.29	0.03	0.33	0.02	0.20	0.01	0.72	0.13	0.85	0.22	0.66	0.12

LCA Medium Concentration (μM)	GHDCA (μM)					
	6 hr		12 hr		24 hr	
	Mean	SD	Mean	SD	Mean	SD
0					0.00	0.00
100	3.05	0.03	2.60	0.43	1.08	1.08
125	6.90	2.00	6.50	1.83	1.84	3.18
150	7.89	1.33	2.31	4.01	4.98	0.83
200	13.65	5.90	16.62	14.59	18.75	3.31

(C) Mouse

LCA Medium Concentration (μM)	TCDCA (μM)						GCDCA (μM)					
	6 hr		12 hr		24 hr		6 hr		12 hr		24 hr	
	Mean	SD	Mean	SD	Mean	SD	Mean	SD	Mean	SD	Mean	SD
0					0.38	0.09					0.00	0.00
100	13.56	2.20	19.20	4.52	26.33	5.57	0.96	0.20	1.31	0.11	1.48	0.27
125	13.96	8.38	14.53	3.30	17.89	3.56	0.74	0.18	1.20	0.13	0.96	0.13
150	8.28	1.89	8.35	2.02	12.47	1.04	0.70	0.05	0.92	0.21	1.04	0.14
200	11.17	2.76	11.86	7.77	15.81	5.79	0.82	0.30	1.07	0.32	1.01	0.29

LCA Medium Concentration (μM)	TMCA (μM)					
	6 hr		12 hr		24 hr	
	Mean	SD	Mean	SD	Mean	SD
0					6.58	0.93
100	1.34	0.64	3.68	1.00	1.93	0.58
125	1.09	1.45	1.65	0.69	0.61	0.53
150	0.00	0.00	0.41	0.37	0.00	0.00
200	0.41	0.70	0.88	1.12	0.49	0.85

(D) Dog

LCA Medium Concentration (μM)	TCDCA (μM)						GCDCA (μM)					
	6 hr		12 hr		24 hr		6 hr		12 hr		24 hr	
	Mean	SD	Mean	SD	Mean	SD	Mean	SD	Mean	SD	Mean	SD
0					1.23	0.22					1.18	0.21
100	0.94	0.09	0.71	0.06	0.40	0.05	0.97	0.21	0.83	0.12	0.54	0.10
125	0.79	0.07	0.58	0.05	0.42	0.03	0.89	0.16	0.65	0.10	0.41	0.05
150	0.70	0.17	0.73	0.12	0.36	0.06	0.79	0.35	0.78	0.15	0.41	0.11
200	0.55	0.10	0.61	0.08	0.52	0.18	0.54	0.02	0.53	0.07	0.49	0.12

LCA Medium Concentration (μM)	TCA (μM)					
	6 hr		12 hr		24 hr	
	Mean	SD	Mean	SD	Mean	SD
0					0.48	0.08
100	0.29	0.08	0.22	0.06	0.13	0.11
125	0.25	0.06	0.24	0.09	0.16	0.13
150	0.26	0.09	0.35	0.21	0.11	0.10
200	0.30	0.13	0.14	0.13	0.00	0.00

Supplementary Figure 6.2.

(A) Rat

CDCA Medium Concentration (μM)	MCA (μM)						TMCA (μM)					
	6 hr		12 hr		24 hr		6 hr		12 hr		24 hr	
	Mean	SD	Mean	SD	Mean	SD	Mean	SD	Mean	SD	Mean	SD
0	0.00	0.00	0.00	0.00	0.00	0.00	3.45	1.05	5.74	2.49	14.00	3.94
50	0.00	0.00	0.00	0.00	0.00	0.00	30.68	9.87	33.66	12.41	46.28	17.25
100	24.12	9.33	0.00	0.00	0.00	0.00	28.23	2.55	13.18	4.16	18.37	3.02
250	72.25	13.63	135.56	37.14	88.75	7.62	8.22	1.91	1.94	0.49	1.79	0.33
375	63.87	24.68	113.44	18.10	55.44	12.66	7.12	2.80	0.00	0.00	0.00	0.00
500	101.37	25.99	62.27	42.55	1.53	2.65	5.33	3.29	0.00	0.00	0.00	0.00
1000	0.00	0.00	0.00	0.00	0.00	0.00	0.00	0.00	0.00	0.00	0.00	0.00

CDCA Medium Concentration (μM)	GMCA (μM)						GCA (μM)					
	6 hr		12 hr		24 hr		6 hr		12 hr		24 hr	
	Mean	SD	Mean	SD	Mean	SD	Mean	SD	Mean	SD	Mean	SD
0	0.00	0.00	0.00	0.00	0.87	0.10	0.00	0.00	0.00	0.00	0.00	0.00
50	120.61	10.12	95.64	19.74	102.50	16.20	0.00	0.00	0.00	0.00	0.00	0.00
100	305.97	15.05	127.47	13.50	115.58	12.55	0.36	0.03	0.00	0.00	0.00	0.00
250	202.90	11.34	150.74	11.60	117.49	13.47	0.18	0.01	0.00	0.00	0.00	0.00
375	117.37	25.60	44.25	6.11	12.22	5.38	0.00	0.00	0.00	0.00	0.00	0.00
500	80.99	40.40	8.19	2.73	0.00	0.00	0.00	0.00	0.00	0.00	0.00	0.00
1000	0.00	0.00	0.00	0.00	0.00	0.00	0.00	0.00	0.00	0.00	0.00	0.00

(B) Human

CDCA Medium Concentration (μM)	CA (μM)						TCA (μM)					
	6 hr		12 hr		24 hr		6 hr		12 hr		24 hr	
	Mean	SD	Mean	SD	Mean	SD	Mean	SD	Mean	SD	Mean	SD
0	0.59	0.04	0.75	0.06	0.62	0.08	5.88	0.25	7.31	0.38	8.33	0.67
250	9.49	0.41	5.93	0.26	4.24	0.69	0.50	0.03	0.32	0.06	0.20	0.03
375	10.95	0.58	6.60	0.66	3.99	0.45	0.58	0.02	0.26	0.04	0.19	0.03
500	11.72	0.68	5.37	0.83	3.15	0.24	1.03	0.05	0.28	0.03	0.14	0.12
650	7.85	0.66	2.94	0.32	1.71	0.09	1.44	0.09	0.32	0.01	0.00	0.00
800	6.27	0.36	1.93	0.06	0.32	0.28	2.13	0.19	0.36	0.02	0.00	0.00
1000	5.11	0.13	1.28	0.11	0.00	0.00	2.49	0.08	0.40	0.03	0.00	0.00

CDCA Medium Concentration (μM)	GCA (μM)					
	6 hr		12 hr		24 hr	
	Mean	SD	Mean	SD	Mean	SD
0	20.38	0.89	28.39	4.10	44.47	1.05
250	2.22	0.15	1.25	0.03	1.01	0.11
375	2.35	0.21	1.33	0.07	0.90	0.06
500	2.78	0.22	1.17	0.04	0.87	0.07
650	4.18	0.26	0.81	0.15	0.65	0.02
800	6.11	0.49	1.27	0.10	0.00	0.00
1000	8.93	0.41	1.40	0.15	0.00	0.00